General Disclaimer

One or more of the Following Statements may affect this Document

- This document has been reproduced from the best copy furnished by the organizational source. It is being released in the interest of making available as much information as possible.

- This document may contain data, which exceeds the sheet parameters. It was furnished in this condition by the organizational source and is the best copy available.

- This document may contain tone-on-tone or color graphs, charts and/or pictures, which have been reproduced in black and white.

- This document is paginated as submitted by the original source.

- Portions of this document are not fully legible due to the historical nature of some of the material. However, it is the best reproduction available from the original submission.

Produced by the NASA Center for Aerospace Information (CASI)

SPACECRAFT ANTENNA SYSTEMS

INTERIM ENGINEERING REPORT (PHASE I – FINAL REPORT)

(OCTOBER 1963 – JANUARY 1965)
NASA 5-3545

COMSAT RESEARCH BRANCH
CODE 625
GODDARD SPACE FLIGHT CENTER
GREENBELT, MARYLAND

GPO PRICE $ _____

CFSTI PRICE(S) $ _____

Hard copy (HC) $6.00

Microfiche (MF) 1.00

ff 653 July 65

BY
- W. H. KUMMER
- A. T. VILLENEUVE

AEROSPACE GROUP
RESEARCH AND DEVELOPMENT DIVISION

HUGHES

HUGHES AIRCRAFT COMPANY
CULVER CITY, CALIFORNIA

FACILITY FORM 602

N66 24121 (ACCESSION NUMBER) (THRU)

263 (PAGES) (CODE)

CR-91797 (NASA CR OR TMX OR AD NUMBER) 07 (CATEGORY)

Report No. P65-35

INTERIM ENGINEERING REPORT

(Phase I - Final Report)

for

STUDY OF SPACECRAFT ANTENNA SYSTEMS

(October 1963 - January 1965)

Contract No. NAS 5-3545

W. H. Kummer and A. T. Villeneuve

Prepared by

Antenna Department
Hughes Aircraft Company
Culver City, California

APPROVED:

L. L. Bailin

L. L. Bailin, Manager
Antenna Department

for

Goddard Space Flight Center
Greenbelt, Maryland
Comsat Research Branch Code 625
A. Kampinsky, Technical Officer

BLANK PAGE

CONTENTS

1. INTRODUCTION. 1

1.1 The Communication Link and the Antenna Systems 1

1.2 Purpose of this Study 3

1.2.1 General Phases 3

1.2.2 Organization of Data 6

1.3 System Parameters 7

1.3.1 Earth-Satellite Systems 7

1.3.2 Satellite-to-Satellite Systems 11

1.4 Antennas for Present Communication Satellites . 11

1.5 Frequency of Operation 15

1.5.1 Allocated Frequencies and Allowable Power Densities. 15

1.5.2 Antenna Considerations in Relation to Operating Frequency 16

1.5.3 Frequency Selection Based on Fixed Satellite Antenna Gain. 17

1.5.4 Frequency Selection Based on Fixed Satellite Antenna Size 18

1.6 Relative Applicability of Techniques 18

1.7 Summary of Antenna Characteristics. 21

1.7.1 Characteristics of Switched Multiple-Beam Antennas 22

1.7.2 Properties of Self-Phased Arrays. 22

1.7.3 Characteristics of Adaptive Arrays 23

1.7.4 Characteristics of Conventional Phased Arrays . 24

1.7.5 Tabulated Characteristics 24

1.8 Recommendations 25

CONTENTS (Continued)

2. SATELLITE COMMUNICATION SYSTEMS 31
2.1 Orbital Characteristics and Scan Requirements . 31
2.2 Scan Requirements and Beamwidth 34
2.3 Beam Scanning Techniques 34

3. COMPONENTS FOR ELECTRONICALLY SCANNED ANTENNAS. 37
3.1 Ferrite Phase Shifters 37
3.1.1 General Characteristics 38
3.1.2 Longitudinal Field Phase Shifter 40
3.1.3 Digital Ferrite Phase Shifters 41
3.1.4 Synchronous Ferrite Phase Shifters 41
3.1.5 Miniature Ferrite Phase Shifters 47
3.2 Semiconductor Phase Shifters 48
3.2.1 Microwave Diodes 48
3.2.2 Continuously Variable Phase Shifters. 53
3.2.3 Stepped Phase Shifters 60
3.3 Diode-Iris Amplitude and Phase Control Unit . . 61
3.3.1 Background 61
3.3.2 Experimental Models 62
3.4 Solid-State Components 65
3.4.1 Switches 65
3.4.2 Broadband Transistor Amplifiers 66
3.4.3 Tunnel Diode Amplifiers 67
3.4.4 Microwave Power Transistors 67
3.4.5 X-Band Mixers 68
3.4.6 Filters 69
3.4.7 Circulators 70
3.5 Log-Periodic Circuits 70
3.5.1 Log-Periodic Structures 71
3.5.2 Log-Periodic Phase Difference Circuits. . . . 73
3.5.3 Log-Periodic Magic-T Circuits 75
3.5.4 Log-Periodic Directional Couplers 75

CONTENTS (Continued)

4.	ANTENNA SYSTEMS		77
	4.1	Phase Scanned Circular Arrays	77
	4.1.1	Pattern Analysis	77
	4.1.2	Array Description	80
	4.1.3	Control Electronics	80
	4.1.4	Array Performance Characteristics	83
	4.2	Diode-Iris Controlled Traveling-Wave Array	85
	4.2.1	Antenna Components	85
	4.2.2	Aperture Distributions	85
	4.2.3	Pattern and Gain Measurements	86
	4.3	Reflector and Feed Systems	90
	4.3.1	Paraboloidal Reflector and Feeds	90
	4.3.2	Spherical Reflectors	94
	4.4	Lenses and Feed Systems	97
	4.4.1	Lenses with an Optical Axis	97
	4.4.2	Spherically Symmetric Lenses	103
	4.5	Multiple-Beam Antennas	112
	4.5.1	The Butler Array	113
	4.5.2	Multibeam Circular Arrays	120
	4.6	Multibeam Horn Antenna System	125
	4.7	Amplitude Scanned Circular Arrays	126
	4.7.1	Required Element Excitations	126
	4.7.2	Experimental Systems	128
	4.7.3	Properties of System	129
	4.8	Amplitude Scanned Time-Controlled Arrays	129
	4.8.1	Theory of Pattern Synthesis	130
	4.8.2	Application to Beam Scanning	132
	4.8.3	Electronic Amplitude Scan by Time Control Synthesis	134
	4.9	Pseudo Passive Satellite Techniques	135
	4.9.1	Basic Configuration	135
	4.9.2	Number of Components Required	138

CONTENTS (Continued)

	4.10	Weight Considerations of Multiple-Beam Antennas	139
	4.10.1	Reflector and Feed Antennas	139
	4.10.2	Spherical Lens Antennas	141
	4.10.3	Thin Optical Lenses and Feeds	142
	4.10.4	Constrained Lenses and Feeds	143
5.	ELECTRONICALLY SELF-STEERING SYSTEMS		145
	5.1	The Effective Gain of Self-Steerable Arrays	145
	5.1.1	Transmit Case	145
	5.1.2	Mutual Coupling Effects on Element Power	148
	5.1.3	Receive Case	150
	5.1.4	System Operation	150
	5.2	Redirective Array	152
	5.2.1	Analysis of Operation	152
	5.2.2	Retransmission Process	157
	5.2.3	Representative Systems	160
	5.3	Simple Retrodirective Array	166
	5.3.1	Description	166
	5.3.2	Analysis of System	168
	5.3.3	Noise Considerations in System with Separate Amplifiers in Each Line	170
	5.3.4	Experimental Systems	172
	5.4	Adaptive Antenna Arrays	178
	5.4.1	General Description of Operation	178
	5.4.2	Independent Loop Configuration	180
	5.4.3	Sum Signal Reference Configuration	182
	5.4.4	Experimental Phase-Locked Loops	184
	5.4.5	Adaptive Arrays used as Retrodirective Antennas	185
6.	NEW TECHNOLOGY SECTION: THE TRANS-DIRECTIVE ARRAY		187
	6.1	General Description	187
	6.2	Two-Station Operation	188
	6.3	Multi-Station Operation	190

CONTENTS (Continued)

7.	MILLIMETER-WAVE ANTENNAS		193
	7.1	Scaling Considerations	193
	7.2	Phase Shifters for the Radiating Elements of a High-Gain Planar Array	195
	7.3	Ferrite Phase Shifters	197
	7.3.1	Applications to Arrays	197
	7.3.2	Linearity	199
	7.3.3	Insertion Loss	200
	7.4	Scanning by Control of Ferrite Slab in Wavefront	200
	7.5	Optical Antennas	202
	7.5.1	Lens Scanning Antennas	204
	7.5.2	Hemispherical Mechanical Scanning	207
	7.5.3	Electronic Switches	209
	7.6	Millimeter-Wave Components	211
	7.6.1	Power Source	211
	7.6.2	Amplifiers	212
	7.6.3	Hexagonal Ferrite Isolators	212
8.	ACKNOWLEDGMENTS		215
9.	REFERENCES		217
10.	APPENDIX		225

BLANK PAGE

ILLUSTRATIONS

1-1.	Typical missions and corresponding possible antenna configurations	5
1-2.	Representative link parameters	7
1-3.	Telstar communication antenna	13
1-4.	Pattern coverage of Telstar antennas	13
1-5.	Syncom communications antenna	14
1-6.	Pattern coverage of Syncom antennas	14
1-7.	Basic theory of Trans-Directive Array	29
1-8.	Basic theory of retrodirective array	29
2-1.	Angles subtended by satellites in different orbits	32
2-2.	Region of required beam pointing directions for gravity-stabilized satellite.	33
2-3.	Region of required beam pointing directions for spin-stabilized satellite.	33
3-1.	Effect of temperature compensation in a ferrite phase shifter	39
3-2.	Characteristics of 32 phase shifters	40
3-3.	Longitudinal field ferrite phase shifter	41
3-4.	Waveguide digital ferrite phase shifter	41
3-5.	Circular waveguide r-f field configuration	45
3-6.	Control magnetic field configuration	45
3-7.	Modified Fox phase shifter.	46
3-8.	General equivalent circuit representation of variable capacitance diode.	50
3-9.	Simplified equivalent circuit of a continuously operated variable capacitance diode.	51
3-10.	Equivalent circuits for extreme bias conditions of forward and reverse breakdown voltages	51
3-11.	Junction capacitance and current as a function of applied bias voltage	51

ILLUSTRATIONS (Continued)

3-12.	Operation and equivalent circuit of PIN diode	53
3-13.	Delay line semiconductor phase shifter	53
3-14.	Equivalent circuit of capacitance-controlled phase shifter	54
3-15.	Schematic of experimental voltage-controlled phase shifter	56
3-16.	Characteristics of voltage-controlled phase shifter	56
3-17.	Variable capacitance diode phase shifter configurations	57
3-18.	Reflection phase shifter with 3-port circulator	58
3-19.	Phase shift of output signal	59
3-20.	Phase shift and insertion loss as functions of diode bias at 1 Gc	59
3-21.	A two-stage, three-step phase shifting system	60
3-22.	Iris-controlled slot	62
3-23.	Mechanically-controlled complex slot	62
3-24.	Experimental phase and amplitude data for mechanical complex slot	63
3-25.	Four-diode-iris phase and amplitude control device	64
3-26.	Noise temperature of various r-f amplifiers as a function of operating frequency	67
3-27.	Example of one-port log-periodic network	71
3-28.	Constant phase difference circuit	73
3-29.	Two-port log-periodic transmission-line network	73
3-30.	Octaline magic-tee	74
3-31.	Quadriline hybrid junction	75
4-1.	Circular array geometry	78
4-2.	Applications Technology Satellite circular phased array	81
4-3.	System diagram of control electronics for circular phased array	83
4-4.	Departure of incremental phase shift versus programmed phase shift for various temperatures	84
4-5.	Ten-element diode-iris array	86

ILLUSTRATIONS (Continued)

4-6.	Phase bridge circuit used for obtaining phase and amplitude distribution in linear array aperture	87
4-7.	Measured sum patterns illustrating 90 degrees of electronic beam scanning	88
4-8.	Comparison of predicted and measured sum and difference patterns for selected scan angles	89
4-9.	Paraboloidal reflector geometry	91
4-10.	Paraboloidal reflector with array primary feed for scanning	93
4-11.	Spherical reflector geometry	95
4-12.	Wide-angle scan dielectric lens	99
4-13.	Constrained lens	100
4-14.	Typical ray in an ideal Luneberg lens	105
4-15.	Approximate theoretical electromagnetic field near the focus point of a 10-inch Luneberg lens at f = 6 Gc	108
4-16.	Experimental far field radiation pattern of a 10-inch Luneberg lens at f = 6 Gc	108
4-17.	Exact theoretical electric field near the focus point of a 10-inch Luneberg lens at f = 6 Gc	108
4-18.	Typical pattern of 10-inch Luneberg lens with open-end waveguide at 6 Gc	109
4-19.	Constant-K lens showing focusing of rays by refraction	110
4-20.	Relationship of dielectric constant and radius of a broad-beam Luneberg lens	112
4-21.	Phase shift convention for directional couplers and hybrid rings	113
4-22.	Simplest beam-forming matrix	114
4-23.	Amplitude and phases of different beam signals in a 4-element matrix	115
4-24.	Sixteen-element beam-forming matrix	116
4-25.	Phase shifts in a Butler array	118
4-26.	Circular array with beam-forming matrix	122
4-27.	N-element circular array	122
4-28.	Lincoln Laboratory multibeam horn antenna system	125

ILLUSTRATIONS (Continued)

4-29.	Diagram of k'th control channels for experimental amplitude scanned circular array	128
4-30.	Linear array	130
4-31.	Method of exciting elements	132
4-32.	Phasor diagram	133
4-33.	Scattering surface of elements distributed on spherical cap	136
5-1.	Excitation of single element by matched voltage source	146
5-2.	Geometry of far field of self-steerable array	151
5-3.	Basic elements of a two-way repeater	153
5-4.	Circular array of spiral antennas	160
5-5.	Retrodirective array techniques	167
5-6.	Specific configuration for a retrodirective array	173
5-7.	Van Atta array	174
5-8.	Van Atta array on circular curve	175
5-9.	Active Van Atta system with separate arrays for reception and retransmission	177
5-10.	Modulated Van Atta array	178
5-11.	Typical phase-locked loop receiving array	179
5-12.	Servo diagram of phase-locked loop	180
5-13.	Servo diagram of simplified phase-locked loop	180
5-14.	Proportional plus integral network	181
5-15.	Block diagram of the active adaptive antenna array system simulator	184
5-16.	Acquisition time of the 8-channel antenna array simulator versus mixer output voltage	185
5-17.	Oscillograms showing the adaptiveness of the phase-locked system	185
5-18.	Adaptive retrodirective antenna modules	186
6-1.	Trans-Directive Array	189
6-2.	Specific configuration for a Trans-Directive Array	191

ILLUSTRATIONS (Continued)

7-1.	1000-element round-hole 56-Gc array	194
7-2.	Detail of small ferrite phase shifters	199
7-3.	Ferrite slab in wavefront	201
7-4.	Basic arrangement of ferrite slab scanner	202
7-5.	Radiation patterns of ferrite slab scanner	203
7-6.	Cylindrical lens scanner	205
7-7.	Radiation pattern at 56 Gc in the plane of scan of the cylindrical lens scanner	206
7-8.	Hemispherical mechanical scanner	208
7-9.	Multiple feed scanning antenna utilizing switches	210

TABLES

1-1.	Typical system parameters for down link	8
1-2.	Typical system parameters for up link	9
1-3.	Effects of atmospheric absorption	10
1-4.	Vehicle surfaces	25
1-5.	Multiple-beam antennas	26
1-6.	Self-steerable arrays	27
3-1.	Typical characteristics of longitudinal ferrite phase shifters at various frequencies	42
3-2.	Waveguide digital ferrite phase shifter characteristics at various frequencies	43
3-3.	Comparison of step and continuously variable phase shifters	49
3-4.	Representative X-band crystals	68
3-5.	Applicable commercial filters for space-earth communications systems	69
3-6.	Performance of commercially available strip transmission line circulators	70
4-1.	Array characteristics for Tchebyscheff patterns	129
7-1.	Typical design parameters for nonscanned millimeter-wave antennas	196
7-2.	Power characteristics of available oscillators	212
7-3.	Characteristics of hexagonal ferrite isolators	213

PRECEDING PAGE BLANK NOT FILMED.

SUMMARY

An antenna systems study for spacecraft communications was performed that included a review of the literature, a field survey, and an assessment of the present state-of-the-art in all electronic beam formation shaping and steering techniques. Multiple-beam formation methods, phased-locked loops, electronically scanned antenna systems, electronically self-steering antenna systems, and millimeter-wave antenna systems are discussed in detail as potential parts of spacecraft systems.

Several specific implementations of beam forming and shaping are included. Among these are diode-iris control of the amplitude and phase of slot radiation, a multibeam-forming Trans-Directive Array, amplitude scanning by time-control synthesis, a mechanically scanned millimeter-wave cylindrical lens system, and a multibeam Luneberg lens antenna with a mosaic feed. A survey of electronic and mechanical steering for the millimeter wavelengths (to 100 Gc) is also included.

Components for the implementation of the various antenna systems are described and include standard and miniature ferrite phase shifters, semiconductor variable capacitance and PIN diode phase shifters, and log-periodic circuits. Where techniques are critically dependent upon certain components, these critical component areas are identified and are assessed for the appropriate applications.

PRECEDING PAGE BLANK NOT FILMED

BLANK PAGE

1. INTRODUCTION

1.1 THE COMMUNICATION LINK AND THE ANTENNA SYSTEMS

The continuation of activities now underway in space depends in large measure on the degree to which satisfactory communication can be established and maintained with and between the participating vehicles. A similar dependence on communication will also be true of future missions undertaken by NASA through the Applications Technology Satellite Programs, by the Comsat Corporation and other commercial firms, and by the Department of Defense. Although each program will of course have special needs and requirements with respect to vehicle configurations and sizes, the ultimate success of all will depend largely on the establishment of efficient communication links: earth-earth, satellite-satellite, and earth-satellite-earth. The Telstar, Relay, and Syncom programs are important examples of recently successful pioneering efforts in the field of communications. But these early satellites are inefficient portions of an overall communications link; typically, for example, they have stationary antennas that radiate energy in all directions. The promise of more complex future missions in space emphasizes the need for maximizing communication bandwidth and gain and has stimulated the demand for better performance from the requisite subsystems. Among these subsystems is the antenna system and the associated processing equipments.

An interesting variety of special communication problems are generated for the spacecraft antenna system that involve unique considerations and difficulties differing in both degree and kind from those associated with earth-based facilities and terminals. Highly efficient point-to-point communications are going to be required in which the space vehicle itself may constitute either a point of origin of transmissions

or simply a relay station, depending on the particular mission. A higher signal-to-noise ratio will be required of the energy from the satellite, especially in the final, possibly power-limited, link down to earth. Motion is to be expected, also, of either or both terminals of a communication link with respect to any particular choice of reference frame. New environmental demands must be met, including those imposed by the ambient vacuum, by temperature extremes, and by micrometeorite bombardment as examples. Reliability assumes extreme importance with spacecraft antenna systems since neither repair nor servicing is possible with present-day technology.

The stringent weight restriction on equipment that is inherent in all space missions translates for the antenna system rather directly into limitations on the available power and on the size of communication equipment. Transmission of signals to and from space vehicles will involve communication over vast distances. Even for an earth-orbiting satellite, the range is great, although this distance may be considered short for a space mission. The implications of the weight limitations and the long distances again point to the desirability and necessity of achieving as much directivity and efficiency in the antenna structure as the mission situation will permit.

As the directivity is increased, the necessary degree of pointing accuracy required of the spacecraft antenna also increases. Two limitations are encountered here: in the capability of a vehicle to control its mechanical orientation and in the accuracy with which this orientation may be determined at any given time. To achieve good performance, high gain is the basic requirement and controls the characteristics of a satellite communications antenna. High gain implies

a) A beam from the satellite that is narrower than a beam that would subtend the earth.

b) An aperture which is large compared with wavelength and thus is a physically large aperture at the lower wavelengths.

c) A steering mechanism which points this beam continuously at one or more selected locations on earth. The beam motion is an integral part of the antenna problem. Three types of beam motion are

possible, of which the most promising is also the least developed: mechanical, including large appendage antennas; electro-mechanical; and electronic or inertialess.. Short of these limitations, the question exists of the extent to which control of the vehicle attitude is advisable in a given set of circumstances. The answers from an engineering standpoint entail practical compromises and depend on the techniques available for antenna searching and tracking as compared with vehicle control methods. A consideration of antenna techniques must thus be incorporated into any overall system design for a mission in order that essential trade-offs in weight, accuracy, and reliability can be determined.

1.2 PURPOSE OF THIS STUDY

The primary objective of this study of spacecraft antenna systems was to survey the state-of-the-art in electronic scanning and steering techniques — specifically, to compare the generic types. The applicable techniques are identified, the critical areas are delineated, and the components which comprise these systems are critically examined for suitability. The techniques are projected to practical devices for satellite applications.

1.2.1 General Phases

Various kinds of space communication links have been considered in this program in an effort to provide descriptions of antenna and antenna system techniques that would improve overall gain characteristics. Available techniques for all-electronic beam formation, shaping, and steering were surveyed and their applicability to specific space missions was assessed, even though the devices presently available for the reliable control of individual radiating elements involve considerable bulk and weight.

The functions of the communication systems studied demand high-gain beams that can be despun and pointed at electronic speeds. This demand implies lightweight antennas that can be integrated into the surface of the vehicle. Those functions which require high power gains

in certain areas of space need antennas of sufficient size in wavelengths to effectively collimate the radiated or received energy. Each antenna system must be capable of finding a small target and tracking it under diverse operating conditions. One phase of this program thus was concerned with the needs imposed by the attitude and fundamental characteristics of the space vehicle. In this phase two approaches were used to determine the state-of-the-art. Reports and published articles on electronic scanning were obtained and studied. Visits were made to establishments (see Appendix) in which programs in electronic scanning and steering are being pursued.

In a second phase, several novel techniques were analyzed from a fundamental antenna point of view. The state-of-the-art in antenna techniques falls into two generic types: the antenna techniques that require external controls and those that are self-steering. In the externally controlled systems, an external sensor (i-r, r-f, or ground station) is required for beam acquisition, and a phasing network is required to point the beam appropriately to correct the direction when necessary. The self-steering or focusing system requires electronic circuitry that can sense the phase of incoming pilot signals to lock-on and track an earth station or another vehicle. The restrictions imposed by the probable vehicle configurations as well as by available on-board weights are examined. Certain multiple beam or electronic scanning techniques are presently severely limited by these considerations.

In a third phase of the program, detailed consideration was given to those techniques that are promising and appropriate to communication antennas situated on satellites. Various stabilization configurations were studied and suitable antenna techniques were juxtaposed with the missions. (See Figure 1-1.) Five satellite orbits and degrees of stabilization of immediate interest to NASA communications systems were studied:

a) synchronous altitude, 35,790 Km, spin-stabilized
b) synchronous altitude, 35,790 Km, gravity-stabilized
c) 6,000 n. mi. (11,120 Km) orbit, spin-stabilized
d) 6,000 n. mi. (11,120 Km) orbit, gravity-stabilized
e) unstabilized satellite.

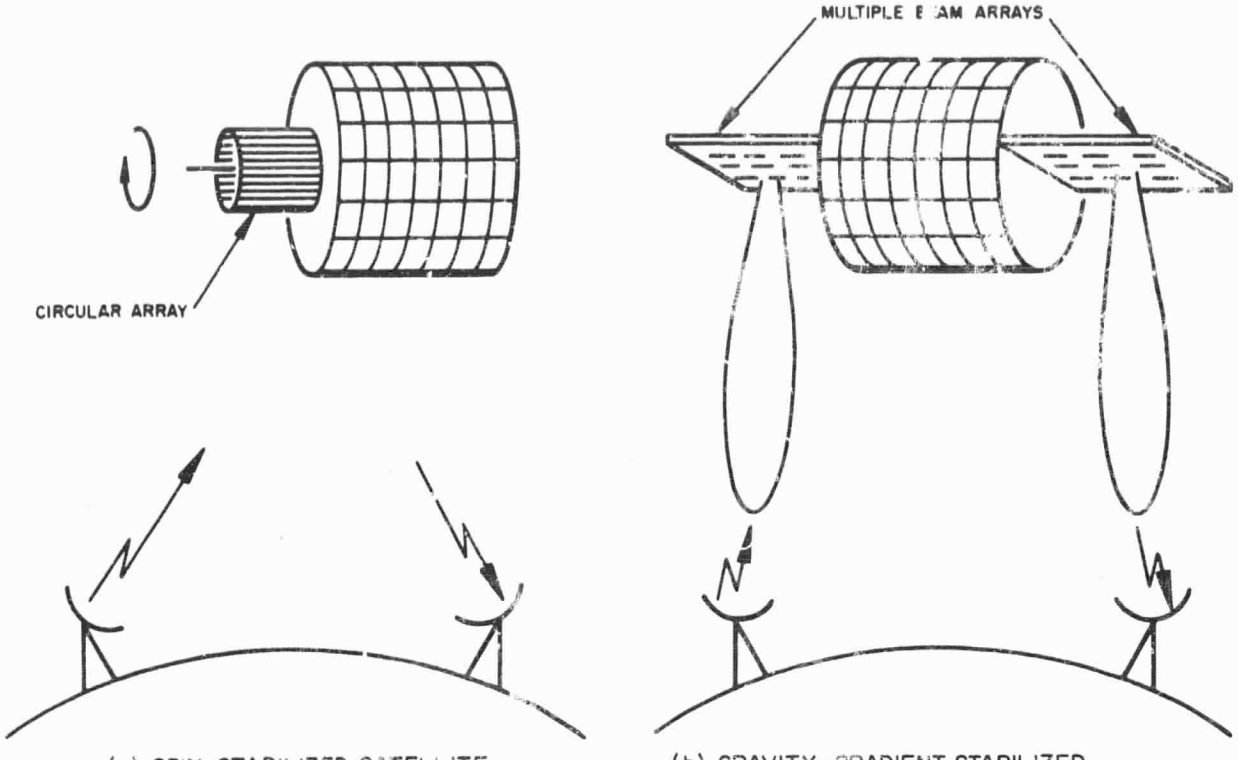

(a) SPIN-STABILIZED SATELLITE

(b) GRAVITY-GRADIENT STABILIZED SATELLITE WITH MULTIPLE BEAM ARRAYS

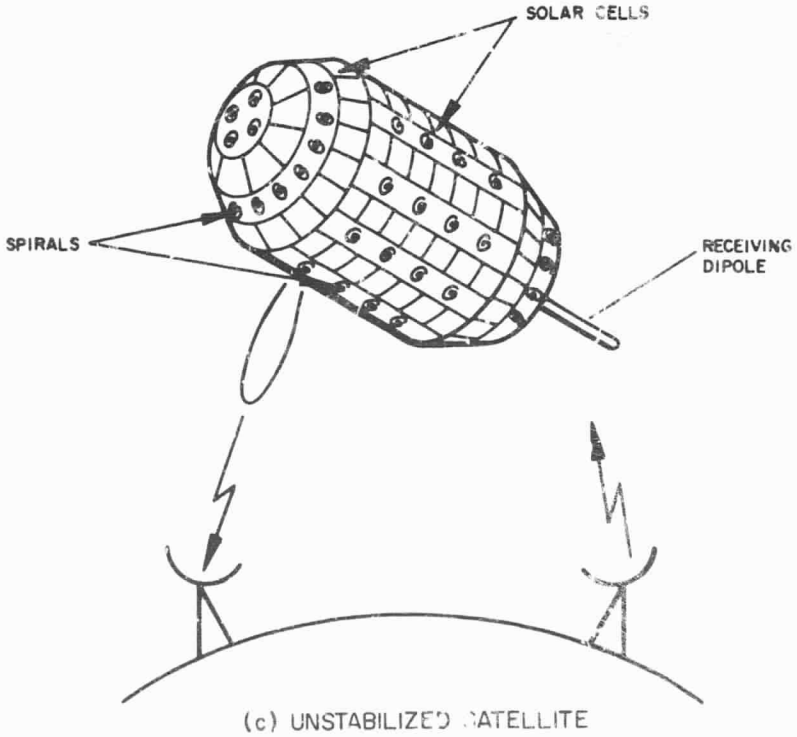

(c) UNSTABILIZED SATELLITE

Figure 1-1. Typical missions and corresponding possible antenna configurations.

1.2.2 Organization of Data

To provide the background against which the various antenna techniques can be reviewed, this beginning section presents data on system considerations. The effect on a satellite communication system of such factors as vehicle stabilization method, type of orbit, atmospheric attenuation, and choice of operating frequency are presented and discussed in some detail. Typical system parameters for both earth-satellite and satellite-earth links of a representative system are discussed and given in tabular form. The three present communication satellites — Telstar, Relay, and Syncom — are described in terms of their antennas; these represent the present operational antenna systems. The antenna techniques surveyed are summarized in the first section in terms of their relative applicability to spacecraft communications systems and described in detail in subsequent sections.

Following the system summary, the components for electrically scanned antennas are discussed in detail (Section 3), including ferrite and semiconductor phase shifters, a diode-iris control unit, various solid-state components, and wideband log-periodic circuits. These and other critical components are considered as constituents of certain systems in Sections 4, 5, and 6. In Section 4 are discussed systems which require an external control for orientation of the beam direction. Phase-scanned and amplitude-scanned circular arrays, traveling-wave arrays, reflectors, lenses, multiple-beam antennas, and time-controlled arrays are described in detail.

Antennas that do not require external control for beam orientation are considered in Section 5 as electronically self-steering systems. These include redirective and retrodirective arrays of various kinds and self-adaptive antenna arrays that utilize phase-locked loops.

The New Technology section (6) incorporates new techniques formulated during the course of this study. The section is devoted to the description of a Trans-Directive Array which uses multiple beams. Antenna techniques in the millimeter-wavelength band and the problems associated with the extension of lower frequency techniques into this band are presented in Section 7. Several new scanning techniques and the state-of-the-art in millimeter component development are also described.

The list of applicable references utilized directly in this survey is given at the end of the report, and a brief compilation of establishments visited and key personnel interviewed is presented in the Appendix.

1.3 SYSTEM PARAMETERS

In this section system parameters are listed for systems that should find use in the next several years in spacecraft communications.

1.3.1 Earth-Satellite Systems

Typical system parameters for earth-satellite systems are presented in Tables 1-1 and 1-2. It should be emphasized that these numbers are only representative and can be adjusted to suit particular requirements, as is illustrated in Figure 1-2. The parameters selected depend on many trade-offs beyond the scope of the present study. For instance, if only voice channels are required, then a 10-Mc bandwidth would not be needed. The antenna gains and transmitter powers can be achieved in practice.

For the frequencies below 10 Gc, an antenna size of 15 feet was chosen since it appears to be a good compromise between cost and performance. At the millimeter wavelengths, the diameter was selected on the basis of compatibility between beamwidth, achievable gain, and tracking accuracy. The 1-db beamwidth is only 0.12° at 35 and 94 Gc. If the signal is to be maintained to ±1/2 db, then a tracking capability of 0.1° must be engineered into the ground stations. To achieve the 58-db gain, rigid tolerances must be maintained on the antenna surfaces.

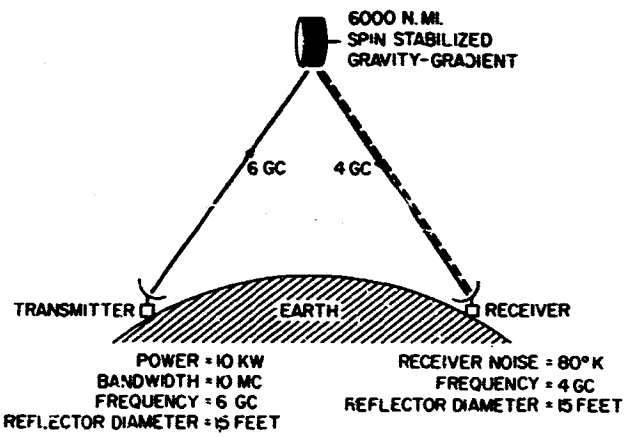

Figure 1-2. Representative link parameters.

There are some unknowns, such as the atmosphere losses at 35 and 94 Gc. These estimated losses are shown in Table 1-3 and are additive.

Orbit Altitude	11, 120 Km (6, 000 n. mi.)				35, 790 Km (Synchronous)			
Angle Subtended by Earth	43°				17. 4°			
Frequency, Gc	4	8	35	94	4	8	35	94
Free space path loss, db*	189	195	207. 5	216. 5	197	203	216	224. 5
Paraboloid diameter of receiving and transmitting antenna, feet	15	15	10	3. 6	15	15	10	3. 6
3-db beamwidth, degrees	1. 1	0. 57	0. 20	0. 20	1. 1	0. 57	0. 20	0. 20
Gain (55-percent efficiency), db	43	49	58	58	43	49	58	58
1-db beamwidth, degree	0. 66	0. 33	0. 12	0. 12	0. 66	0. 33	0. 12	0. 12
Line losses, db	1. 5	1. 5	2	2	1. 5	1. 5	2	2
Atmospheric losses, db	—	—	2	8	—	—	2	8
R-f bandwidth, Mc	100	100	100	100	100	100	100	100
Carrier S/N, db	15	15	15	15	15	15	15	15
Bandwidth and S/N product, db	95	95	95	95	95	95	95	95
Satellite effective radiated power required, dbw**	40. 5	40. 5	40. 5	40. 5	48. 5	48. 5	48. 5	48. 5
Noise temperature at ground station, °K	80	80	80***	80***	80	80	80***	80***

*For maximum distances of 16, 330 Km (10, 150 statute miles) for the 40° angle and 41, 700 Km (25, 900 statute miles) for the 17. 4° angle.

**ERP = antenna gain in db + transmitted power in dbw.

***These figures are projections of the art; achieving them could require engineering development.

Table 1-1. Typical System Parameters for Down Link.

Orbit Altitude Angle Subtended by Earth	11,120 Km (6,000 n. mi.) 43°				35,790 Km (Synchronous) 17.4°			
Frequency, Gc	6	8	35	94	6	8	35	94
Free space path loss, db*	192.5	195	207.5	216.5	200.5	203	216	224.5
Paraboloid diameter of transmitting antenna, feet	15	15	10	3.6	15	15	10	3.6
3-db beamwidth, degrees	0.76	0.57	0.20	0.20	0.76	0.57	0.20	0.20
Gain (55-percent efficiency), db	46.5	49	58	58	46.5	49	58	58
1-db beamwidth, degree	0.44	0.33	0.12	0.12	0.44	0.33	0.12	0.12
Line losses, db	1.5	1.5	2	2	1.5	1.5	2	2
Transmitter power	10 Kw 40 dbw	10 Kw 40 dbw	3.2 Kw 35 dbw	500 w** 27 dbw	10 Kw 40 dbw	10 Kw 40 dbw	3.2 Kw 35 dbw	500 w** 27 dbw
Atmospheric losses, db	—	—	2	8	—	—	2	8
Power received at satellite, dbw	-107.5	-107.5	-118.5	-141.5	-115.5	-115.5	-127	-149.5
R-f bandwidth, Mc	100	100	100	100	100	100	100	100
Carrier S/N, db	15	15	15	15	15	15	15	15
Bandwidth and S/N product, db	95	95	95	95	95	95	95	95
Power required at satellite input, dbw***	109	109	109	109	109	109	109	109

*For maximum distances of 16,330 Km (10,150 statute miles) for the 43° angle and 41,700 Km (25,900 statute miles) for the 17.4° angle.

**These numbers are projected from present designs at other frequencies; achieving these powers would require development effort.

***Components are assumed to be at 290°K.

Conversion factors: radius of earth = 6.37×10^6 meters

1 nautical mile = 1.853 Km

Table 1-2. Typical System Parameters for Up Link.

Characteristics of Atmosphere	Attenuation at 35 Gc for Various Elevation Angles (db)			Attenuation at 94 Gc for Various Elevation Angles (db)		
	5°	10°	90° (Zenith)	5°	10°	90° (Zenith)
Clear weather	2.5	1.2	0.25	10	5	<1
Fog: visibility 2000 feet ($0.032\ g/M^3$)	1.2	0.6	0.1	5.7	2.9	0.5
Fog: visibility 400 feet ($0.32\ g/M^3$)	7.4	3.8	0.7	57	29	5.0
Fog: visibility 100 feet ($2.3\ g/M^3$)	63	32	5.5	>100	>100	40
Light rainfall: 1 mm/hr	11.4	5.7	1.0	40	20	<4
Moderate rainfall: 4 mm/hr	57	29	5	100	70	12.5
Heavy rainfall: 16 mm/hr	>100	>100	17.5	>100	>100	50

Table 1-3. Effects of Atmospheric Absorption.

For example, at 35 Gc the assumed atmospheric loss is

For clear weather path at 10° above horizon		1.2 db
Light fog add		0.6 db
Total	about	2 db

The actual values depend on the location, elevation, and local weather of the terminal.

From Table 1-1 it is clear that the down link is the most critical one because the satellite is limited in both transmitter power and antenna gain. The down link is thus part of the communication satellite

which can use high-gain antennas to best advantage and is the link which will receive first consideration in the application of electronic techniques.

1.3.2 Satellite-to-Satellite Systems

Typical system parameters for satellite-to-satellite communications are more difficult to define than for earth-to-satellite systems. They will depend on various factors such as types of orbits, stabilization of satellites, distances involved, and the types of communications systems envisioned. Because of the rather broad range of possibilities and the number of unknowns, no typical system calculations have been performed.

1.4 ANTENNAS FOR PRESENT COMMUNICATION SATELLITES

The three communications satellites presently operational, Telstar, Relay, and Syncom, have antenna systems which do not scan. Their antennas are designed to take advantage of the mission and orbit parameters as far as possible. Telstar has a quasi-omnidirectional antenna since the satellite does not have a preferred orientation with respect to the earth, and both Syncom and Relay have antennas that produce a doughnut-shaped pattern for the down link. The characteristics of the communication antennas for Telstar, Syncom, and Relay are listed below.

Telstar I

Orbit: inclination to equator 45°
apogee 3,531 miles
perigee 600 miles
Stabilization: spin-stabilized
Orientation with respect to earth: no constant plane
Down link: 4 Gc, left circular polarization
Up link: 6 Gc, right circular polarization
Antenna location: equatorial on satellite (Figure 1-3)
Generic type: circumferential slot on sphere
(D. S. Bugnolo, 1962)

Pattern coverage at both frequencies and gain with respect to isotropic circularly polarized antenna (Figure 1-4 ab):

equatorial: 1 db ± 1 db

polar to ±50° for -3 db

Syncom II and III

Orbit: synchronous

Stabilization: spin-stabilized

Orientation with respect to earth: spin axis perpendicular to orbit plane

Syncom II - inclined to equator

Syncom III - in equatorial plane

Down link: 1.8 Gc, linear polarization

Up link: 7.4 Gc, linear polarization

Antenna location: parallel to spin axis

Generic type: collinear three-element skirted dipole (Figure 1-5)

array axis parallel to spin axis

beamwidth 23° between 3-db points (Figure 1-6)

gain 5.0 db ± 1 db on equator

Relay:

Orbit: elliptical

apogee 4,612 miles

perigee 820 miles

Stabilization: spin-stabilized

Down link: 4.08 Gc and 4.17 Gc, left circular polarization

Up link: 1.725 Gc, right circular polarization

Antenna location: mounted along the spin axis of satellite on mast at one end

Generic type: biconical horn

Pattern coverage: essentially doughtnut-shaped

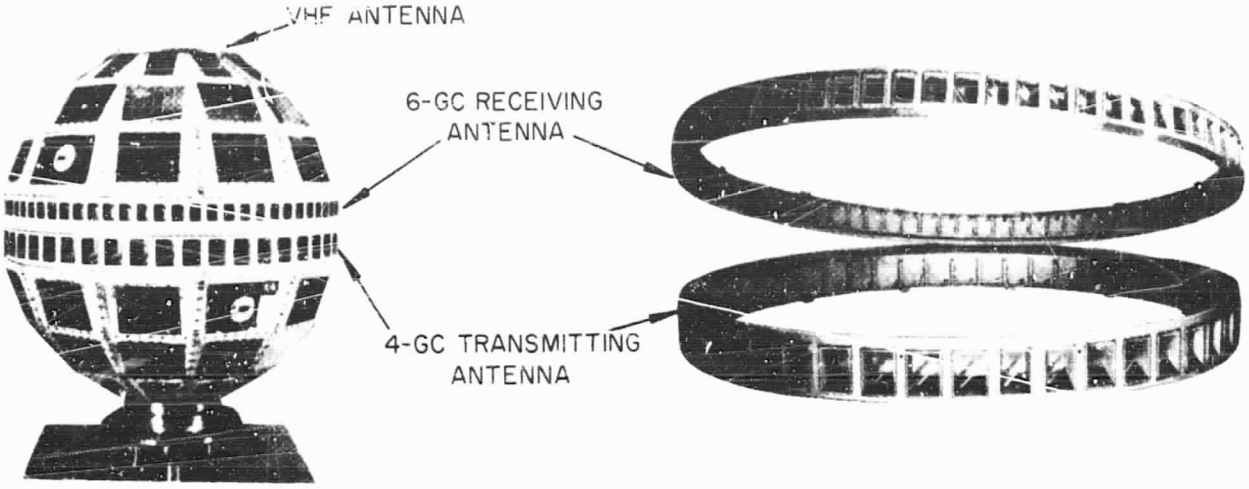

Figure 1-3. Telstar communication antenna (Bangert et al., 1963).

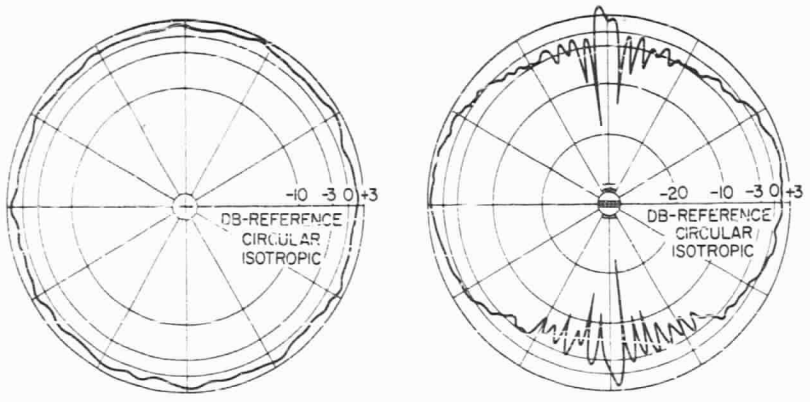

(a) TRANSMITTING PATTERN (4GC)

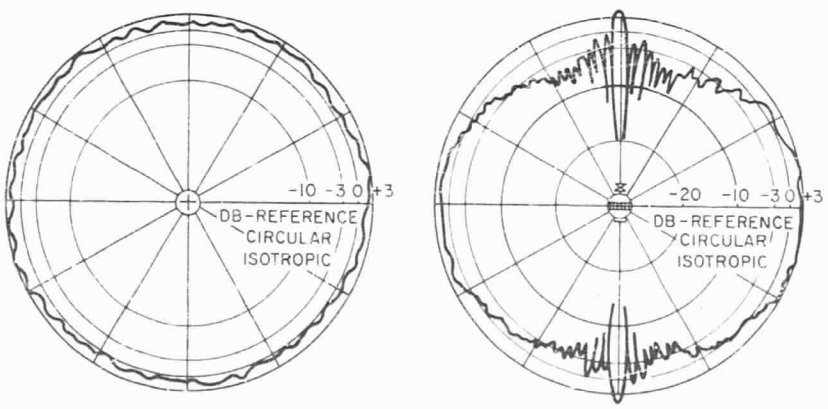

(b) RECEIVING PATTERN (6 GC)

Figure 1-4. Pattern coverage of Telstar antennas (Bangert et al., 1963).

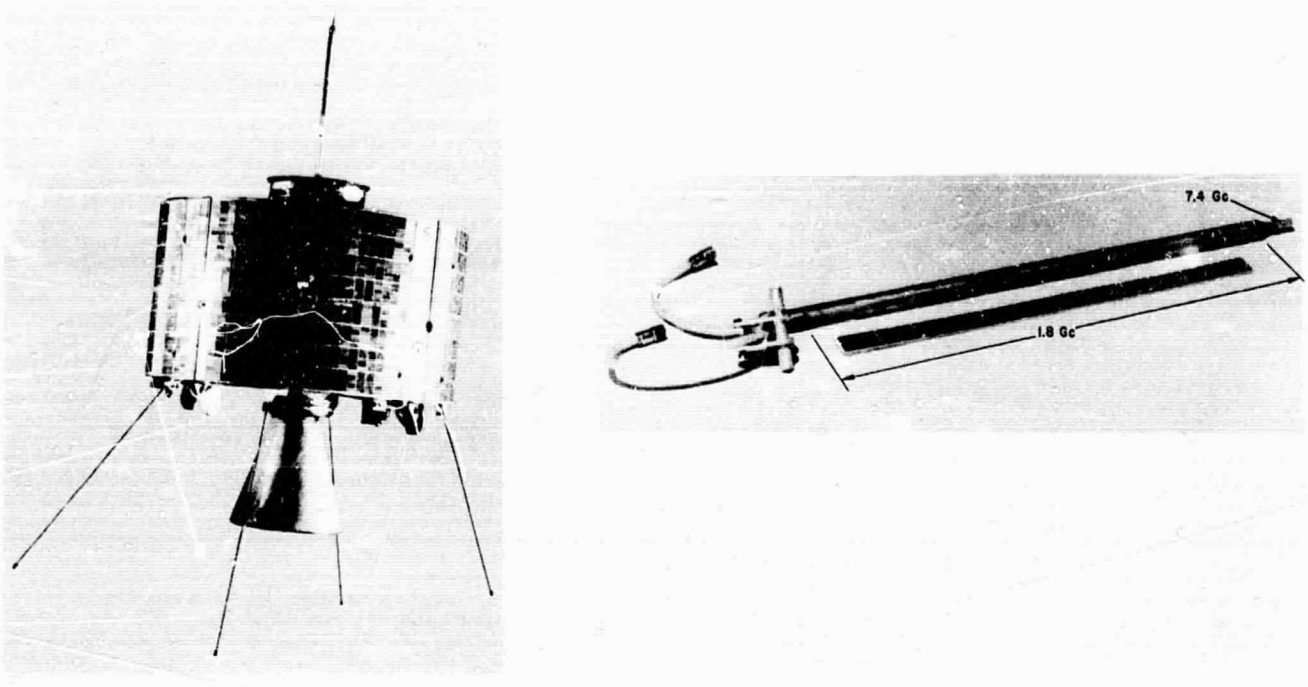

Figure 1-5. Syncom communications antenna.

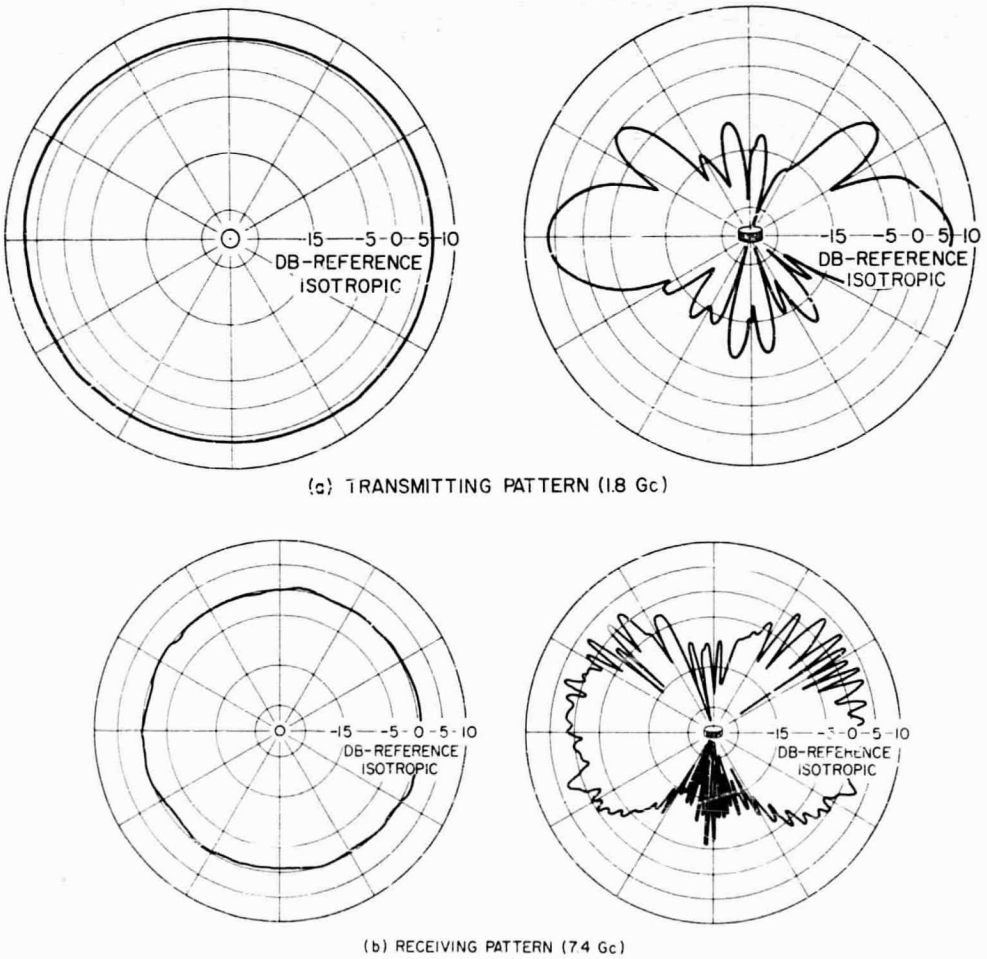

Figure 1-6. Pattern coverage of Syncom antennas.

1.5 FREQUENCY OF OPERATION

The selection of a frequency of operation depends on many considerations; among these are the availability of suitable components for every part of the communication link, the physical laws which determine the system characteristics, and the availability of frequencies in the spectrum suitable for satellite communications. Frequency availability may outweigh any trade-offs based on component or system considerations. The allocated frequencies are listed first in this subsection, followed by a discussion of the choice of operating frequency in terms of antenna considerations.

1.5.1 Allocated Frequencies and Allowable Power Densities

Among many other factors, the operation of satellite systems also depends on the cooperation between various users and the noninterference with other communication services. Below are listed applicable sets of the EARC, ITU, Geneva, 1963. (This information was kindly supplied by the ComSat Research Branch, Goddard Space Flight Center.)

Frequencies: up link 4400-4700 Mc
5800-5850
5850-5925
5925-6425
7250-7750
7900-8400

down link 3400-4200 Mc
7250-7700

31-31.3 Gc on secondary basis (noninterference)

31.5-31.8 Gc on primary basis for space research

31.8-32.3 Gc, 34.2-35.2 Gc } secondary basis

Power transmitted: up link 65 dbw in any Kc band
45 dbw in any 4-Kc band along horizon

Power density:

Required minimum carrier dispersal	300 Kc on up link
Maximum power density on down link, wideband FM or PM	Not to exceed -130 dbw/m^2 for all angles of arrival
Telephone channel, 4 Kc wide	-149 dbw/m^2
Passive or active narrow-band (modulation other than wide deviation FM or PM) for 4-Kc bandwidth	-152 dbw/m^2

At a joint technical advisory committee of IRE-EIA, March 1961, various areas in the United States were delineated with respect to regions of noninterference. This map is contained in their report on "Frequency Allocation for Space Communications."

1.5.2 Antenna Considerations in Relation to Operating Frequency

The choice of frequency depends on many parameters, not all of which are technical in nature. With certain assumptions, a reasonable conclusion can be reached with respect to frequencies to be chosen. The assumptions and the reasons for each are listed first.

Ground terminal:	Noise figure, transmitter power, ground antenna size, signal bandwidth are constant
Satellite:	Antenna has fixed gain instead of fixed size; noise figure, transmitter power, signal bandwidth are constant.

The assumption of fixed satellite antenna gain is made because the antenna on a communications satellite is likely to be one of the following four types:

1) An antenna forming a beam which blankets the entire earth and has a beamwidth slightly larger than the solid angle the earth subtends at the satellite. In this type of antenna, the beam shape and width are determined by a fixed geometry and do not depend on the frequency of operation; hence, the gain is fixed.

2) A multiple-beam antenna having narrow overlapping beams that can be combined to blanket the entire earth. One beam is used at any one time for receiving and another is used for transmitting. For this type of antenna, the gain of each beam is approximately proportional to N, the number of beams, although the gain of the overall antenna system decreases somewhat with higher frequency since the beam-switching circuits become more lossy. As in type (1) the gain of each beam does not depend on the operating frequency.

3) A retrodirective array having N elements. For this type of antenna, the gain is approximately proportional to N, the number of elements. The retrodirective system consists of antenna elements whose size is inversely proportional to frequency and of circuit components, such as mixers and i-f amplifiers, whose size is basically independent of the frequency. At the present level of technology, the allowable number of elements is limited by the weight of the circuit components; hence, the antenna gain is controlled by the number of components, not by the frequency used. (See Table 1-6.)

4) Mechanically and electronically scanned arrays. The useful gain of these arrays is not limited by the antennas themselves but at this time seems limited by the complexity and weight of the control circuitry that would be necessary to steer the antenna towards a selected location on earth. Since the beamwidths now considered are such that they blanket the entire earth, these types of antennas fall into the first category.

1.5.3 Frequency Selection Based on Fixed Satellite Antenna Gain

For a fixed satellite antenna gain, there is no advantage in an increase in frequency if it is assumed that the signal-to-noise ratio in the system is constant and independent of frequency. From an overall point of view, a lower frequency of operation is desirable because:

1) To use a given size reflector at higher frequencies at the ground terminal requires that the reflector be built to tighter tolerances; in addition, tracking accuracies must be greater.

2) In general, as frequency increases, it becomes more difficult to obtain the same transmitter power and to obtain as low a noise figure in the receiver.

3) Generally, as frequency increases in the microwave region, losses due to atmospheric absorption increase.

1.5.4 Frequency Selection Based on Fixed Satellite Antenna Size

The use of satellite antennas of a fixed size at higher frequencies would be a definite advantage if control circuitry is available to steer a narrow beam anywhere on earth. The weight of mechanically scanned antennas is fairly constant for constant area. Therefore, the gain does increase with frequency. For electronically scanned antennas, the weight of the components, such as the necessary phase shifters, decreases with increasing frequency so that an increase in gain with increasing frequency will be realized without much change in total antenna weight.

The advantages, other than increased gain, in the use of the higher frequencies fall into several categories.

1) The bandwidths as measured in percentage of the radio frequency carrier give larger absolute bandwidths than at lower frequencies; thus, design of several components will be easier.

2) Because of the crowding of the 1- to 10-Gc spectrum, the only available bands are in the 10- to 100-Gc range.

3) The higher frequencies, 30 to 100 Gc, suffer from atmospheric attenuation in several bands. The proper choice of frequencies will provide security between satellites since atmospheric attenuation will absorb transmission toward the earth.

1.6 RELATIVE APPLICABILITY OF TECHNIQUES

As a result of the survey of antenna techniques embodied in this report, several conclusions concerning the applicability of the various methods have been reached. These are presented in the succeeding paragraphs.

a) Paraboloidal Reflectors. These antennas are not desirable for electronically scanning a beam over large angular regions. Problems of aperture blockage are severe, and array type feeds are required to obtain proper beam positions and small spillover. They might be used for restricted angular coverage since, in general, scans of a few beamwidths can be achieved without pattern deterioration. (See Section 4. 3. 1.)

b) Spherical Reflectors. These antennas are also not desirable for satellite communication application. They are capable of wide-angle scan with a single mechanically moved feed, but electronic scanning requires the presence of array feeds which result in aperture blockage. With either type of scanning, inefficient use is made of the aperture. (See Section 4. 3. 2.)

c) Thin Optical Lens Antennas. These antennas also have the problem of requiring array feeds to obtain proper beam spacing. Unless primary phased arrays are used to feed them, they are limited in their achievable scan angle before pattern deterioration occurs. Aperture blockage is not a problem with lenses, however. Solid dielectric lenses are broadband but may be heavy. Zoned lenses are less broadband but lighter. The use of artificial dielectrics can decrease weight but will increase dissipative losses and frequency sensitivity. (See Section 4. 4. 1.)

d) Constrained Lenses. These antennas, which force rays to follow prescribed paths, can be designed for wide-angle coverage. They still have the requirement that array feeds are necessary to obtain overlapping beams. They may also be frequency sensitive because of dispersion in the constraining paths.

All of the above antenna systems (a) through (d) have an additional drawback in their requirement for approximately as much depth as aperture size; they operate best with focal distances nearly equal to aperture dimensions and are not very suitable for applications in which conformal antennas are desirable. They might best be considered as appendage antennas. The second common problem of requiring array type feeds to obtain proper beam positioning might be solved by proper feed design. (See Section 4. 4. 1.)

e) Spherical Lenses with Multiple Feeds. These consist of Luneberg and constant dielectric lenses. They provide wide angular coverage. With a cluster of feeds arranged on a spherical cap, the antenna is applicable to a gravity-gradient stabilized satellite. With a belt of feeds surrounding the lens on a great circle, the antenna is applicable to a spin-stabilized vehicle. In the first configuration, for example, the antenna could be placed on the earth-directed face of the satellite. The feeds and somewhat less than half the lens would be set in a recessed portion of the satellite. In the second configuration, the lens and feeds would have to be supported on the satellite spin axis but far enough away from the satellite to avoid interference between lens and satellite. In this form, it would be an appendage antenna. Weight is a problem if solid dielectrics are used for the lenses. Artificial dielectrics are lighter but have higher losses that can be up to 2 db more than for the solid lenses. In addition, the volume of these lenses, as with thin optical and constrained lenses, is relatively large since their depth is equal to their aperture. (See Section 4.4.2.)

f) Multiple-Beam Arrays Using Beam-Forming Matrices. These antennas use a single array of radiators that are fed by a matrix with multiple inputs which forms a number of independent beams. The beam-forming matrices require combinations of hybrids or directional couplers. The fact that the matrix consists of passive elements makes it inherently reliable; however, their number depends on the number of beams required and rapidly becomes very large. At frequencies up to X-band, strip transmission line techniques can be used in the matrix to keep down size and weight. The extensive networks required can introduce dissipation losses of several db into the antenna.

Of the multiple-beam arrays studied, the most attractive appear to be the spherical lens and the array with beam-forming matrix, the former for its wide angle scan capability and the latter for its capability to be arranged in a compact planar configuration. (See Sections 4.5, 4.6.)

g) Self-Steerable Antennas. The class of antennas termed "self-steerable" are those which, through the use of electronic processing

equipment, can automatically form a beam in the direction of an incident pilot signal. These antennas may be subdivided into several groups depending on how the steering is accomplished. These groups are listed here as

(1) Switched multiple-beam antennas

(2) Self-phased arrays

(3) Adaptive arrays

Group (1) may use the multiple-beam antennas mentioned with appropriate switching and control circuitry to select the proper beam automatically as indicated by the pilot signal. Group (2) is composed of conformal arrays of elements, each of which has its own electronic circuitry that automatically phases the elements to produce a beam in the direction dictated by the pilot. Group (3) is closely related to group (2) but uses phase-locked loops at each element to accomplish the element phasing. The term adaptive comes from certain properties of the phase-locked loops. (See Section 5.)

h) Conventional Phased Arrays. These arrays obtain beam-pointing direction through the use of phase shifters to control the phase distribution across the aperture. They differ from the self-phased and adaptive antennas in that the beam-pointing information is not obtained directly at each element but must be obtained from some other information, such as the interelement phase shift of a pair of elements, an i-r sensor, or some preprogrammed pointing instructions. This information must then be used to generate control signals which will adjust the individual phase shifters to point the beam in the proper direction. The control functions must be tailored to the phase shifter characteristics. (See Sections 4.1, 4.2.)

1.7 SUMMARY OF ANTENNA CHARACTERISTICS

In this section, the salient characteristics of the various antennas studied during the course of this program are outlined and also listed in tabular form.

1.7.1 Characteristics of Switched Multiple-Beam Antennas

Some of the more important characteristics of switched multiple-beam antennas are listed.

Advantages

a) They do not require variable phase shifters to scan the beam.

b) Their gain is not limited by the requirement that each beam cover the entire visible earth.

c) They are applicable to both nonsynchronous and synchronous gravity-gradient stabilized orbits.

d) They require no earth sensor and no preprogrammed controls.

e) They utilize inherently reliable r-f components (matrix or lens).

f) Satellite attitude information is inherently available.

Disadvantages

a) They require large numbers of couplers or hybrids (array with beam-forming matrix).

b) They require generation of pilot signal at the receiver.

c) Their weight may be a problem, depending on the configuration (use of a lens, for instance).

d) They require electronically controlled r-f switches and switch control circuitry.

e) Switching among the beams may result in switching transients in the information signal.

f) The minimum useful signal is determined by the gain at the switch-over point. For smooth transfer, variable power dividers instead of switches may have to be used between beams (additional circuitry and control circuitry).

1.7.2 Properties of Self-Phased Arrays

The various types of self-phased arrays, arrays whose beams are steered automatically by use of the interelement phase shift of an

incident pilot signal, have certain properties in common. Some of their more important properties are given.

Advantages

a) The array is made up of independent channels so that failure of one is not catastrophic.

b) Controlled phase shifters are not required to steer the beam.

c) Their gain is not limited by the requirement that the beam cover the entire visible earth.

d) They are applicable to nonsynchronous, synchronous, stabilized, or unstabilized systems.*

e) They require no earth sensor and no preprogrammed controls.

f) They are applicable to satellite-to-satellite communications.

g) They are capable of being enlarged (growth potential).

h) They require no switches or switch controls.

i) Satellite attitude information is inherently available.

Disadvantages

a) The components needed for implementation in flight-qualified, lightweight form need further development (essentially true of most systems).

b) They require generation of pilot signal at receiver.

c) An N element array requires N phase-matched channels.

d) Each channel requires a complete receiver and transmitter.

1.7.3 Characteristics of Adaptive Arrays

The characteristics of adaptive arrays are very similar to those of the self-phased arrays except in certain details of operation.

---

*To obtain the correct phase distribution over the aperture, the Van Atta array should be used only in planar configurations. A number of these arrays placed about an unstabilized satellite will produce interference patterns as the satellite spins or tumbles. It appears that the Van Atta array should be restricted to vehicles with gravity-gradient or similar stabilization.

Their advantages and disadvantages are similar to the self-phased arrays except for the following:

Advantages

a) The use of servo-controlled phase shifts can achieve very low tracking errors.

b) Phase shifters can handle large transmitted powers.

c) Satellite attitude information is inherently available.

Disadvantages

a) A servo loop and a controlled-phase shifter are required for each element in the array.

b) A trade-off is required between pointing accuracy and rapidity of beam positioning.

1.7.4 Characteristics of Conventional Phased Arrays

The conventional phased array, when properly steered, has radiation characteristics similar to those of the self phased and adaptive arrays. However, it also has certain different properties:

Advantages

Phase sensing devices may not be required at each element.

Disadvantages

a) Satellite attitude information is required for beam steering.

b) Complex control and waveform generating circuits are required.

c) Element phases are not individually adjusted but are determined from separate sources of beam pointing information.

1.7.5 Tabulated Characteristics

The vehicle surfaces on which an antenna could be mounted conformally are listed in Table 1-4. The different surfaces are paired with various modes of stabilization, orbit, and problem areas. In Table 1-5, the characteristics of multiple-beam antennas are summarized, and in Table 1-6, the characteristics of self steerable arrays.

Type of Vehicle Surface	Applicable Type of Stabilization	Type of Orbit	Problem Areas for Antennas
Planar	Gravity	Synchronous 6000 n. mi.	Projected Aperture
Cylindrical	Spin Gravity	Synchronous 6000 n. mi.	Sidelobes
Spherical	Unstabilized* Spin Gravity	Synchronous 6000 n. mi.	Sidelobes

*Tumbling satellite or satellite whose axis does not bear a known relation with respect to earth.

Table 1-4. Vehicle Surfaces.

1.8 RECOMMENDATIONS

From the summary of the relative applicability of the various generic antenna types, it is evident that the several techniques considered offer a wide variety of potential capabilities. Their ultimate performance characteristics depend to a large part upon the availability of certain critical components. Of course, the most desirable technique to use in any particular application will be dictated by the details of the application in its special requirements. However, a comparison of the techniques studied will indicate that the self-steerable antennas offer great versatility with regard to communications between satellites and earth, between satellites and airborne vehicles and ships at sea, and even between satellites themselves. Once implemented in some form and with the appropriate components, they provide a startling simplicity of operation which increases the system reliability and longevity. Because of their versatility of application and potential simplicity of operation, it is recommended that self-steerable arrays receive additional study and development to advance them to the point in the laboratory at which their capabilities may be empirically assessed. Once their assets and problems are completely verified, an extensive qualification and flight test program should be planned and executed.

Type of Antenna ④	Applicable Type of Stabilization	Type of Orbit	Coverage	External Pointing Control	Type of R-F Control Required	Bandwidth	Weight in Kilograms (See Section 4.10)	Reliability Factors	Problem Areas
Reflectors and Feeds	Gravity	Synchronous	A few beam-widths off axis	Pilot signals or pre-programmed controls	Switches and control circuitry (See Section 3.4)	Inherently broadband; limited by feed and crossover level change	① $W = \frac{\sqrt{G}}{f_{Gc}^2}(0.0251\sqrt{G} + N)$	Failure of switch causes loss of beam(s)	Gain degradation beyond a few beam-widths Aperture blockage
Thin optical lenses and feeds	Gravity	Synchronous	A few beam-widths off axis	Pilot signals or pre-programmed controls	Switches and control circuitry (See Section 3.4)	Unzoned solid dielectric: broadband Zoned: less broadband $BW = \frac{25}{M}\%$ (dielectric) ⑤	$W = \frac{NK}{f^2} + A'\left(\frac{\sqrt{\frac{G}{\eta}}}{f}\right)^3$ $W = \frac{NK}{f^2} + A''\left(\frac{G}{\eta f^2}\right)$	Failure of switch causes loss of beam(s)	Weight and Feed Array
Spherical optical lenses and feeds	Gravity	6000 n. mi. Synchronous	Beams may be positioned within cone of half-angle 60° - 70°	Pilot signals or pre-programmed controls	Switches and control circuitry (See Section 3.4)	Solid dielectric: broadband (octave) Artificial: less broadband	② $W = 0.354\left(\frac{\sqrt{G}}{f_{Gc}}\right)^3$ ③ $W = 0.177\left(\frac{\sqrt{G}}{f_{Gc}}\right)^3$	Failure of switch causes loss of beam(s)	Weight
Constrained lenses and feeds	Gravity	6000 n. mi. Synchronous	Beams may be positioned within cone of half-angle 50°	Pilot signals or pre-programmed controls	Switches and control circuitry (See Section 3.4)	Narrow band (on the order of 10 percent)	$W = \frac{NK}{f^2} + A'\left(\frac{\sqrt{\frac{G}{\eta}}}{f}\right)^3 + B'\frac{G}{f^2}$ $W = \frac{NK}{f^2} + A''\frac{G}{\eta f^2} + B''\left(\frac{\sqrt{\frac{G}{\eta}}}{f}\right)$	Failure of switch causes loss of beam(s)	Feed Array
Arrays with beam-forming matrices	Gravity	6000 n. mi. Synchronous	Beams may be positioned within cone of half-angle ≈ 45°	Pilot signals or pre-programmed controls	Switches and control circuitry (See Section 3.4)	Matrices can be made broadband (octave) Beam positions frequency sensitive ⑥	$W = 2.7 \times 10^{-3} \quad (G)^3$	Failure of switch causes loss of beam(s)	

NOTES:
G = Peak gain (cross-over gain will be lower depending on configuration)
N = Number of feeds
η = Efficiency
① = $\eta = 0.41$
② = $\eta = 0.56$
③ = $\eta = 0.355$
④ = Considered for use in a transdirective array. See Table 1-6.
⑤ = M = number of one wavelength steps between axial path and path through lens edge.
6 = See Section 4.5.1.

Table 1-5. Multiple-Beam Antennas

Type of Array	Applicable Type of Stabilization	External Pointing Control Required	Type of Orbit	Components Required for Steering	Bandwidth ①	Coverage	Reliability Factors	Problem Areas	Weight	Multiple Access Capability
Trans-Directive (requires multiple beams; see Table 1-6)	Gravity-gradient	All require r-f pilot signals	6000 n.mi. or synchronous	Logic circuits and r-f switch	See Table 1-5	See Table 1-5	Fails gracefully except for i-f amplifier	Cross-over level of beams are 4-8 db down from peak	1 Kg ② per beam approximately	Yes
Self-phased arrays	Gravity Unstabilized Spin			Local oscillators, modulators, mixers, amplifiers	Limited by size of array and by scan coverage ④	Large, depends on configuration-up to 4π steradians	Fails gracefully	Lightweight components are needed; phase coherence required between channels is limited by component characteristics	0.5 Kg ③ per element approximately	Yes
Adaptive Arrays	Gravity Unstabilized			Electronically controlled phase shifter and/or phase-locked loop			Fails gracefully			No

NOTES:

① Instantaneous bandwidth

② Weight is for power supplies and all other necessary components using Trans-Directive array in prototype form – based on existing components. Excluded are satellite structure, telemetry, solar cells and batteries.

③ Weight is for all components including power supplies. Components are in prototype form – based on existing components except for r-f amplifiers (100 mw at 4 Gc/element, 10 percent efficiency).

④ See formulas in Sections 5.2.2 and 5.2.3.

Table 1-6. Self-steerable arrays.

Of importance in the study and development recommended and implied above is the concurrent or even preceding development of rugged, small, lightweight components so that package size, weight, and power consumption can be minimized. In the area of new component developments, consideration and effort should be given to the following:

a) Lightweight, phase-coherent, i-f amplifiers.

b) Solid-state amplifiers with power outputs on the order of 100 mw at 4 Gc that would be greater than outputs presently available from tunnel diodes.

c) Lightweight and compact circulators, mixers, and up-converters which operate in the microwave frequency region.

d) Solid-state local oscillators.

Once a device is perfected, it should be space qualified as soon as possible and checked out for reliability. Each of these components plays a key role in the various techniques discussed, and consequently, their unavailability inhibits the development and even the consideration of many useful approaches to spacecraft antenna systems.

Two experimental configurations of the recommended self-steerable or self-phasing arrays are being developed as laboratory breadboards within the Hughes Aircraft Company Antenna Department. One is the Trans-Directive Array* described in detail in the New Technology Section (6) of this report and shown schematically in Figure 1-7, and the other is a retrodirective array such as is indicated by Figure 1-8. The breadboard of the Trans-Directive Array will utilize a Butler matrix to generate 16 high-gain, overlapping, independent beams. The antenna has two sets of beams superimposed on each other; one set operates at the up-link frequency and the other at the down-link frequency. A ground station wishing to utilize the system's up link transmits a band of information plus a low-power, c-w "pilot" signal. This pilot tone is received by the array on all the receiving beams. The system then selects the "best" beam, i.e., the receiving beam with the highest signal level, and connects to it the input of the communications equipment.

---

*Patent disclosure filed.

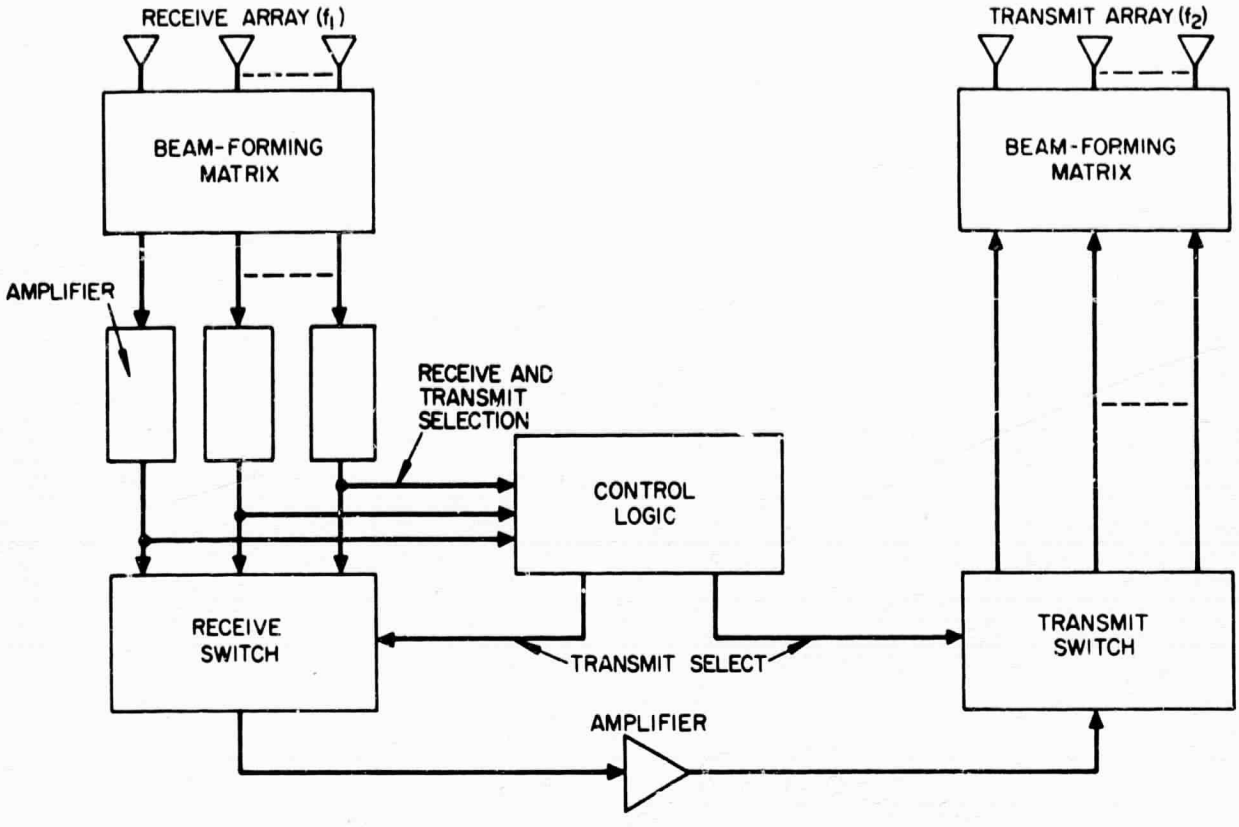

Figure 1-7. Basic theory of Trans-Directive Array.

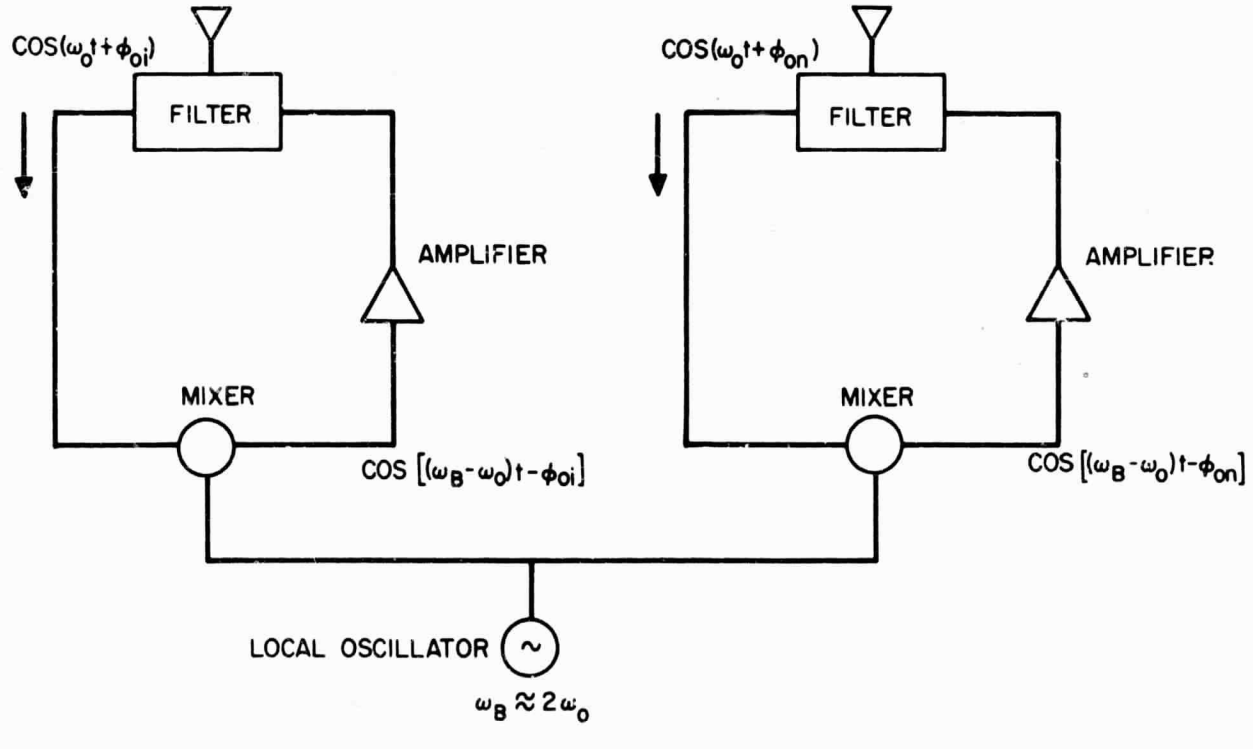

Figure 1-8. Basic theory of retrodirective array.

A second ground station, this one desiring to utilize the down link, also sends up a low-power c-w pilot signal which the system uses to select the "best" beam for transmitting. More sophisticated versions of this basic system would contain several electronically variable power dividers and use several of the adjacent overlapping beams simultaneously to form one high-gain beam which moves continuously and without transients to track the pilot signals.

The retrodirective array breadboard under development contains 16 antenna elements which receive a c-w pilot signal from the ground station desiring to use the down link. In this system, the relative phase of the pilot signal as received at the various antenna elements is used to appropriately phase the down-link information signal which is simultaneously being transmitted out of the same elements. This results in the transmitted signal being confined to a narrow high-gain antenna beam on the down link. The beam is continuously scanned by the system. The down link operation is applicable to the up-link as well, but the breadboard incorporates the retrodirective feature only on the down link and uses a nonscanning, broad beam for receiving the up-link information. Another aspect of the breadboard development will be the testing of mounting surfaces of many shapes, since the elements of the retrodirective array may be mounted on almost any surface.

2. SATELLITE COMMUNICATION SYSTEMS

The characteristics of the electronic beam forming and steering techniques to be used on communications satellites are dictated by the orbits and mission requirements of particular satellites. Five orbital cases are considered in this report:

1. Synchronous altitude (35, 790 Km), spin-stabilized satellite
2. Synchronous altitude (35, 790 Km), gravity-stabilized satellite
3. Six-thousand nautical mile orbit (11, 120 Km), spin-stabilized satellite
4. Six-thousand nautical mile orbit (11, 120 Km), gravity-stabilized satellite
5. Unstabilized satellite

The particular missions of interest are:

1. earth-satellite and satellite-earth
2. earth-satellite-satellite and satellite-spacecraft, -aircraft, or -earth

Based on the above missions, orbital and stabilization characteristics of these antenna techniques that can satisfy the scan requirements for the several cases will be presented and their relative merits will be discussed.

2.1 ORBITAL CHARACTERISTICS AND SCAN REQUIREMENTS

As is shown in Figure 2-1, the earth subtends an angle of approximately 17.4° at a satellite in a synchronous orbit (35, 790 Km altitude). For a satellite in an orbit of 6, 000 n. mi. (11, 120 Km altitude), the earth subtends approximately 43.0° at the satellite. Therefore, for

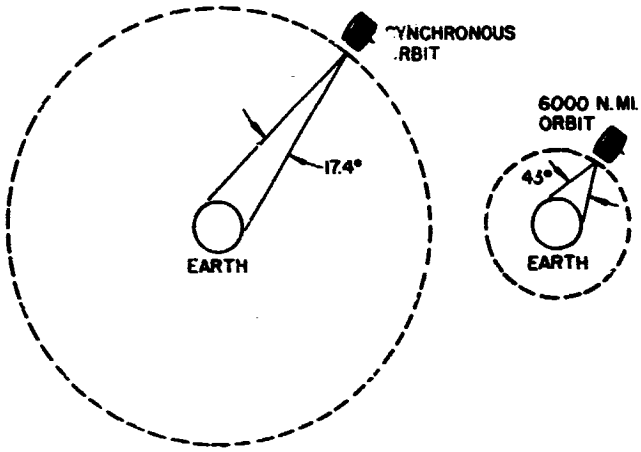

Figure 2-1. Angles subtended by satellites in different orbits.

the two-way link of mission 1, the beams of the satellite array must be positionable within these regions. Since stabilization conditions of the satellite will affect this region of coverage as viewed from the satellite, the scanning requirements were investigated in relation to a set of axes fixed on the satellite itself. Convenient choice of axes depends to some extent on the satellite shape and the type of stabilization used. Several cases were considered.

The first is a gravity-gradient stabilized satellite in which the satellite has one axis coincident with a line through the center of the earth. Slow oscillations or librations of the axis about this line do occur, however. If the satellite axis pointing earthward is selected as the z-axis, then in the absence of librations, the region of required beam pointing direction is determined by the cone which the earth subtends at the satellite. If the satellite axis undergoes librations which fall within a cone of half angle θ_L, then that angular variation must be added to the half angle of the cone which the earth subtends, θ_E. The total determines the region within which it must be possible to position the beam, as is shown in Figure 2-2. For the synchronous orbit $\theta_E = 8.75°$, while for the 11,120 Km orbit $\theta_E = 21.5°$. A typical value for θ_L for gravity-gradient stabilization is $\theta_L = 10°$.

For the spin-stabilized orbit in which the spin axis is normal to the plane of the orbit, it is convenient to take the θ reference axis as the spin axis. In this case the region of required beam pointing directions is as shown in Figure 2-3. The relation between θ_E and altitude is the same for this case as for the gravity-stabilized case. For the spin-stabilized satellite, values of θ_L of about 1° are realizable although 3° is considered a limiting value.

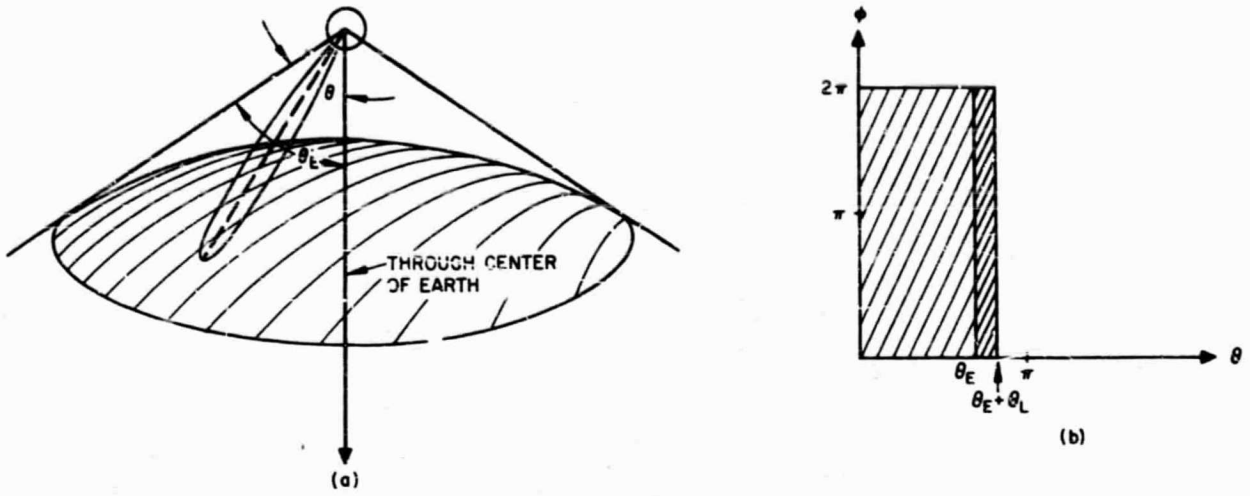

Figure 2-2. Region of required beam pointing directions for gravity-stabilized satellite.

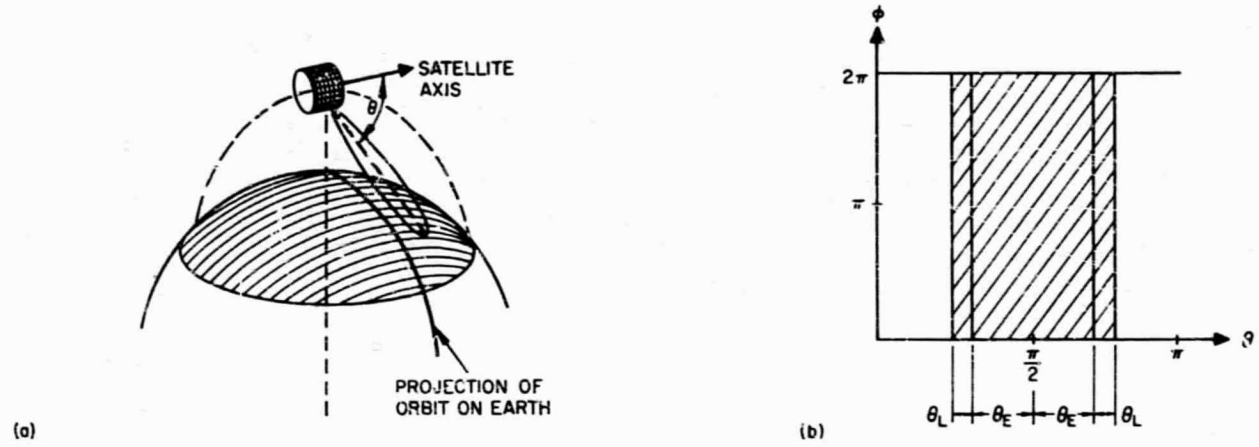

Figure 2-3. Region of required beam pointing directions for spin-stabilized satellite.

For the unstabilized satellite it must be possible to position the beam anywhere within the range $0 < \theta < \pi$ and $0 < \phi < 2\pi$.

For the three-way links of mission 2, the same coverage as that of the unstabilized satellite is required since the relative angular positions of two spacecraft may take on all possible values.

It should be pointed out that both mission 1 and mission 2 indicate that, when narrow beams are considered, simultaneous multiple beams are necessary for real-time communication channels between two stations using the satellite as a link. However, in applications in which the satellite may store a transmission and then relay it at a later time, single steerable beam antennas would suffice.

2.2 SCAN REQUIREMENTS AND BEAMWIDTH

The antenna scan requirements are not independent of the antenna beamwidth characteristics. If it is postulated that the signal directed to a prescribed point be within a certain fraction of the signal on the peak of the beam, then it is not necessary to scan the center of the beam to that point. For example, if an acceptable fraction were 3 db, then it would only be necessary to scan the beam center to within one-half a 3-db beamwidth of the extreme edge of the desired coverage region. For broad beams this relationship could result in a considerable reduction in scan requirements, but it has little effect on reducing scan requirements for narrow beams. Since the study here is quite general, the more stringent requirements of the narrow beam antennas were used, and the effects of beamwidth in reducing scan requirements were neglected unless otherwise specified. It was assumed that positioning the beam center anywhere in the required coverage region is required.

2.3 BEAM SCANNING TECHNIQUES

The scan requirements result directly from the missions themselves and not from any considerations of ease of implementation, mean times to failure of the various components which are used to implement the techniques, primary power requirements, complexity, weight, or cost. All these considerations do have significant bearing on the applicability of any one technique to a particular orbit-mission situation. Considerations of the components necessary for implementation of a particular system were included in this study. Of course, not all conceivable situations and systems could be given thorough consideration, and engineering judgment was used in the selection of those techniques that were investigated most fully.

A number of techniques exist which can be used to collimate a beam in a given direction in space. For reference, the techniques considered are listed:

1. reflector and feed systems
2. lens and feed systems

3. multiple-beam systems using beam-forming matrices or lenses
4. phased array techniques
5. self-phased array techniques
6. adaptive array techniques

One electronic technique, frequency scanning, does not require phase shifting devices and uses the inherently dispersive waveguide transmission lines as the scanning mechanism. The transmitter frequency is programmed to give the desired beam direction. The receiver is slaved to the operating frequency so that the beam direction is identical on receive. Usually a 10-percent r-f bandwidth is needed to realize a 1-percent communication channel bandwidth. Radar is a logical application for frequency scan since transmitter and receiver are located together. However, frequency scanning is unsuitable for satellite communications because of (a) the narrow r-f bandwidth available, (b) the need for a large r-f spectrum per useful transmission bandwidth, (c) the complexity of the resultant system, and (d) incompatibility with present and contemplated ground terminals. The technique is not considered further in this report.

BLANK PAGE

3. COMPONENTS FOR ELECTRONICALLY SCANNED ANTENNAS

Electronic scan is an antenna technique which permits a stationary array of radiators to rapidly steer a radiation pattern in free space. The technique has been used in radio-astronomy as an interferometer method and, more recently, in ground and shipbased radars. The concern in this report is the application of electronic scan to space vehicle communication. Here the implementation of techniques for electronic control is a challenging task, but several methods do show considerable promise.

In all electronic scan techniques the disposition of the radiation pattern in space is controlled by varying the uniform progressive phase shift between the elements in the aperture. The progressive phase shift is the sum of a phase factor which accounts for the external spacing between the elements and a phase factor which represents the common phase difference between the currents that drive adjacent elements. To electronically scan a radiation pattern, the relative phase of the driving currents is varied by some device such as ferrite phase shifters, semiconductor diodes, or switches.

3.1 FERRITE PHASE SHIFTERS

The ability to take advantage of the interaction of electromagnetic waves with statically oriented magnetization in ferrites has resulted in many useful microwave and millimeter-wave devices. Among these are phase shifters, isolators, gyrators, and circulators (Lax and Button, 1962). The phase shifter is one of these devices which is most useful in the construction of antenna arrays with electronically steerable beams. Two general configurations of ferrite phase shifters are available. One uses a transverse magnetizing field; the second uses a longitudinal magnetizing field. The former is reciprocal only for certain configurations

while the latter is intrinsically reciprocal, a property desirable in arrays to be used for both transmission and reception. Phase shifters that use longitudinal magnetization also produce greater phase shifts at lower levels of applied magnetic field than do those that use transverse magnetization. General characteristics of ferrite phase shifters that affect spacecraft scanning applications are discussed below, followed by descriptions of a longitudinal field ferrite phase shifter, a digital ferrite phase shifter, and several kinds of synchronous phase shifters.

3.1.1 General Characteristics

A number of electrical considerations are involved in any assessment of ferrite phase shifters for use in scanning arrays. The following is a list of some of the more important of these considerations.

a) Reciprocity

The longitudinal field phase shifter is reciprocal. The transverse field phase shifter is reciprocal only for certain ferrite locations in the waveguide.

b) Impedance Matching

Various techniques have been used to match into and out of the ferrite section. These include use of tapered ferrite ends (Reggia and Spencer, 1957), quarter-wave transformers (Reggia and Spencer, 1957), and step reductions in ferrite cross section (Clavin, 1960a). Well-matched devices show reduced losses and improved phase shift characteristics.

c) Frequency Dependence of Phase Shifts

For use in arrays whose beam pointing direction is to be independent of frequency, it is necessary that the differential phase shifts introduced by the phase shifters be proportional to frequency. For phase shifters whose ferrite cross-sectional dimensions lie between two "critical" values, this condition is approximately satisfied but not much information is available.

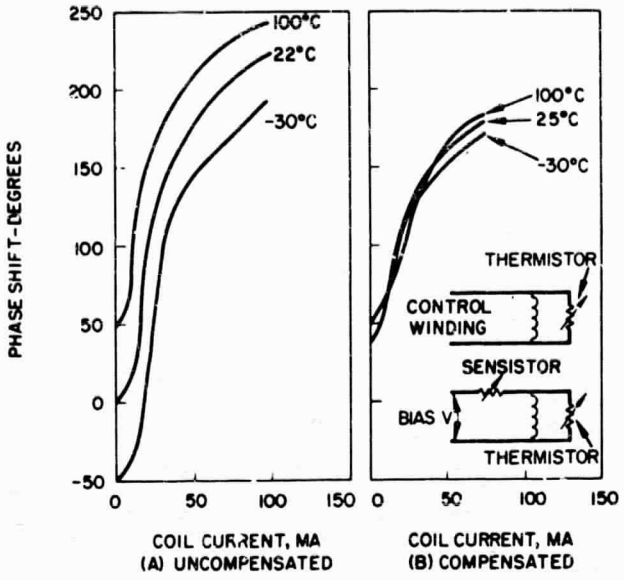

Figure 3-1. Effect of temperature compensation in a ferrite phase shifter (Clavin, 1960b).

d) Temperature Sensitivity

The ferrite material itself is inherently temperature sensitive so that the phase shifts are also temperature sensitive. In applications in which all phase shifters are at the same temperature, only the change in differential phase shift is important. Otherwise change in the absolute phase must be minimized. As an example of the phase change that can occur, it has been observed that a change of one degree Centigrade in a rod 0.3 inch in diameter and 5.5 inches long caused a 4.5 degree phase shift at X-band (Goodwin and Nussmeier, 1959). Clavin (1960b) reported a scheme which uses temperature compensation in a secondary coil as indicated in Figure 3-1. This scheme greatly reduces the effects of temperature changes on the phase shifts.

e) Shorted Turn Effects

The presence of the conducting walls of the waveguide provide a path for induced currents when the applied magnetic field is changing. If fast changes in phase are required, these induced currents can limit the achievable spe ' This effect can be reduced by making the waveguide walls thin to increase their resistance to the induced currents or by interrupting the current path by slotting the waveguide. The latter technique requires choking arrangements to prevent r-f leakage.

f) Hysteresis Effects

Hysteresis effects are encountered in both transverse and longitudinal field ferrite phase shifters. The longitudinal field phase shifter operates with the ferrite below saturation and suffers from hysteresis within the ferrite itself. The transverse field phase shifter operates above ferrite saturation but requires external iron magnetic circuits

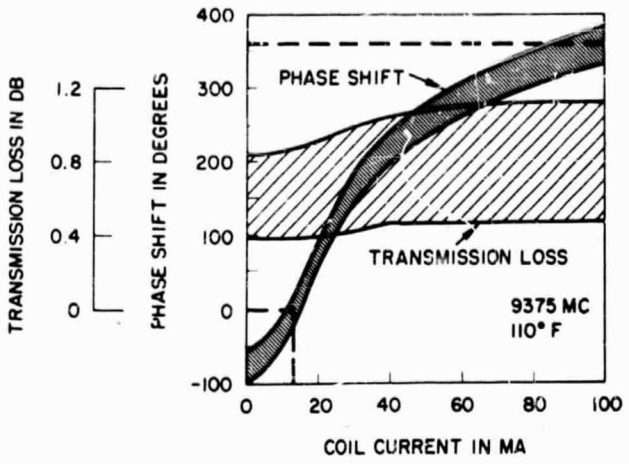

Figure 3-2. Characteristics of 32 phase shifters (ESSA, 1959).

which exhibit hysteresis effects. To obtain repeatability of phase shifts with coil current, the magnetic circuits must be driven into saturation between settings and a saturation pulse time plus a time to switch out of saturation to the desired phase setting are required. More driving power is also needed.

In addition to electrical considerations, weight and material inconsistencies pose problems. The reproducibility of characteristics in ferrite devices is not very good due to variations in the material itself. Figure 3-2 compares the phase shift and loss characteristics of 32 X-band longitudinal phase shifters constructed to identical specifications from three batches of the same material (ESSA, 1959). The phase shift variations of ±30 degrees and insertion loss variations of ±0.2 db among these 32 phase shifters were primarily caused by differences in the ferrite material of the three batches.

Weight can also be a great problem with ferrite phase shifters. Spaceborne arrays with large numbers of such phase shifters would be unacceptably heavy compared with other possible phase shifting schemes. But for systems that require only a relatively few phase shifters, however, such as the ATS satellite, the devices have promise.

3.1.2 Longitudinal Field Phase Shifter

The longitudinal field ferrite phase shifter consists of a ferrite rod or slab magnetized by the magnetic field of an axial solenoid (Button and Lax, 1962). An example is shown in Figure 3-3. The principle of operation can be explained from perturbation theory in which the change in one of the diagonal components of the effective permeability tensor is treated as a perturbation on the problem of a centered longitudinal dielectric slab of permeability μ_o. The large phase shifts result from a

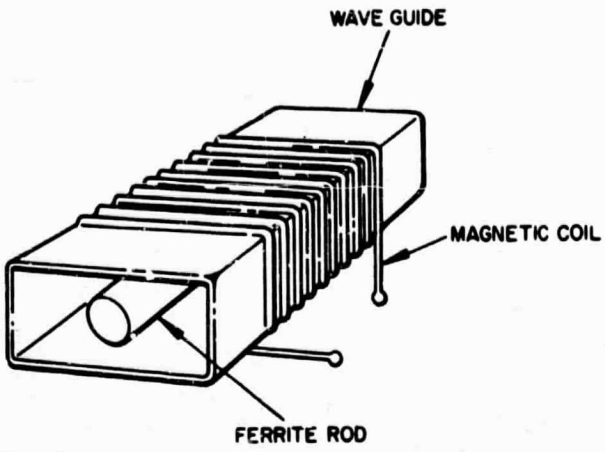

Figure 3-3. Longitudinal field ferrite phase shifter (Shnitkin, 1961).

relatively small change in the effective permeability of a slab with a high dielectric constant. Typical characteristics of both waveguide and coaxial longitudinal field phase shifters are presented at several different frequencies in Table 3-1. Switching times and switching powers are interrelated insofar as faster switching times can be obtained with greater switching powers.

3.1.3 Digital Ferrite Phase Shifters

Recently, a digital type of ferrite phase shifter has been developed which uses a transversely magnetized ferrite tube along the axis of a waveguide or transmission line. A waveguide version is illustrated in Figure 3-4. The ferrite is a rectangular hysteresis loop and is magnetized in either one of two saturated conditions by a pulse of current in a wire along its axis. Because of the rectangular hysteresis loop, no holding power is necessary to maintain the ferrite in either state. These phase shifters are non-reciprocal because of the static magnetic field configuration. They can be made reciprocal merely by reversing the magnetization between transmit and receive. Table 3-2 lists some typical characteristics of available digital ferrite phase shifters.

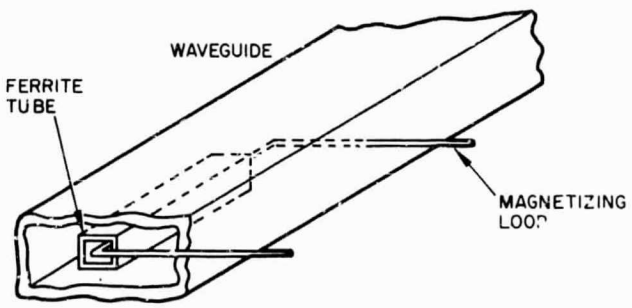

Figure 3-4. Waveguide digital ferrite phase shifter.

3.1.4 Synchronous Ferrite Phase Shifters

The synchronous ferrite phase shifter can be made in several different forms. One type operates in a manner similar to the well-known Fox phase shifter (Fox, 1947). To understand the

Characteristic	Frequency		
	C	X	K_u
Phase shift, degrees	360	360	360
Insertion loss, db	1.0	1.0	1.0
Peak power (max), KW	20	4	5
Temperature sensitivity, deg/°F	6.0	4.5	3.0
Frequency variation, deg/Mc	0.1	0.1	0.1
Drive, ampereturns	250	150	150
Switching power, watts	4	2	1.5
Switching time, microseconds	100	100	100
Length, inches	12	8	5
Weight, pounds	3	1.5	1.3

a) Waveguide Devices

Characteristic	Frequency		
	L	S	C
Phase shift, degrees	360	360	360
Insertion loss, db	2	1	1
Peak power, KW	2	5	10
Temperature sensitivity, deg/°F	3	3	4
Frequency variation, deg/Mc	0.5	0.3	0.1
Drive (approximate), ampereturns	1000	500	200
Switching power, watts	20	10	4
Switching time, microseconds	100	100	100
Length, inches	20	10	8
Weight, pounds	6	3	2-1/2

b) TEM Transmission Line Devices

Table 3-1. Typical Characteristics of Longitudinal Ferrite Phase Shifters at Various Frequencies

Characteristic	Frequency	
	C	X
Phase shift/insertion loss, deg/db	360	350
Phase versus frequency	same as equivalent line length ±5°	±2°
Temperature sensitivity, deg/°C	2	<1
Bandwidth, percent	10	10
Power handling (VSWR < 1.5:1)		
peak	10 KW	30 KW
average	--	50 W
Switching currents, amps	10-100	10-100
Switching times, microseconds	2-10	2-10
Switching energy, microjoules	200-2000	5000
Dimensions	standard waveguide cross section or less	
Weight	essentially that of waveguide	

Table 3-2. Waveguide Digital Ferrite Phase Shifter Characteristics at Various Frequencies.

operation of the synchronous phase shifter, the Fox phase shifter is described first.

Fox Phase Shifter. The Fox phase shifter essentially consists of three differential phase shift sections of waveguide assembled in tandem. The first of these converts incident linearly polarized waves into circularly polarized waves. The second serves to rotate the instantaneous orientation of the circularly polarized waves to shift the phase of the output. The third section then reconverts the circularly polarized waves to linearly polarized waves. The required 90°, 180°, and 90° differential phase shifts, respectively, of the three sections are produced by dielectric birefringence. By judiciously squeezing circular waveguide to have an elliptical cross section or by inserting fins, septa, or rods into the circular waveguide, a sufficiently different phase velocity is achieved

for waves whose electric fields are aligned in two perpendicular longitudinal planes to provide the required differential phase shift.

Synchronous Ferrite Phase Shifter. In the synchronous ferrite phase shifter the center 180° differential phase shifter (or half-wave plate, as it is sometimes referred to) is rotated electrically rather than mechanically. The movement is accomplished by the introduction of magnetically induced birefringence by ferrite loading of the half-wave section and by the application of a synchronously rotating transverse magnetic field from an external motor stator. Within the ferrite loaded half-wave plate, the plane parallel to the electric field of waves traveling with maximum phase velocity and the perpendicular plane (parallel to the electric field of waves traveling with minimum phase velocity) are both rotated in the same sense and by the same amount as is the transverse magnetic field of the motor windings. This electrical rotation of the high and low velocity planes produces the identical phase shift as would the mechanical rotation of the Fox phase shifter.

The operation of the ferrite loaded half-wave plate can be explained by considering the interaction between an electromagnetic wave and the electron spins of the ferrite which exhibit a gyroscopic like behavior when a static magnetic field is applied. When the polarization of the magnetic field in the electromagnetic wave is circular in the plane perpendicular to the static magnetic field, there will be maximum interaction. There is no interaction when the r-f magnetic field polarization is linear and parallel to the static magnetic field. The permeability of the ferrite to the electromagnetic wave is greater or less than μ_o when the sense of circular polarization and the sense of precession of the electron gyroscope are the same or opposite, respectively. At point A, slightly inside the wall of the dominant mode circular waveguide, shown in Figure 3-5, the r-f magnetic field is circularly polarized, rotating in a time sequence 1-2-3-4 as indicated by the vectors (Brooks, 1963). At point B, slightly inside the guide wall, the r-f magnetic field is linearly polarized. For points along a circular arc from A to B, the r-f magnetic field is first circularly polarized and then progressively more elliptically polarized. Further along the arc, 180° from A, the polarization is circular but of

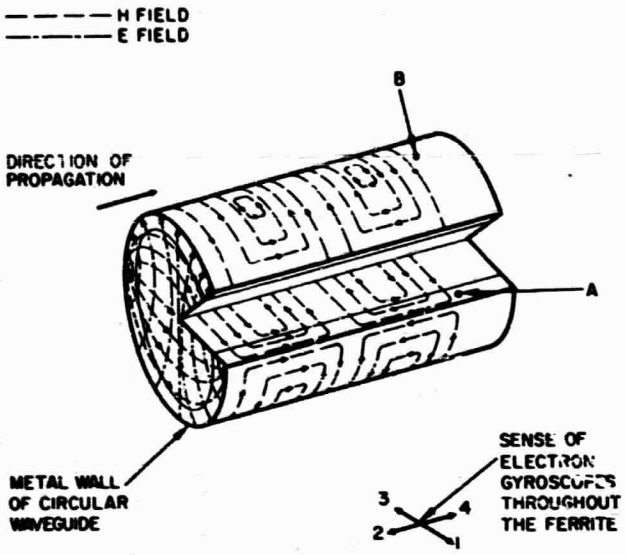

Figure 3-5. Circular waveguide r-f field configuration (Brooks, 1963).

the opposite sense of what it was at A. The polarization again is linear 180° from B.

A thin-walled ferrite ring is now assumed to be inserted inside the metal waveguide such that it is in contact with the metal wall as shown in Figure 3-6. By applying the static transverse magnetic field, the ferrite will present a permeability greater than μ to the r-f wave of polarization e_x and a permeability less than μ to the r-f wave of polarization e_y. This difference constitutes magnetically induced birefringence in that r-f waves of polarization e_x will not propagate through the ferrite loaded waveguide section as fast as r-f waves of polarization e_y. When the length of the section is chosen to allow 180° differential phase shift between the two orthogonal waves (or modes) and the transverse magnetic field is rotated, a rotating half-wave plate is achieved which, when combined with two circular polarizers at the input and output of the half-wave plate, will result in an electrical device similar to the mechanical Fox phase shifter that is capable of continuous unlimited phase shift.

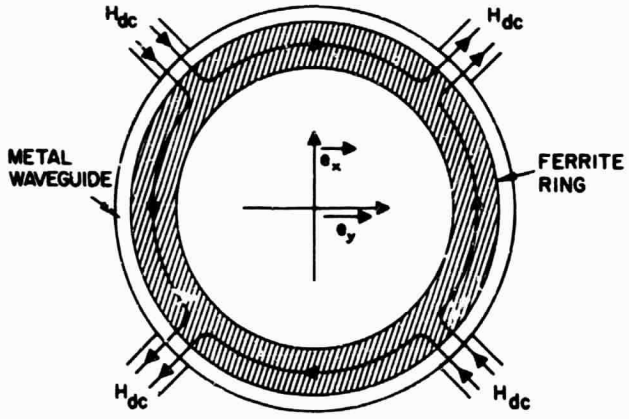

Figure 3-6. Control magnetic field configuration (Brooks, 1963).

Modified Fox Phase Shifter. In a variation of the basic version of the synchronous ferrite phase shifter, one quarter-wave plate is eliminated and two orthogonal coupling probes are incorporated at the output. The device is being used in the circular phase array antenna for the Applications

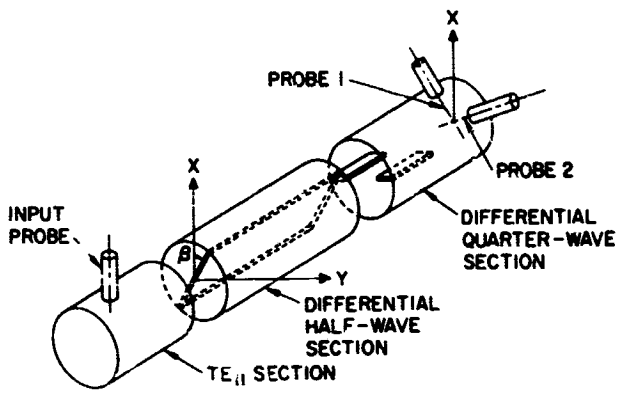

Figure 3-7. Modified Fox phase shifter (Erhardt et al., 1963).

Technology Satellite (Erhardt et al., 1963). (See Section 4.1 for a description of the antenna system.) Eight of these devices are utilized in the array, each with a total of 0.9 db insertion loss and cycled at 100 cps.

The operation of the device can be described with the aid of Figure 3-7. The input probe excites the TE_{11} mode along the X-axis in the input section. In the differential half-wave section the component of the electric field along the plate is delayed by 180° over the component normal to the plate. This results in a rotation of the field structure through an angle 2β so that A_x and A_y, the x and y components of the fields at the output of the half-wave section, are

$$A_x = A \cos 2\beta \tag{3-1a}$$

$$A_y = A \sin 2\beta \tag{3-1b}$$

Next, the quarter-wave plates in the third section delay the y polarized field by 90° so that the voltages induced in probe 1 and probe 2 are, respectively,

$$V_1 = \frac{A}{2} \cos 2\beta + j\frac{A}{2} \sin 2\beta = \frac{A}{2} e^{j2\beta} \tag{3-2a}$$

$$V_2 = \frac{-jA}{2} \sin 2 + \frac{A}{2} \cos 2\beta = \frac{A}{2} e^{-j2\beta} \tag{3-2b}$$

It is evident that the phase shifts are in opposite directions. One voltage may be fed to one antenna element and the other to an element diametrically opposite it. The phase shift is twice the angle of plate rotation. In the electronic version of the device, the differential half-wave plate is

replaced by a cylindrical section of transversely magnetized ferrite. The magnetization is obtained from the stator of a 4-pole, 2-phase induction motor. When two sinusoidally varying voltages in phase quadrature are applied to the stator windings, the field magnetizing the ferrite rotates through one-half revolution in every cycle of applied voltage. This results in a total phase shift of 360° per cycle and therefore a continuously increasing phase shift is available. For this application, however, continuously variable phase shifts are not required. As discussed in Section 4.1.1, the required phase shifts are given by Equation (4-8) and vary cosinusoidally with time. For a given phase shift, ψ, the required voltages for the two phases are

$$V_1 = V_o \cos \psi \tag{3-3a}$$

$$V_2 = V_o \sin \psi \tag{3-3b}$$

In view of the form of ψ_n given by (4-8) the required driving voltages are of the form

$$V_{1_n} = V_o \cos\left[kR \cos\left(\omega t + n\frac{2\pi}{N} + \zeta\right)\right] \tag{3-4a}$$

$$V_{2_n} = -V_o \sin\left[kR \cos\left(\omega t + n\frac{2\pi}{N} + \zeta\right)\right] \tag{3-4b}$$

where ζ is determined by the beam pointing direction at $t = 0$. These voltages with the proper value of ω and ζ must be supplied by the control electronics of the array. The actual array and the control electronics are briefly described in Sections 4.1.2 through 4.1.4.

3.1.5 Miniature Ferrite Phase Shifters

Recent investigators (Jones and Reggia, 1964) describe some interesting modifications of ferrite phase shifters. Miniaturization is achieved by waveguide folding rather than by any new principles. In effect, a phase shifter is produced with the waveguide ports close

together. Some economy of magnetization and of field coil size result from the folding process. The miniature phase shifter offers interesting possibilities in an electronically scanned microwave antenna. While it is too early to evaluate this device in an actual design, it merits serious consideration.

3.2 SEMICONDUCTOR PHASE SHIFTERS

Phase shifters that use diodes to control the driving current phasing for slot radiators can be designed to operate in a continuously variable or a stepped fashion. Those components that provide continuous phase shift utilize varactor diodes while those that produce discrete phase shifts employ PIN diodes. Two types of the continuous phase shifter components are in current use. One is basically a transmission structure which uses the varactor diodes periodically located along a transmission line. The other is inherently reflective in nature and is converted to a transmission component by the employment of 3-db couplers or circulators and reflective terminations. This latter device uses varactor diodes for continuous phase shift. Digital phase control can be obtained with the reflective device just described with the substitution of PIN diodes as the control element. This effectively switches different line lengths in and out of the system thereby changing the phase shift through it. In all phase shifters the diode may be used either in shunt or in series with the line; the choice depends on the phase shift required and the desire to minimize the insertion loss of the device. Table 3-3 presents a comparison of the continuous and stepped types of semiconductor phase shifters, and detailed descriptions are given in the subsequent paragraphs.

3.2.1 Microwave Diodes

At microwave frequencies the nonlinear behavior of diodes can be described in terms of linear lumped parameters in an equivalent circuit. These representations accurately predict the performance of the diode in many applications and for a limited range in frequency and applied bias. The two types of diodes which are used in phase shifting devices are the varactor diode and the PIN diode.

Characteristics	Step Phase Shifter	Continuously Variable Phase Shifter
Phase	Incremental, step values unlimited -- dependent only on line lengths and insertion loss limits (as much as 360° steps)	Continuous, range limited by capacitance change and insertion loss limits (up to 220°/unit)
Insertion Loss	Least dependent on diode -- 0.4 db at L-band	Dependent on diode -- 1.5 db at L-band
Peak Power (Voltage Limited)	Fewer r-f voltage or current swing restrictions -- 50 kw	R-f voltage swing restricted by capacitance change -- 100 w or less
Average Power	100 w at L-band	25 w at L-band
Phase Power (Level Sensitivity)	None (within power rating)	Dependent on r-f voltage swing compared with breakdown of varactors
Phase Stability		
a. Temperature	Independent up to about 150°C	Dependent on capacitance change -- 0.1°/°C
b. Control	Not critical as long as forward or reverse bias is maintained; no hysteresis effects	No hysteresis effects Dependent on capacitance change and on bias voltage -- 0.4°/percent ΔV
Speed	Moderate, less than 100 ns	Highest, nanosecond range
Control Power	Forward state: few 100 mw/step Reverse state: drive 10 - 100 pf/step	Reverse bias only. Less than 1 mw. Drive 10 - 100 pf

Table 3-3. Characteristics of Step and Continuously Variable Phase Shifters (with Present Diodes Operating in the Reflective Mode)

Varactor Diode. The varactor diode is a nonlinear crystal which changes capacitance with applied bias voltage. A general representation for a variable capacitance diode is shown in Figure 3-8. The diode parameters, L, C_j, C', R_s, R_b, and ω, are defined:

L = whisker and lead inductance

C_j = junction (or barrier) capacitance

C' = parasitic and holder capacitances

R_s = spreading resistance

R_b = nonlinear barrier resistance

$\omega = 2\pi f$ where f = frequency

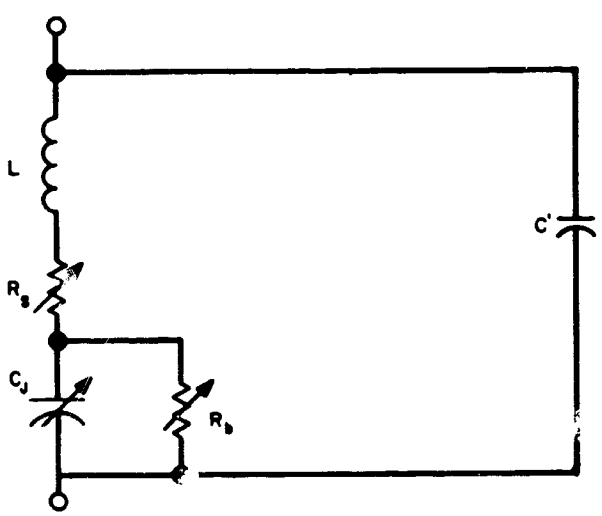

Figure 3-8. General equivalent circuit representation of variable capacitance diode.

Since the shunt capacitance C' and series inductance L can be assumed to be tuned out by the diode holding mechanism, the circuit of the microwave diode can be simplified further; also, the value of R_b is much larger than the junction reactance $X_c = (1/\omega C_j)$ at the high frequencies used here so that it too can be ignored. The variation in capacitance with the applied bias voltage V across the diodes is given by the approximate relation (Houlding, 1960):

$$\left(\frac{1}{C_j}\right)^n = K(\phi - V) \qquad (3\text{-}5)$$

where K and ϕ are constants, and n is around 2 for a step-junction and around 3 for a diffused junction. From this relation it can be seen that the capacitive reactance X_c approaches zero as the forward bias voltage V approaches ϕ. A diode which is operated over its bias range can be represented by the equivalent circuit of Figure 3-9; the representations for the extreme forward and reverse bias conditions (that is, for forward

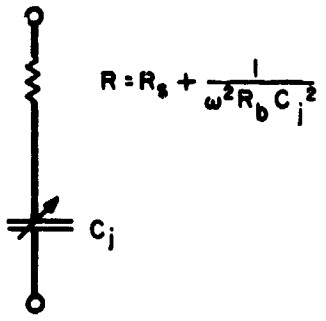

Figure 3-9. Simplified equivalent circuit of a continuously operated variable capacitance diode.

and reverse breakdown voltages) and the corresponding current flow can be drawn as in Figures 3-10ab. An indication of the electrical behavior of a typical diode can be obtained from Figure 3-11, in which the junction capacitance C_j and the junction current I are plotted as a function of voltage.

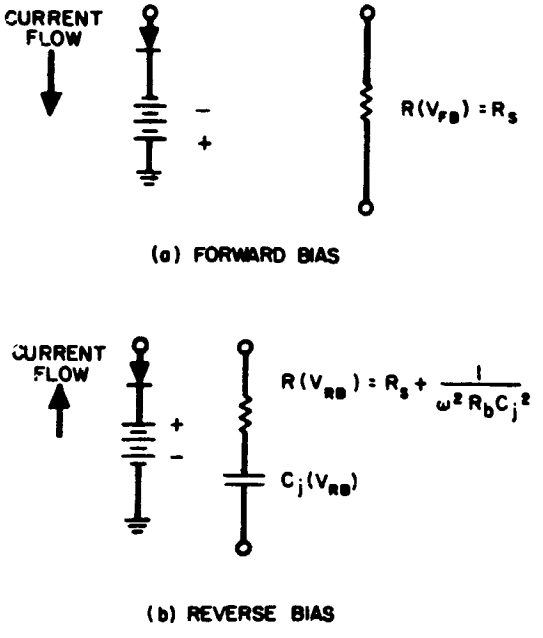

Figure 3-10. Equivalent circuits for extreme bias conditions.

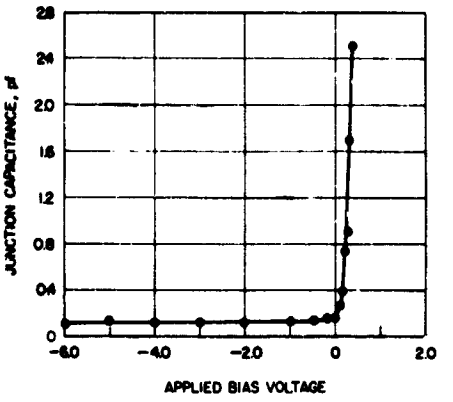

a) Diode junction capacitance versus voltage

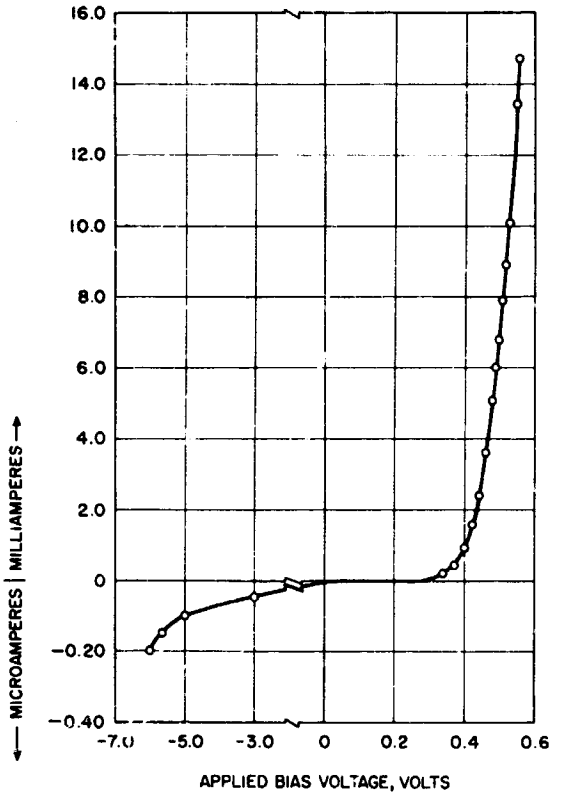

b) Diode current versus voltage

Figure 3-11. Junction capacitance and current as a function of applied bias voltage.

A quality rating or figure of merit for a varactor diode, stated by Houlding (1960), is given by the formula

$$f_c = \frac{1}{2\pi R C_{jmin}} \tag{3-6}$$

where f_c is called the cutoff frequency; the equivalent series resistance, R, and the minimum junction capacitance, C_{jmin}, are measured at reverse breakdown. An equivalent figure of merit is the Q of the diode which can be expressed as

$$Q = \frac{f_c}{f} \tag{3-7}$$

where f is the frequency at which R and C_{jmin} are measured. These parameters give a convenient, useful, and accurate description of the diode, but the methods by which they are measured are not sufficiently standardized to make possible direct comparisons between the products of various manufacturers.

A high Q can be achieved if the product RC_j is minimized. To achieve maximum capacitance change in the waveguide, C_j must also be minimized. But because of the physical geometry, a compromise must be made between the values of R and C_j. The junction capacitance is directly proportional to the area of the junction, while R varies approximately inversely with the junction area for a mesa (distributed) junction diode and inversely as the circumference of the area for a point contact diode.

Varactor diodes are especially attractive for high frequency use because of their small dimensions, fast response, and low noise. Since the diodes are physically small, they can serve as variable reactance elements in shunt or in series in a waveguide transmission line and still be matched to the waveguide. The essential purpose of using varactor diodes, then, in microwave phase shifters, is to exploit the very large range of reactance available. Varactors have been fabricated which require from several volts to as high as several hundred volts of driving voltage. In pulse operation the latter types are capable of handling several amperes of current.

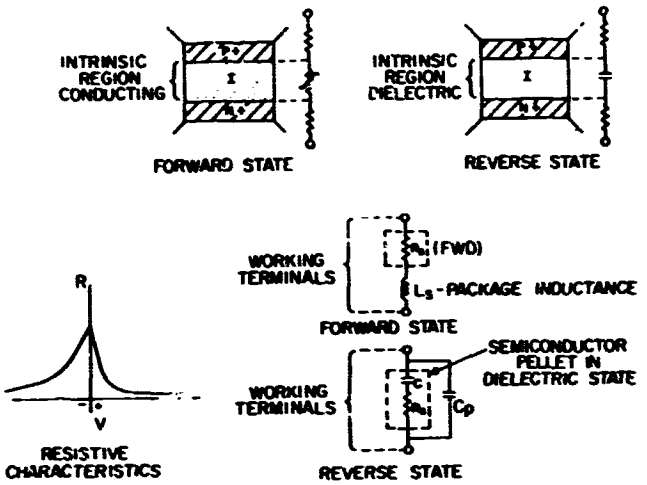

Figure 3-12. Operation and equivalent circuit of PIN diode (Mortenson, 1964).

PIN Diodes. The PIN diode behaves as a variable resistance element with applied bias (Mortenson, 1964). The operation and equivalent circuit for this crystal is shown in Figure 3-12. As shown, the PIN diode has a sandwich structure with a sizable intrinsic region. In reverse bias the structure behaves as a series RC circuit. The capacitance is determined by the geometry of the resistivity of the P and N regions. For forward bias the I region behaves like a variable resistance, while the P and N regions have essentially constant resistance values. The values of resistance vary from several thousand ohms at zero bias to less than one ohm with a bias current of milliamperes. The crystal can be operated as a variable resistance device in forward bias with the current determining the value of resistance or as a dual-state, switching device with the forward current and reverse bias voltage establishing the proper diode impedance values.

PIN diodes have been constructed to operate with breakdown voltages varying from a few hundred volts up to many kilovolts and with currents on the order of hundreds of amperes under pulse conditions.

3.2.2 Continuously Variable Phase Shifters

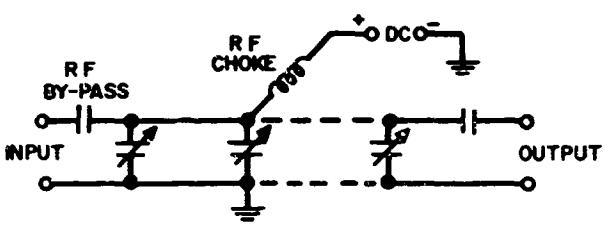

Figure 3-13. Delay line semiconductor phase shifter (Shnitkin, 1961).

Transmission-Type Phase Shifter. A configuration which will result in a continuous phase shift in a microwave transmission line is a tandem arrangement of varactor diodes in shunt in a waveguide as shown in Figure 3-13. Here each diode shifts the phase of the transmitted signal no more than 45 degrees

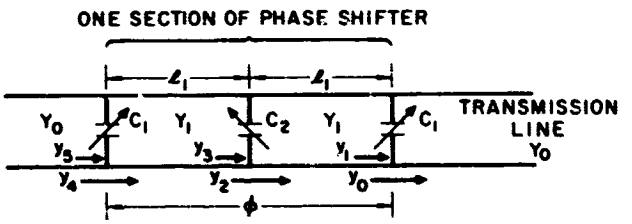

Figure 3-14. Equivalent circuit of capacitance-controlled phase shifter (Dawirs and Swarner, 1962).

and thus requires the employment of at least eight elements to obtain a total phase shift of 360 degrees. This design exhibits an insertion loss of several db since the loss of each diode is 0.3 db or more. In addition it causes a change in the characteristic impedance of the waveguide transmission line and thus introduces an impedance mismatch.

A series device employing varactor diodes has been devised by H. N. Dawirs and W. G. Swarner (1962); this design minimizes the number of diodes needed for a given phase shift and a tolerable mismatch. An equivalent circuit of a prototype section of the device is shown in Figure 3-14. In the figure, C_1 and C_2 represent variable capacitance diodes shunted across a line whose characteristic admittance is Y_c. The two capacitors, C_1, at the end of a section are used to vary the phase shift of the section, and the capacitor in the middle of the section, C_2, is used to adjust the characteristic admittance Y_c to be equal to the characteristic admittance of the terminating lines Y_o. The phase shift $\Delta\phi$ as a function of the capacity variation is approximated by the relation

$$\Delta\phi \simeq \frac{2\pi f}{Y_c}\Delta C_1 \qquad (3\text{-}8)$$

where

f = frequency in megacycles

Y_c = characteristic admittance of the prototype phase shifter in ohms

ΔC_1 = change in control capacitance C_1 in picofarads

The range of phase variation is ±45 degrees for Equation (3-8). As the phase is changed, the characteristic admittance Y_c of the prototype should be kept equal to the terminating admittance Y_o to minimize mismatches and spurious phase shifts. The adjustment is accomplished by

control of the variable C_2. From these considerations, then, the following two expressions can be derived for determining the circuit parameters Y_1 and ℓ_1. (With reference to Figure 3-14, Y_1 is the characteristic admittance of the prototype section without the diodes, and ℓ_1 is the length of transmission line section separating C_1 and C_2.)

$$Y_1 = \sqrt{\frac{n_2}{n_1}\frac{Y_c^2}{2} - (2\pi f C_1'')^2} \tag{3-9}$$

$$\tan\frac{2\pi\ell_1}{\lambda} = \sqrt{\frac{n_2}{n_1}\left(\frac{Y_c}{2\pi f C_1''}\right)^2 - 1} \tag{3-10}$$

In Equations (3-9) and (3-10), n_1 is the number of diodes in shunt whose total capacitance adds up to C_1, and n_2 is the number of diodes in shunt with a fixed capacitance C_o which is added to minimize the number of diodes required.

$$C_1 = n_1(C' + C'') \tag{3-11}$$

and

$$C_2 = C_o + n_2(C' + C'') \tag{3-12}$$

where C'' is a fixed midrange diode capacitance and C' is the variable diode capacitance. Hence, the other quantity C_1'' is defined as $C_1'' = n_1C''$, and λ is the wavelength in the transmission line.

To obtain an optimum design, intermediate matching sections are introduced at the ends of the phase shifter. If, for example, quarter-wave transformers are used to match the characteristic impedance ($Z_c = 1/Y_c$) to the terminating impedance, ($Z_o = 1/Y_o$), increased values of Z_o can be used and the sensitivity of phase shift to variation in capacitance can be increased [see Equation (3-8)]. In addition, examination of the design relationships show that fewer diodes are required for a given

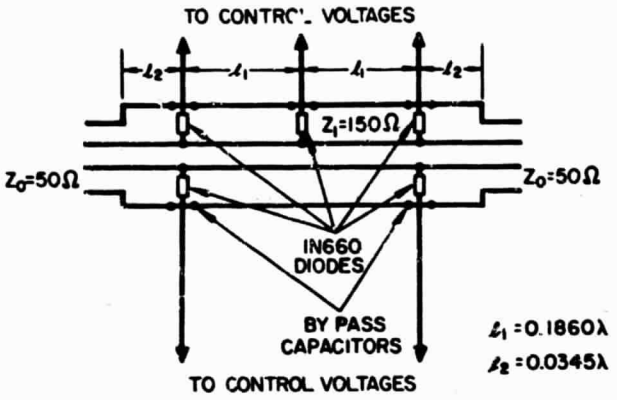

Figure 3-15. Schematic of experimental voltage-controlled phase shifter (Dawirs and Swarner, 1962).

phase shift. Using these relationships, Dawirs and Swarner give the complete design procedure and theory for building a diode phase shifter so that a prescribed phase shift can be achieved with a minimum number of diodes and relative ease of construction.

Figure 3-15 shows the schematic of an experimental model of a diode phase shifter which was built with end sections designed to be used in a 50-ohm circuit at 300 megacycles. This model, as shown in the schematic, employs only 5 diodes (type 1N660) but is capable of providing 100 degrees of phase shift. The performance of this model is summarized in Figure 3-16 which shows that, for attenuation restricted to 1 db or less, the phase shift range is limited to 50 degrees while the VSWR over this range remains less than 1.03. Another feature of this delay line configuration is that broadband response in terms of good impedance match can be computed. If there is a ±10 percent variation in frequency, for example, then the input VSWR should be less than about 1.1.

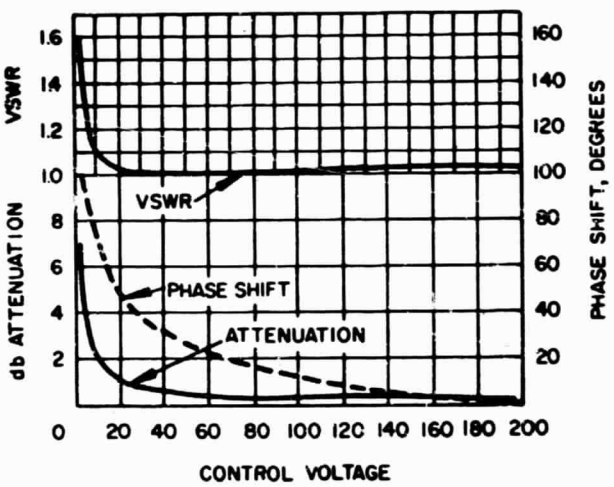

Figure 3-16. Characteristics of voltage-controlled phase shifter (Dawirs and Swarner, 1962).

Reflection-Type Phase Shifter. The reflection mode of the continuously variable phase shifter uses a transmission line terminated in a pure reactance; it operates on the principle that all energy incident upon the termination will be reflected, and the phase shift of

the reflected wave will be a function of the change in magnitude of the reactance. By using hybrid circuits with two ports of the four ports terminated with ideal (lossless) varactor diodes having identical characteristics, the two reflected waves can be completely separated from the two incident waves and combined in phase in the output port. When the bias voltage on the diodes is changed, the phase shift in the output wave will equal the phase shift produced in either reflected wave, and the complete unit will still be well matched. Such a device would also be highly efficient and capable of providing close to 180° of phase shift in a continuous fashion. Figure 3-17 shows two of the hybrid configurations which have been used in practice. For some applications, a three-port circulator with one port terminated in one diode may be used similarly, as shown in Figure 3-18.

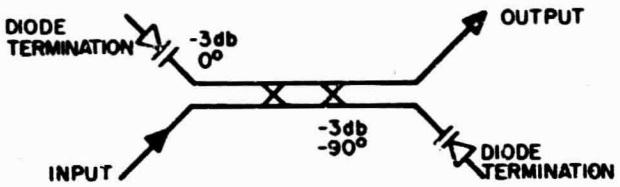

a) With a 3-db coupler (Hardin et al., 1960)

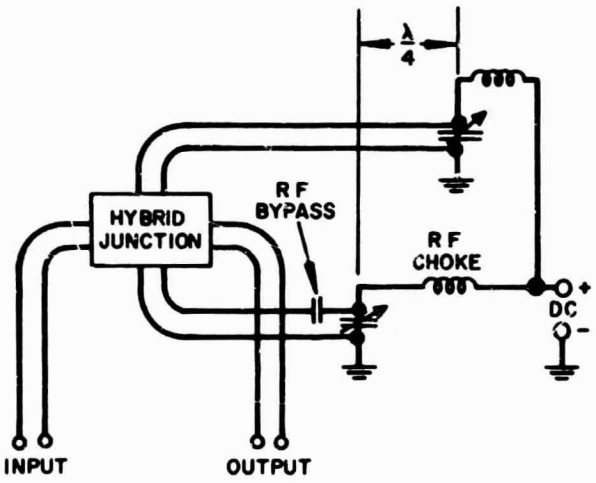

b) With a magic tee hybrid coupler (Shnitkin, 1961)

Figure 3-17. Variable capacitance diode phase shifter configurations.

To realize complete control of 180 degrees is quite difficult because varactor diodes can only approximate pure, voltage-variable reactances; in fact, because the diode resistance and capacitance characteristics are practically independent of frequency, the range of phase control diminishes steadily as the frequency is raised. The problem of producing a large amount of phase control at the high frequencies might, therefore, be recognized as a problem of requiring high Q diodes at these frequencies. To fully appreciate the meaning of this dependence of phase control on the frequency of operation of a particular diode, the following simplified example is given. It is assumed that the diode is shunted across the line and positioned

a quarter-guide wavelength ($\lambda_g/4$) from the short circuit termination and that the case capacitance of the diode is tuned out. In terms of the normalized equivalent circuit parameters, $x_c = (X_{C_j})/Z_c$ and $r_s = R_s/Z_c$, where Z_c = characteristic waveguide impedance and the maximum Q value of the diode is $Q(V_{RB}) = \frac{f_c(V_{RB})}{f}$, the phase of the reflected wave is given by

$$\text{Phase} = \Phi = \text{Arc tan}\left[\frac{2r_s Q \frac{C_{min}}{C}}{\left(1 + Q^2 \frac{C_{min}^2}{C^2}\right) r_s^2 - 1}\right] \qquad (3\text{-}13)$$

In Figure 3-19, Φ is plotted as a function of C for Q = 132 at 1 Gc and 13.2 at 10 Gc; r_s is taken to be a constant 0.0125 = R_s/r_c = 6 ohms/480 ohms (a valid assumption provided the voltage bias does not exceed forward breakdown). It can be noted that the product $r_s Q$ is essentially independent of r_s so that the curves are insensitive to large changes in r_s if $r_s^2 \ll 1$.

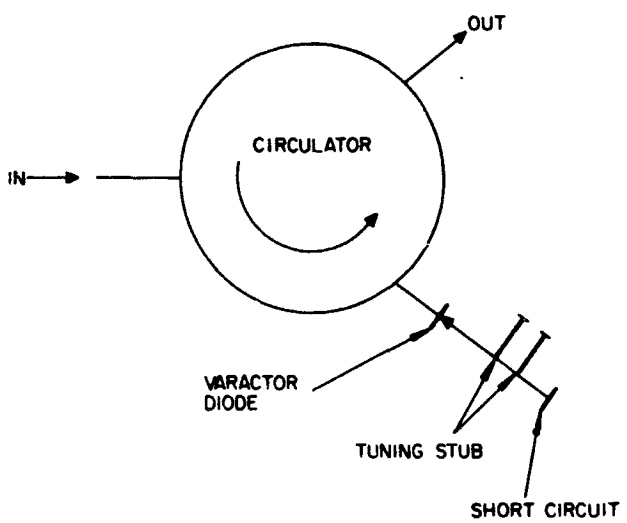

Figure 3-18. Reflection phase shifter with 3-port circulator.

An actual diode, of course, has a limited range of capacity variation, which is about 0.2 to 9.0 pf. The diode would, therefore, provide a total phase shift of 114 degrees at 1 Gc and 19 degrees at 10 Gc (see Figure 3-19). An extrapolation between the curves indicates a diminishing range of phase control with increasing frequency.

Hardin, Downey, and Munushian (1960) have experimented with units using the configuration shown in

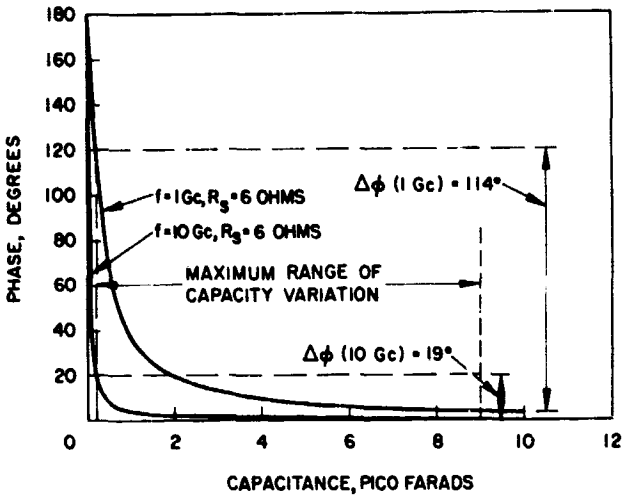

Figure 3-19. Phase shift of output signal.

Figure 3-17a and the resultant data bear out this frequency dependence. The units were built and tested at 0.5, 1.0, 6.0, and 9.0 Gc with the units at 1.0 and 9.0 Gc demonstrating, respectively, a phase change of 110° with an insertion loss of 1.2 db and a phase change of 40°, with an insertion loss of 3.9 db. However, the lower loss can be obtained by a reduction in the total phase change. These researchers explain the trade-off between decreased insertion loss and range of phase shift on the basis that both minimum insertion loss and phase variation (and hence the range of phase shift) are greatest when the diode termination (including tuning slabs, etc.) is designed for resonance in the center of the range of capacity variation of the diodes. The variations in phase shift and in the insertion loss with respect to bias voltage are shown in Figure 3-20 for the unit built at 1.0 Gc. The diodes used to obtain the data were Hughes MPA 2800 diodes which have a capacitance variation from about 2.5 to 1.0 pf for a corresponding bias voltage change from 0 to -5 volts and a reverse breakdown voltage of -7 volts.

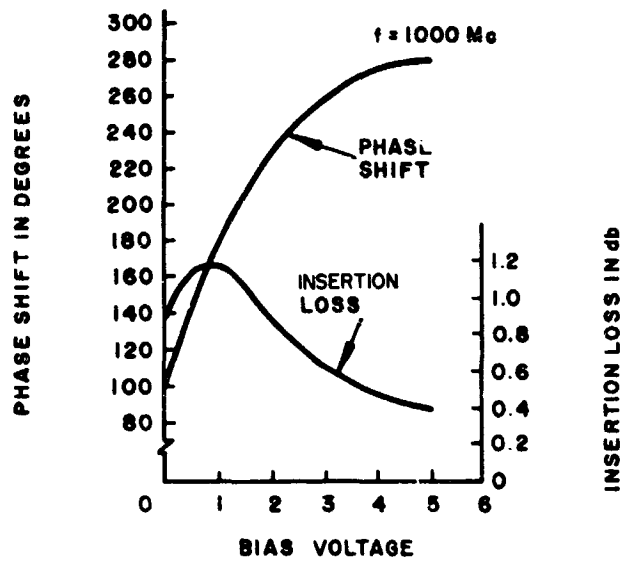

Figure 3-20. Phase shift and insertion loss as functions of diode bias at 1 Gc (after Hardin et al., 1960).

The data at 1 Gc were obtained for an r-f input power level of 1 milliwatt. However, because of r-f rectification and the generation of harmonics by the diodes, a rapid

increase in loss was observed at higher power levels. For example, when the r-f power was increased to 20 mw, the loss increased from 1.2 db to 6.4 db. Thus, at the higher power levels, the device behaved more like a power limiter.

If these diodes were to have higher reverse breakdown ratings, then the limiting action would occur at higher r-f power levels. Harmonic generation would consequently be reduced, since there would be less variation in capacitance with change in voltage.

3.2.3 Stepped Phase Shifters

The step or discrete phase shifter is essentially the same component as the continuous phase shifter with the varactor diode replaced by the PIN diode. The PIN diode is located at a fixed distance from a short termination and is biased to produce either an open or a short circuit impedance in the transmission line. As such, the incremental phase shift is directly proportional to twice the distance between the diode and the short termination. This unit is termed a single-step or one-bit phase shifter since only one change in phase is possible. To provide additional phase increments, multi-step phase shifters can be constructed as individual units or several can be placed in cascade; in addition, one-bit phase shifters can be fabricated as multi-step phase shifters. Figure 3-21 illustrates an incremental phase shifter which consists of two three-step phase shifters in cascade. One phase shifter produces incremental phase changes of 15, 30, and 45 degrees while the other provides 60, 120, and 180 degree phase variations. Both phase shifters require three pairs of PIN diodes and produce phase variations from 0-180 degrees in 15 degree increments. Step phase shifters

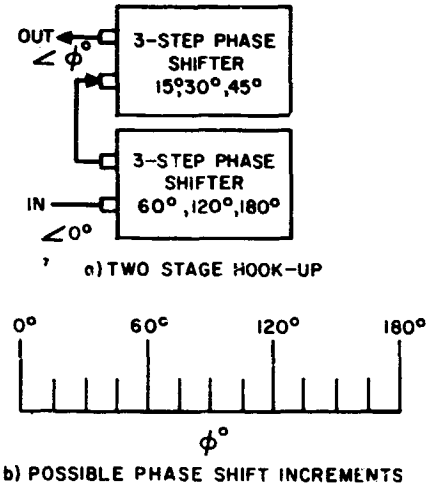

Figure 3-21. A two-stage, three-step phase shifting system (Matthei, 1964d).

exhibit lower insertion loss and higher power handling capability than the continuous type because of the nature of operation and fabrication of the PIN diode compared with the varactor diode. However, these advantages are at the expense of additional diodes and an increase in complexity of the diode circuitry.

3.3 DIODE-IRIS AMPLITUDE and PHASE CONTROL UNIT*

One of the most promising techniques for the implementation of complete electronic control in both phase and amplitude over the radiation from a slot array involves the use of semiconductor diodes in each slot element of an array. The control requires a small d-c voltage across a semiconductor material. Experimental iris configurations have been used that consist of two and four diodes symmetrically disposed about a longitudinal broadwall slot in a standard waveguide appropriate to the frequency region. Variation in the bias voltage across each diode can make the slot couple to both series and shunt currents in the broad wall of the waveguide and provides independent phase and amplitude control over the radiation emanating from the slot. Phase control over an array aperture is obtained by independent control of each element.

3.3.1 Background

The concept of using a waveguide iris configuration to control the radiation from a slot is relatively new. Control of this type was first demonstrated by Tang (1956) who used a single, mechanically-operated metal iris to control only the amplitude of slot radiation over a 50-db range at X-band. The mechanical device, shown in Figure 3-22, consists of a longitudinal, centered, broadwall slot and a resonant metallic iris which is inserted into the waveguide through nonradiating slots in the narrow walls and driven by a micrometer mechanism. When the iris is positioned symmetrically in the waveguide, the slot does not radiate; as the iris is moved to one side or the other, the slot radiates

*This work has been supported by the NASA Langley Research Center under Contracts NAS 1-2621 and NAS 1-4053.

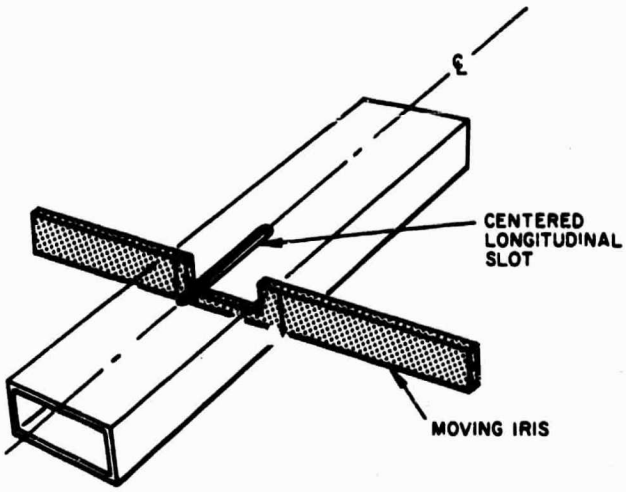

Figure 3-22. Iris-controlled slot.

with an amplitude dependent on the iris displacement. Iris-controlled elements of this type have been successfully used in linear arrays to produce a variety of radiation patterns.

The most general type of broadwall slot is that which is displaced and inclined from the centerline of a waveguide. Maxum (1957) has shown that this "complex" slot couples to both series and shunt currents in the waveguide broadwall and thus is capable of providing variable phase and amplitude values. It was demonstrated that two resonant metallic irises (Figure 3-23) could successfully be used to mechanically control a complex slot. Figure 3-24 illustrates the experimental amplitude (40 db range) and phase (180° range) control that was obtained by operating the device over only a portion of its range; the solid and dashed lines indicate constant settings for irises No. 1 and No. 2, respectively. By operating the device over its complete iris displacement range, 360° of phase control can be obtained.

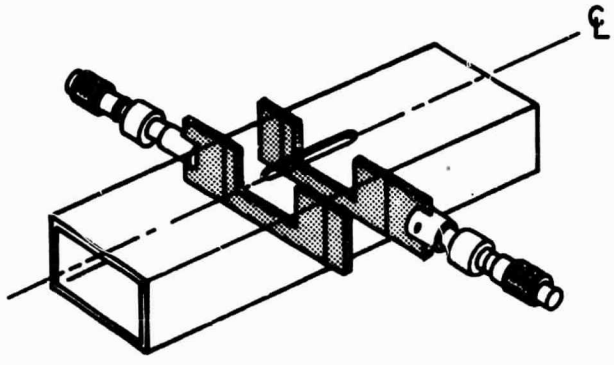

Figure 3-23. Mechanically-controlled complex slot.

3.3.2 Experimental Models

The metallic-iris techniques have been adapted at the Hughes Aircraft Company to electronic control by the use of semiconductor irises (Forman and Goebels, 1962). Initially, the investigations dealt with two-diode-iris units which primarily controlled the amplitude or the phase of the radiation from a slot at X-band.

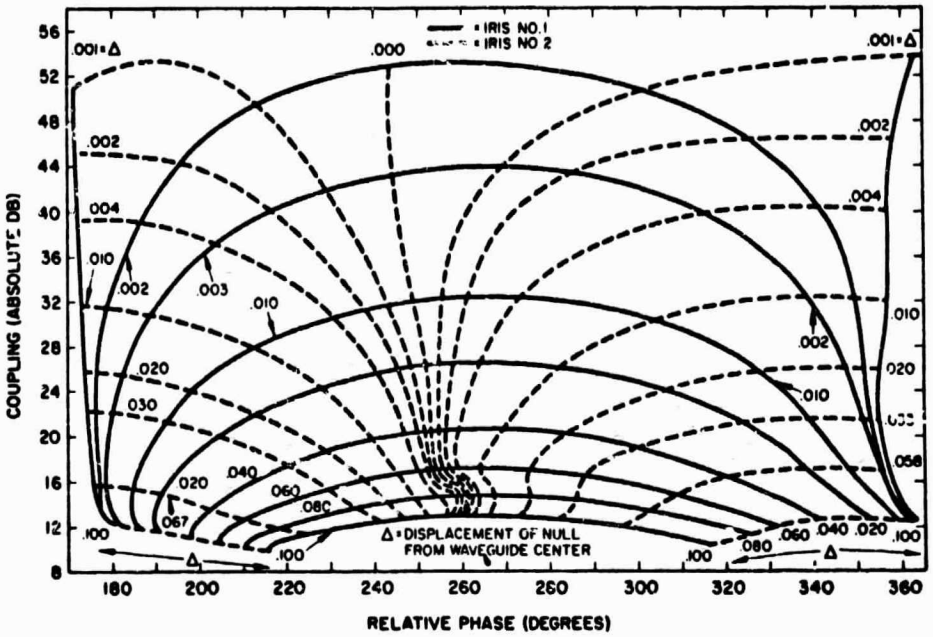

Figure 3-24. Experimental phase and amplitude data for mechanical complex slot.

Several amplitude control units were constructed in which two symmetrically disposed varactor diodes were located in the transverse plane of the waveguide. One of the units exhibited 44 db of control with a maximum slot radiation of 6.2 db down from the input power. Phase control units were also designed in which the diodes were placed in a transverse plane but offset by one-fourth the slot length. When the bias voltage across a diode was changed, the phase of the slot radiation varied ±87 degrees. Over this range of phase control the amplitude varied by about 13 db.

The studies were extended to four-diode-iris units that demonstrated complete phase control in addition to independent amplitude control. Two pairs of diodes were positioned in two transverse planes along a slot 0.225 inch from the narrow wall, that is, at a distance equal to one-fourth the waveguide width. The interspacing of diode pairs along the axis of the waveguide was $\lambda_g/4 = 0.440$ inch. At this interval reflections from the two pairs of diodes are out of phase and cancel. R-f chokes were mounted on the broad wall opposite the slot arm to permit the diodes to be externally biased. The diodes

and their chokes are shown in an assembled test unit in Figure 3-25. Experimentation was conducted at 9.375 Gc with Hughes silver-bonded germanium diodes (HD-5610). A rectangular brass tuning element one-half guide wavelength in length, 0.900 inch in width, and 0.140 inch in height was used to match the unit.

With the matching element, the VSWR for -50 db coupling (minimum coupling) was 1.19:1 and less than 1.4:1 over nearly the entire control range of the four-diode device. Amplitude coupling control to -15 db was observed with a phase control range of 360 degrees. At minimum slot coupling the reflective and dissipative insertion loss was 1.4 db; the extreme values of this insertion loss were measured to be 1.1 db and 1.8 db at -36 db coupling (VSWR = 1.39:1) and -9.1 db maximum coupling (VSWR = 1.10:1), respectively. It should be emphasized that full control of the slot radiation characteristics was accomplished with merely microwatts of driving power.

The four-diode-iris control unit was used in the design and testing of a 10-element traveling-wave array that is described in detail in Section 4.2.1.

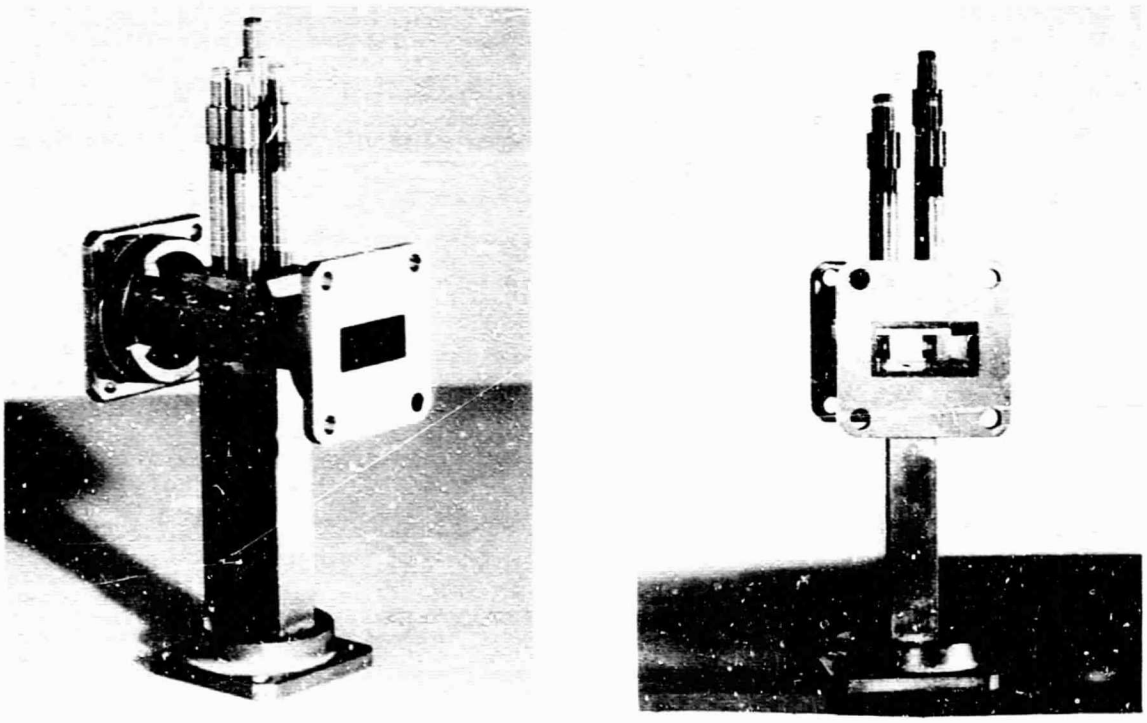

a) Overall view b) End View

Figure 3-25. Four-diode-iris phase and amplitude control device.

3.4 SOLID-STATE COMPONENTS

During the past year the technical literature has reported significant improvement in solid-state devices and circuitry for electronically self-phasing arrays. Some typical advances include switches, broadband amplifiers, tunnel-diode amplifiers, microwave power sources, mixers, filters, and circulators.

3.4.1 Switches

In multiple-beam arrays and in amplitude-scanned time-controlled arrays, switches are needed to implement the scanning systems. To assess the state-of-the-art in semiconductor switches, a survey of commerically available switches was made. Some of these switches and their characteristics are tabulated below.

Manufacturer	Frequency Range	Bandwidth	Minimum Isolation (db)	Insertion Maximum (db)	Peak Power (kilowatts)	Average Power	Switch	Switching Time (nanoseconds)	Type
Micro State	8-12 Gc	60 Mc	32	–	–	0.5 watt	SPDT	2.5	Waveguide
	5.3-8.2 Gc	–	30	–	–	–	–	–	Coaxial
	1.25-1.35 Gc	–	20	0.75	1	–	–	–	–
	1.25-1.35 Gc	–	35	1.0	1	20 watts	SPDT	200	Coaxial
	2.7-2.9 Gc	–	20	1.0	2.5	20 watts	SPDT	200	Coaxial
	2.7-2.9 Gc	–	35	1.5	2.5	20 watts	SPDT	200	Coaxial
	5.4-5.9 Gc	–	20	1.26	6	20 watts	SPDT	200	Coaxial
	5.4-5.9 Gc	–	35	1.6	6	20 watts	SPDT	200	Coaxial
	8.6-9.5 Gc	–	20	1.5	10	20 watts	SPDT	200	Coaxial
	8.6-9.5 Gc	–	35	2.0	10	20 watts	SPDT	200	Coaxial
	145-155 Mc	–	20	0.5	–	2 watts	SPDT	500	Coaxial
	145-155 Mc	–	40	0.7	–	2 watts	SPDT	500	Coaxial
	145-155 Mc	–	60	0.8	–	2 watts	SPDT	500	Coaxial
	400-450 Mc	–	20	0.5	–	2 watts	SPDT	100	Coaxial
	400-450 Mc	–	40	0.7	–	2 watts	SPDT	100	Coaxial
	400-450 Mc	–	60	0.8	–	2 watts	SPDT	100	Coaxial
	1050-1150 Mc	–	20	0.5	–	1 watt	SPDT	45	Coaxial
	1050-1150 Mc	–	40	0.75	–	1 watt	SPDT	45	Coaxial
	1050-1150 Mc	–	60	1.0	–	1 watt	SPDT	45	Coaxial
	2100-2300 Mc	–	20	0.75	–	1 watt	SPDT	35	Coaxial
	2100-2300 Mc	–	40	1.25	–	1 watt	SPDT	35	Coaxial
	2100-2300 Mc	–	60	1.50	–	1 watt	SPDT	35	Coaxial
	5400-5900 Mc	–	20	1.25	–	0.5 watt	SPDT	25	Coaxial
	5400-5900 Mc	–	40	1.5	–	0.5 watt	SPDT	25	Coaxial
	8600-9500 Mc	–	20	1.5	–	0.5 watt	SPDT	10	Coaxial
	8600-9500 Mc	–	40	2.00	–	0.5 watt	SPDT	10	Coaxial
	1200-1400 Mc	–	20	0.5	–	500 mw	SPDT	10	Coaxial
	1200-1400 Mc	–	40	0.75	–	500 mw	SPDT	10	Coaxial
	2100-2300 Mc	–	20	0.75	–	500 mw	SPDT	10	Coaxial
	2100-2300 Mc	–	40	1.0	–	500 mw	SPDT	10	Coaxial

Manufacturer	Frequency Range	Bandwidth	Minimum Isolation (db)	Insertion Maximum (db)	Peak Power	Average Power	Switch	Switching Time (nanoseconds)	Type
Micro State (continued)	5400-5900 Mc	–	20	1.25	–	250 mw	SPDT	7	Coaxial
	5400-5900 Mc	–	40	1.5	–	250 mw	SPDT	7	Coaxial
	8600-9500 Mc	–	30	1.5	–	100 mw	SPDT	4	Coaxial
	8600-9500 Mc	–	40	1.75	–	100 mw	SPDT	4	Coaxial
Hughes	8.2-10.0 Gc	–	45	2.5	–	–	SPST	–	Waveguide
Philco	4.3-5.6 Gc	–	28	0.75	–	–	–	–	Waveguide
	5.6-8.2 Gc	–	28	0.75	–	–	–	–	Waveguide
	8.2-11.8 Gc	–	28	0.75	–	–	–	–	Waveguide
	13-14.2 Gc	–	28	0.75	–	–	–	–	Waveguide
	16.1-16.9 Gc	–	28	0.75	–	–	–	–	Waveguide
Sanders Assoc.	DC-400 Mc	–	20	0.8	–	0.25 watt	SPDT	10	Coaxial
	1-4 Gc	–	30	2.5	–	1 watt	SPDT	50	Coaxial
	4-8 Gc	–	40	3.0	–	1 watt	SPST	50	Coaxial
Antenna Radome Research Associates, Inc.	200-4000 Mc	–	60	3.0	150 watts	–	SPST	10	Coaxial
	4000-8000 Mc	–	20	1.5	1 kw	–	SPST	50	Coaxial
	200-1250 Mc	–	25	1.0	1 kw	–	SPDT	50-100	Coaxial
	1000-2000 Mc	–	20	1.0	1 kw	–	SPDT	50-100	Coaxial
	2000-4000 Mc	–	20	1.5	1 kw	–	SPDT	50-100	Coaxial
	4000-8000 Mc	–	20	1.5	1 kw	–	SPDT	50-100	Coaxial
	7.05-10.0 Gc	100 Mc	50	3.0	150 watts	–	SPST	10	Waveguide
	8.2-12.4 Gc	100 Mc	70	5.0	150 watts	–	SPST	10	Waveguide
	8.2-12.4 Gc	100 Mc	50	3.0	150 watts	–	SPST	10	Waveguide
	12.4-18.0 Gc	300 Mc	40	2.5	150 watts	–	SPST	10	Waveguide
	12.4-18.0 Gc	200 Mc	90	9.0	150 watts	–	SPST	10	Waveguide
	7.05-10.0 Gc	1000 Mc	20	3.0	150 watts	–	SPDT	10	Waveguide
	8.2-12.4 Gc	500 Mc	20	3.0	150 watts	–	SPDT	10	Waveguide
Hewlett-Packard Co.	500 Mc - 12.4 Gc	–	27 500 Mc to 1 Gc 35 1 to 2 Gc 45 2 to 12.4 Gc	0.7 500 Mc to 2 Gc 1.5 2 to 12.4 Gc	100 watts	3 watts	SPST	300	Coaxial

3.4.2 Broadband Transistor Amplifiers

For some time the transistorized i-f preamplifier has been at least equal to comparable tube amplifiers. These solid-state counterparts are especially attractive for applications which require relatively low power consumption and are light in weight. At higher frequencies, Hamasaki (1963) has reported a microwave amplifier with a gain of 32 db, a bandwidth of 450 Mc, and a measured noise figure of 6.5 db at 1.25 Gc.

Several U.S. manufacturers are developing improved microwave transistors. An example is the TIX-3015 (Matthei, 1964a) silicon planar transistor with interdigital geometry. It is expected that the design objective of a 3-stage amplifier operating at 1.3 Gc with a 200 Mc bandwidth will realize a noise figure of 3.5 db.

3.4.3 Tunnel Diode Amplifiers

Tunnel diode amplifiers have shown some improvement in the past year. Steinhoff and Sterzer (1964) report the development of tunnel diodes and amplifiers with low noise figures (3.8 - 4.9 db) and large dynamic signal ranges (65 to 90 db). Sepoff and Wheeler (1964) report an octave bandwidth tunnel diode amplifier operating from 2 - 4 Gc with a gain in excess of 10 db and a noise figure of less than 4 db. Micro State Electronic Corporation markets a tunnel diode amplifier with 15 db gain, a dynamic range of 62 db, and a system noise figure of 4.0 db over a 4.4 - 5.0 Gc frequency range.

The current status of noise temperature versus frequency for the different types of microwave amplifiers is shown in Figure 3-26.

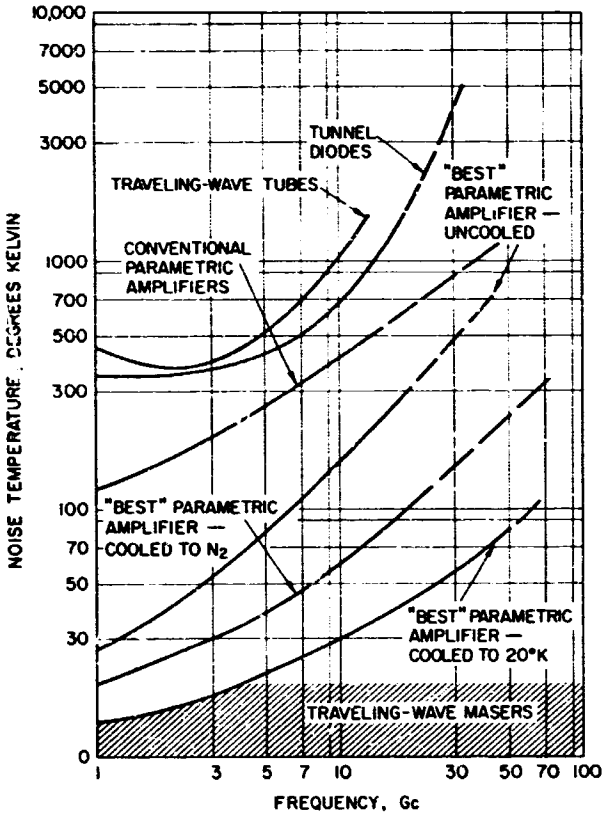

Figure 3-26. Noise temperature of various r-f amplifiers as a function of operating frequency (Matthei, 1964).

3.4.4 Microwave Power Transistors

Improvement has also been made in the development of solid-state power transistors. Powers of 25 watts at 100 Mc and 5 watts at 500 Mc have been reported (Matthei, 1964b). These lower frequency devices can be used to drive varactor or step-recovery diodes to produce harmonic frequencies with surprising efficiencies: for example, to multiply 100 Mc at 45 mw to 2000 Mc at 15 mw (Atalla, 1964) to multiply 5.55 Gc at 540 mw to 22.2 Gc at 100 mw (Rofuse and Steinbracher, 1964).

Tunnel diodes are well established microwave oscillators. Some recent developments report

(Matthei, 1964c) increased power output (24 mw) at 1.66 Gc and to 1.2 mw at 10.5 Gc. The paralleling of four improved diodes is expected to produce 8 mw at X-band frequencies. These power sources provide an attractive means for lightweight local oscillators and parametric amplifier pumps, especially in space vehicles in which weight and power consumption are important.

3.4.5 X-Band Mixers

There has been a significant improvement in the reduction of the noise figure of commercially available silicon diodes which are employed as balanced X-band mixers in superheterodyne receivers. Some of the advances are due to a reduction of losses in the case and the spreading resistance loss due to thinner slabs and better doping of the semiconductor material. The r-f and i-f impedances are being held to closer electrical tolerances to provide improved performance in standard mounts. These improved units also have a higher burn out rating. A list (Microwave Associates, 1964) of representative crystals available for X-band use is shown in Table 3-4.

An improved version of an X-band silicon diode appears in the current literature (Sylvania, 1965). This device, Sylvania's IN23G, is rated with a 6.5 db overall noise figure.

Improved Types: For low noise superheterodyne mixer performance											
Style E				Style G	Test Frequency (Mc)	Maximum Conversion Loss (db)	Maximum Output Noise Ratio (times)	Maximum VSWR in Standard Mixer	Calculated Overall Receiver Noise Figure N_{if} = 1.5 db	I-f Impedance (ohms)	Burnout Rating (ergs)
Fixed Base Types		Matched Pair									
Forward Polarity	Reversed Polarity	Forward Pair	Forward and Reversed	Reversible Polarity Types							
1N23B	1N23BR	1N23BM	1N23BMR	1N415B	9375	6.5	2.7	---	11.4	300-600	0.3
1N23C	1N23CR	1N23CM	1N23CMR	1N415C	9375	6.0	2.0	1.5	9.8	325-475	1.0
1N149	1N149R	1N149M	1N149MR	MA-414	9375	5.5	1.5	1.5	8.3	325-475	1.0
1N23D	1N23DR	1N23DM	1N23DMR	1N415D	9375	5.0	1.7	1.3	8.2	350-450	1.0
1N23E	1N23ER	1N23EM	1N23EMR	1N415E	9375	--	---	1.3	7.5	335-465	2.0
		1N23WEM	1N23WEMR	1N23WE	9375	6.0	1.4	1.3	7.5	335-465	2.0
1N23F	1N23FR	1N23FM	1N23FMR	---	9375	---	---	1.3	7.0	335-465	2.0
MA-451 series and MA-458 series are designed for 150°C operation and are hermetically sealed using metal-to-ceramic solder-seal construction. They replace and are electrically equivalent to the 1N23 and 1N415 types.											
Higher Burnout Types: For use in pulse radars or other receivers exposed to high r-f radiation fields											
MA-4133	MA-4133R	MA-4133M	MA-4133MR	MA-4134	9375	6.0	2.0	---	9.8	325-475	5.0

Table 3-4. Representative X-band Crystals (Microwave Associates, 1964).

3.4.6 Filters

Excellent filters are commercially available in the frequency range up through X-band and beyond. These include filters employed in communication systems, for example, band pass (nominally flat), band rejection, diplexers, and high Q stabilizing cavities. In these higher frequency ranges, the structures may be waveguide, strip transmission line, or coaxial, but for space applications, the small, light strip transmission line and coaxial devices are most attractive. In many cases the performance of the latter are equal to comparable waveguide filters. A number of companies specialize in making a representative line of filters. Rantec Corporation is one well-known California firm which specializes in standard filters as well as in filters for special requirements. Hughes Aircraft Company has also developed a capability in the design and construction of filters for communication and spacecraft applications in the microwave field.

Some representative examples of Rantec filters applicable to space-earth communication are given in Table 3-5. The specifications listed are drawn from catalogs of commercially available devices.

Type of Filter	Center Frequency (Mc)	Bandwidth (Mc)	Maximum VSWR	Maximum Insertion Loss (db)	Stop Band	Manufacturer
Bandpass Waveguides	4080	25	1.2:1	0.30	40 db at 3940 Mc 35 db at 4175 Mc	Rantec
Bandpass Coaxial	Pass Band 2200-2300	100	1.2:1	0.30	-40 db at 1900 Mc -40 db at 2500 Mc	Rantec
					Isolation	
Diplexer	4080 ± 5		1.3:1	0.30	40 db Band 1	Rantec
Waveguide	4175 ± 5		1.2:1	0.20	40 db Band 2	
Diplexer	2213 ± 4		1.2:1	0.1	145 db Band 2	Rantec
Waveguide	2295 ± 4		1.2:1	0.3	30 db Band 1	

Table 3-5. Applicable Commercial Filters for Space-Earth Communications Systems.

3.4.7 Circulators

At the frequencies used in satellite communications (2, 4, and 6 Gc), waveguide circulators tend to be heavy and bulky. More attractive solutions utilize strip transmission line with coaxial connectors which are lighter in weight and more compact. These devices are of the three-terminal "Y" type.

Typical performance of commercially available strip transmission line circulators is indicated in Table 3-6.

Frequency Band (Gc)	Insertion Loss (db maximum)	Isolation (db)	VSWR	Bandwidth (percent)	Size (Inch)	Temperature	Manufacturer
9.5-10.5	0.1-0.25	22 min. 28 max.	1.15:1	10	7/8 by 3/4 by 5/8	Note ①	Western Microwave Laboratory
2	0.2-0.3	25 min.	1.23:1	30		Note ②	Hughes Aircraft Company
4	0.2-0.3	25 min.	1.23:1	30		Note ②	
6	0.2-0.3	40 min. ③	1.23:1	10		Note ②	

Notes:

① -35° to +55° C (with insulation or cooling, range extends from -85° to +145° C).

② In general, the temperature effects of the circulators listed are of the same order of magnitude. The isolation of an isolator will be degraded as the temperature varies from the design temperature, which is, for example, room temperature or 20° C. The effect of an elevated temperature is the more serious effect: the maximum temperature is determined by the minimum isolation which the system can tolerate. To extend the temperature range requires a design to produce greater isolation at room temperature. The lowering of temperature which decreases the temperature below the Curie point has a relatively small degrading effect.

③ The narrower band tends to improve the isolation at room temperature and at mid-band. Thus, the 2, 4, and 6 Gc models used for space application, such as those in the ComSat Early Bird, use relatively narrow bands and provide a higher isolation. This characteristic can be used as a trade-off for operation over wider range of temperatures with the isolation dropping, say, to 20 db.

Table 3-6. Performance of Commercially Available Strip Transmission Line Circulators.

3.5 LOG-PERIODIC CIRCUITS

The ability to operate antenna systems over wide frequency ranges rests on the availability of components which can operate properly over the desired range. In some applications broadband hybrids are required. In others, components with fixed phase relationships between outputs are required. The use of log-periodic

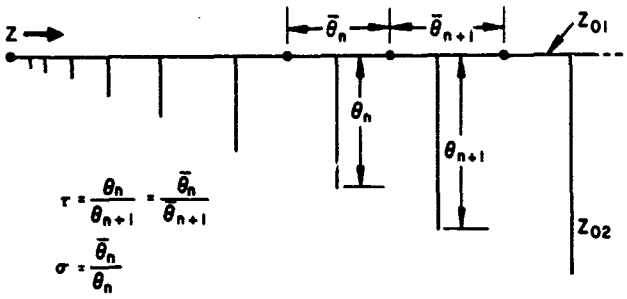

Figure 3-27. Example of one-port log-periodic network (Duhamel and Armstrong, 1964a).

networks to achieve such broadband characteristics appears to offer promise.

3.5.1 Log-Periodic Structures

The basic structure which illustrates the type of performance obtainable is shown in Figure 3-27 (Duhamel and Armstrong, 1964a). The circuit may be considered as a cascade of symmetrical sections consisting of transmission lines of characteristic impedance Z_{01} and electrical length $\bar{\theta}_n$, shunt-loaded by open-circuited transmission lines of impedance Z_{02} and electrical length θ_n. The design ratio τ relates similar lengths of transmission lines in adjacent sections. The ratio $\bar{\theta}_n/\theta_n$ is denoted by σ. Ideally, the circuits should extend indefinitely to the right and there should be an infinity of sections between the feed point and the first stub shown. The circuit is defined so that

$$V_n(f) = V_{n+1}(\tau f) \quad \text{for all } \underline{n} \tag{3-14}$$

where V_n is the voltage at the n^{th} node, $\underline{f}$ is the normalized frequency, and $\underline{n}$ is an integer. It may be shown that, under these conditions, the input reflection coefficient is a periodic function of the logarithm of the frequency; i.e., $\Gamma(f) = \Gamma(\tau f) = \Gamma(\tau^n f)$.

The behavior of the circuit may be explained approximately as follows. An incident wave applied at the input propagates down the structure toward the reflection region (which is defined as the region at which a shunt stub is approximately one-quarter wavelength long). Along the first part of the structure, the loaded transmission line behaves as a slowly varying, nonuniform transmission line. At the reflection region, the shunt stubs effectively short the wave and reflect it back to the feed point. If complete reflection takes place at this region, then calculations show that the input reflection coefficient is given approximately by

$$\Gamma = \exp\left[j\left(\frac{2\pi \log f}{|\log \tau|} + \phi\right)\right] \tag{3-15}$$

where ϕ is a constant. The reflection coefficient has been normalized to the impedance Z_0, which is given by

$$Z_0 = Z_{01}\left[1 + \frac{Z_{01}}{\sigma Z_{02}}\right]^{1/2} \tag{3-16}$$

This is simply the limiting form, as $n \rightarrow -\infty$, of the image impedance of a symmetrical section. It can be seen that the phase varies linearly with the logarithm of the frequency and changes by 2π when the frequency is changed by the factor τ. These expressions assume a structure with an infinite number of sections. For a structure with a finite number of sections, the performance of the circuit will approach that of the infinite circuit over a finite bandwidth. The low cut-off frequency is determined when the longest stub is approximately one-quarter wavelength long, and the upper cut-off frequency when the shortest stub is somewhat less than one-quarter wavelength long.

The circuit of Figure 3-27 has another important property: if all dimensions of the circuit are scaled gradually from the original dimensions to τ times their starting dimensions, it will be found that the phase curve slides up by an amount 2π. This property is useful in the design of phase difference circuits.

Extensive computer computations indicate that it is possible to design a single port log-periodic circuit such that the phase of the input reflection coefficient closely approximates the ideal linear phase variation with the logarithm of the frequency. The magnitude of the reflection coefficient is essentially independent of frequency, and values greater than 0.9 or 0.95 can be achieved in practice.

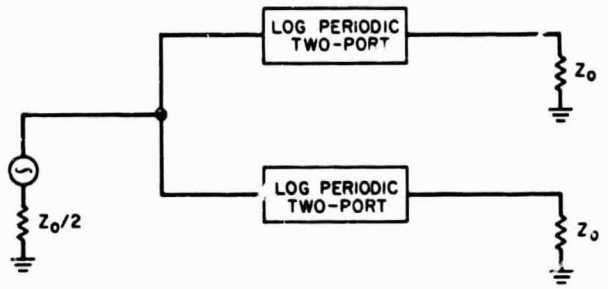

Figure 3-28. Constant phase difference circuit (Duhamel and Armstrong, 1964b).

3.5.2 Log-Periodic Phase Difference Circuits

As indicated, one-port log-periodic circuits can be combined to give networks whose output phases at two output ports differ by a fixed amount over wide frequency ranges (Duhamel and Armstrong, 1964b). Figure 3-28 is a schematic of the types of constant phase difference circuits to be discussed. It consists of two similar two-port log-periodic circuits with their inputs connected in parallel. The component two-port networks may be obtained by coupling two one-port networks as illustrated in Figure 3-29a and b. The elements of the scattering matrix of the two ports are approximately of the form

$$S_{11} = S_{22} \simeq 0 \tag{3-17a}$$

$$S_{12} = S_{21} \approx \exp\left\{-j\left[\frac{2\pi f}{|\log \tau|} + \epsilon + \frac{1}{2}\left(\log\frac{Z_{oe}}{Z_{oo}}\right)\sin\left(\frac{2\pi \log f}{|\log \tau|} + \epsilon\right)\right]\right\} \tag{3-17b}$$

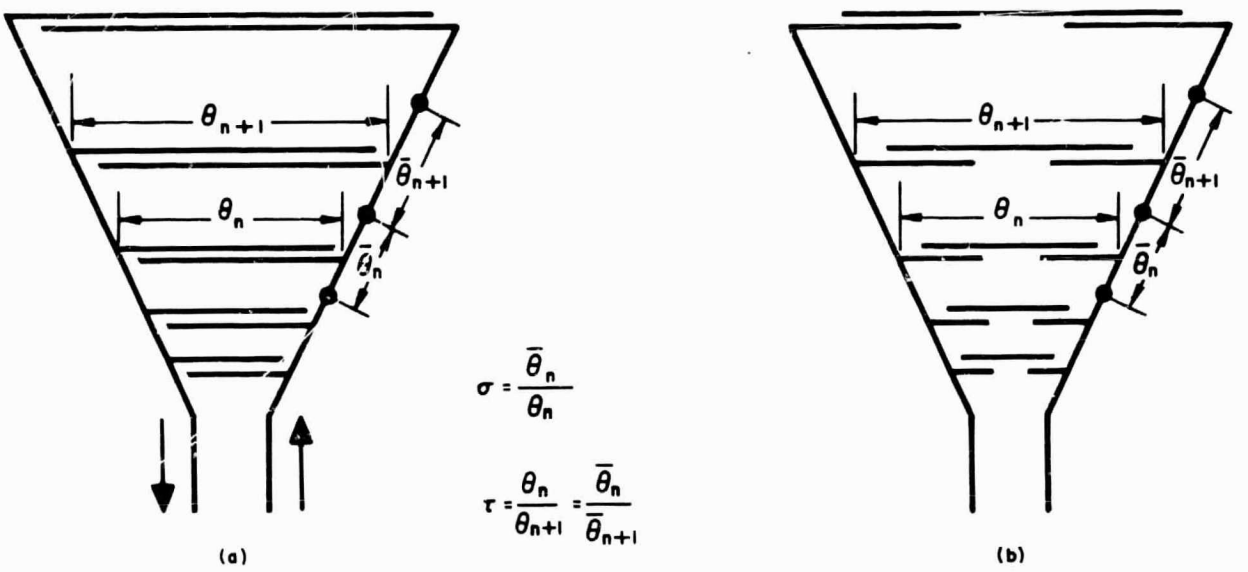

Figure 3-29. Two-port log-periodic transmission line network (Duhamel and Armstrong, 1964b).

where Z_{oe} and Z_{oo} are the even and odd mode characteristic impedances of the types of section shown in Figure 3-29. The last term represents an error term (ripple) which is small if Z_{oe}/Z_{oo} is near unity. Computer analysis indicates that it is possible to make $|S_{11}| < 0.03$ and the phase ripple of S_{12} less than 1.5 degrees. When two of the two port networks of proper dimensions are connected as shown in Figure 3-28, the phase difference between the two outputs is of the form

$$\psi = \epsilon_2 - \epsilon_1 + \frac{1}{2}\log\left(\frac{Z_{oe2}}{Z_{oo2}}\right)\sin\left(\frac{2\pi \log f}{|\log \tau|} + \epsilon_2\right) - \frac{1}{2}\log\left(\frac{Z_{oe1}}{Z_{oo1}}\right)\sin\left(\frac{2\pi \log f}{|\log \tau|} + \epsilon_1\right) \qquad (3\text{-}18)$$

When $\frac{Z_{oe2}}{Z_{oo2}}$ and $\frac{Z_{oe1}}{Z_{oo1}}$ are near unity, ψ is nearly independent of frequency. An experimental balun was built using this technique. It was designed to operate over the range 500 Mc to 5000 Mc. Preliminary measurements indicate that, by proper parameter adjustments, balance to unbalance ratios greater than 26 db and phase deviations ($\Delta\psi$) of 3 degrees may be obtained. Input VSWR's less than 1.10 over most of the bandwidth may be practical. More precise fabrication techniques are being studied to improve the balance to unbalance ratio.

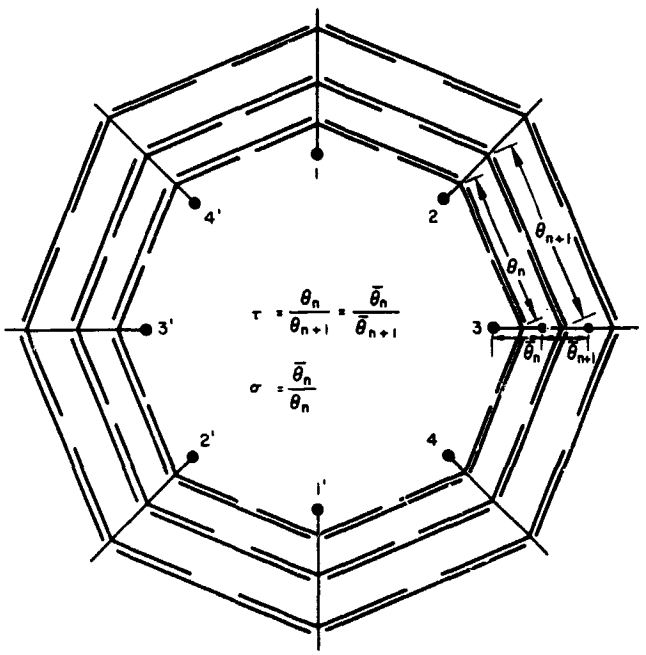

Figure 3-30. Octaline magic-tee (Duhamel and Armstrong, 1964c).

3.5.3 Log-Periodic Magic-T Circuits

Log-periodic circuits may also be used to obtain broadband magic-T junctions (Duhamel and Armstrong, 1964c). Figure 3-30 illustrates the octaline

arrangement. The device is operated using terminals 1-1', 2-2', etc., as balanced pairs. Excitation of terminals 1-1' gives equal, in-phase outputs at 2-2' and 4-4' and zero output at 3-3'. Excitation of terminals 3-3' gives the same output at 2-2' but reverses the phase at 4-4'. Zero output is obtained at 1-1'. This operation is magic-T performance. An experimental stripline model was built to operate from 300 Mc to 900 Mc. The isolation between terminals 1-1' and 3-3' was greater than 24 db over the desired band. The coupled outputs were equal to within ±0.5 db and the phase difference between the outputs was less than ±5 degrees. The coupled outputs were 1 to 1.5 db below the desired level of -3 db. The VSWR was high and about 1.6 over the band. This result is attributed to poorly matched input and output coax to stripline transitions. More careful transition design could reduce this VSWR.

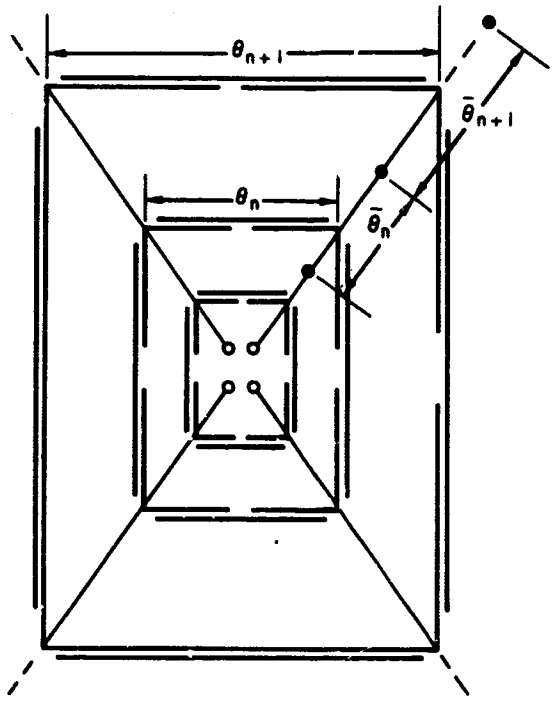

Figure 3-31. Quadriline hybrid junction.

3.5.4 Log-Periodic Directional Couplers

Hybrid junctions in which the coupled outputs are 90° out of phase can also be constructed using log-periodic circuits. Figure 3-31 illustrates a configuration capable of such operation. This device has an advantage over the octaline arrangement in that the terminals are unbalanced rather than balanced. It is expected that performance up to X-band may be obtained.

BLANK PAGE

4. ANTENNA SYSTEMS

A survey of electronically scanned antenna space systems is presented in this section. Wherever possible, the techniques are evaluated with respect to satellite applications. Most of the systems fall within current engineering capability. They either are demonstration models or could be made into such models with a reasonable degree of additional development. The various systems include scanned arrays and multiple beam antennas of various configurations. All these systems usually require external sensors or commands to obtain the proper beam pointing direction.

4.1 PHASE SCANNED CIRCULAR ARRAYS

Ferrite phase shifters of the modified Fox type (Section 3.1.4) have been used to despin the beam of a circular array developed for use in the Applications Technology Satellite (ATS). The array consists of sixteen vertical elements equally spaced about a circle. The individual elements are linear arrays whose length is determined by the required pattern beamwidth in the planes containing the spin axis, i.e., the array axis. Some directivity in these planes results from the array factor also, but the primary source of directivity is the element factor. The radiation pattern in the azimuth plane, the plane normal to the array (spin) axis, is determined by the excitations of the elements. In the ATS array the amplitude distribution is uniform while the phases are adjusted to produce a beam in a given azimuth direction. The direction is changed by adjusting the relative phases of the excitations.

4.1.1 Pattern Analysis

The locations of elements in a circular array of N elements and radius R and the position vectors to a point in the far field are shown

in Figure 4-1. The distance from the n^{th} element to the field point is r_n which in terms of $\underline{r}$ is given approximately by

$$r_n \approx r - R \sin\theta \cos(\phi - \phi_n) \tag{4-1}$$

so that the array factor is given by

$$F(\theta, \phi) = \sum |a_n| \; e^{j\psi_n} \; e^{jkR \sin\theta \cos(\phi - \phi_n)} \tag{4-2}$$

where $|a_n|$ is the amplitude and ψ_n the phase of the n^{th} element excitation. To obtain a beam at angle ϕ_b in the $\theta = \pi/2$ plane, the ψ_n should be adjusted so that all terms in the series add in phase in that direction, i.e., so that

$$\psi_n = -kR \cos(\phi_b - \phi_n) \tag{4-3}$$

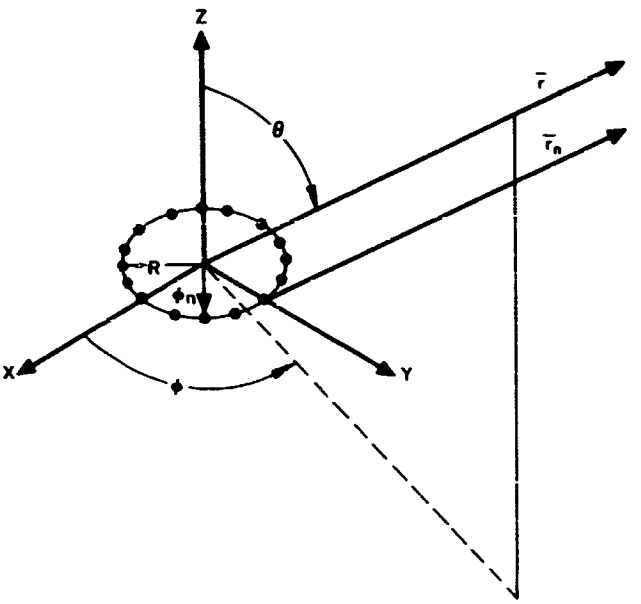

Figure 4-1. Circular array geometry

The total array pattern for a uniform amplitude distribution and elements which are omnidirectional in azimuth is

$$E_\phi(\theta, \phi) = f_\phi(\theta) \sum e^{jkR \left[\sin\theta \cos(\phi - \phi_n) - \cos(\phi_b - \phi_n)\right]} \tag{4-4a}$$

$$E_\theta(\theta, \phi) = f_\theta(\theta) \sum e^{jkR \left[\sin\theta \cos(\phi - \phi_n) - \cos(\phi_b - \phi_n)\right]} \tag{4-4b}$$

where f_ϕ and f_θ are the element factors for the ϕ and θ components, respectively, of the radiation field. The angles ϕ_n are given by

$$\phi_n = n\frac{2\pi}{N} \qquad 0 \le n \le N - 1 \tag{4-5}$$

so that the patterns are given by

$$E_\phi(\theta, \phi) = f_\phi(\theta) \sum_{n=0}^{N-1} e^{jkR \left[\sin\theta \cos(\phi - n\frac{2\pi}{N}) - \cos(\phi_b - n\frac{2\pi}{N})\right]} \tag{4-6a}$$

$$E_\theta(\theta, \phi) = f_\theta(\theta) \sum_{n=0}^{N-1} e^{jkR \left[\sin\theta \cos(\phi - n\frac{2\pi}{N}) - \cos(\phi_b - n\frac{2\pi}{N})\right]} \tag{4-6b}$$

If the spacecraft spins at an angular velocity, ω, about an axis coinciding with the antenna axis, keeping the beam stationary necessitates adjusting the element phases so that ϕ_b compensates for the spin. Therefore, it is necessary to have

$$\phi_b = -\omega t \tag{4-7}$$

This adjustment requires that the element phases must go through the values

$$\psi_n = -kR \cos(\omega t + n\frac{2\pi}{N}) \tag{4-8}$$

Thus, the relative phases must undergo cosinusoidal variations displaced in time by $\frac{2\pi}{N}$. Equation (3-21) indicates that, if N is even,

then

$$\psi_{n\pm N/2} = -\psi_n \tag{4-9}$$

and, therefore, diametrically opposite array elements require opposite phase shifts. The device used to accomplish the required phase shifts electronically is essentially a modification of the Fox phase shifter technique (Fox, 1947) and the synchronous ferrite phase shifter. (See Section 3. 1. 4)

4. 1. 2 Array Description

The ATS circular array consists of 16 elements spaced on a circle of one wavelength radius. Each element of the circular array consists of a colinear array of half wave dipoles. The dipoles are fed by gaps in the outer conductor of a coaxial feed line. The line is filled with Teflon so that the dipoles can be fed in phase and the separation can still be kept to about 0. 7 free space wavelength. The power divider which feeds the phase shifters is a stripline assembly and the coupling from the phase shifters to the linear arrays is also a stripline assembly. Figure 4-2 shows the completed array and the details of a disassembled stripline circuit output coupler and ground planes. The ground planes are numbered consecutively from 1 to 4. The coupler is shown in various stages of disassembly. Starting with the complete assembly, components are consecutively removed from the right assembly (top views) and reassembled on the left (bottom views).

4. 1. 3 Control Electronics

The control electronics generates the set of 16 control voltages for the ferrite phase shifters. A system diagram is shown in Figure 4-3. The system uses an input reference of one pulse per spacecraft revolution. The pulse is obtained from a sun sensor as the vehicle spins and feeds a frequency lock loop which generates $2^9 = 512$ pulses for every input pulse. The output of the frequency lock loop drives the beam positioner, which, in turn, drives 16 sine wave generators in the

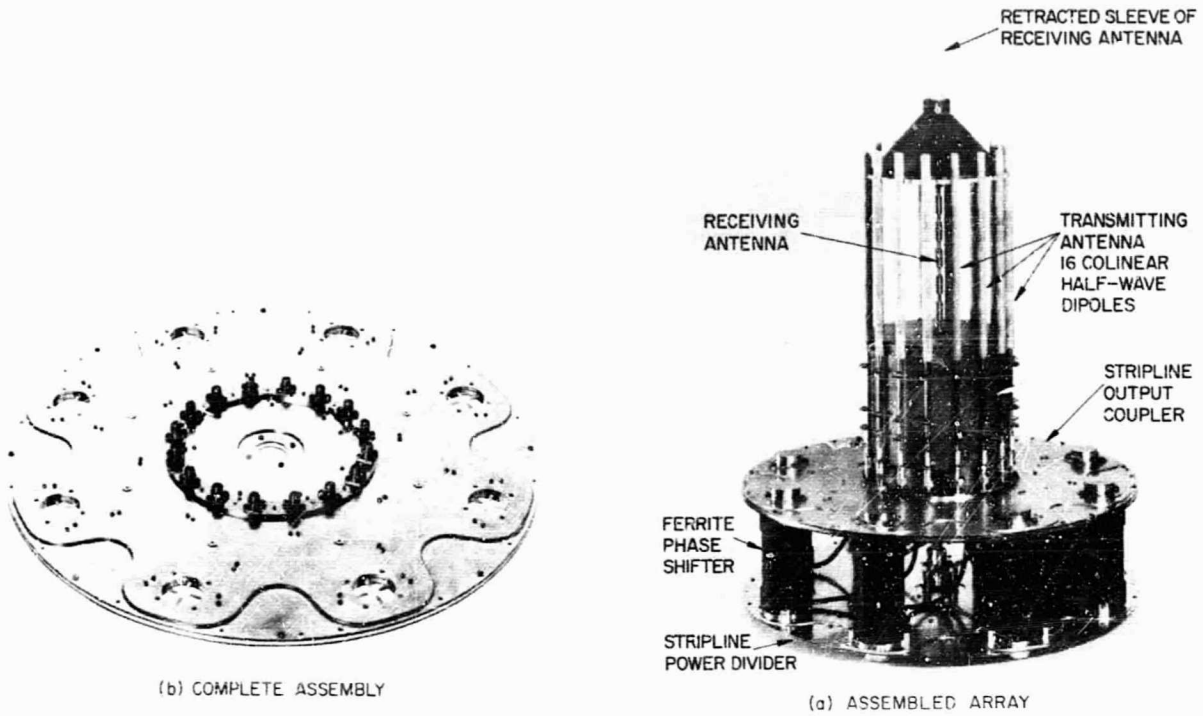

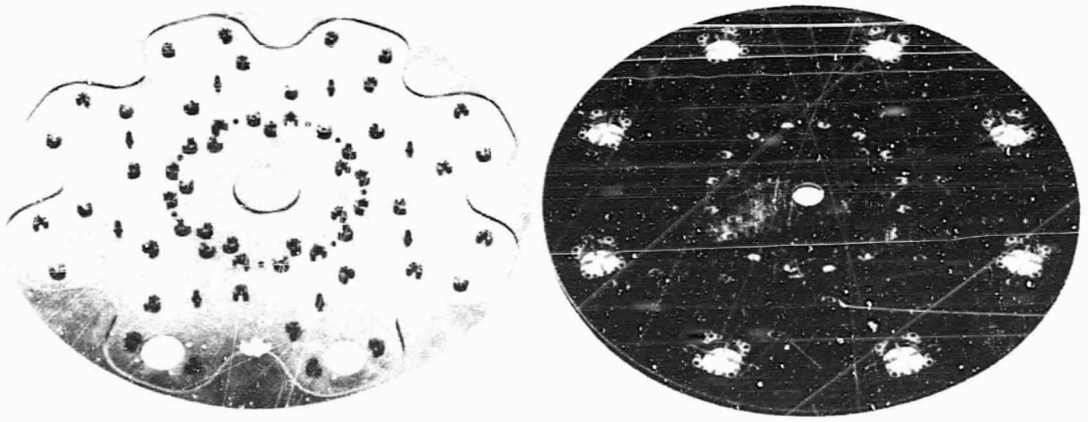

(c) LEFT: BOTTOM VIEW, GROUND PLANE
RIGHT: STRIPLINE BOARD, TOP VIEW

Figure 4-2. Applications Technology Satellite circular phased array.

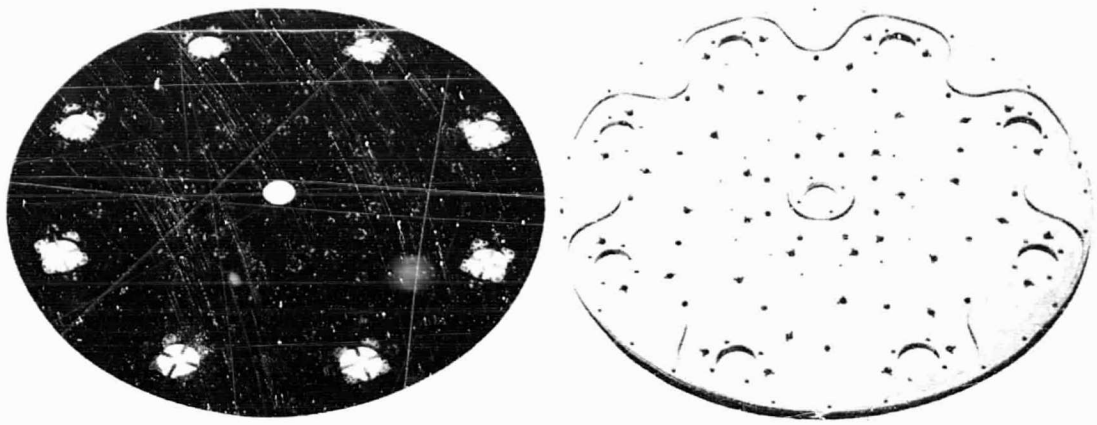

(d) LEFT: TOP STRIPLINE BOARD, BOTTOM VIEW
RIGHT: GROUND PLANE 2, TOP VIEW

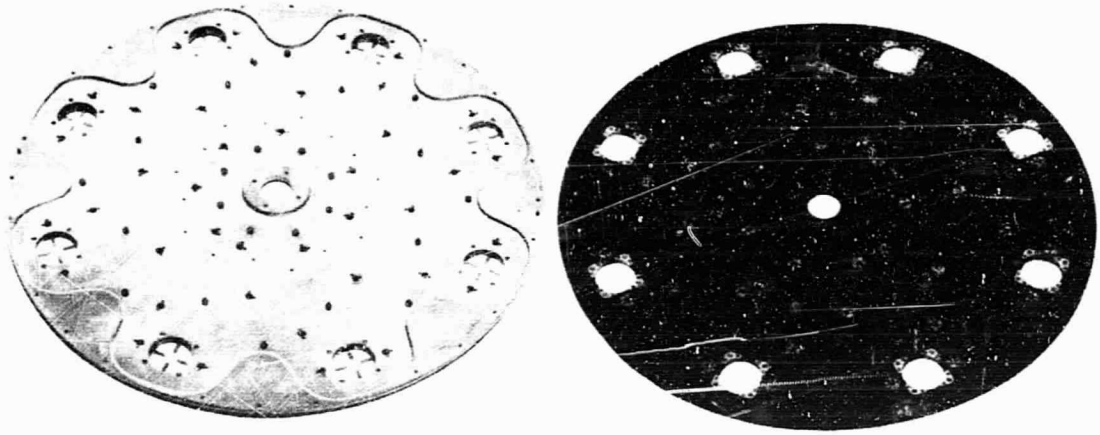

(e) LEFT: GROUND PLANE 3, BOTTOM VIEW
RIGHT: BOTTOM STRIPLINE BOARD, TOP VIEW

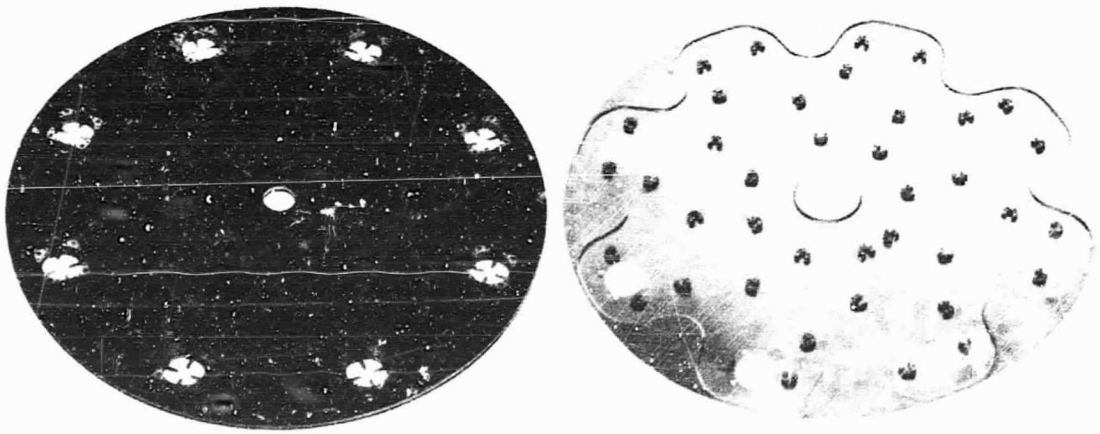

(f) LEFT: BOTTOM STRIPLINE BOARD, BOTTOM VIEW
RIGHT: GROUND PLANE 4, TOP VIEW

Figure 4-2 (Continued)

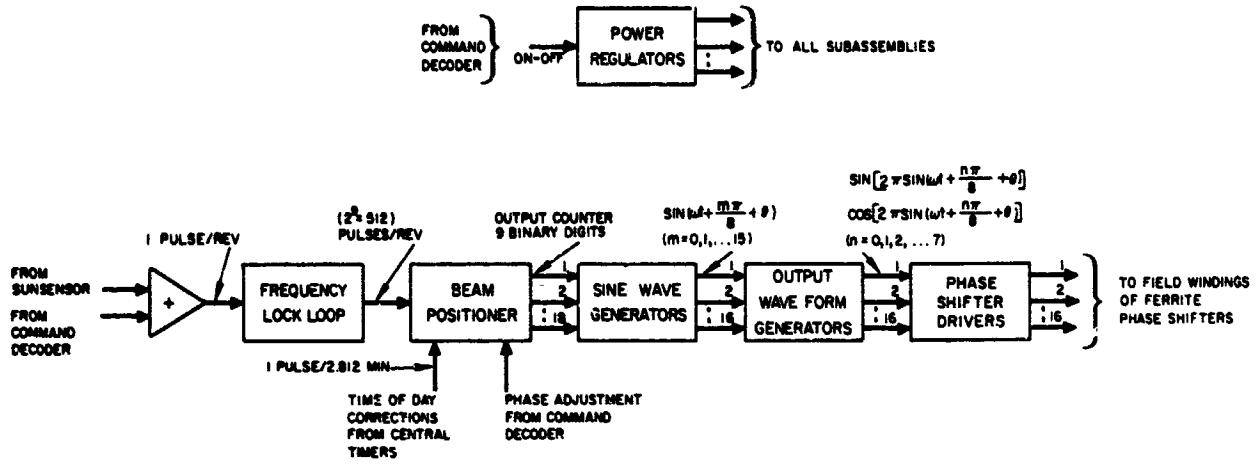

Figure 4-3. System diagram of control electronics for circular phased array.

proper phase to position the beam. The change in the relationship between the spacecraft, the earth, and the sun is automatically accounted for by injection of an additional pulse into the beam positioner every 2.812 minutes. The sine wave generators drive output waveform generators and phase shifter drivers which provide the required waveforms for the coils of the phase shifters.

4.1.4 Array Performance Characteristics

The array gain as measured at 4100 Mc is just over 13 db. This value includes losses due to mismatch, shadowing of elements in the array, stripline losses, element matching network losses, and phase shifter losses. Combined stripline and phase shifter losses are between 1.5 and 2.0 db. Loss through a typical phase shifter is about one db. This figure will vary over the range of operating temperatures by about ±1/4 to ±1/2 db, depending on the operating frequency. Measurements of departure of phase shift from linearity for various temperatures are not available for the presently used ferrite, but from the available data, performance similar to that of previous models is expected. The results of measurements on the earlier models are illustrated in Figure 4-4. In the figure, the departure of the incremental phase shift of five units

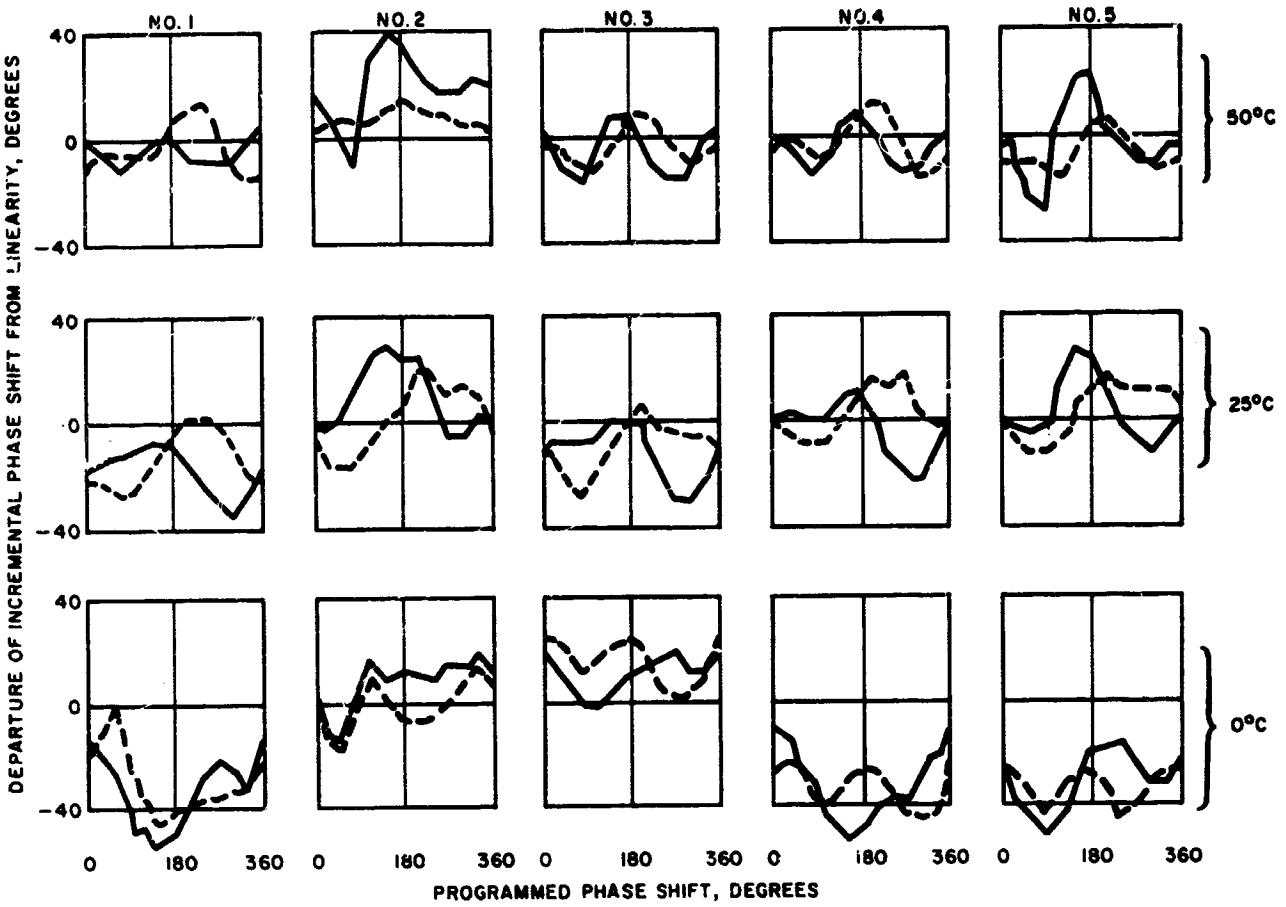

Figure 4-4. Departure of incremental phase shift versus programmed phase shift for various temperatures.

is plotted as a function of the programmed phase shift for temperatures of 0°, 25°, and 50° C. Each unit has two outputs which feed diagonally opposite elements in the array.

Matching network losses for the circular array are 1 to 2 db, and mutual coupling losses are estimated at about 0. 5 db. These losses and those of the strip transmission line and phase shifters essentially account for the reduction from the calculated gain figure (excluding losses) of about 18 db. It is thought that the losses could be reduced by at least 2 db yielding an antenna with a gain of nearly 16 db. The amplitude modulation of the beam peak as it is spun is about ±0. 4 db from the average level.

4.2 DIODE-IRIS CONTROLLED TRAVELING-WAVE ARRAY

The feasibility of accomplishing electronic scanning of an antenna with diode-iris slot control has been demonstrated in the design of an experimental 10-element traveling-wave array. Ten four-diode-iris devices (Section 3.3.2) were fabricated for use in this array.

4.2.1 Antenna Components

The linear array proper consisted of a milled-rectangular waveguide fixture, 0.900 inch wide and 0.260 inch high, and a top plate that contained ten uniformly spaced slots on the center line. Each diode was inserted into the waveguide through holes in the bottom wall and fastened by one lead in the top plate and by the other lead through the bottom wall to an r-f choke assembly (see Figure 4-5). Control of the slot excitation was achieved by biasing the four diodes through their choke assemblies.

The slot interspacing $\underline{d}$ was chosen to be 0.586 λ_o or 0.738 inch to accommodate a reasonable spacing between consecutive four-diode-iris clusters. The reduced height waveguide array utilized linear-tapered transitions as impedance transformers at the ends to provide a smooth transition into standard X-band waveguide test equipment. The VSWR for each transition was about 1.05:1.

In addition to the array proper, diode-bias control circuits and chokes were designed and fabricated.

4.2.2 Aperture Distributions

The demonstration of electronic scanning included the generation of sum and difference patterns at selected positions in space in a 90-degree angular sector. The aperture phasing was selected to generate sum patterns at θ = 0 degree, ±28.2 degrees, and ±45 degrees, and difference patterns at θ = 0 degree and +45 degrees. The necessary progressive phase shift α along the array for a particular scan angle θ was computed from the equation

$$\alpha = \pm \frac{2\pi d}{\lambda_o} \sin \theta = \pm 211^\circ \sin \theta \qquad (4\text{-}10)$$

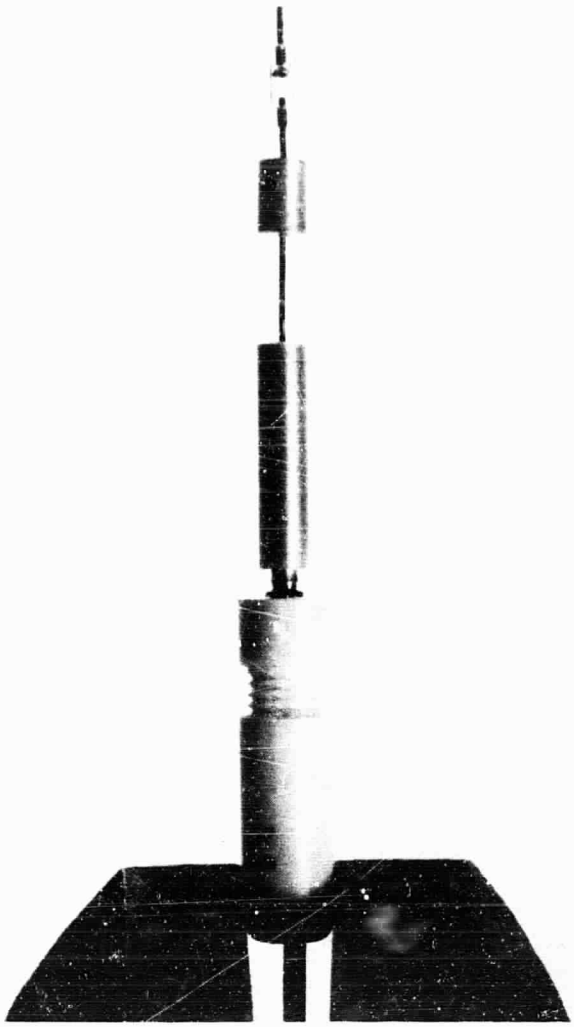

a) diode mounted on choke assembly

where

λ_o = free space wavelength

d = 0.586 λ_o = element interspacing

Seven aperture distributions were set up in the array with the diode-irises using a microwave phase bridge circuit. The bridge circuit utilized a radiation sampling probe, mounted on an accurately driven carriage, to obtain the relative phase and amplitude of each element in the aperture. A close view of this portion of the phase bridge is shown in Figure 4-6 along with a schematic of the entire phase bridge circuit.

4.2.3 Pattern and Gain Measurements

After the diode voltages needed to generate the seven aperture distributions had been recorded, the linear array and associated control panel were

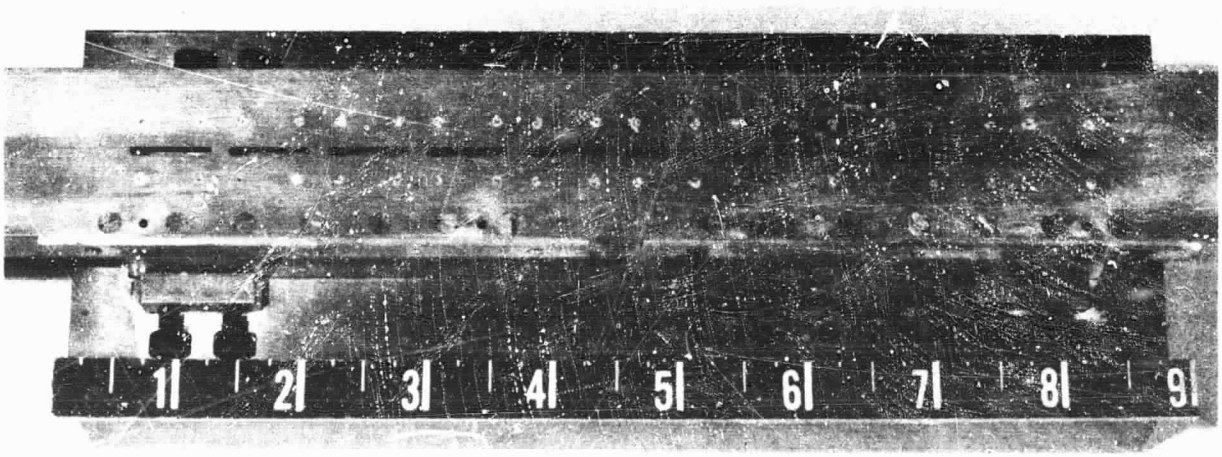

b) top view of array

Figure 4-5. Ten-element diode-iris array.

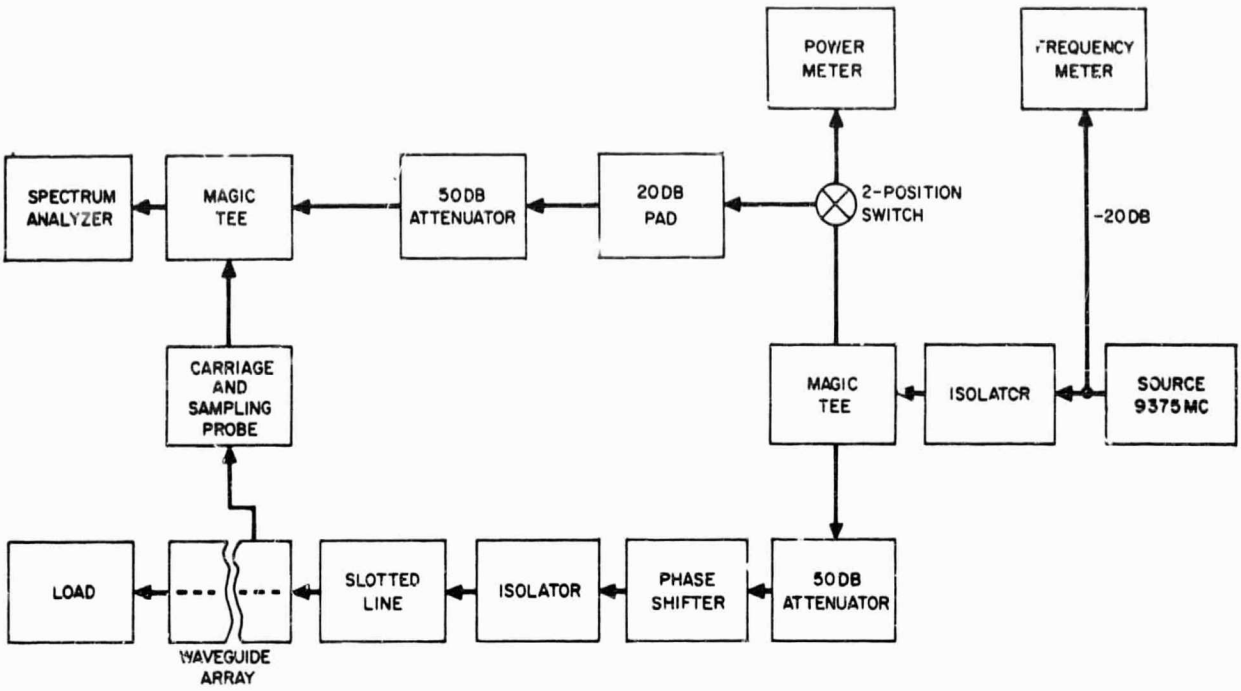

a) schematic of entire circuit

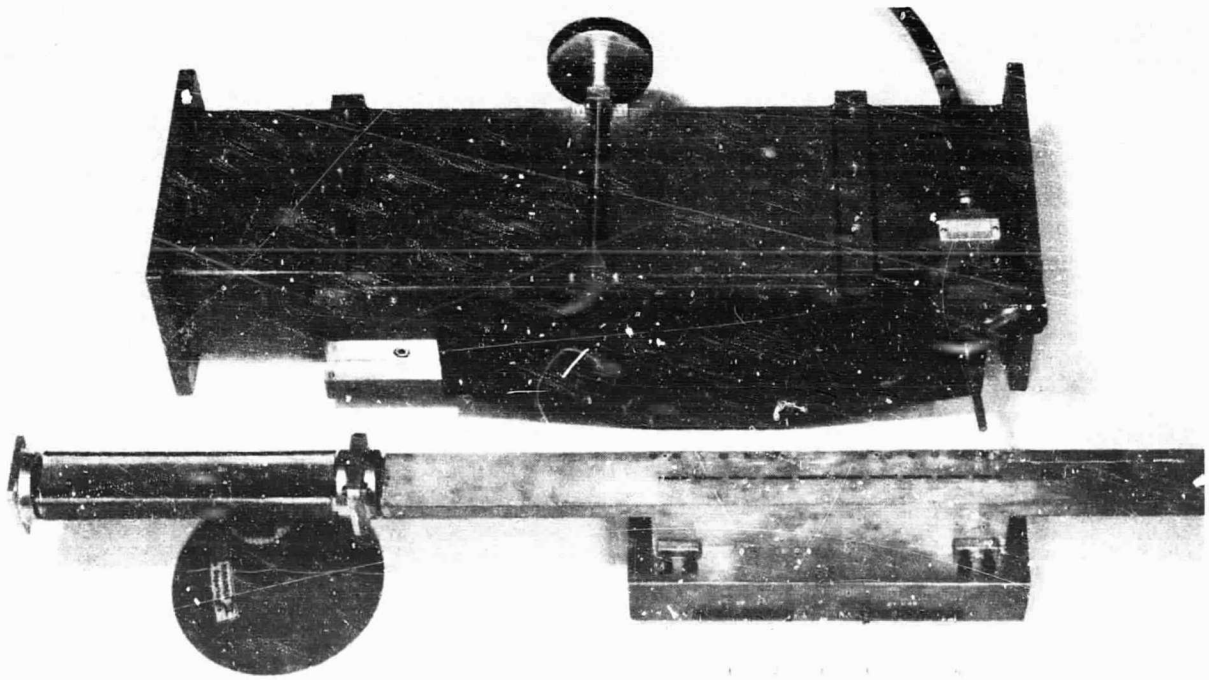

b) carriage and sampling probe

Figure 4-6. Phase bridge circuit used for obtaining phase and amplitude distribution in linear array aperture.

moved and mounted on the turntable in the Hughes anechoic chamber; in addition, ground planes were attached to the linear array. The diode voltages were reproduced for each distribution, and patterns and gain measurements were taken. Figure 4-7 shows a composite grouping of the five sum patterns that were taken at 9.375 Gc. These patterns demonstrate the feasibility of the diode-iris technique to electronically scan the main beam of the linear array ±45 degrees about the array normal. All beam pointing directions were accurate to within one degree of theoretical prediction.

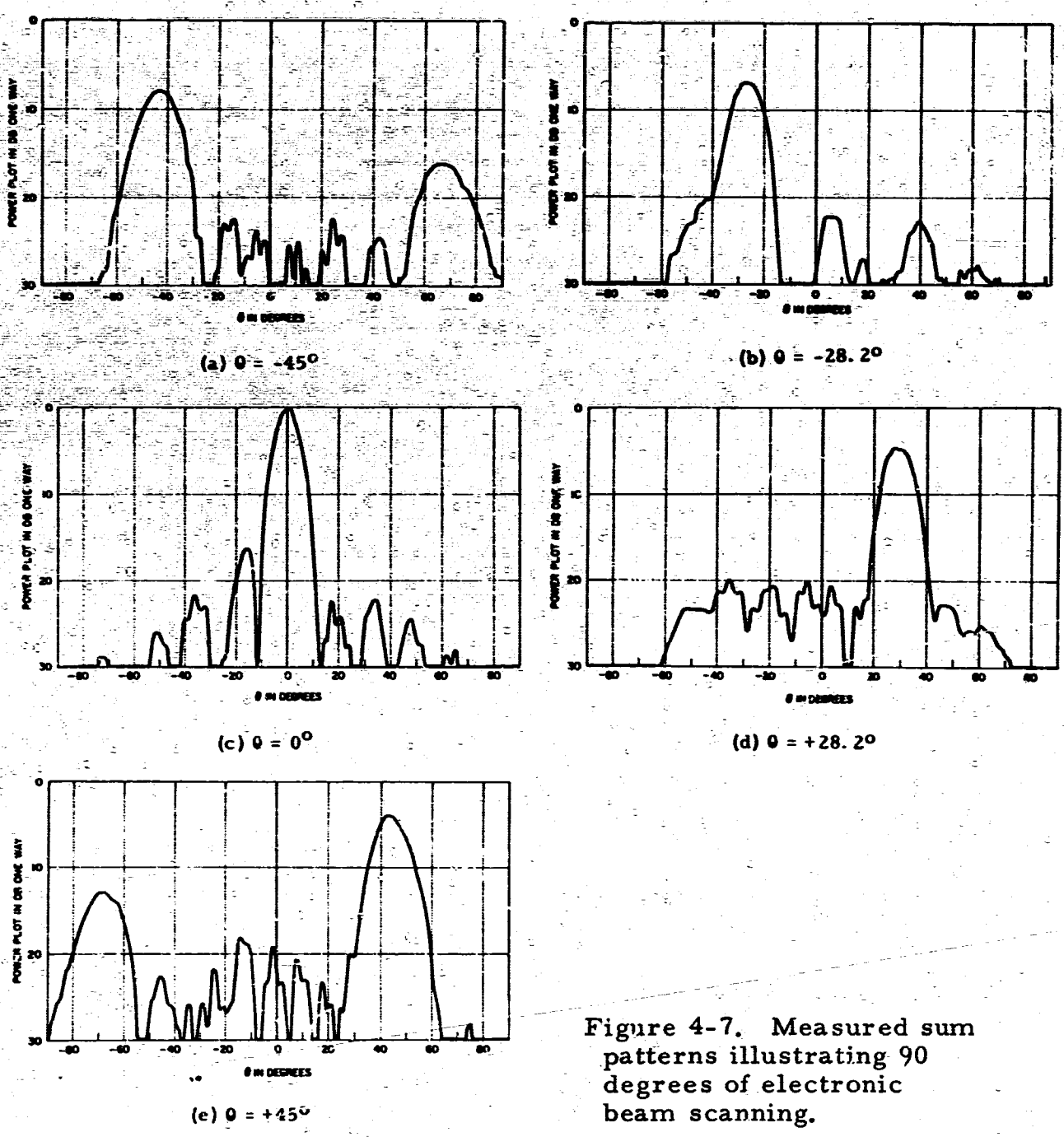

Figure 4-7. Measured sum patterns illustrating 90 degrees of electronic beam scanning.

Difference patterns at θ = 0, +45 degrees were recorded and the corresponding sum patterns are compared with the predicted patterns in Figure 4-8. The predicted patterns were calculated using the amplitude and phase values of each element obtained in the phase bridge circuit; these excitations were then programmed into a computer and the patterns calculated. Good agreement between prediction and measurement was realized. These results are indicative of the accuracy achieved in controlling the phase progression and amplitude distribution in the aperture. The high sidelobes seen in the sum patterns for θ = ±45

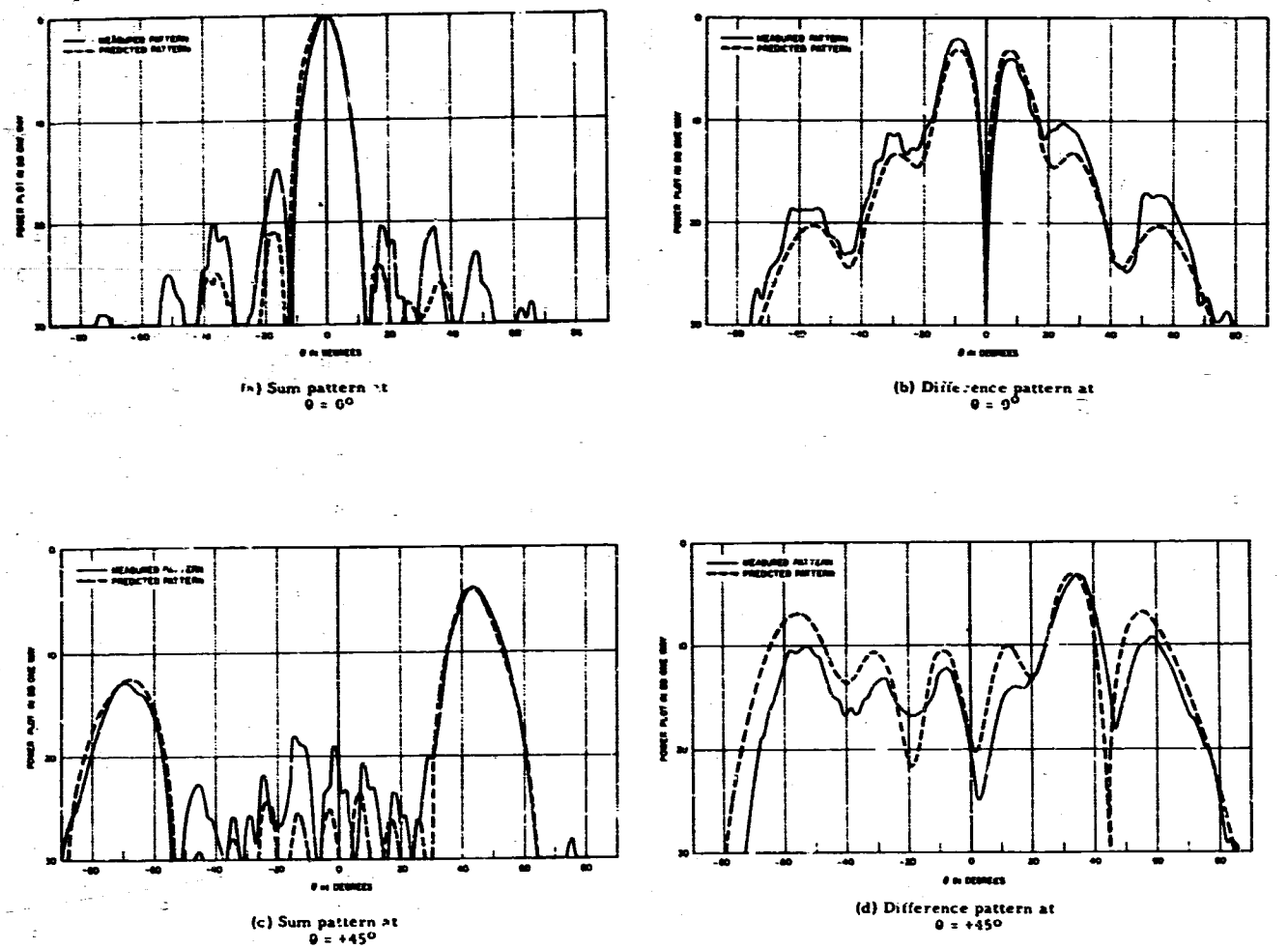

Figure 4-8. Comparison of predicted and measured sum and difference patterns for selected scan angles.

degrees are second-order beams due to the position of the scanned beam and the spacing between slot radiators. These beams are predicted by the theory and are not a limitation of the technique.

For the broadside pattern, the antenna gain was computed to be 13.2 db. The measured gain for the array was 5.7 db. The power delivered to the load and the reflection loss account for 0.75 db of this gain difference; the ten diode-iris devices account for 6.75 db, or about 0.68 db per unit which agrees with the value anticipated.

4.3 REFLECTOR AND FEED SYSTEMS

The possibility of using reflector and feed systems to obtain electronic beam positioning has been considered. The beam pointing direction could theoretically be controlled by switching among various feeds that would be positioned to direct their corresponding beams in the desired pointing directions; adjacent beam crossover levels of -3 db have been assumed to give satisfactory coverage. It has not been possible to investigate all conceivable reflector feed configurations, but several representative configurations were considered.

4.3.1 Paraboloidal Reflector and Feeds

The possibility of using a paraboloidal reflector on a gravity-gradient stabilized satellite has been considered. In this application the reflector would be located on the base of a cylindrical or cubical satellite structure with the antenna axis directed along the satellite axis. In the absence of librations this axis would be directed through the center of the earth.

Kelleher and Coleman (1952) and Jasik (1961a) have reported the off-axis scanning capabilities of paraboloidal reflectors. They found that only limited scan angles may be achieved without serious sidelobe and gain degradation. For example, a scan of about 5 half-power beamwidths with a 30-inch reflector, which had a 3-degree half-power beamwidth and a 20-db aperture taper showed a gain loss of about 1.5 db. The sidelobe level increased from about -26 db to about -14 db, an increase of approximately 8 db. These measurements were taken using a single feed horn mechanically moved off the axis.

The use of multiple feeds to obtain electronic beam positioning poses even more of a problem. To scan the beam off axis by an angle, Θ, it is necessary to move the feed off the axis by an angle, Φ, subtended at the reflector vertex. (See Figure 4-9.) The angle Φ is somewhat greater than Θ but for a particular value of f/D the two angles are proportional. For f/D = 0.75, which was the best value examined by Kelleher and Coleman, the value of Φ is given by

$$\Phi \approx 1.05\Theta \tag{4-11}$$

From Figure 4-9b it may be seen that the feed displacement, d, required for a given scan angle is

$$d = \left(\frac{f}{D}\right) D \tan \Phi \tag{4-12}$$

which, for $\frac{f}{D} = 0.75$, becomes

$$d = 0.75\ D \tan(1.05\Theta) \tag{4-13}$$

For purposes of illustration the aperture distribution is assumed to vary as $(1 - r^2)$ over the plane of the aperture, where r is a normalized

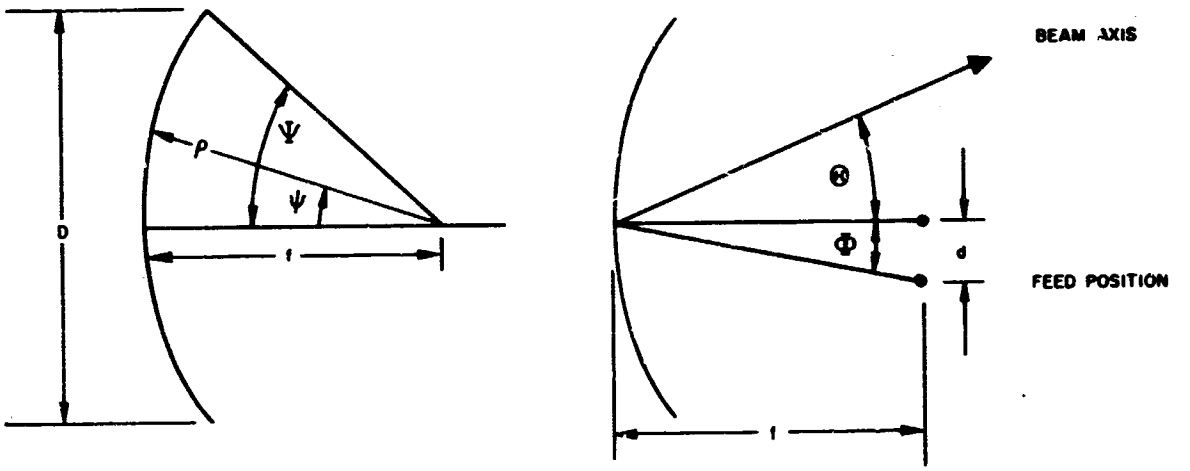

(a) PARABOLOIDAL COORDINATE SYSTEM (b) SCAN ANGLE AND FEED POSITION

Figure 4-9. Paraboloidal reflection geometry.

aperture variable (r = 1 at edge). Then for the half-power beamwidth of the pattern, there is the relationship from Silver (1949a)

$$(BW)_{HP} = 1.27 \frac{\lambda}{D} \tag{4-14}$$

If the minimum scan angle is to be one-half power beamwidth, then

$$d_{min} = 0.75\ D \tan (1.34 \frac{\lambda}{D}) \tag{4-15}$$

which, for large D/λ, reduces to

$$d_{min} \approx \lambda$$

The second feed must be located one wavelength distant from the axis regardless of the diameter of the dish. To position another beam scanned one additional half-power beamwidth off axis, a third feed spaced 2 wavelengths off the axis is required, etc.

In addition to feed spacing, the sizes of the primary feed apertures necessary to obtain desirable secondary aperture distributions are of importance. For an f/D ratio of 0.75 and a 10 db secondary aperture taper, the primary radiation pattern at the reflector edge (Silver, 1949b) must be down by

$$\frac{G_P(\psi)}{G_P(0)} = \frac{1}{10 - 5 \sin^2 \psi} = \frac{1}{9.19} = 0.109 \tag{4-16}$$

or 9.63 db below the peak of the primary pattern. If this figure is to be obtained in the H-plane of a primary horn radiator, the horn dimension in that plane must be at least $1.67\ \lambda$. In the E-plane a dimension of $1.17\ \lambda$ is necessary to obtain the proper primary pattern (Jasik, 1961b). It appears that the requirements on feed dimensions and relative feed positions are incompatible if a separate feed is considered for each beam position. This problem might be solved by using some more

complicated feed system of overlapping feed horns in which groups of smaller horns would be shared in various manners for the individual beam positions. Another approach would be to locate arrays of small radiators in the focal plane to synthesize the primary feed aperture. Switching groups of elements in the array on and off would provide the required effective motion of the primary aperture. Continuous shifting of power from one group of primary radiation to another, rather than discontinuous switching, would make possible continuous beam scanning.

A similar but somewhat more sophisticated approach has also been described in the literature (White and DeSize, 1963). An array of feeds is disposed on a spherical surface of radius r concentric with the reflector focus (illustrated in Figure 4-10). By adjusting amplitudes and phases of these primary feed elements, the reflector illumination can be adjusted to obtain beam scanning. The phase errors that usually result when a single feed is moved away from the focus may be reduced with this technique by phasing the elements to correct for these errors. In effect, the beam of a large aperture is scanned by feeding it with a smaller aperture formed by a phased array. Finer control of amplitude and phase is obtainable as the spherical radius r is made larger. However, the maximum size is limited by the amount of aperture blockage that results as well as by the number of elements and control equipment

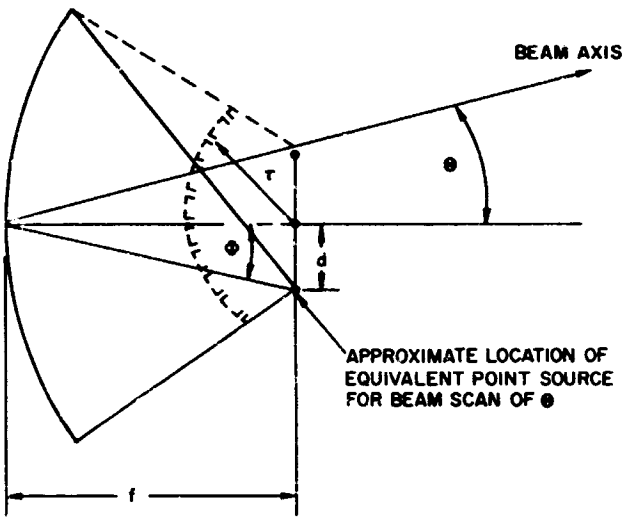

Figure 4-10. Paraboloidal reflector with array primary feed for scanning

required in the primary array. White and DeSize have presented calculations for a system using 31 feeds and a 120-λ aperture. For a ten-beamwidth scan, pattern deterioration was not excessive. First sidelobes changed from -22 db at zero scan to about -18 db at maximum scan. The first nulls also tended to fill in to a great extent. The main beam shape was relatively unaffected.

The use of horn clusters or arrays for scanning presents aperture blockage problems which will degrade gain and sidelobe levels from the ideal design values. For a satellite in a synchronous orbit, such a cluster would be required to position the beam within a cone of half angle 18°. A planar cluster in the focal plane would result in aperture blockage of close to 47 percent. A spherical cluster as illustrated in Figure 4-10 would result in somewhat greater blockage. Since this blockage occurs in the region in which the aperture illumination is normally maximum, the resulting reduction in aperture efficiency due to blockage alone would be about 3 db or more. The degradation predicted by Kelleher and Coleman (1952) is optimistic since their investigation was limited to only a single feed horn. Methods exist for reducing the effect of aperture blockage for non-electronically scanned reflectors. These use polarization rotation techniques to reduce the effect of the blocking structure on the secondary wavefront. However, the complicated nature of the feeding structures required for electronically scanned reflectors make the applicability of such techniques questionable at this time.

For these reasons, the use of a paraboloidal reflector for electronically scanning a narrow beam over the angular regions of interest in this application does not appear too desirable. For situations requiring scanning of only a few beamwidths, it may be acceptable.

4.3.2 Spherical Reflectors

A second type of reflector which might be considered for application of gravity-gradient stabilized satellites on mission 1 is the spherical reflector. Ashmead and Pippard (1946) and Li (1959) have demonstrated that the symmetry of the spherical surface eliminates

beam deterioriation over wide scan angles, at least when a single movable feed is used to scan the beam. When a cluster of switched feeds is used for electronic beam steering, however, perfect symmetry is not maintained as various feeds are connected, so that some beam shape changes might be expected to occur as the beam is stepped throughout the required coverage region. Other factors also affect the applicability of the spherical reflector to electronically scanned antennas.

Figure 4-11 illustrates the geometry and some of the parameters of importance in spherical reflector antennas. The distance a is the radius of the effective aperture which subtends an angle ψ at the primary feed which is located on the focal locus and is directed at the reflector along a radius from the reflector center. If the beam is to scan to a maximum angle, ζ_m, from the reflector axis, then the following must hold if excessive spillover is to be avoided.

$$a = R \sin \left(\frac{\Theta}{2} - \zeta_m\right) \tag{4-17}$$

The aperture dimension a is determined by system beamwidth requirements and may therefore be considered as a fixed quantity. This then gives a relation between R and Θ

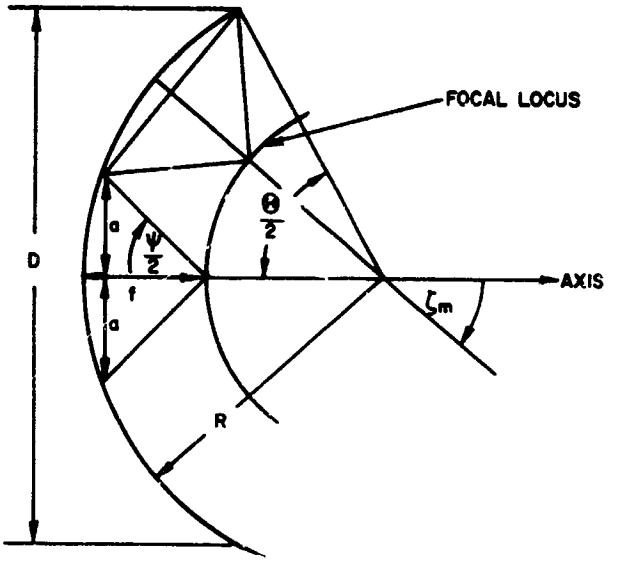

Figure 4-11. Spherical reflector geometry.

The spherical reflector does not have a well defined focus so that a point source feed gives rise to phase errors over the aperture. According to Li these are minimized, for a given ratio $\frac{a}{R}$, when f is given by

$$\frac{f_{cpt}}{R} = \frac{1}{4}\left(1 + \sqrt{1 - \left(\frac{a}{R}\right)^2}\right) \tag{4-18}$$

Li also states that, for a given aperture size a, the minimum value of R that may be used to keep the total phase deviation over the aperture within a value $(\Delta/\lambda)_{total}$ is

$$R_{min} = a\left[\frac{(a/\lambda)}{14.7(\Delta/\lambda)_{total}}\right]^{1/3} \tag{4-19}$$

where Δ is the path length deviation and λ is the wavelength. This value of R also minimizes the total reflector diameter D, given by

$$D_{min} = 2R_{min}\sin\left(\frac{\theta}{2}\right)$$

$$\frac{D_{min}}{2a} = \left[\cos\zeta_m + \sin\zeta_m\sqrt{\left(\frac{(a/\lambda)}{14.7(\Delta/\lambda)_{total}}\right)^{2/3} - 1}\right] \tag{4-20}$$

If now it is assumed that the aperture 2a is uniformly illuminated (the primary pattern must in reality be tapered in order that a be limited to a specific value) and a/λ results in a 3° beamwidth, the minimum value of D is

$$\frac{D_{min}}{2a} = \cos\zeta_m + 1.98\sin\zeta_m \tag{4-21}$$

A maximum scan angle of $\zeta_m = 18°$, corresponding to a synchronous altitude orbit, gives the following result

$$\frac{D_{min}}{2a} = 1.56 \tag{4-22}$$

Therefore, only about 41 percent of the physical aperture is available to produce the beam. If the aperture taper is taken into account this area is further reduced. It is apparent that such a system makes very inefficient use of the physical aperture. In addition, aperture blockage will also be a problem area when clusters of feeds are used. The feed problem might be solved by using arrays to form the primary aperture as discussed in the previous section on paraboloidal reflectors. For these reasons the spherical reflector is not too attractive for a scanning antenna.

Other types of reflectors may appear to be adaptable to electronic scanning requirements in certain respects. However, it is felt that the aperture blockage and feeding techniques will remain problem areas and this type of antenna system has not been pursued further.

4.4 LENSES AND FEED SYSTEMS

The use of lenses (Jasik, 1961c) with multiple switched feeds for electronic scanning would apply most readily to a satellite using the gravity-gradient type of stabilization. Various types of dielectric and metal plate lenses have been studied by a number of investigators and are reported in several places (Jasik, 1961d). Summaries of the general principles of the lenses are available in these reports. Only overall results are presented here. The types of lenses to be considered fall into two general categories: lenses with an optical axis and spherically symmetrical lenses.

4.4.1 Lenses with an Optical Axis

Both dielectric lenses and metal-plate lenses whose radiation characteristics are optimum along or symmetrical about a certain axis fall into the class of lenses with an optical axis.

Dielectric lenses are designed on the basis of geometrical optics (Snell's law). The surfaces are chosen in such a way that rays emanating from a point (focus) on one side of the lens emerge as parallel rays on the opposite side of the lens. The radiation pattern of the lens is computed from the resulting field distribution over an aperture near the lens surface.

Metal plate lenses may be designed on a similar optics basis, but one type, the so-called constrained lens, does not depend on Snell's law for its operation and merits separate discussion.

General Scanning Considerations. Most optical systems can be designed so that there are no phase errors over a given plane aperture for one particular position of the feed, usually the lens axis. When the feed is removed from this position, however, the resulting aperture distribution has phase errors which contribute to beam pointing error, pattern asymmetry, gain reduction, and increased sidelobe levels. With dielectric lenses it is possible, through use of the Abbe sine condition (Drude, 1925), to improve the off-axis pattern characteristics. When this condition is satisfied, "coma" effects are reduced for source positions near the lens focus and lens scanning performance is improved. Even with this improvement, scanning is still restricted to relatively small angles.

With the constrained type of metal-plate lenses, it is possible to design a system with no phase errors over the aperture for two positions of the feed. This design can result in greatly improved wide angle scan performance for well-designed lenses. Examples of these two types of lenses are discussed in the following paragraphs.

A Wide-Angle Scanned Dielectric Lens. An example of a wide-angle scanned dielectric lens that employs the Abbe sine condition to improve scanning performance is discussed by Friedlander (1946). The lens has a constant dielectric with a plane surface on the feed side, as illustrated in Figure 4-12. The ideal value of the index of refraction, n, was found to be $n = 1.618$ but Friedlander used a slightly different value. For a lens in which $D = 50\,\lambda$, he was able to obtain a scan of $\pm 10°$ from the axis with satisfactory beam performance. If it is assumed that the aperture illumination was tapered as $\left[1 - \left(\frac{\rho}{2D}\right)^2\right]$, then the half-power beamwidth of the antenna is given by

$$(BW)_{1/2} = 1.27 \frac{\lambda}{D} \text{ radians}$$

$$(BW)_{1/2} = 1.45° \qquad (4\text{-}23)$$

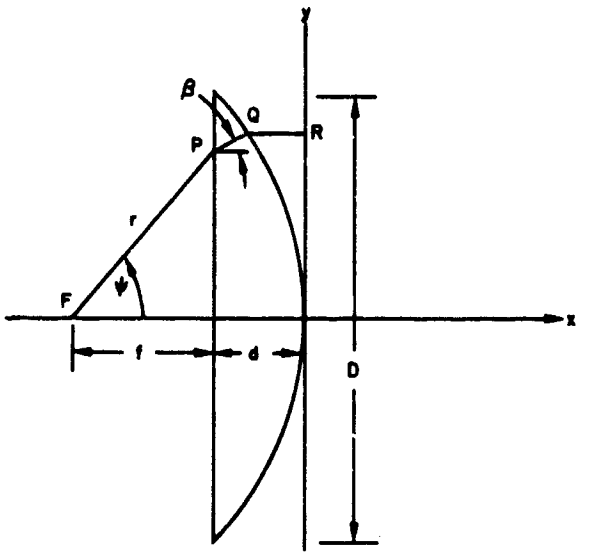

Figure 4-12. Wide-angle scan dielectric lens.

Thus, the scan angle is equivalent to 6.9 half-power beamwidths. If the D/λ ratio is halved by reducing the frequency, the beamwidth would increase to about 3° and a scan angle of ±15° to ±20° might be achievable within the same limits of phase error over the aperture. This result would depend on how the phase error distribution over the aperture varied with feed position, so that the number of beamwidths which would be scanned is not independent of frequency. Even lenses designed for wide-angle scanning of fairly narrow beams are still restricted rather severely in their scan capabilities.

Another area of interest, similar to that involved in the reflector scanners discussed in Section 4.3, is the compatibility of feed dimensions and required feed positions when multiple feeds are used. As an example, the lens discussed by Friedlander had a ratio of focal length, f_o, to lens diameter, D, of unity. To scan the beam off the axis by a small angle, θ, the feed had to be moved off the axis by an amount a, where a is given by

$$a \approx f_o \theta$$

For the aperture taper assumed above, a must take on the following value to scan off axis by a half-power beamwidth:

$$a \approx \frac{f_o}{D} 1.27\lambda \qquad (4\text{-}24)$$

For f/D = 1.0 this value gives

$$a = 1.27\lambda \qquad (4\text{-}25)$$

The aperture subtends a half angle of 2[illegible] at the feed and if the primary pattern is to be confined to this region of the lens, i.e., no excessive spillover, a minimum feed aperture of the order of 1.5λ is required (Jasik, 1961b). Therefore, primary feed apertures for adjacent beams must overlap to obtain the desired scan. Thus, an array technique would be required for feeding such a lens. However, in order to obtain wide angle scan, this primary feed array would have to be phased to correct for lens aberrations; otherwise, only limited scan is achievable. In view of the rather limited scan angle achievable without phasing, this lens system is apparently not generally applicable to the space missions of interest.

Wide-Angle Scanned Constrained Lens. Constrained lenses, which do not obey Snell's law, may be designed to scan over fairly broad angular regions. These lenses use parallel metal plates which constrain the waves to follow prescribed paths. If the metal plates are arranged in an egg-crate fashion so that they form square dominant mode waveguides, then waves of any polarization will be accepted and constrained to follow these waveguides. By adjustment of the input and output surfaces of these lenses, desirable radiation characteristics may be obtained over relatively wide scan angles. Such lenses are discussed by Ruze (1950), and the example considered here is as illustrated in Figure 4-13.

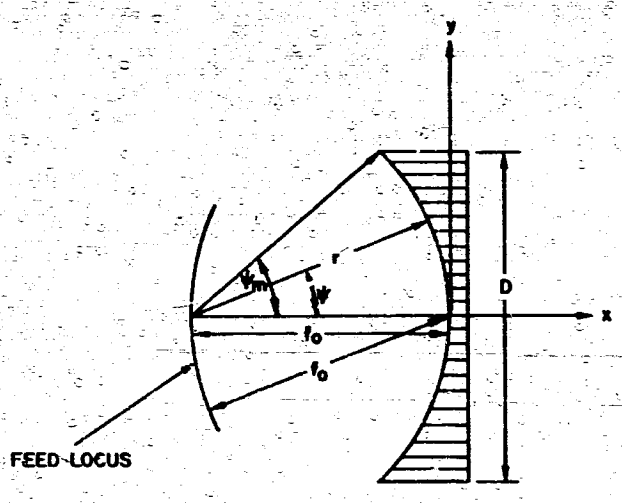

Figure 4-13. Constrained lens.

The lens considered is a two-dimensional lens. However, the general technique applies to three-dimensional lenses, though the actual numbers obtained for that case would be different. The lens aperture, D, is 72 wavelengths

and $f_o/D = 1.5$. It is so designed that, with the feed located on a feed locus of radius f_o, there are no phase errors in the aperture for feeds positioned at angles of ±45° with the axis. With the feed on axis at $-f_o$, there is no quadratic phase error over the aperture. Under these conditions the antenna was capable of scanning a 1° (half-power beamwidth) beam over a ±50° range. Ruze also gives a relation between the f/D ratios, the half-power beamwidth, and θ_s, the <u>total</u> scan angle, for this type of lens as

$$\theta_s = 93° \left[BW^{o}_{1/2} \left(\frac{f_o}{D} \right)^2 \right]^{1/3} \qquad (4\text{-}26)$$

For the particular antenna considered, it can be found that $BW^{o}_{1/2} = 65° \lambda/D$ so that

$$\theta_s = 374° \left[\lambda/D \left(\frac{f_o}{D} \right)^2 \right]^{1/3} \qquad (4\text{-}27)$$

For $D = 75\lambda$ and $f_o/D = 1.50$, this relation gives $\theta_s = 113°$, in substantial agreement with the experimental results. If D/λ were decreased by a factor of 3, i.e., if the beam had a half-power width of 3°, then the scan angle θ_s, is increased to $\theta_s = 163°$ so that a sector of ±81 degrees could be scanned.

It is also of interest to relate the required feed aperture size to the relative feed positions required to move the beam by a half-power beamwidth. For the wide-angle constrained lens, the half-power beamwidth corresponds approximately to that due to an amplitude distribution over the aperture given by (Ruze, 1950)

$$g(y) = \cos^2 \left(\frac{\pi}{m} y \right) \qquad m > D \qquad (4\text{-}28)$$

where m is adjusted so that at the aperture edge $g(D/2) \approx 0.38\, g(0)$. This relationship corresponds to an efficiency (including primary pattern spillover) o 85 percent (reflection and dissipation losses neglected). At $\psi = \psi_m$ the primary pattern required to give this taper must be 0.388 of its maximum value. For the f_o/D ratio of 1.50, $\psi_m = 18.75°$ and the minimum feed aperture must have a dimension of 2.8 λ (Jasik, 1961b). However, to scan the beam by a half-power beamwidth, the feed moves only

$$\ell = BW_{1/2}\, f_o \tag{4-29a}$$

which, for this lens, gives

$$\ell \approx 1.96\, \lambda \tag{4-29b}$$

Once again, primary feed apertures must overlap to obtain proper coverage. However, in view of the relatively wide-angle scan achievable with such a lens, investigation of feeding techniques that would permit electronic scan of such a lens might be worthwhile.

Feeding Techniques. In all the reflector antennas and lens antennas considered, it was shown that the primary aperture dimensions required are greater than the displacement of the primary aperture necessary to obtain a scan of one half-power beamwidth. Thus, to obtain electronic scanning, it appears that the primary aperture must be composed of an array of small (i. e., approximately half wavelength) radiators which can be excited in combinations to produce the desired effective primary aperture. If this array were conformal with the locus of the focal point as the array is scanned, then the array elements could be fed in phase and only on-off switching or a smooth transfer of power between elements would be required to obtain beam scanning. This technique would not be able to correct for aberrations resulting from the effective motion of the primary aperture.

The technique of White and DeSize (1963) already mentioned in Section 4. 3. 1, on the other hand, uses a surface which usually does not coincide with the locus of focal points and thereby requires phase as well as amplitude control to achieve proper illumination. It is capable of correcting for various aberrations that might otherwise occur in electronic scanning but is more complicated than the system without phase control. Since in lens antenna systems aperture blocking would not be a problem, either technique might be applied. The relative merits of each would depend on the particular system requirements. In any event additional investigation of the techniques would be required before any specific recommendations could be made.

Losses. Several effects contribute to losses in lens antennas (Jasik, 1961e). In both dielectric and metal-plate lenses, reflection losses occur at the air-dielectric or air-metal plate interfaces. These losses depend on polarization and incidence angle of the radiation as well as on the effective lens dielectric constant and may result in a gain reduction of 1/2 db. They may be reduced by the use of matching techniques into and out of the lens. Dissipation losses in dielectric lenses may also be a problem; however, they depend on the type of lens and the loss tangent of the material used. For low-loss dielectric lenses (loss tangent = 0. 001) which are zoned to keep them thin, dissipative losses are on the order of less than 0. 1 db.

Spillover losses of 1 to 2 db may also occur in lens antennas. The exact amount depends on the type of lens used, its f/D ratio, the required aperture distribution, and the type of feed used, so that specific numbers cannot be given.

4. 4. 2 Spherically Symmetric Lenses

Spherically symmetric lenses are those that do not have any preferred optical axes and, therefore, maintain their radiation characteristics for all positions of a feed. They are inherently wide-angle scan lenses. Several types are of interest:

1) Luneberg lens

2) Constant dielectric lens

3) Broadbeam Luneberg lens

Luneberg Lens. The Luneberg lens is a sphere of dielectrically loaded, radar-transparent material. The dielectric constant increases from that of air at the periphery to twice this value at the center. The rate of increase is such that a plane striking the lens from any one direction is focused at a point on the opposite side of the sphere. If an open waveguide feed is placed at this focus, the energy will propagate down the waveguide. A second waveguide placed adjacent to the first will produce a second beam adjacent to the first, and if the two waveguides are sufficiently close, the two beams will overlap. Because of diffraction effects, the beams that are formed have finite angular beamwidths and sidelobes; in fact, the complete radiation pattern of one of these beams is very much like the radiation pattern of a planar aperture of the same diameter.

Eaton (1953) and others have shown that the paths followed by the rays in an ideal Luneberg lens lie in planes and have elliptical shapes. For the standard Luneberg lens with one focus on its surface and the other diametrically opposite at infinity, the equation of a ray is given by

$$\rho^2 = \frac{\sin^2 \delta}{1 - \cos \delta \cos (2\theta - \delta)} \qquad (4\text{-}30)$$

where ρ and θ are the polar coordinates in the plane containing the ray as defined in Figure 4-14. The ray makes the initial angle δ with respect to the axis of the lens and leaves the lens at E in a direction parallel to the lens axis. The two solutions for θ in Equation (4-30) for which $\rho = 1$ are $\theta = \pi$ and δ. Therefore, the angular polar coordinate of the ray exit point, E, is the initial angle which the ray makes with respect to the axis of the lens at the focal point F. Thus, if the primary pattern of a feed at the focus point F is omnidirectional and has a radiation pattern of one ray per degree for $-\pi/2 \leq \delta \leq \pi/2$, then there will also be one ray per degree for $-\pi/2 \leq \theta \leq \pi/2$ on the periphery of that plane of the Luneberg lens. The rays on line AB will have a sec θ distribution, θ being measured as the angular polar coordinate to the ray exit point on the periphery of the plane of this Luneberg lens.

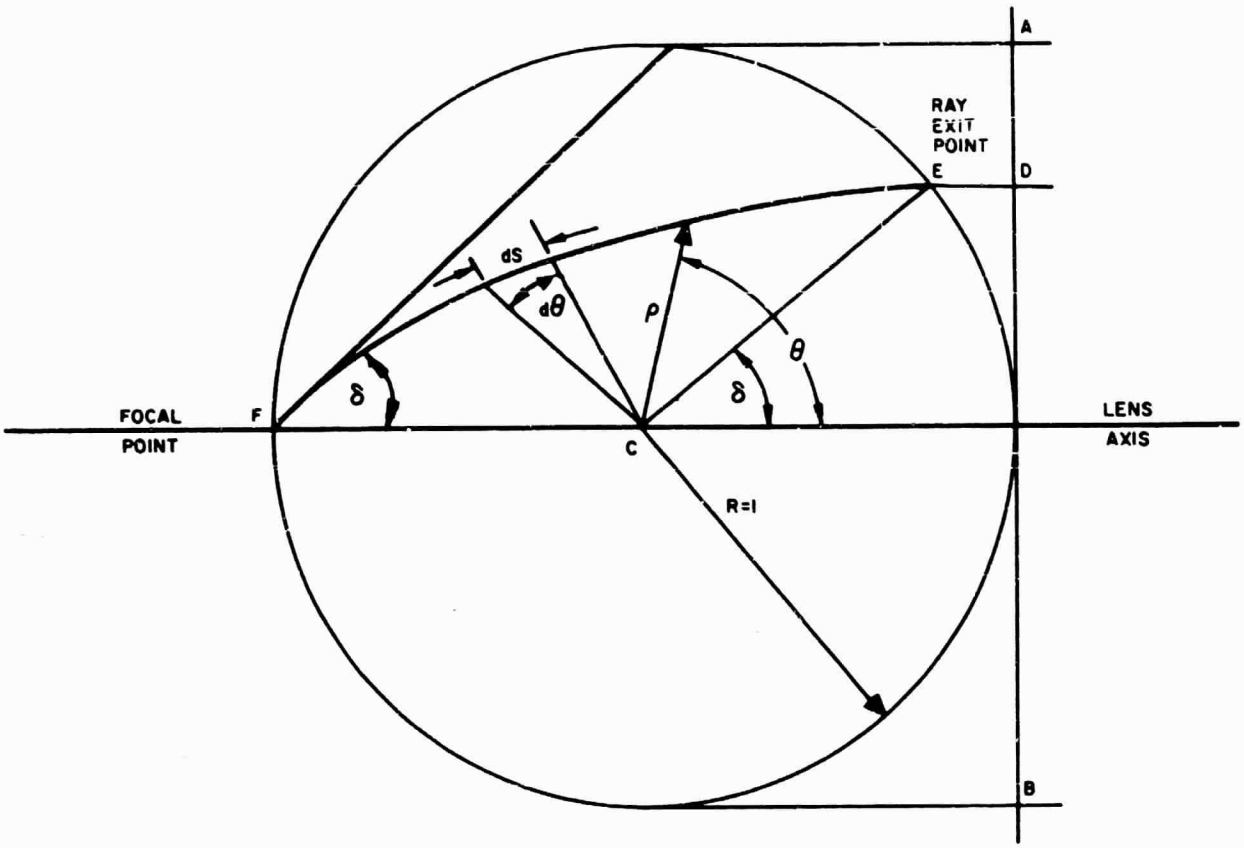

Figure 4-14. Typical ray in an ideal Luneberg lens.

When the primary pattern is that of a horn, which has forward directivity in the form of a cos θ distribution, there results a similar pattern of rays on the periphery of the lens in this plane. The rays on line AB will now have a cosθ secθ or uniform distribution. This reasoning can be carried further to show that a horn feeding a three-dimensional Luneberg lens is analogous to a uniformly illuminated circular aperture which has the size of a great circle of the lens and a center tangent to the lens at a point diametrically opposite the feed horn.

That the uniformly illuminated circular aperture is a constant phase front can be verified with reference to Figure 4-14. The change of phase, $d\phi$, for a small change of angle, $d\theta$, is

$$d\phi = \omega \sqrt{\mu\epsilon}\ dS \qquad (4\text{-}31)$$

where

$$dS = \sqrt{\rho^2 + \left(\frac{d\rho}{d\theta}\right)^2}\, d\theta \tag{4-32}$$

and (Luneberg, 1944)

$$\omega\sqrt{\mu\epsilon} = \omega\sqrt{\mu_o\epsilon_o}\sqrt{2 - \rho^2} \tag{4-33}$$

The substitution of Equations (4-30), (4-32), and (4-33) into Equation (4-31) and the integration of θ from δ to π will yield the total change of phase between E and F:

$$\phi_{EF} = \int_{\delta}^{\pi} \omega\sqrt{\mu_o\epsilon_o}\sqrt{2 - \rho^2}\sqrt{\rho^2 + \left(\frac{d\rho}{d\theta}\right)^2}\, d\theta \tag{4-34}$$

The phase difference between D and E is

$$\phi_{DE} = (1 - \cos\delta)\,\omega\sqrt{\mu_o\epsilon_o} \tag{4-35}$$

The total change in phase between D and F is

$$\phi_{DF} = \omega\sqrt{\mu_o\epsilon_o}\left[1 - \cos\delta + \int_{\delta}^{\pi}\sqrt{2 - \rho^2}\sqrt{\rho^2 + \left(\frac{d\rho}{d\theta}\right)^2}\, d\theta\right] \tag{4-36}$$

It can be shown that

$$\frac{\partial\phi_{DF}}{\partial\delta} = 0$$

Thus ϕ_{DF} is constant with respect to δ and the line AB has a constant phase front. This reasoning also can be carried further to show that

there is a constant phase front over a circular aperture whose size is that of a great circle of the lens and whose center is tangent to the lens at a point diametrically opposite the feed.

It has been shown by this heuristic argument that a horn feeding a Luneberg lens is analogous to a circular aperture of uniform phase and illumination whose radius is that of the lens and whose center is tangent to the lens at a point diametrically opposite the feed horn. The far field radiation pattern of the Luneberg lens is that of the circular aperture or

$$|E| = \left| \frac{2J_1(ka \sin \theta)}{ka \sin \theta} \right| \tag{4-37}$$

where k is the propagation constant and a is the radius of the lens. The plot of $\frac{2J_1(ka \sin \theta)}{ka \sin \theta}$ versus θ for a 10-inch lens at 6 Gc is shown in Figure 4-15. It shows close correspondence to an actual experimental pattern for a 10-inch lens at 6 Gc (Figure 4-16) and to the exact theoretical electric field pattern for a 10-inch lens at 6 Gc (Figure 4-17; Shapiro, 1963).

A mosaic arrangement of feeds on the surface of the Luneberg lens will generate a similar mosaic of overlapping beams in space on the diametrically opposite side of the lens. The amount of beam overlap can be controlled by the spacing between adjacent feeds. Use of loaded waveguide feeds allows their size and their spacing to be tailored to the particular requirements for any application. Beam overlap at the 3-db points is easily obtained. The gain, beamwidth, and radiation pattern of each beam would be essentially identical. Overall gains of about 3 db and 2-1/2 db below area gain have been obtained, respectively, with an 18-inch diameter Luneberg lens operating at 12.4 Gc and with a 10-inch diameter Luneberg lens operating at 6 Gc (Shapiro, 1962a).

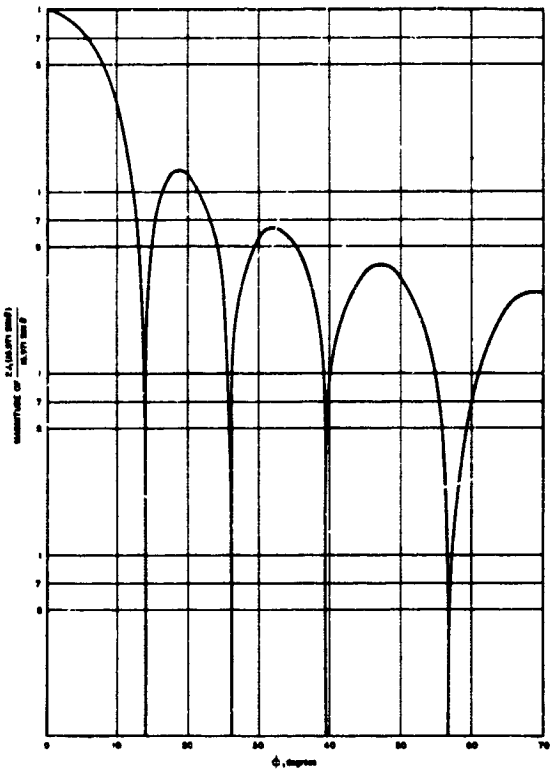

Figure 4-15. Approximate theoretical electromagnetic field.

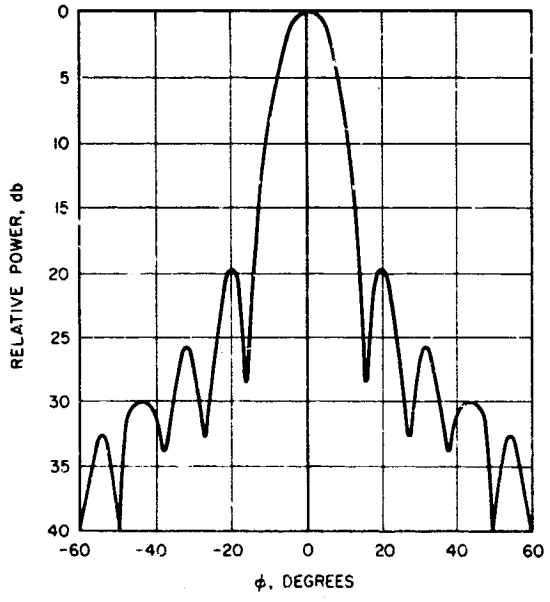

Figure 4-17. Exact theoretical electric field.

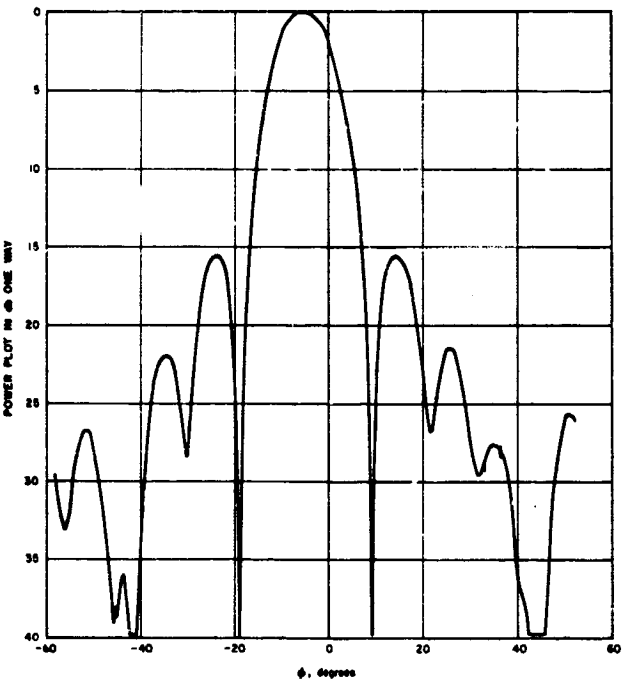

Figure 4-16. Experimental far field pattern.

The mutual coupling effects between a number of feeds placed in close proximity to obtain overlapping beam coverage have been considered. It has been found experimentally that the presence of well-matched adjacent feeds has only a slight effect on radiation patterns. A typical pattern of a 10-inch diameter lens fed by open-ended waveguides at 6 Gc are shown in Figure 4-18 (Shapiro, 1962b). Such a pattern would be acceptable for communication systems.

In addition to the effects of adjacent feeds on the radiation pattern, the effects of aperture blockage at wide scan angles due

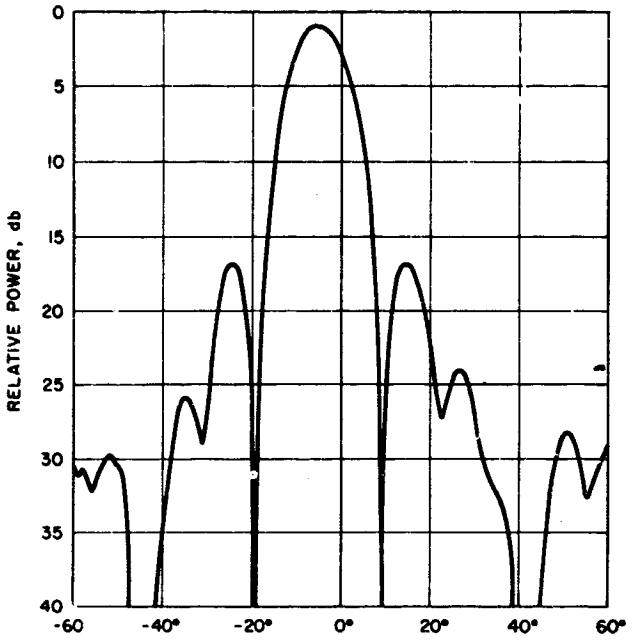

Figure 4-18. Typical pattern of 10-inch Luneberg lens with open-end waveguide at 6 Gc.

to the presence of multiple feeds distributed over the rear of the lens have been measured experimentally. It was found that the effect was negligible for scan over cones of half-angle less than 67° (Shapiro, 1962c).

Several problems exist in the use of Luneberg lenses. One of these is weight; for example, the 18-inch lens discussed above weighs about 36 pounds. A Luneberg lens cannot be zoned to reduce weight as can the other lenses, but artificial dielectrics can be used. A lightweight version of the 18-inch lens would weigh 9 pounds. The artificial dielectric material restricts the use of these lenses to frequencies for which the loading objects and their spacings are small in terms of wavelength. The problem of controlling the dielectric constant in sufficiently small steps also limits the high frequency application of such lenses to the X-band region at the present time. In addition, less gain (about 2 db) is to be expected because of the artificial dielectric material. The beamwidth, however, would be unchanged.

Constant Dielectric Lenses. A spherical lens of uniform dielectric material, commonly referred to as the "constant-K" lens, can be used to obtain wide angle scan. This type of lens has focusing

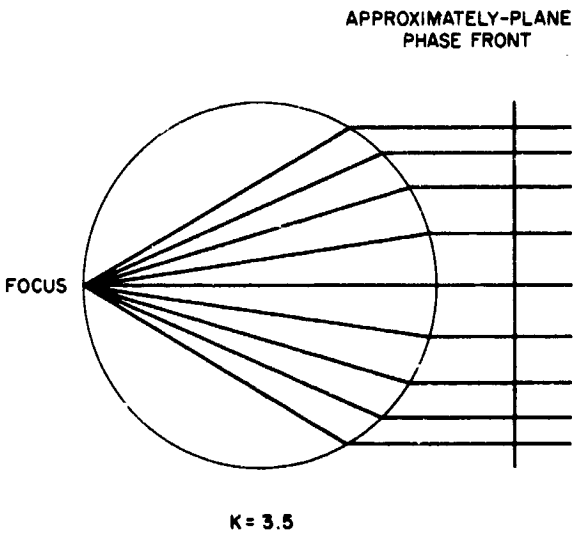

Figure 4-19. Constant-K lens showing focusing of rays by refraction.

properties similar to those of Luneberg lenses, except that small aberrations, sufficiently small to be negligible for most practical applications, are present (Bekefi and Farnell, 1956; Assaly, 1958; Cheston and Luoma, 1963). Figure 4-19 shows a constant-K lens and indicates the manner by which the rays are brought to a focus with ray refraction. Such lenses are inherently of simpler mechanical design than Luneberg lenses and should therefore have electrical symmetries far more accurate than those attainable for Luneberg lenses.

The focus is within the lens if the dielectric constant of the constant-K lens is greater than 3.5. As the dielectric constant is reduced from 3.5, the focus progressively moves away from the surface.

Constant-K lenses with diameters in excess of 100 wavelengths should perform well according to theoretical investigations. However, as the aperture gets larger in terms of wavelength, the aberrations become more significant and degrade the pencil beam pattern and reduce the gain. Overall gains of about 3 db below area gain have been obtained with a constant-K-type lens of diameter equal to 12 wavelengths (15-1/2 inches) operating at 9.375 Gc (Cheston and Luoma, 1963).

A multiple-beam antenna formed by a constant-K-type lens or a Luneberg lens backed with a mosaic or array of feed elements has a unique advantage over multiple-beam antennas that use beam-forming matrices. In the lens array, the pointing direction of each beam is independent of frequency; it depends only on the location of the feed with respect to the center of the lens. This advantage will reduce the complexity of a wideband system which must operate at widely different frequencies and with the multiple beams.

The weight of a constant-K-type lens would probably be greater than that of a Luneberg lens of similar size. The figure would be a serious problem in many space applications.

Broad Beam Luneberg Lens. To minimize the problem of aperture blockage by increasing the size of the lens and retaining the same beamwidth, a shaped beam modification of the Luneberg lens is considered. This lens has a broader pencil beam than a Luneberg lens of the same diameter, since the emergent phase front is not plane but rather a slightly curved sphere. The rays are not collimated, and the lens design may be thought of as being of the "shaped beam" type. Geometrical optics should give a reasonable first approximation to the actual patterns achieved by these lenses, just as it does for the shaped-beam metal reflectors described by Silver (1949c). Since this type of analysis leads to patterns that are frequency independent, one application of the shaped beam lens is for "pencil beams" with constant beamwidth over a broad band. As DeSize (1957) points out, this application permits broadband, wide-angle coverage with a multiplicity of fixed feeds without failure of coverage at the high-frequency end of the band or wasteful overlap at the low-frequency end.

Kay (1959) and Morgan (1959) have developed design procedures for finding the index variation of a spherically symmetric lens which will produce a uniform exit beam of any desired width. For the broad-beam Luneberg lens with a cosine-tapered feed at the surface, Morgan has verified Kay's work and derived the index of refraction of a lens with a sector beam $2\psi_o$ wide as

$$n = \exp\left[\omega(\rho, 1) - 2\omega(\rho, \csc \tfrac{1}{2}\psi_o)\right] \tag{4-38}$$

where $\omega(\rho, S)$ are as developed in a series by Fletcher et al. (1954) as

$$\omega(\rho, S) = \sum_{i=o}^{\infty} C_i(\rho) S^{-2i-1} \tag{4-39}$$

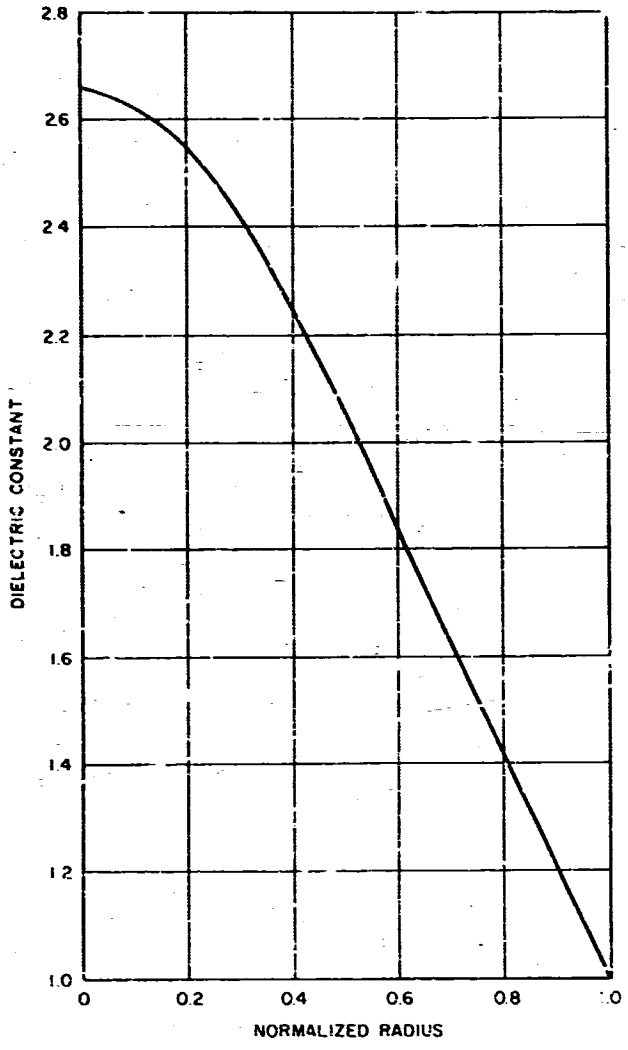

Figure 4-20. Relationship of dielectric constant and radius of a broad-beam Luneberg lens.

The latter authors have tabulated the values of C_i for use in Equation (4-39).

Equation (4-39) was substituted into Equation (4-38) to solve for the variation of dielectric constant (n^2) as a function of normalized radius for a 25.7-degree beamwidth lens. Such a beamwidth would allow fourteen 25.7-degree beams to successively cover the earth which, at a synchronous orbit of approximately 22,000 miles, would subtend 17-1/2 degrees at the satellite.

The broad-beam Luneberg lens would produce a 25.7-degree beamwidth regardless of size and frequency, when fed with a cosine primary pattern. It has a dielectric constant which varies with the normalized lens radius as plotted in Figure 4-20.

As far as is known, there are no lenses of this design available commercially. Thus the potential of the theoretical work remains to be reduced to practice.

4.5 MULTIPLE-BEAM ANTENNAS

The multiple-feed lens antenna systems discussed previously are essentially multiple-beam antennas in that a number of feeds can be used simultaneously. Another class of multiple-beam antennas employs arrays of elements that are interconnected through a beam-forming matrix to produce multiple beams.* A promising example is the

*Shelton and Kelleher, 1961; Butler and Lowe, 1961; and Delaney, 1962.

so-called Butler array which consists of an r-f beam-forming matrix circuit in which extensive use is made of 3-db directional couplers and fixed phase shifter. The beam-forming matrix technique has been modified and adapted to use in circular arrays (Chadwick and Glass, 1962).

4.5.1 The Butler Array

One of the basic components of the Butler type of beam-forming array is the 3-db directional coupler which connects the antenna elements to the output terminals (Butler and Lowe, 1961; Delaney, 1962). When the voltages at the two input terminals of the coupler have the amplitude and relative phase angles shown in Figure 4-21, all the input signal power will appear at the indicated terminal. This 3-db directional coupler, used in conjunction with two antenna elements, will form the simplest kind of multibeam array. Figure 4-22 shows such a 2-beam, 2-element array.

A 4-beam array can be built by the interlacing of two 2-beam arrays with a second level of directional couplers provided to combine the outputs into beams. Fixed phase shifters must be inserted between the upper and lower levels of couplers to form the output beam. Figure 4-23 shows such a 4-element, 4-beam array using directional couplers. The amplitudes and phases of an incident "Beam 1 Left" signal are shown at various points in the matrix. Figure 4-23b shows the

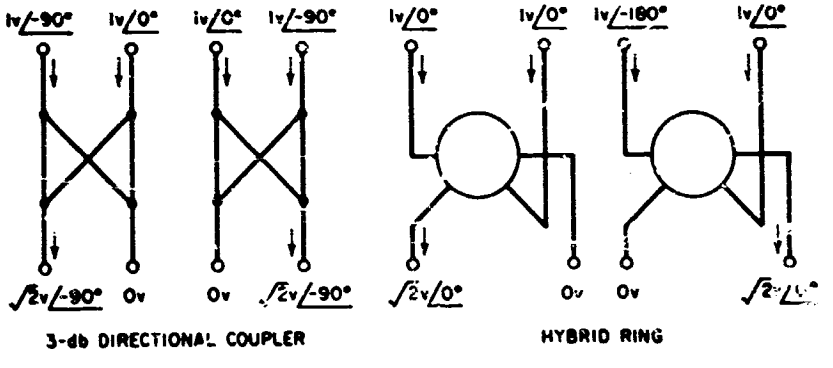

Figure 4-21. Phase shift convention for directional couplers and hybrid rings.

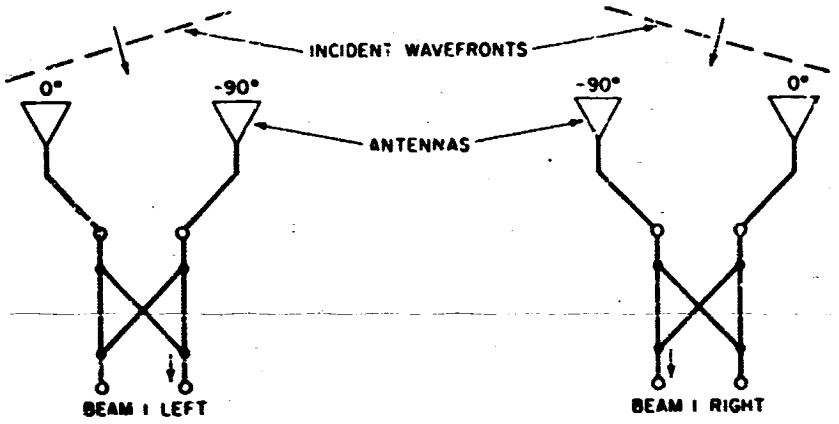

Figure 4-22. Simplest beam-forming matrix.

amplitudes and phases of an incident "Beam 2 Left" signal. "Beam 1 Right" and "Beam 2 Right" are obvious because of the symmetry of the matrix. The "shaded" directional couplers are the ones used to form the particular beam. It can be seen that the beam-forming matrix behaves like a multiple corporate feed structure which routes a signal originating at a particular point in space to a particular output part of the matrix.

A 16-beam array, shown in Figure 4-24, can be though of as four interlaced 4-beam arrays. Two extra levels of phase shifters and 3-db directional couplers are required to form the beams.

These arrays can be built to have any power of 2 beams, 2, 4, 8, 16, 32, etc. The number of beams is equal to the number of array elements. This beam-forming technique can be used in two-dimensional (planar) arrays by first combining the outputs of the columns of antenna elements into matrices and then combining the outputs of the column matrices in a group of row matrices.

Theory of Butler Array. The normalized magnitude of the field intensity in the far field of a linear array of n isotropic sources is given by (Jasik, 1961c)

$$\left|E\right| = \frac{1}{n}\frac{\sin(n\psi/2)}{\sin(\psi/2)} \qquad (4\text{-}40)$$

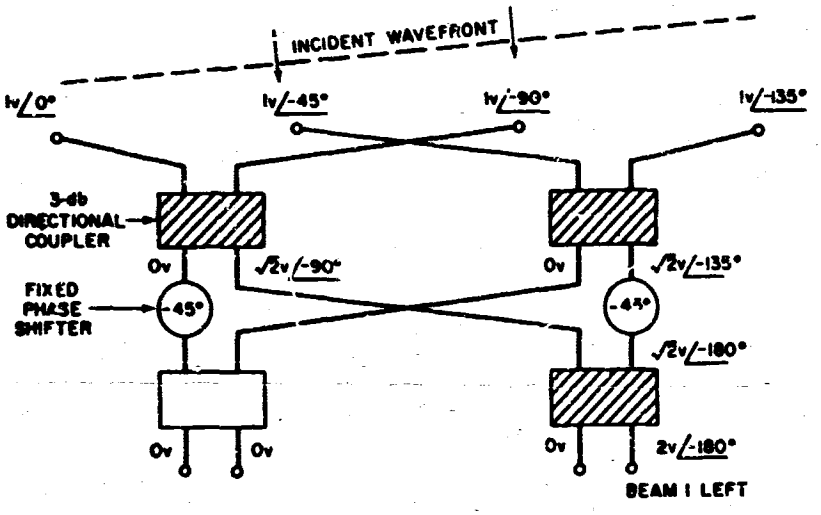

a) beam 1 left

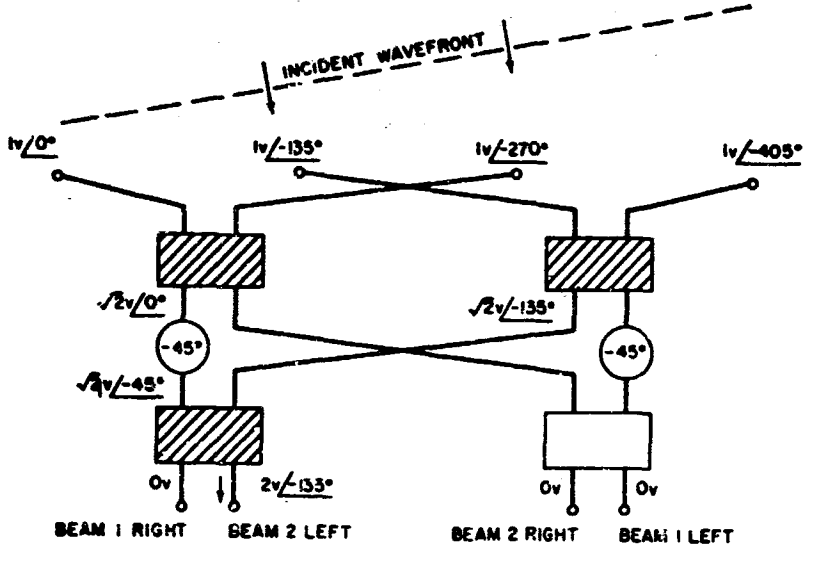

b) beam 2 left

Figure 4-23. Amplitude and phases of different beam signals in a 4-element matrix.

The number of directional couplers required to build the matrix of the Butler array can be shown to be equal to $\frac{n}{2} \log_2 n$, where n is the number of elements in the array. The number of fixed phase shifters required is $\frac{n}{2} (\log_2 n - 1)$. A major drawback of this beam-forming technique, when large arrays are considered, is the complexity of the matrix arrangement. For example, a 64-element

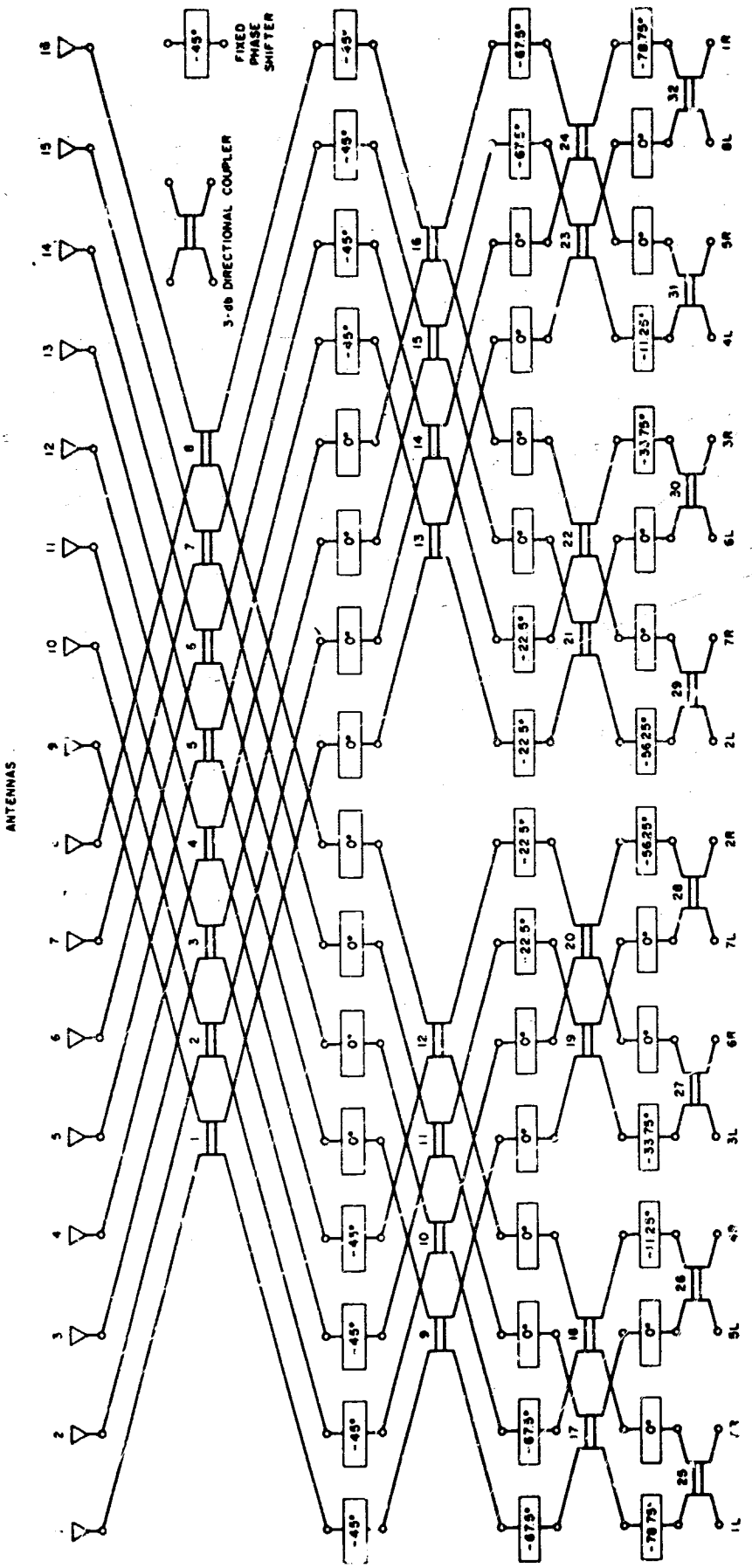

Figure 4-24. Sixteen-element beam-forming matrix.

matrix requires 192 directional couplers and 160 fixed phase shifters. However, unlike another frequently proposed beam-forming technique, sometimes referred to as the Maxson array, the directional couplers of the Butler array are all identical; i.e., they are all of the 3-db type. This duplication would certainly reduce the costs if not the complexity of building and packaging such a matrix. Use of strip transmission lines would permit the fabrication of several directional couplers and phase shifters on individual boards which could be stacked closely together. This arrangement might alleviate the packaging complexity.

Other pertinent characteristics of the Butler array are:

1. The peak of any beam occurs at the null of beams adjacent to it; therefore, the use of amplitude comparison monopulse as the angle tracking technique would require comparison of maximum signals as found at the peak of one beam with minimum signals hidden below the noise in the system because they occurred at the null of the adjacent beam.

2. There will be a significant amount of beam degradation off broadside as the envelope of the beam peaks follows the antenna element pattern as predicted from the principle of pattern multiplication.

3. There is considerable beam movement with changes in frequency (and the beam movement tends to increase for beams far from the broadside direction). When the phase shifters and the couplers in the matrix are ideal, the near-to-broadside beam position will be shifted by about 10 percent, and beams close to endfire will have their positions shifted by 28 percent when the frequency is changed by 10 percent.

Figure 4-25 depicts a wave front at a Butler array of four elements. The angle of incidence is θ and is described by

$$\theta = \text{arc sin} \frac{c\delta}{2\pi fd} \tag{4-41}$$

where

δ = the phase difference between two adjacent array elements

d = the element separation

c = the speed of light

f = the frequency

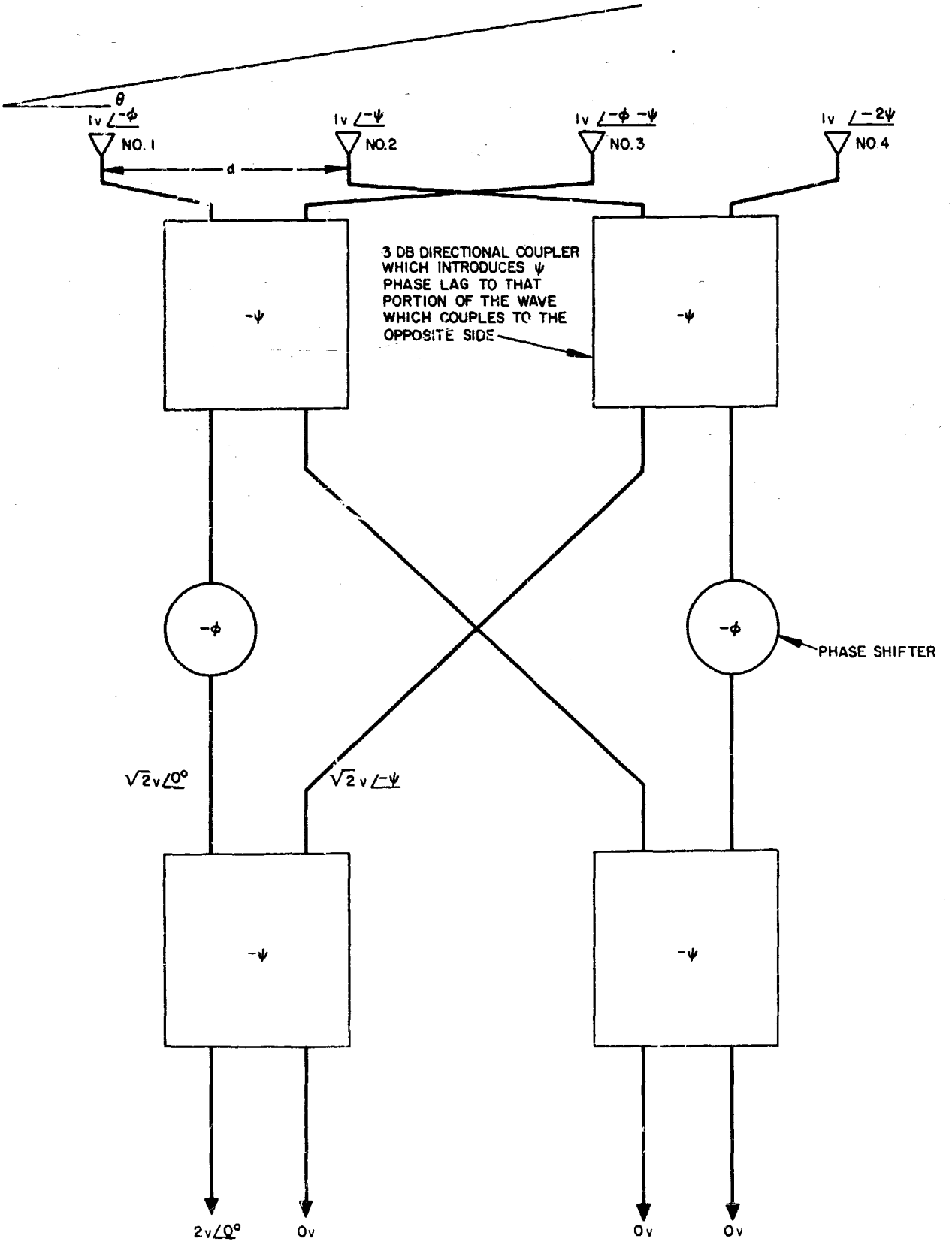

Figure 4-25. Phase shifts in a Butler array.

It is noticed from Equation (4-41) that θ, the angle of incidence, will remain constant with respect to frequency if δ, the phase difference between the adjacent array elements, is directly proportional to frequency. It is obviously desirable therefore to have all the phase shifters and couplers in the matrix with phase shifts that are directly proportional to frequency. This can be seen when one solves for δ_{mn} between the four elements of the array in Figure 4-25, where m and n refer to the particular two elements involved:

$$\begin{aligned} \delta_{12} &= \phi - \psi \\ \delta_{23} &= -\phi \\ \delta_{34} &= \phi - \psi \end{aligned} \tag{4-42}$$

It is seen from Equation (4-42) that ψ must equal 2ϕ to provide equal phase shifts between adjacent elements and that θ of Equation (4-41) will remain stationary when the phase shifters and couplers introduce phase shifts of ϕ and ψ, respectively, which are directly proportional to f.

The Butler array would be applicable to gravity-gradient stabilized satellites in either the 11, 120-Km or the synchronous orbit. In this application it would consist of a planar array. If the Butler array were employed in a spin-stabilized satellite, a number of such arrays would have to be dispersed about the spin axis in such a way that full 360-degree coverage was obtainable as the satellite rotated about its axis. To avoid the necessity of scanning each array too far off axis, four arrays would be required. Each would cover a 90-degree sector of ±45 degrees from broadside in the circumferential plane of the satellite. The extension to an unstabilized satellite would require six arrays symmetrically disposed about the satellite.

Number of Components Required. It is of interest to examine the number of components required for a possible application of a two-dimensional Butler array to obtain scan in two planes. A 16-by-16

element array at X-band (e. g., 9. 375 Gc) spaced 0. 7 λ will produce a beam with a null-to-null width at broadside of about 10 degrees and a gain of about 32 db. The number of 3-db couplers required for such an array is 768, while 512 fixed phase shifters are required. The phase shifters may consist of only sections of transmission line and so would be no problem but the number of 3-db couplers is quite large. However, it appears that all relatively high gain scanning systems require large numbers of elements.

Shelton and Kelleher (1961) describe alternative methods for building up the feed matrix of uniformly illuminated multiple-beam arrays. In addition to the hybrid junctions of the Butler matrix, they consider the use of six- and eight-port junctions. With these it is not necessary that the number of radiating elements equal a power of two. The number of elements may take on the values $2^{\ell} 3^{m} 4^{n}$, where ℓ, m, and n are integers (including 0). By using a combination of 4- and 8-port junctions, it is possible to obtain a 128-element linear array which requires 64 hybrids and 96 8-port junctions for a total of 160 junctions. A butler matrix for the same number of radiating elements requires 448 hybrids. Thus, the use of different building blocks can drastically reduce the number of junctions required and might more than offset the increased complexity of the multi-port junctions. As a further comparison, a 16-by-16 element planar array using 8-port junctions would require only 256 such junctions as compared to the 768 2-by-2 hybrids required for the same aperture using a Butler matrix. It appears that development of low-loss 6- and 8-port junctions for use in such matrices might make such a system feasible.

4. 5. 2 Multibeam Circular Arrays

Adaptation to circular arrays of the Butler beam-forming matrix technique (Chadwick and Glass, 1962) makes use of an approximate analogy between the exponential Fourier series expansion in ϕ of the aximuth pattern of a circular array and the pattern of a linear array in the variable $u = kd \sin \phi'$. If the excitations of the elements of a circular array are expressed in terms of their phase sequence modes,

then each phase sequence mode is responsible for exciting primarily one specific term in the exponential Fourier expansion of the pattern in ϕ. For example, the zero phase sequence mode excites an essentially omnidirectional pattern with uniform phase; the first positive phase sequence excites a pattern which is essentially omnidirectional in ϕ, but whose phase varies linearly in ϕ; the second phase sequence mode excites an essentially omnidirectional pattern whose phase varies as 2ϕ; etc. Actually, the phase sequence mode patterns are not ideal and have additional harmonics which are error terms. If the error terms are sufficiently small, then excitation of the phase sequence modes with the same relative amplitudes and phases as those of the element excitations of the equivalent linear array will result in a pattern as a function of ϕ which is identical with the linear array patterns as a function of kd sin ϕ'. Therefore, techniques for synthesizing linear array patterns as a function of kd sin ϕ' may be applied to synthesizing patterns of circular arrays as a function of ϕ.

The heart of the technique is the so-called mode-forming matrix which transforms the excitation coefficients of the reference linear array into the proper phase sequence component of the circular array excitation and combines these excitations at the elements of the circular array to produce the desired pattern in ϕ. This matrix is illustrated in Figure 4-26.

The errors in the fields of the various phase sequence modes are greatest for the modes whose mode numbers are approximately equal to half the number of array elements. These errors increase with element spacing. They appear to be relatively small for spacings less than one-quarter wavelength but increase beyond this spacing. As an example, for a 16-element array with half-wavelength spacing, whose elements have patterns of the form $\cos^{16}\left(\frac{\phi - \phi_n}{2}\right)$, where ϕ_n is the angular position of the n^{th} element, only 10 out of 16 phase sequence modes are very pure. This means that a pattern corresponding to a linear array of only ten elements can be faithfully reproduced. As the patterns of the individual elements become more nearly omnidirectional, even fewer phase sequence modes have sufficient purity; i.e., the

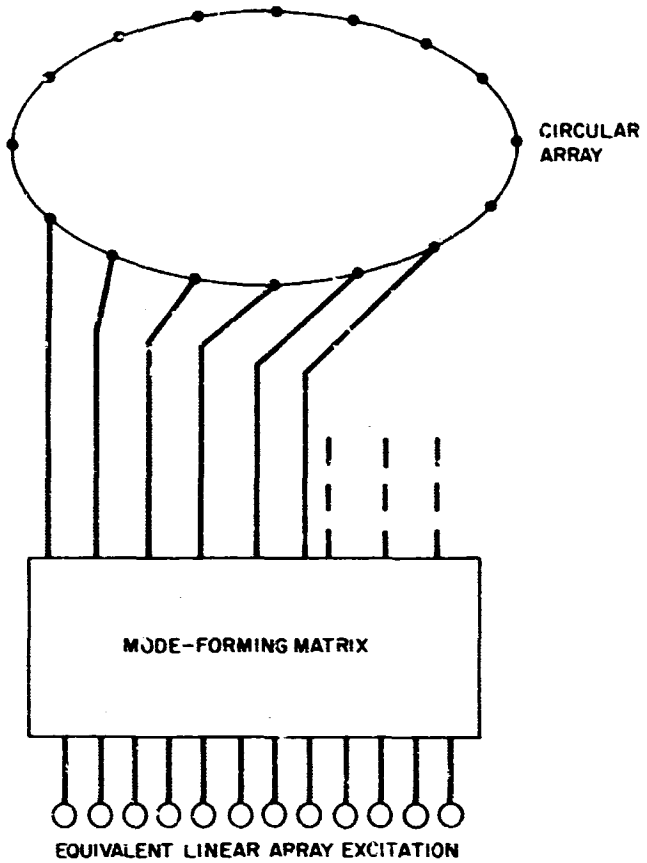

Figure 4-26. Circular array with beam-forming matrix.

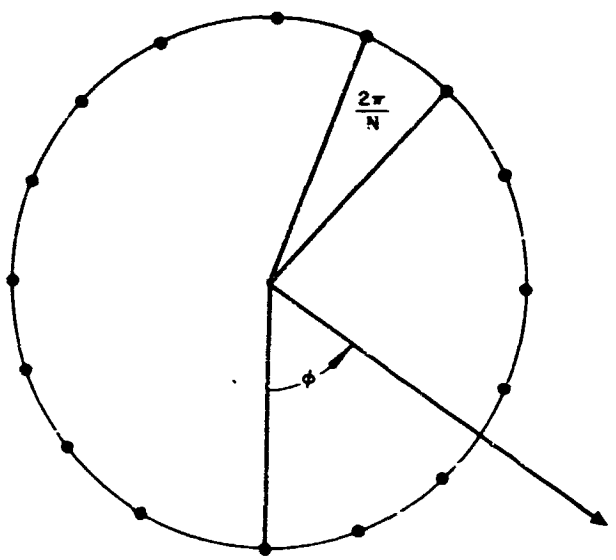

Figure 4-27. N-element circular array.

number of elements in the equivalent linear array whose pattern can be faithfully reproduced becomes less.

The arrangement of Figure 4-27 can be used to illustrate how the phase sequence excitations are related to the Fourier coefficients of the circular pattern. If the elements are numbered starting from n = 0 at $\phi = 0$, the element pattern of the elements about the array can be written as $f\left(\phi - \frac{n2\pi}{N}\right)$ where $-N/2 \leq n \leq N/2$. The relative element excitations for the p^{th} phase sequence are

$$a_{n_p} = a_o e^{jnp\frac{2\pi}{N}} \qquad (4\text{-}43)$$

so that the pattern for the p^{th} phase sequence excitation may be written as

$$E_p(\phi) = \sum_n e^{jnp\frac{2\pi}{N}} f\left(\phi - \frac{2\pi n}{N}\right) \cdot e^{-jkR\left[1 - \cos\left(\phi - \frac{n2\pi}{N}\right)\right]} \qquad (4\text{-}44)$$

$$-\frac{N}{2} < p < \frac{N}{2}$$

This expression may be written as a complex exponential Fourier series as

$$E_p(\phi) = e^{-jkR} \sum_{m=-\infty}^{\infty} A_m e^{jm\phi} \tag{4-45a}$$

where

$$A_m = \frac{1}{2\pi} \int_0^{2\pi} E_p(\phi) e^{-jm\phi} d\phi \tag{4-45b}$$

If the phase sequences were pure, all the A_m would vanish except when $m = p$ and

$$E_p(\phi) = e^{-jkR} A_p e^{jp\phi} \tag{4-46}$$

Then it would be possible to reproduce exactly a pattern which had Fourier terms from -N/2 to N/2. However, if the A_m are computed, the following expression results:

$$A_m = 0 \qquad m \neq p + \ell N \qquad (\ell \text{ integer}) \tag{4-47a}$$

$$A_{p+\ell N} = N j^{-(p+\ell N)} \sum_{q=-\infty}^{\infty} j^q B_{qo} J_{q-p-\ell N}(kR) \tag{4-47b}$$

where $J_n(x)$ is the Bessel function of the first kind and of order n and B_{qo} is given by

$$B_{qo} = \frac{1}{2\pi} \int_0^{2\pi} f(\phi) e^{-jq\phi} d\phi \tag{4-48}$$

Equations (4-47) show that A_p and the error terms $A_{p+\ell N}$ are not independent. It is desirable to make $A_{p+\ell N}$ small for $\ell \neq 0$. The method for doing this is by controlling the B_{qo} by adjusting the element pattern and by controlling N, the number of elements in the array. The larger the value of N for a given array diameter, the purer the phase sequences. For the limit of continuous circular apertures the error terms vanish.

As examples of the technique, multiple-beam antennas have been designed which use beam-forming matrices in addition to mode-forming matrices. These matrices transform the input signal into the excitation coefficients of a linear array with a specified beam pointing direction and sidelobe level. The beam-forming matrices then feed mode-forming matrices to form the circular array patterns as described above.

Critical Components. The critical components in this technique appear to be the elements in the mode-forming matrix of the array. This matrix requires hybrid couplers and fixed phase shifts to form the individual phase sequence modes. For an N element array N hybrids are necessary. These may be constructed in stripline as is described by Chadwick and Glass. In addition to the mode-forming matrix to convert from linear array excitations to circular array excitations, equipment necessary to obtain the equivalent linear array excitations must also be included as part of the technique. For example, to use the array as a multiple beam array of the Butler type, the inputs for the mode-forming matrix would be taken from a Butler matrix. Therefore this type of array would be scanned electronically by switching among the input lines of the Butler matrix. Since such an array uses two matrices, it is more complex than the linear Butler array.

To use such an array to despin beams also requires techniques for transferring power from one beam to an adjacent beam without the introduction of switching transients and signal modulation as the antenna spins through the cross-over points between two beams. Thus, in addition to the components required for the beam- and mode-forming matrices, application of the technique to despinning beams requires additional control circuitry.

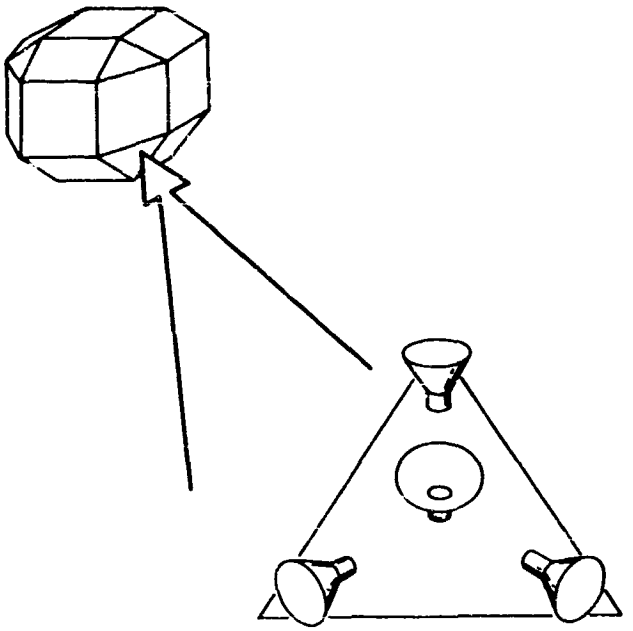

Figure 4-28. Lincoln Laboratory multibeam horn antenna system.

4.6 MULTIBEAM HORN ANTENNA SYSTEM

One of the more direct approaches to multiple-beam antenna systems now under consideration would use clusters of horns with beam switching from horn-to-horn to communicate from earth to satellite and back to earch (Ricardi et al., 1964). Under development at the Lincoln Laboratory of Massachusetts Institute of Technology, this multibeam horn antenna system will be mounted on an unstabilized satellite that has many facets. The horns will be arranged in clusters on 8 triangular panels as illustrated in Figure 4-28. There are to be four circular horns per panel, each pointing in a different direction. Thus, 32 horns in all will be used to cover the complete 4π steradians required with some beam overlap. The switching between horns is accomplished by diode switches and controlled by infrared sensors mounted in groups of four on the antenna panels. Each sensor is oriented to look in the same direction as a horn. The system will operate at 7.75 Gc and 8.35 Gc. The half-power beamwidth of each horn is approximately 48 degrees.

One of the critical components in the system is the 1-to-4 coaxial-to-waveguide diode switch. This switch must operate at both 7.75 Gc and 8.35 Gc and must therefore be fairly broadband. A 4-ounce switch was under development which at the design frequency of 7.75 Gc exhibited a 0.45-db loss from coax input to three waveguide outputs and a 9.65-db loss to the fourth output. Its off-isolation from input to outputs was 30 db at the design frequency. However, at 8.35 Gc the performance deteriorated. Off-isolation at this frequency had dropped to 6-6.5 db, and after removal of reflection loss, it was only 4.5 db.

4.7 AMPLITUDE SCANNED CIRCULAR ARRAYS

Another method of obtaining 360-degree azimuth scan using circular arrays of elements requires only amplitude variation (including sign changes) of the element excitations (Neff et al., 1961).

This scanning technique uses concentric rings of circular arrays. Each ring is used to contribute essentially one term of a Fourier cosine series representation of the desired pattern. A single center element contributes the constant term, the first ring contributes the first harmonic term, the next outer ring contributes the second harmonic term, and so forth. Thus if K harmonic terms are required to synthesize a desired pattern, K circular rings are required to produce that pattern. For example, if all K harmonic terms are equally excited and adjusted to add in phase, they will yield a pattern $F(\phi)$ of the form

$$F(\phi) = \frac{\sin K(\phi - \phi_o)}{\sin \frac{1}{2}(\phi - \phi_o)} \tag{4-49}$$

This pattern has 13-db first sidelobes. The half-power beamwidth, $\Phi_{1/2}$ satisfies the following equation:

$$\sin\left(\frac{K}{2}\,\Phi_{1/2}\right) = \sqrt{2}\,K \sin\left(\frac{1}{4}\,\Phi_{1/2}\right) \tag{4-50}$$

so that the required number of rings is given by solving Equation (4-50) for K when $\Phi_{1/2}$ is specified. It is evident that, since K must be an integer, there is only a discrete set of allowable values for the 3-db beamwidth for this type of pattern.

4.7.1 Required Element Excitations

As described by Neff et al. (1961), the number of elements in the k^{th} ring is assumed to be equal to 4k; r, the radius of the ring, is adjusted so that $\frac{2\pi r}{\lambda} = k$, where λ is the wavelength. The element excitations required to produce an angular variation of the form $\cos k(\phi - \phi_o)$, where ϕ_o is the desired pointing direction, are given by Neff:

$$V_i^{(k)} = V^{(k)} \cos\left(\frac{\pi}{2} i - k\phi_o\right) \qquad i = 0, 1, 2, \cdots, 4k-1 \qquad (4-51)$$

In this equation i represents the number of the element in the ring. The numbering is done in the direction of increasing ϕ. For even-numbered element this becomes

$$V_i^{(k)} = V^{(k)}(-1)^{i/2} \cos k\phi_o \qquad i = 0, 2, 4, \cdots \qquad (4-52)$$

while for odd-numbered elements it becomes

$$V_i^{(k)} = V^{(k)}(-1)^{\frac{i-1}{2}} \sin k\phi_o \qquad i = 1, 3, 5, \cdots \qquad (4-53)$$

The corresponding pattern becomes approximately

$$F^{(k)}(\phi) = A_k(\phi_o) \cos k(\phi - \phi_o) \qquad (4-54)$$

where

$$A_k = C_k(\phi_o)\, V^{(k)}$$

Therefore by applying excitations which satisfy Equation (4-52) to the even-numbered elements and by applying excitations which satisfy Equation (4-53) to the odd-numbered elements, patterns which may be rotated in space are achieved. Calculations have shown that, due to the effects of mutual coupling, some pattern variations occur as ϕ is varied from a value coinciding with the angular location of an element to a value between adjacent element positions. This effect is indicated in Equation (4-54) by showing that A_k depends on ϕ_o. Thus, as a beam is rotated, some modulation of the pattern amplitude may occur. In specific applications this modulation must be considered to see if it would adversely affect the operation of the system in which it might be used.

4.7.2 Experimental Systems

Some experimental antennas based on this technique have been built. They consist of two-ring and three-ring arrays of quarter-wave monopoles above a ground plane. The arrays were used as transmitting arrays only and operated at a carrier frequency of 300 Mc. Electronic scanning was done by varying ϕ_o at a rate of 60 revolutions per second. The system required two channels of electronic controls per ring, one to provide the excitations of the form of Equation (4-52) and one to provide the excitations of the form of Equation (4-53). Figure 4-29 illustrates a typical pair of channels for the k^{th} ring. The arrays were designed for 20-db sidelobe Tchebyscheff patterns. Table 4-1 lists theoretical pattern requirements. The experimental two-ring array had about a 75-degree 3-db beamwidth and sidelobes of at least -20 db, and the experimental three-ring array had a 3-db beamwidth of about 50 degrees and a sidelobe level of about -20 db, both in good agreement with theory.

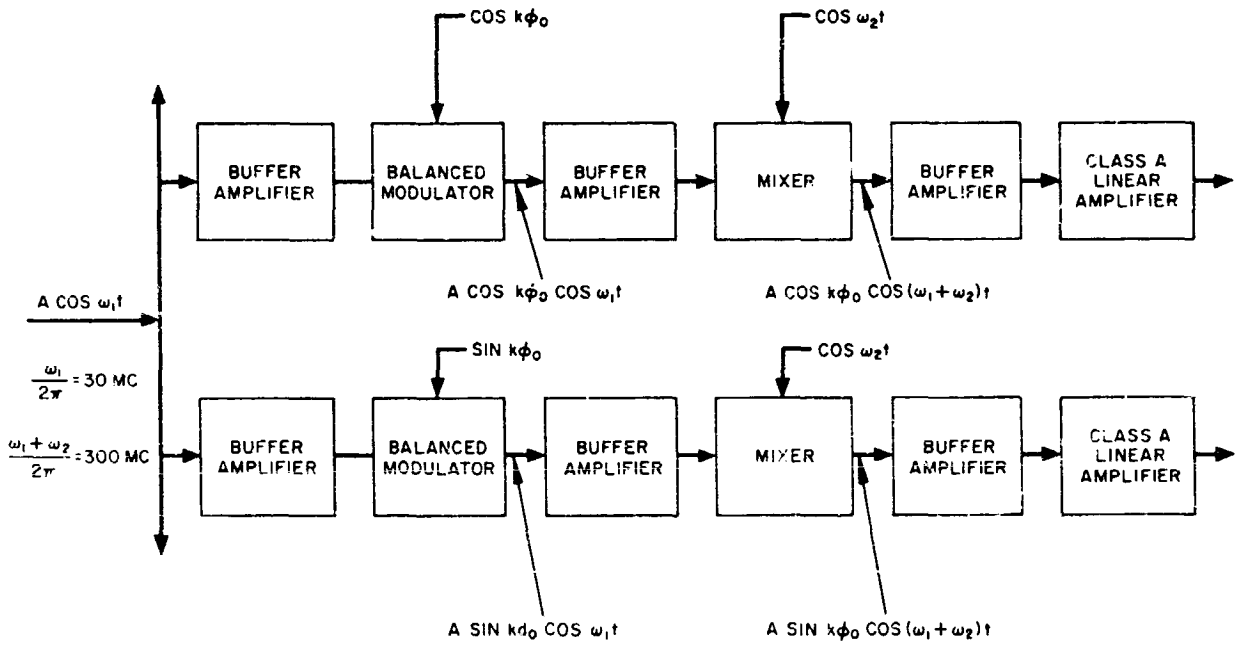

Figure 4-29. Diagram of k'th control channels for experimental amplitude scanned circular array.

Number of Rings	Number of Elements	3-db Beamwidth (degrees)	
		20-db Sidelobes	30-db Sidelobes
1	5	125	130
2	13	74	83
3	25	51	60
4	41	40	46
5	61	32	38
7	113	22	27
10	221	16	18
80	12,961	2	2

Table 4-1. Array Characteristics for Tchebyscheff Patterns (Neff et al., 1961).

4.7.3 Properties of System

1. Full 360-degree azimuth scan is achievable.
2. Control functions are simply related to scan angle.
3. Mutual coupling is taken into account in the basic design.
4. Number of rings is equal to the number of required spatial harmonics of the desired pattern so that for narrow beams a large number of rings is required.
5. For faithful pattern reproduction, the number of elements per ring should be significantly larger than the number of the ring. In the experimental models the number of elements per ring was 4 times the ring number.
6. The number of control channels required is twice the number of rings.

4.8 AMPLITUDE SCANNED TIME-CONTROLLED ARRAYS

Controlled changes in the amplitude between the elements in an array have been used to achieve electronic scanning and to synthesize

arbitrary patterns.* The technique utilizes on-off diode switches and special circuitry to obtain effective amplitude scanning.

4.8.1 Theory of Pattern Synthesis

A uniformly spaced linear array of 2N + 1 identical radiators is considered as shown in Figure 4-30. For such a uniformly spaced linear array of radiators, separated by a distance d, the far field pattern is given by

$$G(u) = \sum_{-N}^{N} e_n(u)\, A_n\, e^{j(nu)} \qquad (4\text{-}55)$$

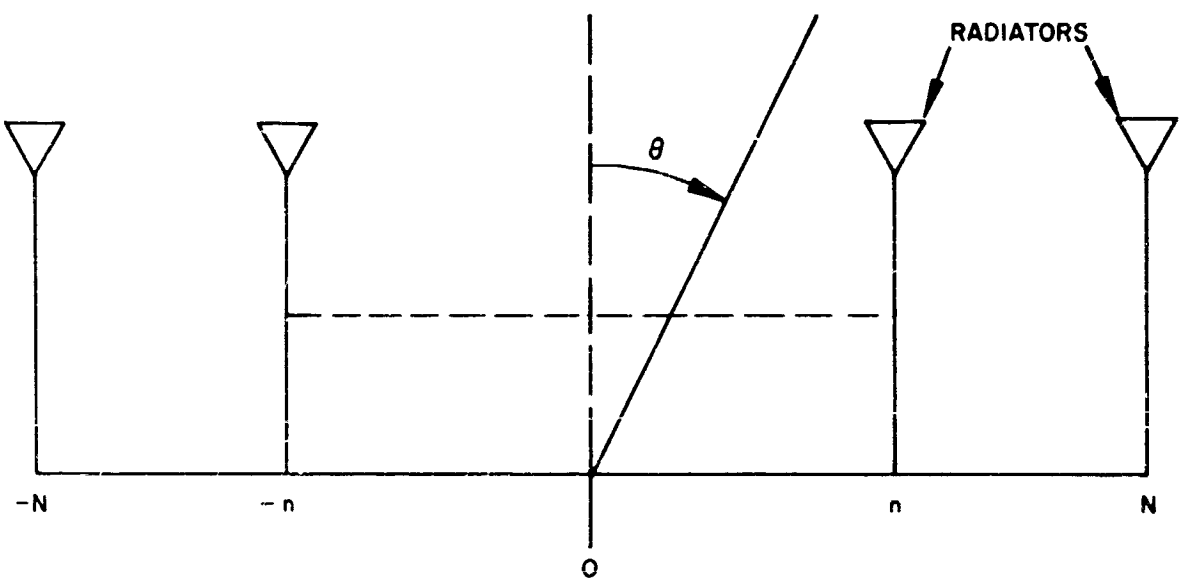

Figure 4-30. Linear array.

*Shanks and Bickmore, 1959; Kummer, Villeneuve, and Terrio, 1963; Kummer et al., 1963; Sletten et al., 1958.

where

$u = kd \sin \theta$

$k = 2\pi/\lambda$

θ = angle off broadside

$2N + 1$ = the number of elements in the array

$e_n(u)$ = element factor

A_n = excitation of the n^{th} element

Now if the n^{th} element is excited by $A_n = C_n - jD_n$ if $n \neq 0$ and by C_o if $n = 0$, and if $C_n = C_{-n}$ and $D_n = -D_{-n}$, then the far field pattern becomes

$$G(u) = e(u) \sum_{-N}^{N} \left(C_n - jD_n\right) e^{jnu}$$

$$= e(u) \left[2 \sum_{1}^{N} \left| C_n \cos nu + D_n \sin nu \right| + C_o \right] \qquad (4\text{-}56)$$

It can be seen from Equation (4-56) that the pattern G(u) can be synthesized by the control of only the amplitude C_n and D_n. The degree of approximation to the pattern desired depends on the number of terms in the series and, hence, on the number of elements in the array.

A simple way by which the element excitation can be obtained lies in coupling symmetrical elements (that is, the n^{th} and the $-n^{th}$ elements) to the sum and difference arms of a magic tee* as shown in Figure 4-31. This design makes use of the fact that the excitation coefficients of the symmetrical elements are complex conjugates of each other. This technique is a modification of one described by Sletten et al. (1958).

*At lower frequencies 3-db couplers are used in a similar manner.

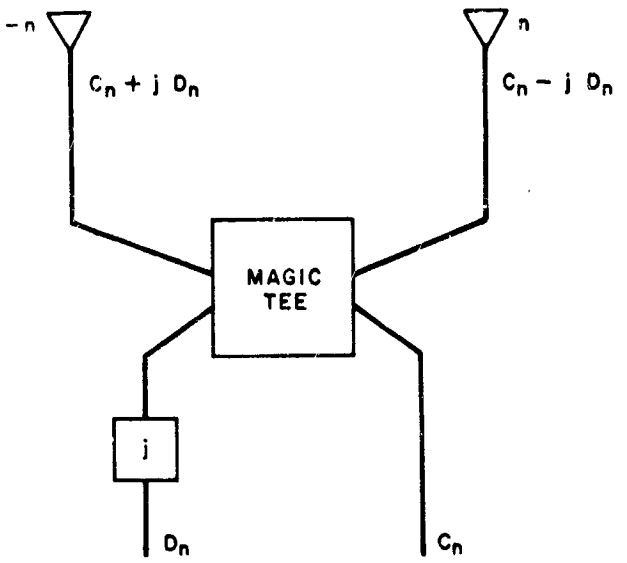

Figure 4-31. Method of exciting elements.

4.8.2 Application to Beam Scanning

The application of the theory of pattern synthesis to beam scanning can be demonstrated by an examination of the far field pattern of a linear array with 2N + 1 radiators, with a constant amplitude distribution across the aperture, and with a beam at $u = u_o$.

$$G(u) = e(u)\,\frac{\sin\left[\frac{1}{2}(2N+1)(u-u_o)\right]}{\sin\left[\frac{1}{2}(u-u_o)\right]} \tag{4-57}$$

or

$$G(u) = e(u)\left[1 + 2\sum_{1}^{N}\cos n(u-u_o)\right]$$

$$= e(u)\left[1 + 2\sum_{1}^{N}(\cos nu_o \cos nu + \sin nu_o \sin nu)\right]$$

It can be seen that in Equation (4-57) $C_n = \cos nu_o$, $D_n = \sin nu_o$, and $C_o = 1$. For arbitrary pattern synthesis the coefficients C_n and D_n may be treated as the Fourier coefficients and may be determined in the usual manner.

It can be shown physically with the aid of a phasor diagram (Figure 4-32) that control of the amplitudes of the elements in a

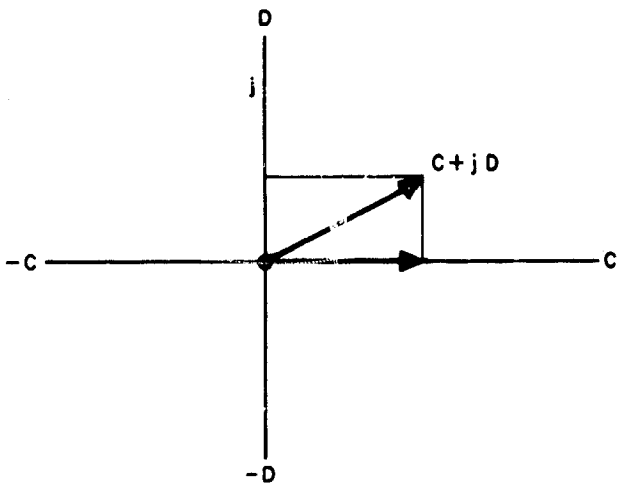

Figure 4-32. Phasor diagram.

prescribed fashion produces an effective phase shift. If D = 0, the phasor lies on the real axis; if C = 0, it lies on the j axis. For various values of C and D the phasor will lie at some prescribed angle in the complex plane. If the quantities C and D are properly chosen, the phase of their sum can be rotated through 360 degrees. The magnitudes of C and D determine the amplitude of their sum. Thus arbitrary phase and amplitude control is achieved.

In place of the continuously varying amplitudes, only two amplitude states, ON and OFF, can be used to achieve the pattern synthesis. In the ON state all amplitudes are equal. The amplitude is effectively varied by control of the ON times of the C_n's and D_n's. When the amplitudes are averaged over an appropriate time interval, the desired amplitudes are effectively obtained. With the ON and OFF amplitude states, the excitation coefficients as a function of time become

$$c_n(t) = \left[U(t) - U(t - \tau_{cn})\right]$$

$$d_n(t) = \left[U(t) - U(t - \tau_{dn})\right] , \qquad \text{for } n \neq 0$$

where $c_n(t)$, $d_n(t)$, τ_{cn}, and τ_{dn} are real and U is the unit step function. If $c_n(t)$ and $d_n(t)$ are made periodic with the same period T, $c_n(t)$ and $d_n(t)$ can be represented by Fourier series and the far field pattern is given by

$$G(u, t) = 2e(u)\, F(u, t)$$

where

$$F(u,t) = \left\{ \sum_{m=-\infty}^{\infty} \sum_{n=1}^{N} \left[C_{mn} \cos nu + D_{mn} \sin nu \right] \exp\left[j \frac{2\pi mt}{T} \right] + \frac{C_o}{2} \right\} \tag{4-58}$$

and

$$\left.\begin{matrix} C_{mn} \\ D_{mn} \end{matrix}\right\} = \frac{1}{T} \int_o^T \begin{pmatrix} c_n(t) \\ d_n(t) \end{pmatrix} \exp\left[-j2\pi m \frac{t}{T} \right] dt , \qquad n \neq 0$$

$$C_{mn} = \frac{\tau_{cn}}{T}$$

$$D_{mn} = \frac{\tau_{dn}}{T}$$

for m = 0 (carrier frequency)

Therefore, the excitation coefficients are now a function of the ON time of each radiator, and filters can be used to eliminate unwanted sidebands. The symbol $\frac{\tau_n}{T}$ is called the duty factor.

4.8.3 Electronic Amplitude Scan by Time Control Synthesis

The practicability of electronic scanning by the use of on-off switching to control the amplitude of the excitation of the various elements has been demonstrated at the Hughes Aircraft Company with an experimental X-band array (Lauriente and Terrio, 1963). This array differed in several minor respects from the array described above. The even and odd parts of the excitation coefficients were not designed to time-share the radiators so that simplicity could be maintained in the array feed. In other words, the magic tee (Figure 4-31) was not used in the experimental array and almost twice as many elements were required and were spaced a quarter-wavelength apart. About half the

elements were used to produce the even part of the pattern and the remainder were used in producing the odd part.

The array was used as a receiver in the experimental set-up, and amplitude control was achieved by means of on-off switching of diode switches. By the techniques employed, the beam of the array was scanned by a variation in the effective amplitudes (produced by variations in the duty factors) of the element excitations while the phase relation between the elements was kept fixed (except for the 180-degree reversals).

4.9 PSEUDO PASSIVE SATELLITE TECHNIQUES

The pseudo passive satellite technique combines tunnel diode amplifiers with a scattering surface in such a way that the scattering cross-section of the surface is increased. A feasibility study of this technique has been made (Sylvania, 1964). The study consisted of several parts:

a) A theoretical study of scattering by large arrays of independent scatterers. Scattering characteristics of various configurations were evaluated by the method of stationary phase. Scattering from arrays with random phase distributions was also considered.

b) A theoretical study of tunnel diode amplifier characteristics including gain, bandwidth, and stability criteria, taking into account the effects of natural coupling among adjacent amplifiers.

c) A consideration of power supplies and feeding techniques.

d) Experimental studies of tunnel diode failure characteristics.

e) Experimental studies of tunnel diode amplifier stability, gain, and bandwidths and backscattering from small configurations of scattering elements incorporating the tunnel diode amplifiers.

4.9.1 Basic Configuration

The basic configuration of interest is a spherical cap, large with respect to wavelength, upon which are distributed spiral antenna elements as illustrated in Figure 4-33. The coordinates θ and ϕ are the colatitude and azimuth angle, respectively, θ measured from the

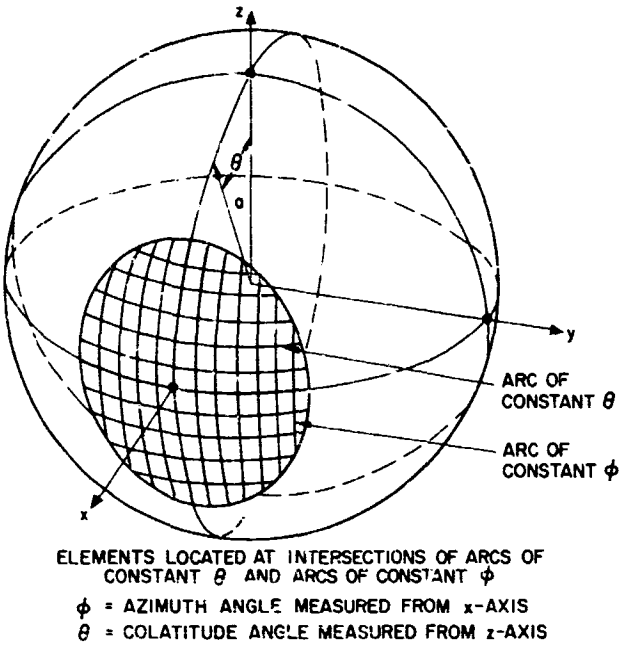

Figure 4-33. Scattering surface of elements distributed or spherical cap.

z-axis and ϕ measured from the x-axis. The scattering surface is centered about the x-axis with its radius of curvature, a, centered at the origin. The spiral elements are assumed to be located at the intersections of arcs of constant θ and arcs of constant ϕ and are all oriented in similar positions. Each element is connected to a transmission line of characteristic impedance Z_o terminated in a load with a reflection coefficient Γ. The coefficient Γ is less than unity in magnitude for passive terminations and greater than one in magnitude for active terminations. If the array is large in terms of wavelength, λ, and the contribution to scattering in any direction comes essentially from elements in the vicinity of a single point of stationary phase (specular reflection), then an approximate expression for the scattering cross-section, σ_s, becomes

$$\sigma_s(\theta_i, \phi_i, \theta_s, \phi_s) \approx \frac{\lambda^4 \, g_e(\theta_i \phi_i) \, g_e(\theta_s, \phi_s) \, |\Gamma|^2}{4\pi \, a^2 \alpha^2 \gamma^2 \left|1 - S_{11}\Gamma\right|^2 \left[\sin^2\theta_i + \sin^2\theta_s + 2 \sin\theta_i \sin\theta_s \cos(\phi_i - \phi_s)\right]} \tag{4-59}$$

where the terms have the following definitions:

θ_i, ϕ_i = angles from which the incident radiation arrives

θ_s, ϕ_s = angles at which the scattered radiation is observed

g_e = effective gain of the elements at the stationary phase point of the scatterer

α = angular element separation in the θ direction

γ = angular element separation in the ϕ direction

S_{11} = reflection coefficient that a single radiating element presents to its transmissive line when all other transmission lines are terminated in Z_o

a = radius of curvature of the spherical surface

The following assumptions were made in arriving at Equation (4-59):

a) The polarization of the incident signal is matched to that of the elements.

b) Mutual coupling among elements is negligible.

c) Scattering from the element itself is negligible compared with the amplified reradiated signal.

If the element spacings are written in the following forms

$$\alpha \approx \frac{d_1}{a} \; ; \qquad \gamma \approx \frac{d_2}{a} \tag{4-60}$$

where d_1 and d_2 are element spacings at the array center, then Equation (4-59) may be put into the more familiar form

$$\sigma_s\left(\theta_i, \phi_i, \theta_s, \phi_s\right) \approx \frac{\lambda^2}{4\pi} g_e(\theta_i, \phi_i)\, g_e(\theta_s, \phi_s)\, \frac{\left|\Gamma\right|^2}{\left|1 - S_{11}\Gamma\right|^2} \cdot \frac{\lambda^2 a^2}{d_1^2 d_2^2 \left[\sin^2\theta_i + \sin^2\theta_s + 2 \sin\theta_i \sin\theta_2 \cos\left(\phi_i - \phi_s\right)\right]} \tag{4-61}$$

The quantity $\dfrac{\left|\Gamma\right|^2}{\left|1 - S_{11}\Gamma\right|^2}$ is the effective power gain of the amplifier. The effective element gain is not independent of the spacing. It cannot exceed $\left(\dfrac{4\pi}{\lambda^2} d_1 d_2\right)$, with the result that

$$\sigma_s \approx \pi a^2 \frac{\left|\Gamma\right|^2 g_e(\theta_i, \phi_i) g_e(\theta_s, \phi_s)\, 4\zeta}{\left|1 - S_{11}\Gamma\right|^2 \left(g_{e_{max}}\right)^2 \left[\sin^2\theta_i + \sin^2\theta_s + 2 \sin\theta_i \sin\theta_s \cos(\phi_i - \phi_s)\right]} \tag{4-62}$$

where ζ is a factor less than or equal to unity.

4.9.2 Number of Components Required

Stable amplifier gains were reported from the Sylvania study and were on the order of 25 db, so that cross-sectional enhancement of this order might be expected. Thus, only relatively low system gain can be realized with a system of this type. The effective cross-section can be increased by increasing the radius of curvature of the surface. However, for a given coverage angle the surface area would have to be increased proportionally to the square of the radius of curvature so that the number of elements required would increase rapidly.

Even surfaces of moderate size require a large number of elements and amplifiers. For example, a spherical cap in a 2000-n. mi. orbit has been estimated to require 173, 000 elements with 23 db amplifier gain at 8 Gc to attain the effective scattering cross-section of a 1000-foot diameter conducting sphere (Sylvania, 1964). These values assume that coverage of the entire earth is to be obtained. An element spacing of 0. 75 λ is assumed. For a 5000-n. mi. orbit, approximately 4580 identical units would be required to simulate a 1000-foot diameter sphere.

The results of life tests indicate that approximately half the amplifiers would fail in the first year. This failure rate would have the effect of about a 6-db reduction in the scattering cross-section of the reflector and would also double the average element spacing. This latter effect might introduce interfering lobes in the pattern and thereby further degrade performance.

The total effective radiated power of such a system is also severely limited by the capabilities of present tunnel diodes. For example, tunnel diode amplifiers in the microwave region (C- or X-band) tend to saturate at outputs of about -40 to -25 dbm. If the latter figure is taken as representative, then 10^4 amplifiers, arranged on a spherical cap to cover a conical region of half angle θ_o, yield a maximum effective radiated power on the order of

$$ERP \approx \frac{2NP_o}{(1 - \cos \theta_o)} = \frac{2 \times 10^4 \times 2.8 \times 10^{-6}}{1 - \cos \theta_o} = \frac{0.056}{1 - \cos \theta_o} \text{ watts} \quad (4\text{-}63)$$

In contrast, active satellites can provide many more db of system gain and effective radiated power with relatively small volume, thereby greatly cutting down on the power requirements of an earth stationed transmitter. Consequently the pseudo-passive technique does not appear to fit the operating characteristics being considered in this study of spacecraft antenna systems.

4.10 WEIGHT CONSIDERATIONS OF MULTIPLE-BEAM ANTENNAS

In estimating the weights of antenna configurations, it is desirable to express these weights in terms of antenna parameters that have meaning in system applications. Usually, the antenna gain and the operating frequency are such parameters, and equations are developed in this section for the variation of the weights of different antenna configurations as a function of these parameters.

4.10.1 Reflector and Feed Antennas

Over a certain range of reflector areas it is assumed that the reflector weight is proportional to its effective density, ρ, and to its area; that is, the thickness of the structure is essentially invariant over the range considered. The area A is related to the gain G and the frequency f as

$$G = \eta \frac{4\pi f^2}{c^2} A \tag{4-64}$$

where η is an efficiency factor and c is the velocity of light. Therefore, the reflector weight, W_r, may be expressed as

$$W_r = K_1 \frac{\rho_r G}{\eta f^2} \tag{4-65}$$

Certain assumptions must also be made about the feed weight. It is assumed that the reflector is front-fed. For a reflector with a circular aperture the length of the feed guide is proportional to the aperture diameter and, thus, proportional to $\sqrt{G}/f$. In addition, transverse or circumferential waveguide and horn dimensions are inversely proportional to frequency; while the wall thickness does not vary significantly with frequency, its weight is proportional to the effective material density. Thus, the feed weight is given by

$$W_f = \frac{\rho_f K_2}{f^2} \sqrt{\frac{G}{\eta}} \tag{4-66}$$

The total weight may be expressed as

$$W_T = \frac{1}{f^2} \sqrt{\frac{G}{\eta}} \left[\rho_r K_1 \sqrt{\frac{G}{\eta}} + N K_2 \rho_f \right] \tag{4-67}$$

where $\underline{N}$ is the number of feeds. The weight of any additional supporting members should be added to this figure. The constants K_1 and K_2 can be evaluated by taking values from particular reflectors and feeds. As an example, a 25-inch diameter, coated fiberglass dish weighs somewhat less than a pound. An estimated weight per feed (for aluminum feed) is about 4 ounces. These values lead to the expression

$$W_T = \frac{\sqrt{G}}{f_{Gc}^2} \left(0.0251 \sqrt{G} + N \right) \quad \text{kilograms} \tag{4-68}$$

for an efficiency, η, of 0.41.

Reduction in the weight of reflector antennas may be possible through the utilization of new plastic materials and special processing techniques. A recent materials investigation of inflatable solar energy concentrators (Schwartz and Bagby, 1964) resulted in parabolic 5-foot diameter reflective surfaces that were similar in quality to surfaces

made with special tooling under ideal earth environmental conditions. Shaped aluminized-Mylar was inflated in a simulated space environment to a true paraboloidal shape and reinforced permanently by a nonreflective plastic that hardened when exposed to the sun. The investigators believe that the process can be applied to radar antennas, as well as to solar concentrators, as large as 50 feet in diameter, weighing less than 0.3 pound per square foot of reflecting surface. Even this weight may be excessive, however, and it is believed that further weight reduction might be possible to, say, 0.15 pound per square foot of reflecting surface.

4.10.2 Spherical Lens Antennas

The weight of a spherical lens is proportional to its volume and, therefore, to the cube of its diameter. The diameter, gain, and frequency are related by

$$f^2 \eta \frac{\pi^2}{c^2} D^2 = G \tag{4-69}$$

so that

$$W_\ell = \rho_1 K_3 \left(\frac{\sqrt{G/\eta}}{f} \right)^3 \tag{4-70}$$

As an example of numbers that apply to these antennas, an 18-inch diameter Luneberg lens which weighs 36 pounds can be considered. If with losses the efficiency η is 0.56, then

$$W_\ell = 0.354 \left(\frac{\sqrt{G}}{f_{Gc}} \right)^3 \text{ kilograms} \qquad \eta = 0.56 \tag{4-71}$$

A lightweight version of this same lens weighs 9 pounds. However, increased losses in the artificial dielectric reduce the efficiency to about 0.355. The weight expression becomes

$$W_{\ell\,W} = 0.177\left(\frac{\sqrt{G}}{f_{Gc}}\right)^3 \text{ kilograms} \qquad \eta = 0.355 \tag{4-72}$$

Weights of feeds must be added to these values to obtain the actual weights. The feed horn circumference and length would each be inversely proportional to frequency. Wall thickness change would not be great so that the feed weight is

$$W_f = K_4 \frac{\rho_f}{f^2} \tag{4-73}$$

The total lens and horn weight then follows the equation

$$W_T = \rho_\ell K_3 \left(\frac{1}{f}\sqrt{\frac{G}{\eta}}\right)^3 + \rho_f N \frac{K_4}{f^2} \tag{4-74}$$

where N is the number of feeds.

4.10.3 Thin Optical Lenses and Feeds

The considerations for unzoned thin lenses and feeds are similar to those for spherical lenses and feeds so the same equation applies with a different value of K_3. With zoned lenses, the overall thickness does not increase with the lens diameter, so that weight is proportional to area. The weight expression for the lens is then

$$W_\ell = K_5 \frac{\rho_\ell G}{\eta f^2} \tag{4-75}$$

and the total weight varies as

$$W_T = \rho_\ell K_5 \frac{G}{\eta f^2} + \rho_f N \frac{K_4}{f^2} \tag{4-76}$$

4.10.4 Constrained Lenses and Feeds

Constrained lenses can be made from thin-walled metal waveguides imbedded in a dielectric binder. The weight of the dielectric depends on volume while the weight of the metal will depend primarily on its surface area. In an unzoned lens the dielectric volume increases as the cube of the lens diameter while the metal surface increases as the square of the lens diameter. The weight with an unzoned lens then varies as

$$W_\ell = \rho_d K_6 \left(\frac{1}{f}\frac{\sqrt{G}}{\eta}\right)^3 + \rho_m K_7 \frac{G}{\eta f^2} \quad \text{(unzoned)} \tag{4-77}$$

For a zoned lens the expression reduces to

$$W_\ell = \rho_d K_8 \frac{G}{\eta f^2} + \rho_m K_9 \frac{1}{f}\sqrt{\frac{G}{\eta}} \quad \text{(zoned)} \tag{4-78}$$

4.10.5 Array and Butler Matrix

The weight of an array will be proportional to the number of elements and therefore to the array gain. It will also depend on the density of the material from which the elements are made. For elements printed on a surface (e.g., spirals, printed dipoles, etc.), the weight will vary inversely as the square of the frequency. Therefore, the array weight is

$$W_a = K_{10}\rho_e \frac{G}{f^2} \tag{4-79}$$

where ρ_e is the effective mass density of the element and supporting material.

The weight of the beam-forming matrix is more difficult to estimate. For a linear array of N elements the number of directional couplers required is

$$N_{dc} = \frac{N}{2} \log_2 N \tag{4-80}$$

The number of fixed phase shifters is

$$N_{ps} = \frac{N}{2} (\log_2 N - 1) \tag{4-81}$$

The phase shifts of the fixed phase shifters and therefore their weights are not all identical. In a strip transmission line configuration, which can be made broadband (for example, by using log-periodic configurations), their sizes are essentially inversely proportional to the center frequency of interest. The weight might therefore be expected to vary as

$$W_m = K_{11} \frac{N}{2} \log_2 N + \sum_{j=1}^{\frac{N}{2}(\log_2 N - 1)} K_{psj} \tag{4-82}$$

In terms of gain this expression becomes

$$W_m = \frac{K_{11}}{2} K_{12} G \log_2 (K_{12} G) + \sum_{j=1}^{K_{12} G(\log_2 K_{12} G - 1)} K_{ps_j} \tag{4-83}$$

No estimates of the K's for the matrix are available at present; however, an actual advertised weight for an eight-element matrix operating between 4 Gc and 6 Gc is 30 ounces. Extension of the weight estimate to two-dimensional matrices is difficult since the matrix configuration might take on several forms.

5. ELECTRONICALLY SELF-STEERING SYSTEMS

Self-steering arrays are a class of antenna systems which use the incident r-f energy to phase the elements so that a beam is formed in the direction from which the energy is received. These arrays are also called self-focusing and self-phasing antennas. This type of array may be contrasted with the usual electronically steerable arrays which require external sensors and information to do the steering. There are a number of configurations which these systems can take, some more sophisticated than others. In general, the systems are redirective (receive r-f energy and retransmit to another station) or retrodirective (receive r-f energy and transmit back to the source). In this section several arrays of this type are considered and their operation analyzed.

5.1 THE EFFECTIVE GAIN OF SELF-STEERABLE ARRAYS

In the most general case, self-steering arrays would be used to receive a signal from one direction and retransmit it in a different direction. Both the transmitting and receiving characteristics of these arrays are of interest. These are considered in the following paragraphs. Since the transmitting situation is more easily treated and since the receiving situation may be determined from it by use of the reciprocity theorem, the transmitting case is considered first.

5.1.1 Transmit Case

To examine the power available at a distant receiver, it is necessary to compute the electric fields produced by the antenna at an arbitrary point in the antenna far field. In the arrays under consideration, each element is assumed to be connected to separate, but identical, generators of internal impedance Z_o through identical transmission lines of characteristic impedance Z_o, where Z_o is assumed to be real. For

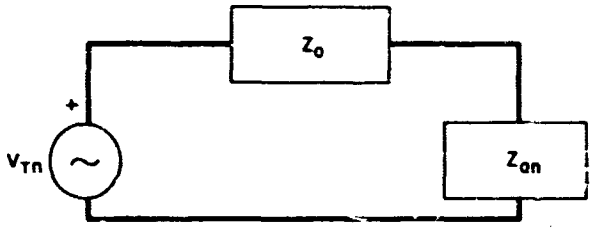

Figure 5-1. Excitation of single element by matched voltage source.

purposes of analysis, Z_{an} is denoted as the input impedance of the n^{th} element with all others passively terminated in Z_o. The equivalent circuit is shown in Figure 5-1. The far-field electric field pattern of the n^{th} element in the presence of all the remaining passively terminated elements is denoted by $\bar{u}_\theta e_{\theta_n}(\theta, \phi) + \bar{u}_\phi e_{\phi_n}(\theta, \phi)$ where θ and ϕ are spherical coordinates and $\bar{u}_\theta$ and $\bar{u}_\phi$ are unit vectors in the θ and ϕ directions, respectively. The directive gain function of the n^{th} element is denoted by

$$g_n(\theta, \phi) = g_{\theta_n}(\theta, \phi) + g_{\phi_n}(\theta, \phi) \tag{5-1}$$

where g_{θ_n} and g_{ϕ_n} denote the gain due to θ and ϕ polarized components, respectively, of the radiation field (Silver, 1949d). They are given by

$$g_{\theta_n} = \frac{4\pi \left| e_{\theta_n} \right|^2}{\iint_{\text{sphere}} \left(\left| e_{\theta_n} \right|^2 + \left| e_{\phi_n} \right|^2 \right) d\Omega} \tag{5-2a}$$

$$g_{\phi_n} = \frac{4\pi \left| e_{\phi_n} \right|^2}{\iint_{\text{sphere}} \left(\left| e_{\theta_n} \right|^2 + \left| e_{\phi_n} \right|^2 \right) d\Omega} \tag{5-2b}$$

With these definitions it may be shown that the electric field intensity at a point in space at a distance R_n from the n^{th} element which is excited by a voltage source V_{T_n} as shown in Figure 5-1 is given by

$$e_{\theta_n} = \sqrt{\frac{\eta R^r_{a_n} g_{\theta_n}}{4\pi}} \frac{V_{T_n} e^{j\psi_{\theta_n}}}{\left(Z_{a_n} + Z_o\right)} \frac{e^{-jkR_n}}{R_n} \tag{5-3a}$$

$$e_{\phi_n} = \sqrt{\frac{\eta R^r_{a_n} g_{\phi_n}}{4\pi}} \frac{V_{T_n} e^{j\psi_{\phi_n}}}{\left(Z_{a_n} + Z_o\right)} \frac{e^{-jkR_n}}{R_n} \tag{5-3b}$$

In these expressions $Z_{a_n} \equiv R^r_{a_n} + R^d_{a_n} + jX_{a_n}$ is the input impedance of the n^{th} element when all others are passively terminated in Z_o. $R^r_{a_n}$ is the radiation resistance of the element and $R^d_{a_n}$ accounts for power coupled to the unexcited elements. The symbols ψ_{θ_n} and ψ_{ϕ_n} are phase functions associated with the θ and ϕ components of the electric field of the element, k is the free space phase constant, and η is the characteristic impedance of free space. The radiation field at some point in the far zone of the array is the sum over all these element fields and is given by

$$E_\theta = \sum_n e_{\theta_n} = \sqrt{\frac{\eta}{4\pi}} \sum_n \sqrt{R^r_{a_n} g_{\theta_n}} \frac{V_{T_n} e^{j\left(\psi_{\theta_n} - kR_n\right)}}{\left(Z_{a_n} + Z_o\right)R_n} \tag{5-4a}$$

$$E_\phi = \sum_n e_{\phi_n} = \sqrt{\frac{\eta}{4\pi}} \sum_n \sqrt{R^r_{a_n} g_{\phi_n}} \frac{V_{T_n} e^{j\left(\psi_{\phi_n} - kR_n\right)}}{\left(Z_{a_n} + Z_o\right)R_n} \tag{5-4b}$$

From these expressions the power density at that point can be computed.

5.1.2 Mutual Coupling Effects on Element Power

The radiation problem has been formulated in terms of the voltages of equivalent generators and the input impedance of each array element when all other elements are terminated in a load Z_o. The total radiated power can then be found by integrating the Poynting vector over a sphere containing the array. It may not be computed directly from the generator voltages and element impedances unless mutual coupling between elements is considered. If mutual coupling is taken into consideration, it may be shown that the current into the n^{th} element is given by

$$I_n = \frac{V_{T_n}}{\left(Z_{a_n} + Z_o\right)} - \frac{1}{\left(Z_{a_n} + Z_o\right)} \sum_{\substack{j=1 \\ j \neq n}}^{N} \frac{Z_{nj}}{Z_{a_j} + Z_o} V_{T_j} = \frac{V_{T_n}}{\left(Z_{a_n} + Z_o\right)} + I'_n \qquad (5\text{-}5)$$

where V_{T_j} is the generator open circuit voltage of the j^{th} element and Z_{nj} is the mutual impedance between element n and element j. It is important to point out that Z_{nj} as used here is not the usual mutual impedance which is determined with all elements open-circuited except the driven element. In this case Z_{nj} is determined with all elements terminated in Z_o except the driven element. The driven element is driven by a generator of internal impedance Z_o. On using this distinction, the terminal voltage at the n'^{th} antenna is given by

$$V_{a_n} = V_{T_n} - I_n Z_o = \frac{Z_{a_n} V_{T_n}}{Z_{a_n} + Z_o} + \frac{Z_o}{Z_{a_n} + Z_o} \sum_{\substack{j=1 \\ j \neq n}}^{N} \frac{Z_{nj}}{\left(Z_{a_j} + Z_o\right)} V_{T_j} \qquad (5\text{-}6)$$

$$= \frac{Z_{a_n} V_{T_n}}{Z_{a_n} + Z_o} - Z_o I'_n$$

The effective element input impedance may now be written as

$$Z^{e}_{a_n} = \frac{Z_{a_n} + Z_o \sum_{\substack{j=1 \\ j\neq n}}^{N} \frac{Z_{nj}}{(Z_{a_j} + Z_o)} \left(\frac{V_{T_j}}{V_{T_n}}\right)}{1 - \sum_{\substack{j=1 \\ j\neq n}}^{N} \frac{Z_{nj}}{(Z_{a_j} + Z_o)} \left(\frac{V_{T_j}}{V_{T_n}}\right)} \tag{5-7}$$

The power radiated by the n^{th} element is therefore given by

$$P_{r_n} = \mathrm{Re}\, \frac{1}{2} V_{a_n} I^{*}_{a_n}$$

$$P_{r_n} = \frac{1}{2} \frac{R_{a_n} |V_{T_n}|^2}{|Z_{a_n} + Z_o|^2} - \frac{1}{2} Z_o |I'_n|^2 + \frac{1}{2} \mathrm{Re} \left\{ \frac{Z_{a_n} - Z_o}{Z_{a_n} + Z_o} V_{T_n} I'^{*}_{n} \right\} \tag{5-8}$$

where Z_o is assumed to be pure real. It is also assumed that dissipation in the element itself is negligible. The first term is the power that would be supplied by the n^{th} generator if only the n^{th} element were excited. The second term is the reduction that results from the excitation of the other elements (effective mismatching). The last term is the change in supplied power due to the mismatch between transmission line and load when only the n^{th} element is excited. This change may increase or decrease the radiated power depending on the phases of the terms involved. Of course, if it is possible to make $Z_{a_n} = Z_o$, the effect of exciting other elements is to reduce the power supplied to the n^{th} element. The total power radiated is now the sum over P_{r_n}.

5.1.3 Receive Case

When the self-steerable array is receiving, each element acts independently of the others as far as internal interconnections are concerned; i.e., each element is separately connected to an impedance, Z_o. V_{L_n}, the voltage across this load resistor, can be computed when an arbitrarily polarized plane wave, with orthogonal components of electric field E_{i_n} and E'_{i_n} is incident on the antenna. This computation can be performed by applying the reciprocity theorem (Harrington, 1961) to a system composed of the antenna under consideration and a remote dipole, oriented first to produce E_{i_n} and then reoriented to produce E'_{i_n} at the receiving antenna. When the theorem has been applied, with the aid of Equation (5-3), the following expression results.

$$V_{L_n} = \frac{Z_o}{\left(Z_{a_n} + Z_o\right)} \frac{\lambda}{j} \sqrt{\frac{R^r_{a_n}}{\pi\eta}} \left\{ \left[E_{i_n} \cos\alpha + E'_{i_n} \sin\alpha \right] e^{j\psi_{\theta_n}} \sqrt{g_{\theta_n}} \right.$$

$$\left. + \left[E_{i_n} \sin\alpha - E'_{i_n} \cos\alpha \right] e^{j\psi_{\phi_n}} \sqrt{g_{\phi_n}} \right\} . \qquad (5\text{-}9)$$

where α is defined in Figure 5-2. Use of Equation (5-9) allows the response of the antenna element to be computed for any type of incident polarization whatsoever. The received signal is then processed in different ways, depending on the exact type of antenna system employed.

5.1.4 System Operation

Both redirective and retrodirective types of self-steerable arrays may be operated in essentially two different manners. In the first manner they operate as linear devices in which the output signal is proportional to the input signal. In this type of operation the transfer functions of the circuit elements are independent of signal amplitude and the system acts essentially as a radar target enhancement device. This type of operation causes returned power at an earth station to vary in a

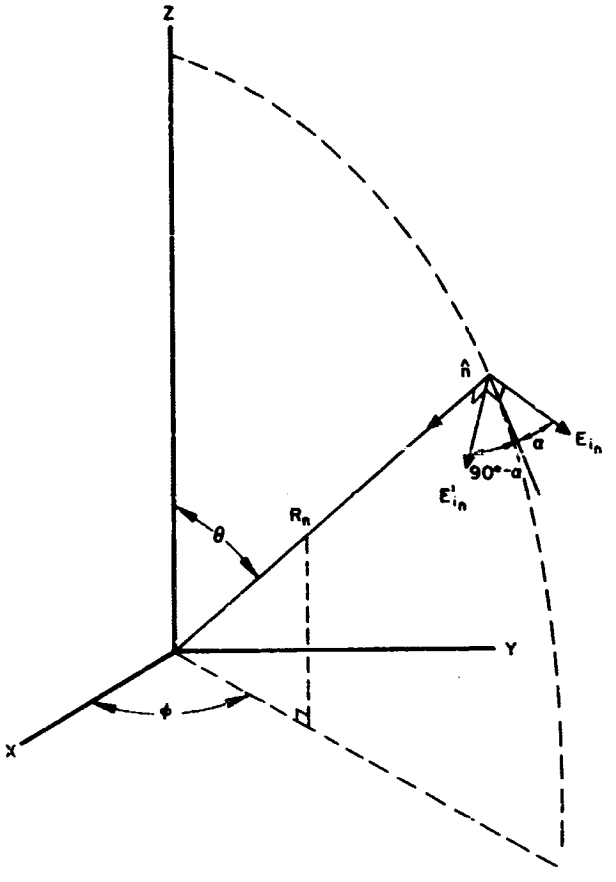

Figure 5-2. Geometry of far field of self-steerable array.

R^{-4} manner, resulting in a wide dynamic range of operation at the earth receiver. The system would have to be designed to give adequate signal-to-noise ratios for the maximum range of operation and, therefore, the minimum power radiated by the satellite would have to provide this signal-to-noise ratio. At closer ranges a linear system would radiate more power than necessary. Therefore, a second mode of operation in which the satellite radiates a signal level independent of range is more attractive. Through the use of limiters, this system has a transfer function which is inversely proportional to incident signal level for signals above a certain threshold and, therefore, its output signal level is independent of the input.

For each mode of operation of the overall satellite, system requirements can be evaluated in terms of the radiated power, antenna gain, and receiver noise figure of the earth stations.

In cases in which sufficient power is available in the up link, it is not necessary to use the directive properties of an array to receive at the satellite. An essentially omnidirectional receiving antenna can be used, and sufficiently high signal-to-noise ratios at the satellite may be obtained. This fact allows the use of essentially only the retrodirective type of system while still maintaining the redirective properties. Thus such a system appears to be very promising.

One property of self-steerable arrays is that they will lock onto any pilot signal of the proper frequency. Two pilot signals from

different points on earth will cause the satellite to radiate back in both these directions. If the system is operated in a linear manner and the signals do not saturate the satellite, no degradation in system performance will result.* If the system is operated at saturation, however, as in the so-called constant radiated power type of operation, then two equal pilot signals will cause the radiated power to be shared by two receiving stations, and the signal level at each station will be degraded.

5.2 REDIRECTIVE ARRAY

Perhaps the most sophisticated of the self-steerable array systems is the "redirective" array (Cutler et al., 1963) which takes a signal from one station and redirects it to a second station. The system requires the generation of six different frequencies to be used in the signal processing. Each element requires a branching filter, two second-order mixers, four third-order mixers, several i-f amplifiers, narrow band filters (e.g., phase-locked loop to process the pilots), and two power amplifiers to supply final transmitted power. A diagram of such a system for a two-way repeater is illustrated in Figure 5-3.

5.2.1 Analysis of Operation

In the analysis to follow, a phase-modulated or frequency-modulated information signal is assumed. An unmodulated pilot signal is also employed by each terminal. Two ground stations, E and W, are assumed with the satellite used for a transmission link between them. The basic idea is as follows. Information is to be transmitted from W to E. Station W transmits a pilot signal and an information signal slightly displaced in frequency. The pilot signal, when received at the satellite, is used to remove phase differences from the information signals received by the array elements. These signals are then added in phase and redistributed to the individual array elements where a

*In the case of the redirective array discussed in Section 5.2, some interaction may occur between signals from two different directions due to the operation of the third-order mixers. Additional investigation is required to determine the extent of this interaction.

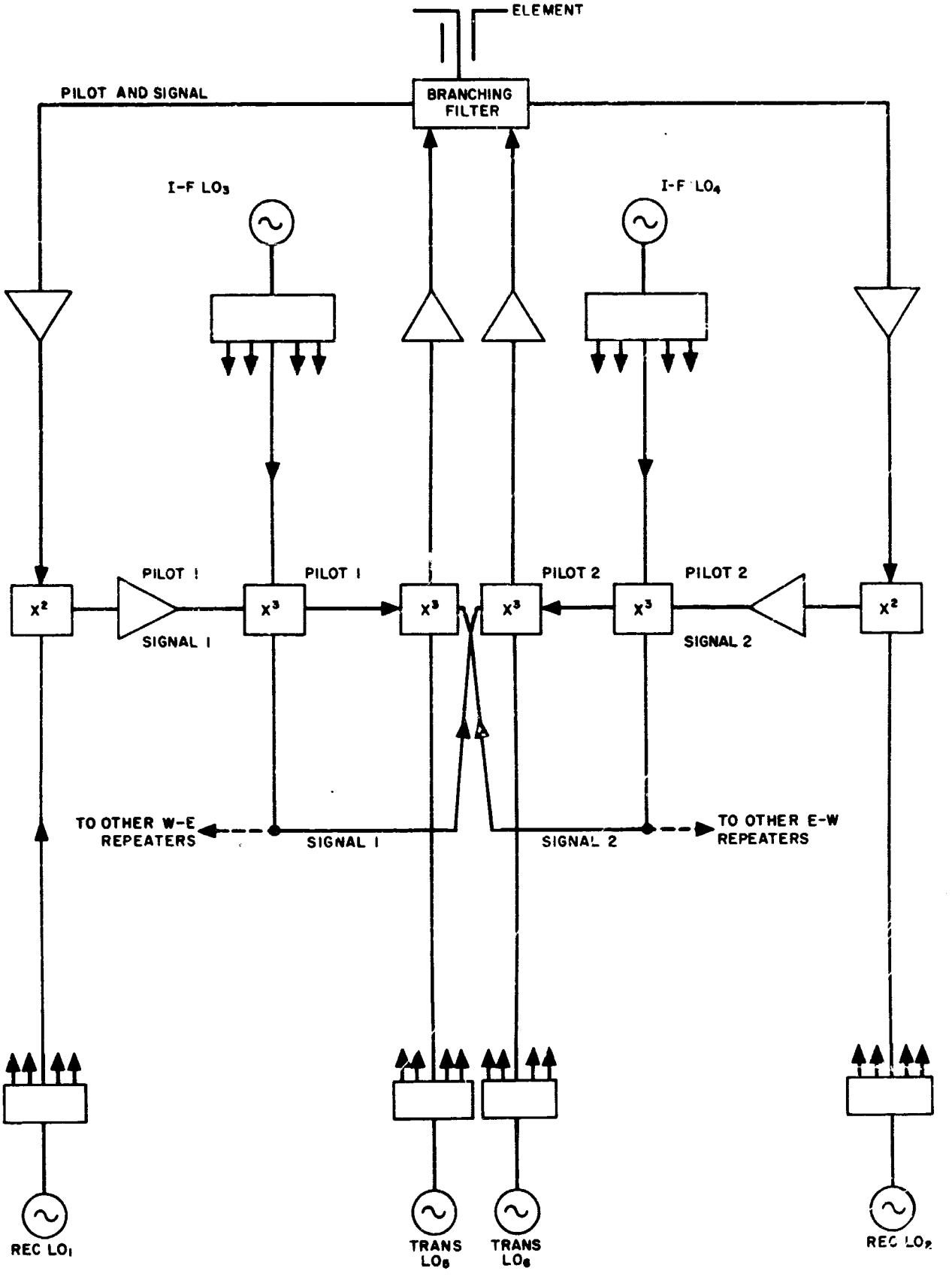

Figure 5-3. Basic elements of a two-way repeater.

pilot signal from the receiving terminal E re-inserts the proper phase on the signal to direct the transmission to E. The in phase addition of the signals received by the individual elements is necessary since not all elements visible to transmitter station and receiver station are the same. In fact, the number visible to both simultaneously may be small. Interconnection of elements allows all those elements visible to either station to be used in forming the receiving and transmitting beam.

The system as illustrated in Figure 5-3 will be analyzed in some detail. A pilot signal at angular frequency ω_{pW} is assumed incident from station W. This signal will induce a voltage across the terminals of the n^{th} element which is denoted by V_{npW} where V_{npW} may be determined from Equation (5-9) by using the proper quantities. For this analysis it may be written as

$$V_{npW} = \left|V_{npW}\right| e^{j\left[\zeta_{npW} + \xi_{npW}(\theta_R, \phi_R)\right]} \qquad (5\text{-}10)$$

where $\zeta_{npW}(\omega_{pW})$ is that portion of the phase of V_{npW} that is characteristic of the element and $\xi_{npW}(\theta_R, \phi_R) = \left(-\omega_{pW}/c\right) h_n(\theta_R, \phi_R)$ is that portion of the phase which depends on element position with respect to a phase front of the incident wave. The quantity c is the free space velocity of light. In a similar manner the incident information signal at the element terminals may be written as (frequency $\omega_{M(W-E)}$)

$$V_{nM} = \left|V_{nM}\right| e^{j\left[\zeta_{nM(W-E)} + \xi_{nM(W-E)}(\theta_R, \phi_R) + \phi_{(W-E)}(t)\right]} \qquad (5\text{-}11)$$

where $\phi_{(W-E)}(t)$ represents the information signal. The subscripts M(W-E) indicate the modulated signal which is to be relayed from W to E. In what follows it is assumed that the received signals V_{npW} and V_{nM} are amplified to such an extent that the signal-to-noise ratio of the information signal is established before the first mixer.

The outputs of the first mixer will consist of the pilot signal and the information signal translated to the frequencies $(\omega_{LO_1} - \omega_{pW})$ and $(\omega_{LO_1} - \omega_{M(W-E)})$, respectively, where ω_{LO_1} is the angular frequency of local oscillator number one. These signals are given by

$$\left|K_{1n}(\omega_{pW})\right| \left|V_{npW}\right| e^{j\left[\beta_{npW} - \zeta_{npW} - \xi_{npW}\right]} \tag{5-12a}$$

$$\left|K_{1n}(\omega_{M(W-E)})\right| \left|V_{nM}\right| e^{j\left[\beta_{nM(W-E)} - \zeta_{nM(W-E)} - \xi_{nM(W-E)} - \phi_{(W-E)}(t)\right]} \tag{5-12b}$$

where $\left|K_{1n}\right| e^{j\beta_n}$ is the transfer function of the first mixer and any preceding amplifiers. It is important that the pilot frequency be filtered from the surrounding noise or modulation and desirable that it be amplified to a level well above that of the modulated signal before entering the second mixer shown in Figure 5-3. These modifications are to keep the pilot from bringing noise into the final modulation band and to assure that the desired products predominate over higher order products. Therefore the pilot signal is amplified to a value

$$\left|A_n\right| \left|K_{1n}(\omega_{pW})\right| \left|V_{npW}\right| e^{j\left[\alpha_n + \beta_{npW} - \zeta_{npW} - \xi_{npW}\right]} \tag{5-13}$$

where $\left|A_n\right| e^{j\alpha_n}$ is the gain of the amplifier. The local oscillator signal for the third-order mixer is a frequency ω_{LO_3}. Two outputs of the third-order mixer are required: the component at frequency $\omega_{LO_3} + \omega_{M(W-E)} - \omega_{pW}$ and a component at the angular frequency for retransmission. The first component is given by

$$\left|K_{2n}(\omega_{M(W-E)}, \omega_{pW})\, A_n K_{1n}(\omega_{pW})\, K_{1n}(\omega_{M(W-E)})\, V_{npW} V_{nM}\right| \tag{5-14}$$

$$e^{j\left[\delta_n + \alpha_n + \beta_{npW} - \beta_{nM(W-E)} + \zeta_{nM(W-E)} - \zeta_{npW} + \xi_{nM(W-E)} - \xi_{npW} + \phi_{(W-E)}(t)\right]}$$

where $|K_{2n}| e^{j\delta_n}$ is the transfer function of the third order mixer. This component is the total received voltage at the n^{th} element. The analysis has assumed that the information bandwidth is sufficiently narrow so that the characteristics of the components are constant over that band and so that the differences in path length from element to element are not significant. If the outputs of these are summed at a common point and redistributed to all the elements again through the third-order mixer associated with LO_6, the signal supplied to each mixer is the average of all signals. If there are $\underline{N}$ elements, the signal supplied to each mixer becomes

$$V_o e^{j\phi_{(W-E)}(t)} = \frac{K_s}{N} \sum_n \left| K_{2n} A_n K_{1n}(\omega_{M(W-E)}) K_{1n}(\omega_{M(W-E)}) V_{npW} V_{nM} \right| \tag{5-15}$$

$$e^{j\left[\delta_n + \alpha_n + \beta_{npW} - \beta_{nM(W-E)} - \zeta_{nM(W-E)}\right.}$$

$$\left. -\zeta_{npW} + \xi_{nM(W-E)} - \xi_{npW} + \phi_{(W-E)}(t) \right]$$

where K_s is a characteristic of the summing device. If all mixers and amplifiers are identical, then the δ_n, α_n, and β_n are identical and the only phase differences of the received signals from each element arise from possible changes with frequency in the phase characteristics of the elements and from the term

$$\xi_{nM(W-E)} - \xi_{npW} = -\frac{(\omega_{M(W-E)} - \omega_{pW})}{c} h_n(\theta_R, \phi_R) \tag{5-16}$$

This latter phase error can be minimized by making $\omega_{M(W-E)}$ and ω_{pW} as close as possible, consistent with filtering capabilities.

It can be seen from Equation (5-15) that in-phase addition of all signals requires that all corresponding mixers and amplifiers behind each element should be identical in electrical characteristics. This requirement may be somewhat difficult to achieve over long periods of time, and allowable tolerances on gain and phase shift would have to be determined from overall system requirements.

5.2.2 Retransmission Process

The retransmission process must still be considered. For retransmission the second output from the third-order mixer is considered, the term at the angular frequency $(\omega_{LO_1} + \omega_{LO_3} - \omega_{pW})$. The component has the form

$$\left|K_{3n}(\omega_{pW})\, A_n K_{1n}(\omega_{pW})\, V_{npW}\right| e^{j\left[\epsilon_n + \alpha_n + \beta_{npW} - \zeta_{npW} - \xi_{npW}\right]} \quad (5\text{-}17)$$

where $\left|K_{3n}\right| e^{j\epsilon_n}$ is the transfer function of the third-order mixer for the signal at this frequency. This signal has the phase information necessary to redirect a signal from station E down to station W. However, at present it is wished to direct a signal from station W, given by Equation (5-15), down to station E. For this process the signal is taken from the mixer connected to LO_6 which corresponds to Equation (5-17) except that it contains phase information from a pilot signal (at ω_{pE}) sent by station E. This signal is at angular frequency $(\omega_{LO_2} + \omega_{LO_4} - \omega_{pE})$ and is given by

$$\left|K'_{3n}(\omega_{pE})\, A'_n K'_{1n}(\omega_{pE})\, V_{npE}\right| e^{j\left[\epsilon'_n + \alpha'_n + \beta_{npE} - \zeta_{npE} - \xi_{npE}\right]} \quad (5\text{-}18)$$

where the primes denote gains and phase shifts of the E-W components analogous to those of the corresponding W-E components.

This signal, together with that given by Equation (5-15), is fed into the third-order mixer of LO_6. The signal at angular frequency $\omega_{T(W-E)} = (\omega_{LO_1} + \omega_{LO_2} + \omega_{LO_4} - \omega_{LO_6} - \omega_{pW} - \omega_{pE} + \omega_{M(W-E)})$ is selected from all the modulation products. It is given by

$$V_{Tn} = \left|K'_{4n}(\omega_{pW}, \omega_{pE}, \omega_{M(W-E)})\, K'_{3n}(\omega_{pE})\, A'_n K_{1n}(\omega_{pE})\, V_{npE}\right| V_o \qquad (5\text{-}19)$$

$$e^{j\left[\sigma'_n + \epsilon'_n + \beta_{npE} - \zeta_{npE} - \xi_{npE} + \phi_{(W-E)}(t)\right]}$$

where $\left|K'_{4n}\right| e^{j\sigma'_n}$ is the transfer function of the mixer for this frequency component. This signal is then the equivalent source voltage exciting the n^{th} element in the array. The far fields radiated by the array can now be written:

$$E_\theta = \sqrt{\frac{\eta}{4\pi}}\,\frac{e^{-jkR}}{R} \sum_n \sqrt{R^r_{a_n} g_{\theta_n}}\,\frac{V_{T_n}}{(Z_{a_n} + Z_o)}\, e^{j\left[\psi_{\theta_n} - \frac{\omega_{T(W-E)}}{c} h_n(\theta,\phi)\right]} \qquad (5\text{-}20a)$$

$$E_\phi = \sqrt{\frac{\eta}{4\pi}}\,\frac{e^{-jkR}}{R} \sum_n \sqrt{R^r_{a_n} g_{\phi_n}}\,\frac{V_{T_n}}{(Z_{a_n} + Z_o)}\, e^{j\left[\psi_{\phi_n} - \frac{\omega_{T(W-E)}}{c} h_n(\theta,\phi)\right]} \qquad (5\text{-}20b)$$

In these expressions all transmitting antenna functions, i. e., gains, phases, etc., are evaluated at the transmitted frequency $\omega_{T(W-E)}$. Using the expression for phase in Equation (5-19) and writing

$$\xi_{npE} = \frac{\omega_{pE} h_n(\theta_T, \phi_T)}{c}$$

where θ_T and ϕ_T are the coordinates of the desired transmitting direction (toward receiving station E), yields

$$E_\theta = \sqrt{\frac{\eta}{4\pi}} \frac{e}{R} \frac{-j\omega_{T(W-E)} R}{c} \sum_n \sqrt{R_{a_n} g_{\theta_n}} \frac{|V_{T_n}|}{(Z_{a_n} + Z_o)} \tag{5-21a}$$

$$\cdot e^{j\left[\sigma'_n + \epsilon'_n + \beta_{npE} - \zeta_{npE} + \frac{\omega_{pE}}{c} h_n(\theta_T, \phi_T) - \frac{\omega_{T(W-E)}}{c} h_n(\theta, \phi) + \psi_{\theta n} + \phi_{(W-E)}(t)\right]}$$

$$E_\phi = \sqrt{\frac{\eta}{4\pi}} \frac{e}{R} \frac{-j\omega_{T(W-E)} R}{c} \sum_n \sqrt{R^r_{a_n} g_{\phi_n}} \frac{|V_{T_n}|}{(Z_{a_n} + Z_o)} \tag{5-21b}$$

$$\cdot e^{j\left[\sigma'_n + \epsilon'_n + \beta_{npE} - \zeta_{npE} + \frac{\omega_{pE}}{c} h_n(\theta_T, \phi_T) - \frac{\omega_{T(W-E)}}{c} h_n(\theta, \phi) + \psi_{\phi n} + \phi_{(W-E)}(t)\right]}$$

Equations (5-21) indicate that the pattern of the array will have a maximum near $\theta = \theta_T$ and $\phi = \phi_T$ if the phase shifts introduced by the processing circuitry are identical from element to element. The terms ζ_{npE} and $\psi_{\theta n}$ can give rise to phase errors if the phases of the element patterns are not idependent of angle. To get a numerical estimate of the effective power at the receiving station E, it would be

necessary to assume an array configuration, element type, and characteristics of circuit components.

It may be pointed out, however, that the errors introduced by the variations in component gains and phase shifts are random and will contribute to beam broadening, gain reduction, and sidelobe increase but not appreciably to beam pointing errors. In addition, for a symmetric element arrangement, such as on a sphere, the phase errors introduced by the element phase characteristics and by the difference in ω_{pE} and $\omega_{T(W-E)}$ would tend to be evenly distributed about the desired pointing direction and result in beam broadening rather than beam pointing error.

5.2.3 Representative Systems

It is of interest to consider the retransmitted signals for several configurations so that the effective system gain may be determined for these configurations. When the elements are arranged in a regularly spaced linear or planar structure, the individual elements are nearly alike in their element factors and impedances. This fact is more nearly true for large arrays in which most elements see similar environments, and edge effects due to different mutual coupling effects are comparatively small perturbations on the whole system.

When the array is distributed over irregular surfaces, the element orientation changes from element to element; and the environment "seen" by each element changes so that both element impedance and element factor may vary from element to element.

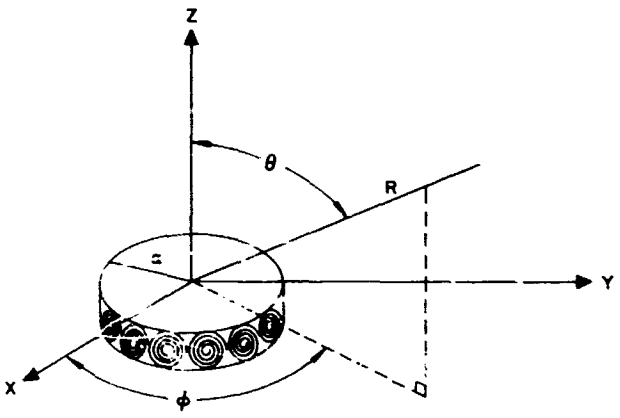

Figure 5-4. Circular array of spiral antennas.

Circular Array of Spirals. To make some of the ideas more concrete, a circular array of spiral antennas can be considered as illustrated in Figure 5-4. The spirals have well defined phase centers located at their physical centers so that ζ_n may be taken as the same for all antennas and

independent of θ and ϕ. These elements produce fields which are circularly polarized. It is assumed that this polarization is maintained for all angles of observation. Then,

$$\sqrt{g_{\theta n}}\, e^{j\psi_{\theta n}} = \sqrt{g_{\phi n}}\, e^{j\left(\psi_{\phi n} \pm \frac{\pi}{2}\right)} = \sqrt{g_n}\, e^{j\left(\psi_n \pm \frac{\pi}{2}\right)} \tag{5-22}$$

All elements are in the same environment so that the Z_{an} are all identical ($Z_{an} \equiv Z_a$). Under these conditions the fields become

$$E_\theta = \sqrt{\frac{\eta R_o^r}{4\pi}}\; e^{-j\frac{\omega_{T(W-E)} R}{c}} \over (Z_a + Z_o)\, R \sum_n \sqrt{g_n}\, \left|V_{Tn}\right| \tag{5-23a}$$

$$e^{j\left[b_n + \frac{\omega_{pE}}{c} h_n(\theta_T, \phi_T) - \frac{\omega_{T(W-E)}}{c} h_n(\theta, \phi) + \phi_{(W-E)}(t)\right]}$$

$$E_\phi = \pm jE_\theta \tag{5-23b}$$

In Equations (5-23) all phase errors due to variations in components have been grouped together in the b_n. Amplitude errors are included in the $\left|V_{Tn}\right|$. Because of the circular geometry of the array the following relationships hold.

$$g_n(\theta, \phi) = g_1\left(\theta, \phi - \frac{[n-1]\,2\pi}{N}\right) \tag{5-24a}$$

$$h_n(\theta, \phi) = a \sin\theta \cos\left(\phi - \phi_1 - \frac{[n-1]\,2\pi}{N}\right) \tag{5-24b}$$

where ϕ_1 is the angular position of element number 1.

The far fields now may be written:

$$E_\theta = \sqrt{\frac{\eta R_a^r}{4\pi}}\, e^{j\phi_{W-E}(t)}\, \frac{e^{-j\frac{\omega_{T(W-E)}R}{c}}}{(Z_a+Z_o)R} \sum_n \sqrt{g_1\left(\theta,\phi - \frac{[n-1]\,2\pi}{N}\right)}\left|V_{Tn}\right| \tag{5-25a}$$

$$e^{j\left[b_n + \frac{\omega_{pE}}{c} a \sin\theta_T \cos\left(\phi_T - \phi_1 - \frac{[n-1]\,2\pi}{N}\right)\right.}$$

$$\left. - \frac{\omega_{T(W-E)}}{c} a \sin\theta \cos\left(\phi - \phi_1 - \frac{[n-1]\,2\pi}{N}\right)\right]$$

$$E_\phi = \pm jE_\theta \tag{5-25b}$$

It is now possible to write ω_{pE} as $\omega_{T(W-E)} + \omega_{e(W-E)}$. Then the signals become

$$E_\theta = \sqrt{\frac{\eta R_a^r}{4\pi}}\, e^{j\phi_{W-E}(t)}\, e^{-j\frac{\omega_{T(W-E)}R}{c}} \sum_n \sqrt{g_1\left(\theta,\phi - \frac{[n-1]\,2\pi}{N}\right)}\left|V_{Tn}\right|$$

$$e^{j\left[b_n + \frac{\omega_{T(W-E)}}{c} a \left\{\sin\theta_T \cos\left(\phi_T - \phi_1 - \frac{[n-1]\,2\pi}{N}\right)\right.\right.} \tag{5-26a}$$

$$\left.\left. - \sin\theta \cos\left(\phi - \phi_1 - \frac{[n-1]\,2\pi}{N}\right)\right\} + \frac{\omega_{e(W-E)}}{c} a \sin\theta_T \cos\left(\phi_T - \phi_1 - \frac{[n-1]\,2\pi}{N}\right)\right]$$

$$E_\phi = \pm jE_\theta \tag{5-26b}$$

From these relationships it is evident that the phase errors introduced by the frequency separation between the transmitted frequency and the pilot frequency are evenly distributed about the required pointing

direction and therefore contribute to beam broadening, sidelobe degradation, and gain reduction, but not to beam pointing error. The b_n (phase errors due to component variation) are essentially random errors and can contribute to beam pointing errors as well as to the errors just mentioned.

In the desired beam pointing direction, the maximum phase error that results from the frequency separation between the received pilot and transmitted frequencies is given from Equation (5-26) as

$$\frac{\omega_{e(W-E)}}{c} a \sin \theta_T = \epsilon \tag{5-27}$$

Therefore, to keep the phase error less than ϵ for all possible θ_T, there should exist

$$\omega_{e(W-E)} < \frac{\epsilon c}{a} \tag{5-28}$$

which in terms of a relative shift may be written

$$\frac{\omega_{e(W-E)}}{\omega_{pE}} < \frac{\epsilon \lambda_{pE}}{2\pi a} \tag{5-29}$$

If it is desired to keep the maximum phase error to less than $\pi/2$, a value that would put the outputs from the end elements in phase quadrature with those from the elements near the center of the radiating section, Equation (5-29) reduces to

$$\frac{\omega_{e(W-E)}}{\omega_{pE}} < \frac{\lambda_{pE}}{4a} \tag{5-30}$$

For an array 10 wavelengths in diameter this relation gives a fractional separation of

$$\frac{\omega_{e(W-E)}}{\omega_{pE}} < 0.05 \tag{5-31}$$

The amount of signal degradation which results from the phase errors due to frequency separation may be written as

$$\left|\frac{E_\phi}{E_{\phi_o}}\right| = \left|\frac{E_\theta}{E_{\theta_o}}\right| = \left| \frac{\sum_n \sqrt{g_1\left(\frac{\pi}{2}, \phi_T - \frac{[n-1]\,2\pi}{N}\right)}\, e^{j\frac{\omega_{e(W-E)}}{c} a \cos\left(\phi_T - \phi_1 - \frac{[n-1]\,2\pi}{N}\right)}}{\sum_n \sqrt{g_1\left(\frac{\pi}{2}, \phi_T - \frac{[n-1]\,2\pi}{N}\right)}} \right| \tag{5-32}$$

For a particular element pattern this expression may be evaluated to determine the actual signal degradation.

Linear Array of Circularly Polarized Elements. As a second example of a redirective array, a linear array may be considered. Once again circularly polarized elements are assumed. They are all similarly oriented and are identical (end effects of array on element patterns and impedance being neglected). Interest in this analysis is only in error in the direction of the re-radiated beam due to the difference in frequency between the transmitted signal and the pilot signal so that only the array factor is of interest. If the angle θ is measured from the array axis, the array factor takes on the form

$$f(\theta) = \sum_n a_n\, e^{j\left[\frac{\omega_T}{c} nd\,(\cos\theta - \cos\theta_R) + \frac{\omega_e}{c} nd \cos\theta_R\right]} \tag{5-33}$$

where $\omega_T = \omega_p + \omega_e$, the a_n are the element excitations, and $\underline{d}$ is the element separation. Ordinarily the a_n are in phase so that the array factor has a principal maximum in the direction for which the exponent vanishes. The last term in the exponent is a progressive interelement phase shift which in effect scans the peak of the beam away from θ_R. The amount of scan is given by

$$\cos \theta_T = \frac{\omega_p}{\omega_p + \omega_e} \cos \theta_R \tag{5-34}$$

where θ_T is the direction of the resulting beam maximum. If this shift is an appreciable fraction of the array beamwidth, a serious degradation in signal will result at the receiver station. The tolerable frequency shift will depend on the array beamwidth and therefore on the array length and its excitation distribution. To get an estimate of the tolerable frequency shift, the array is assumed uniformly illuminated with a pattern that now has the form

$$f(\theta) = \frac{\sin \frac{N}{2} d\left(\frac{\omega_T}{c}\left[\cos \theta - \cos \theta_R\right] + \frac{\omega_e}{c} \cos \theta_R\right)}{\sin \frac{1}{2} d\left(\frac{\omega_T}{c}\left[\cos \theta - \cos \theta_R\right] + \frac{\omega_e}{c} \cos \theta_R\right)} \tag{5-35}$$

In the desired direction this pattern takes on the value

$$f(\theta_R) = \frac{\sin\left(\frac{N}{2} \frac{\omega_e}{c} d \cos \theta_R\right)}{\sin\left(\frac{1}{2} \frac{\omega_e}{c} d \cos \theta_R\right)} \tag{5-36}$$

and has a null for

$$\frac{\omega_e}{\omega_p} = \pm \frac{\lambda_p}{Nd \cos \theta_k} \approx \frac{\lambda_p}{L \cos \theta_R} \tag{5-37}$$

where L is the array length. For values of ω_e greater than this number, the signal is always more than 13 db below the value for $\omega_e = 0$. Therefore, the frequency difference must be kept well below this value. To insure no more than 1 db degradation due to this effect there must exist

$$\frac{\omega_e}{\omega_p} < \frac{0.263}{\cos \theta_R} \frac{\lambda_p}{L} \tag{5-38}$$

5.3 SIMPLE RETRODIRECTIVE ARRAY

The redirective array discussed in the preceding sections is sophisticated in its function and correspondingly complicated in the equipment required to implement it. It is of interest to consider a simpler type of array, the retrodirective array, which has been investigated by a number of researchers (Skolnik and King, 1964; Sichelstiel et al., 1964; Ghose, 1964; Pon, 1964; Rutz-Philipp, 1964; and Gruenberg and Johnson, 1964).

5.3.1 Description

Basically, the retrodirective antenna consists of an array of elements distributed over some surface. Each element is terminated by a frequency converter which sends received signals back out the element with phases inverted. This process effectively directs the signal back toward the source, amplified and with information impressed upon it by the satellite circuitry. A number of physical embodiments of the technique may be realized; the techniques of Rutz-Philipp (1964), Sichelstiel et al., (1964), and Cutler et al., (1963) and Pon (1964) are sketched in Figure 5-5. All these systems do essentially the same thing. The Rutz-Philipp system (Figure 5-5a) does appear to have certain advantages as far as simplicity goes; however, the radiated

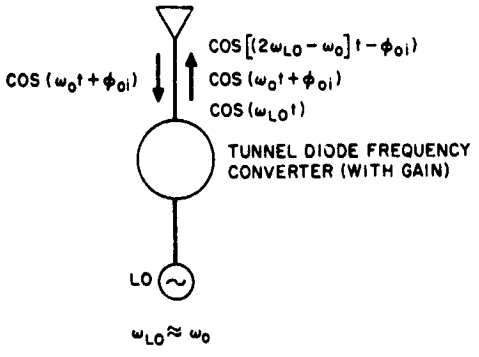

(a) SYSTEM OF RUTZ-PHILIPP (1964)

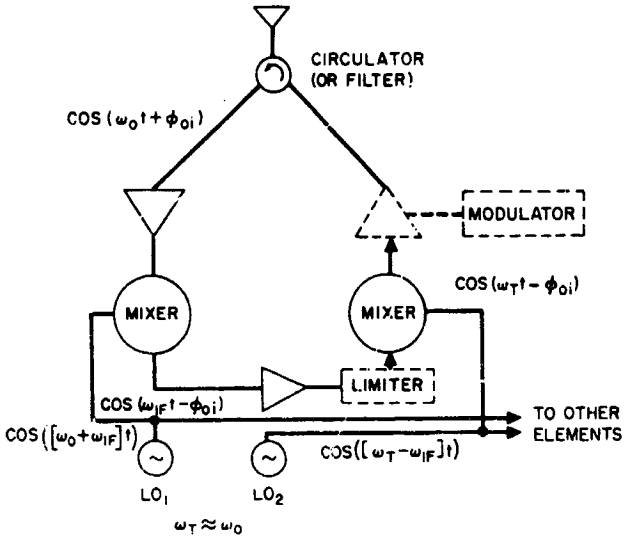

(b) SYSTEM OF SICHELSTIEL ET AL. (1964)

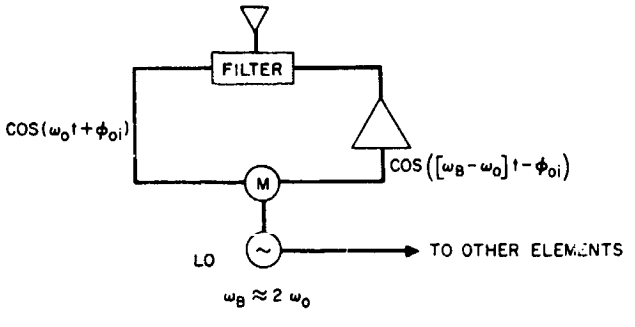

(c) SYSTEM OF CUTLER ET AL. (1963) AND C. Y. PON (1964)

Figure 5-5. Retrodirective array techniques.

energy has an amplified component at the incident frequency. If the gain of the converter is sufficiently large and the antenna element is not sufficiently well matched, the system might tend to be unstable. The other systems circumvent this possibility by the use of branching filters or circulators to isolate the amplified signal from the input signal. Under low-gain, low-power conditions the simpler system appears attractive.

5.3.2 Analysis of System

The operation of the retrodirective system may be analyzed in a manner similar to that used for the redirective array. Let V_n represent the voltage induced across the effective load impedance, Z_o, terminating the n^{th} antenna element, when an incident signal at frequency ω_o is applied. The V_n can be found using Equation (5-9). It may be written as

$$V_{nM} = |V_n| \, e^{j\left[\zeta_n + \xi_n(\theta_R, \phi_R)\right]} \tag{5-39}$$

As in the previous discussion ζ_n is a phase characteristic of the element, and $\xi_n(\theta_R, \phi_R) = (-\omega_e/c)\, h_n(\theta_R, \phi_R)$. The signal fed back to the element is given by

$$\frac{V_{T_n}}{(Z_{a_n} + Z_o)} = \frac{|K_n| \, |V_n| \, e^{j\left[\beta_n - \zeta_n - \xi_n + \phi(t)\right]}}{(Z_{a_n} + Z_o)} \tag{5-40}$$

where the signal is at frequency ω_T and $|K_n| e^{j\beta_n}$ is the overall transfer function of the network behind the element. The quantity $\phi(t)$ is a phase modulation inserted by the satellite. The signal radiated by the antenna may now be written

$$E_\theta = \sqrt{\frac{\eta}{4\pi}} \frac{e}{R} e^{-j\frac{\omega_T}{c}R} \sum_n \sqrt{R^r_{a_n} g_{\theta_n}} \frac{|V_{T_n}|}{(Z_{a_n} + Z_o)}$$

$$e^{j\left[\beta_n - \zeta_n + \frac{\omega_o}{c} h_n(\theta_R, \theta_R) - \frac{\omega_T}{c} h_n(\theta, \phi) + \psi_{\theta_n} + \phi(t)\right]} \tag{5-41a}$$

$$E_\phi = \sqrt{\frac{\eta}{4\pi}} \frac{e}{R} e^{-j\frac{\omega_T}{c}R} \sum_n \sqrt{R^r_{a_n} g_{\phi_n}} \frac{|V_{T_n}|}{(Z_{a_n} + Z_o)}$$

$$e^{j\left[\beta_n - \zeta_n + \frac{\omega_o}{c} h_n(\theta_R, \phi_R) - \frac{\omega_T}{c} h_n(\theta, \phi) + \psi_{\phi_n} + \phi(t)\right]} \tag{5-41b}$$

This expression is basically the same as Equation (5-17). The main difference in the system is one of complexity. The radiation characteristics of this system are identical with those of the redirective array. However, the information signal is not received by a self-focused system but by some other means, such as an essentially omnidirectional antenna.

5.3.3 Noise Considerations in System With Separate Amplifiers in Each Line

A question of interest is the noise contribution in systems such as retrodirective systems or redirective systems which have separate amplifiers in each line as compared with more conventional systems which combine element outputs and amplify with a single amplifier. It will be demonstrated that the noise contribution of the amplifiers are independent of their locations. The case of M transmission lines connected together at P can be considered. Each line has an amplifier of gain G and a noise temperature T_A. For purposes of discussion the junction is assumed to be a parallel connection. The lines of characteristic impedance MZ_o join to form a sum line of characteristic impedance Z_c.

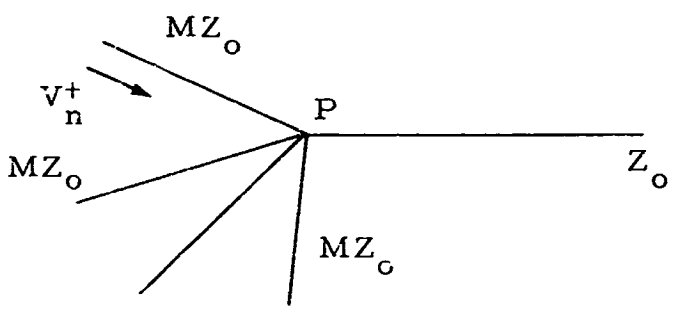

Voltage waves V_n^+ of frequency ω are assumed to be incident on the junction from each feed line. The resulting voltage in the sum line is

$$V_s = \frac{1}{M} \sum V_n^+ \qquad (5\text{-}42)$$

If they are equal to V_o and in phase, the power in the sum line is

$$P_s = \frac{V_o^2}{2Z_o} = M P_o \tag{5-43}$$

where P_o is the incident power in each line. If at the same time there are M noise voltages v_n^+, their value at the junction will also be

$$v_s^+ = \frac{1}{M} \sum v_n^+ \tag{5-44}$$

However, since the noise voltages are uncorrelated, the power they supply to the sum line is

$$P_{Ns} = \frac{1}{2 Z_o} \frac{\sum |v_{Nn}|^2}{M^2} \tag{5-45}$$

and if all the noise voltages have the same mean square values, this power becomes

$$P_{Ns} = \frac{|v_{No}|^2}{2 Z_o M} P_{No} \tag{5-46}$$

Therefore the signal-to-noise ratio is

$$\frac{S}{N} = \frac{M P_o}{P_{No}} \tag{5-47}$$

If the amplifiers have a noise temperature T_N, then

$$\frac{S}{N} = \frac{M P_o}{k T_N B} \tag{5-48}$$

where k is Boltzman's constant and B is the bandwidth.

If instead, a single amplifier with the same effective noise temperature, T_N, is placed in the sum line, its noise power is also $k T_N B$ and the signal-to-noise ratio is the same as in the previous case. The location of the amplifiers is therefore immaterial insofar as their noise contributions are concerned. The same considerations hold true for the retrodirective or redirective arrays, the only difference being that, in some of these arrays, the addition may take place after reradiation. However, there is no difference in the principles which apply and the conclusions are the same.

5.3.4 Experimental Systems

Some models which verify the theory of operation of these techniques have been built and tested.

Linear Array of Horns. Sichelstiel et al. (1964) have described a linear array operating at X-band (Figure 5-5b). The array consists of 25 horn radiators arranged horizontally. Much of the r-f circuitry is waveguide. The 10.7 Mc i-f contains a crystal filter to eliminate unwanted frequencies. The incident r-f frequency was 9.345 Gc and the retransmitted frequency was 9.385 Gc. A number of radiation patterns are shown for 50 λ and 100 λ arrays with the source of incident radiation at different ranges and at on-axis and off-axis positions. The focusing properties are illustrated when a dielectric sheet is partially interposed between the source and the array. The operation for extended sources was also investigated.

Dipole Array. A second experimental retrodirective array based on the type shown in Figure 5-5c is described by C. Y. Pon (1964). This array consists of 4 slot-fed dipoles each with a duplexer and a balanced mixer. The mixers are in waveguide and coaxial line while the duplexer is stripline. The incident frequency was 2.95 Gc, the local oscillator frequency was 5.75 Gc, and the reradiated frequency was 2.80 Gc. Experimental patterns for several angles of signal incidence are presented. The element spacings were such that grating lobes were present in all patterns.

A specific configuration for a retrodirective array, designed by the Hughes Antenna Department, is shown in Figure 5-6. This particular system is designed for a 6,000 n. mi. orbit with a bandwidth of 10 Mc.

Van Atta Array. Perhaps the simplest type of retrodirective system is the Van Atta array (VanAtta, 1959) which has been proposed for use in communications satellites (Ryerson, 1960; Hansen, 1961a). This type of array may be active or passive and directs incident radiation back in the direction of the source. The basic array is illustrated in Figure 5-7. The lines interconnecting pairs of elements all have

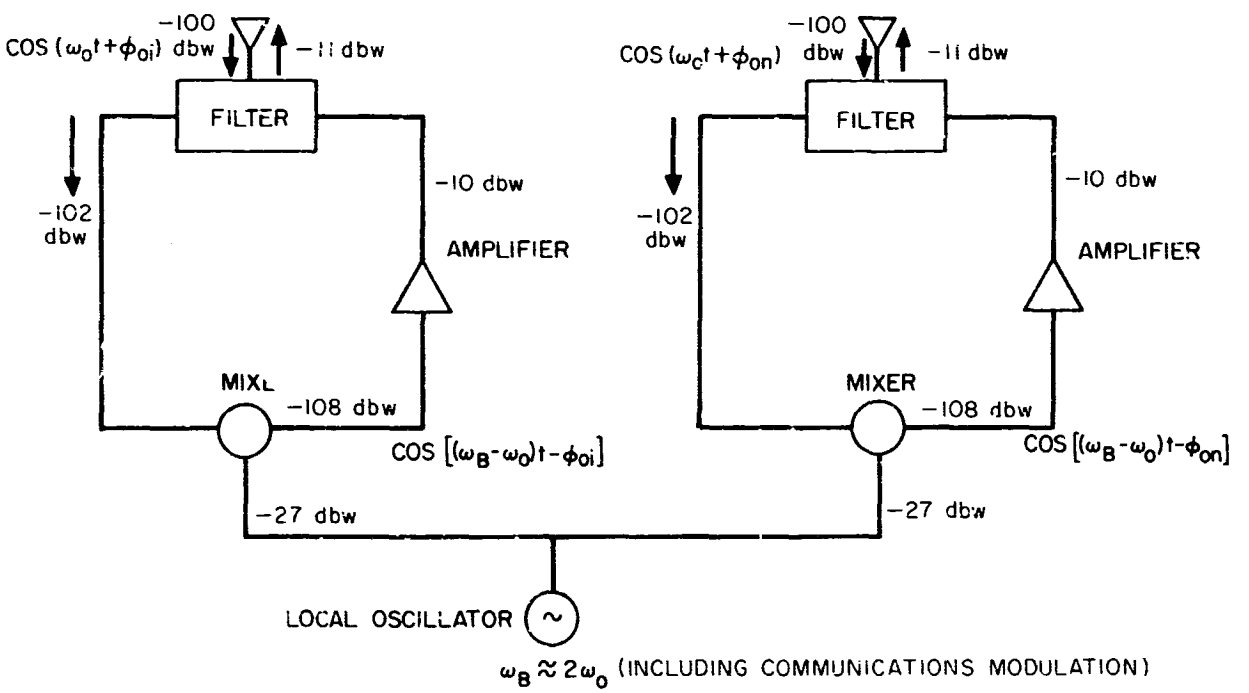

Figure 5-6. Specific configuration for a retrodirective array.

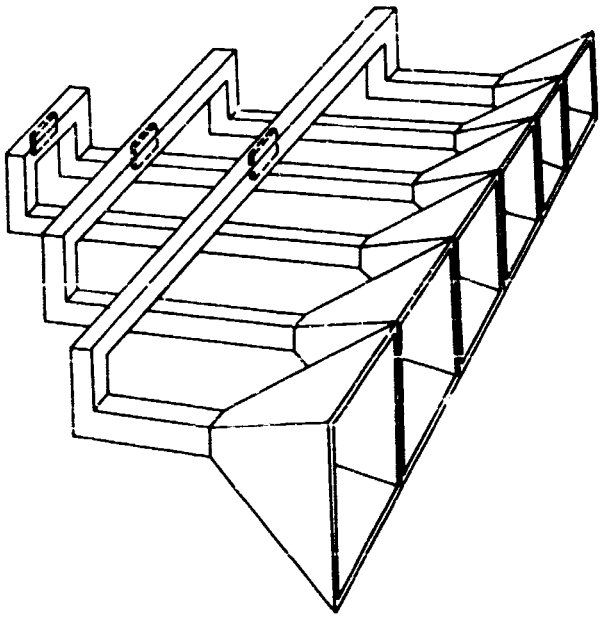

Figure 5-7. Van Atta array (Van Atta, 1959)

the same electrical length. Ideally, in the absence of mismatch and mutual coupling effects, a wave incident at an angle θ with the array axis is redirected with full array gain back toward the source of the incident radiation. Strictly speaking, the Van Atta array is confined to planar array configurations for proper operation (Hansen, 1961b). It is therefore the least general of the types of retrodirective arrays considered since the other could lie on arbitrary surfaces.

An estimate of the effects of placing a Van Atta array on a non-planar surface may be obtained by considering a case in which 2 N+1 elements lie in a circular arc of radius R as illustrated in Figure 5-8. The phase of signals from the n^{th} and $-n^{th}$ elements, referred to the central element, is

$$\phi_n = 2kR\cos\theta + 2\beta\ell_o - h\,R\left[\cos(\theta - n\theta_o) + \cos(\theta + n\theta_o)\right] + \beta\ell_{n-n} \tag{5-49}$$

where β is the phase constant in the connecting lines.
For proper operation this phase should be the same for all values of n and for all values of θ of interest. That is, there must exist

$$\beta\ell_{n-n} = \phi + k\,R\left[\cos(\theta - n\theta_o) + \cos(\theta + n\theta_o)\right] - 2k\,R\cos\theta - 2\beta\ell_o \tag{5-50}$$

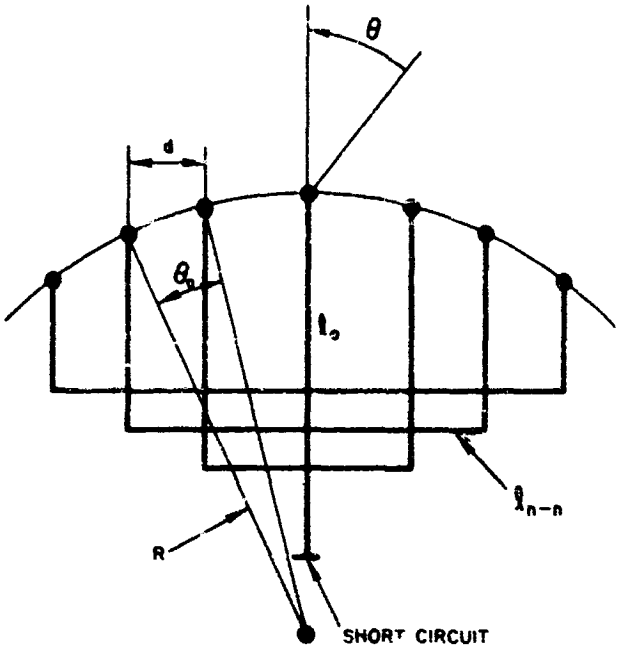

Figure 5-8. Van Atta array on circular curve.

$$\beta \ell_{n-n} = \phi + 2kR\cos\theta\,[\cos n\theta_o - 1] - 2\beta\ell_o \qquad (5\text{-}51)$$

This condition cannot be satisfied for all θ but may be adjusted for one value, say θ_1. Then the expression becomes

$$\phi_n = \phi - 2kR\,[\cos\theta - \cos\theta_1]\cdot[\cos n\theta_o - 1] \qquad (5\text{-}52)$$

The back-scattered pattern (neglecting the element factor) has the form

$$E^s \sim e^{j\phi} \sum_{-N}^{N} e^{-j2kR\,[\cos\theta - \cos\theta_1][\cos n\theta_o - 1]} \qquad (5\text{-}53)$$

Thus it is seen that, unless $\theta = \theta_1$, there is a phase error across the array. If the curvature is small, then the radius of curvature is large. If the element separation is uniform and denoted by d there exists

$$\theta_o \approx \frac{d}{R} \qquad (5\text{-}54)$$

and

$$\cos n\theta_o - 1 \approx \frac{1}{2}\left(\frac{nd}{R}\right)^2 \qquad \frac{nd}{R} \ll 1 \qquad (5\text{-}55)$$

The radiated field then becomes

$$E^s \sim e^{j\phi} \sum_{-N}^{N} e^{-jkd(\frac{d}{R})[\cos\theta - \cos\theta_1]\, n^2} \tag{5-56}$$

Thus the phase error is approximately quadratic. The value of θ_1 would be chosen to give zero error at some angle between $\theta = 0$ and $\theta = \theta_M$, the maximum scan angle. For example, if it is assumed that $\theta_M = 45^o$, then θ_1 would be chosen so that

$$\cos\theta_1 = \frac{1}{2} + \frac{\sqrt{2}}{4}$$

and the expression at broadside would be

$$E^s \sim e^{j\psi} \sum_{-N}^{N} e^{-jkd\left(\frac{1}{2} - \frac{\sqrt{2}}{4}\right)\frac{d}{R}\, n^2} \tag{5-57}$$

To keep the maximum phase error less than $\pi/2$, the condition must be

$$\frac{R}{d} > 0.588\, N^2 \frac{d}{\lambda} \tag{5-58}$$

For an array of given size, the minimum radius of curvature can be determined from the above inequality.

By inserting amplification in the transmission lines between pairs of elements, the system becomes an active system. In accordance with the discussion of Hansen, because of the changes in effective element impedances, bilateral amplifiers are not desirable and back-to-back unilateral amplifiers are more attractive. Circulators would be used to couple into and out of the amplifiers. Additional isolation might be obtained through frequency shifts between received and retransmitted signals. The same type of beam pointing errors as were previously discussed for other redirective and retrodirective arrays would

result from the frequency translation, however. This source of error could be reduced by using two arrays of different sizes scaled to the two frequencies, one for reception and one for transmission. An experimental model using two arrays has been built and tested (Andre and Leonard, 1964), but the arrays were not scaled in size to offset the effect of frequency shift. The model (Figure 5-9) uses two interleaved arrays of orthogonally oriented printed dipoles and employs tunnel diode amplifiers and mixers. The orthogonal orientation of the elements in the two arrays provides isolation between received and retransmitted signals. In this system, the information signal, which has been obtained from some other source, is impressed on the reradiated signal by introducing it on the local oscillator signal at frequency Δf. The experimental array has nine active elements and operates at a nominal receive frequency of 2.0 Gc and transmit frequency of 2.15 Gc. The r-f bandwidth was approximately 120 Mc, and the measured array gain was reported to be 14 db. The array was operated under conditions of both single and multiple access.

A second experimental version of the Van Atta array has been described briefly by Gruenberg and Johnson (1964). It consists of a 25-element Van Atta array in which 24 conjugate elements are pulse code modulated by on-off switches. The switching modulates the reradiated signal. The modulation comes from a signal received by the 25th (center) element. This receiving element accepts the modulated signal from a distant transmitter. A separate receiving station then beams an unmodulated signal to the array. This signal is modulated by the array switches and directed back to the receiving station. A diagram of the system is illustrated in Figure 5-10. No experimental results were given.

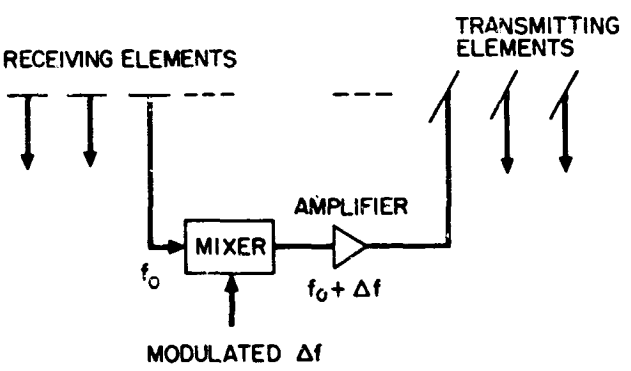

Figure 5-9. Active Van Atta system with separate arrays for reception and retransmission.

A system very similar to the second modified Van Atta array has also been proposed by Margerum and Lees (1964). In one possible version, a partially

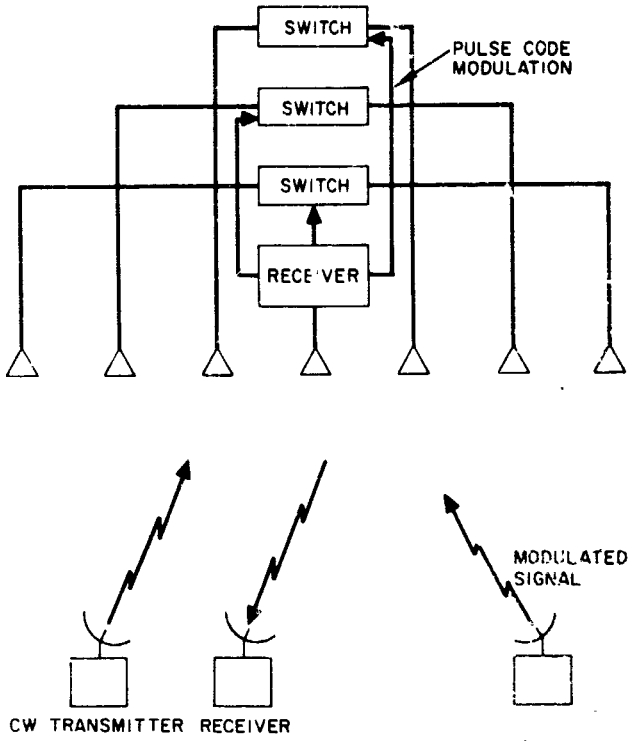

Figure 5-10. Modulated Van Atta array.

silvered Luneberg lens has been considered in place of the Van Atta array. If the conductivity of the silvered portion could be modulated by the receiver output, then the same type of operation as obtained with the array would be achieved. This latter arrangement is essentially passive and therefore provides no r-f signal amplification at the satellite.

5.4 ADAPTIVE ANTENNA ARRAYS

Phase-locked loops have been finding increasing application in recent years as phase synchronizing devices for an arbitrary distribution of radiating elements. An array of elements employing this type of phase is called an electronically adaptive antenna system. A receiving antenna system of this type contains active elements which, unlike passive arrays, automatically adjust the electrical phases of the signals received by the array elements to obtain antenna directivity. These arrays can be made retrodirective.

5.4.1 General Description of Operation

A typical receiving array is shown in Figure 5-11 (Gangi, 1963). The coherent summation of signals from each element or a separate reference oscillator can be used as a reference signal. Each has separate advantages and disadvantages which will be enumerated later. Qualitatively, if one of the elements is receiving at a frequency ω, the total phase of the incoming signal will be $(\omega t + \phi_1)$ when ϕ_1 is an arbitrary phase. The output of the voltage controlled oscillator (VCO) has an

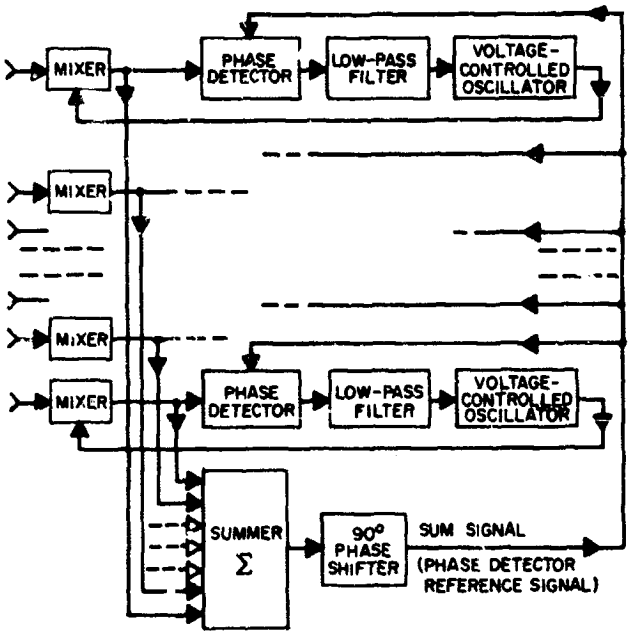

Figure 5-11. Typical phase-locked loop receiving array (Gangi, 1963).

assumed frequency of ω_1 and phase θ_1. The mixer output phase is $[(\omega - \omega_1)t + \phi_1 - \theta_1]$. Now if the reference signal phase is $(\omega - \omega_1)t + \psi$, it is seen that the output from the phase detector is $\phi_1 - \theta_1 - \psi$. The frequency of the VCO is automatically adjusted to minimize this output. Therefore a change in the phase ϕ or frequency ω of an incoming signal tends to be compensated for by the loop, and the output of the mixer remains at a constant frequency and phase.

Parameters of Interest. There are three important parameters of a phase-locked loop which must be considered in a particular application: the lock range, the capture range, and the filter bandwidth. The lock range is the total drift in received frequency which can be exactly compensated for by the phase-locked loop once it is locked in. The capture range is the largest frequency excursion of the received signal over which the system will lock in. The third parameter, the filter bandwidth, describes the system behavior as a noise filter. All of these are interrelated and a change in one will affect the others. It can be shown that a narrow band system will not follow rapid excursion of the incoming signal as might be encountered in a satellite application due to doppler shift. However, a low noise requirement necessitates a narrow bandwidth. Trade-offs must be made to achieve satisfactory operation of such a system. The transfer function of the low-pass filter and the various loop gains determine the three system parameters.

Satellite Application. Either a separate reference oscillator or the coherent summation of received signals can be used as the reference signal. The reference signal should be very stable for proper operation;

however, in a satellite application that requirement is very difficult to meet. If the sum signal is used, a 90^{o} phase shifter is required, thus adding another component to the system. The sum signal is also a noisy signal, but the signal-to-noise ratio of the sum signal is improved in direct proportion to the number of inputs to the summer. With the sum signal as the reference, the VCO frequency change is small since the summer output is at the average of the VCO frequencies. Also, each loop reaches equilibrium in approximately the same amount of time since each loop is interconnected through the sum signal. Most important, the system is automatically adaptive to signal power since the phase-locked loop gain can be shown to be proportional to the square of the signal voltage. These characteristics can be achieved in the system utilizing a separate reference oscillator only at the expense of additional components. Both types of loops can be made adaptive to changes in noise spectral density by the inclusion of a band-pass limiter following the mixer. With a limiter, in addition to its adaptiveness to noise spectral density, the system cannot be driven into non-linear regions. This therefore gives the system a large dynamic range.

5.4.2. Independent Loop Configuration

One of the phase-locked loops of the adaptive antenna array system may be redrawn in servo-loop fashion as shown in Figure 5-12. This loop can be further simplied as shown in Figure 5-13. These diag ams relate only the controlled variable, i.e., the output signal

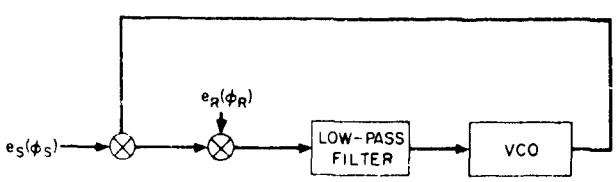

Figure 5-12. Servo diagram of phase locked loop.

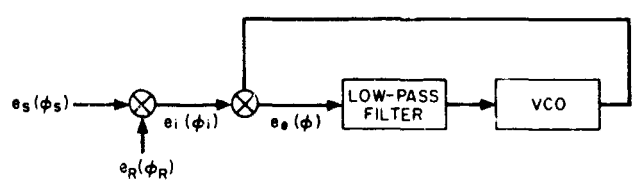

Figure 5-13. Servo diagram of simplified phase-locked loop.

phase, relative to the input signal phase. The Laplace transformed differential equation governing the circuit of Figure 5-13 is

$$p\phi + F(p)K \sin\phi = p\phi_i \tag{5-59}$$

where $\phi = \omega_s t + \theta_s - \omega_R t - \omega_c t - \theta_c$, $F(p)$ is the transfer function of the loop filter, K is the open loop gain, and $\phi_i = (\omega_s - \omega_R)t + \theta_s$ where ω_R is the reference oscillator frequency. The steady-state solution to Equation (5-59) is

$$\sin\phi = \frac{\Delta\omega}{K} \tag{5-60}$$

where $\Delta\omega = p\phi_i = \omega_s - \omega_R$. Equation (5-60) shows that the system will remain locked in for $|\Delta\omega| \leq K$.

In a practical phase-locked loop which has achieved synchronism, ϕ is small. This condition is especially true if the open loop gain K is large. Therefore, $\sin\phi$ can be replaced by ϕ in Equation (5-59), thus linearizing the differential equation. If $F(p) = 1$, the loop behaves like a simple RC filter and has a cutoff frequency of $\omega_c = K$ radians/sec. The noise bandwidth of this loop can be shown to be $2B = \pi K$ (Gruen, 1953). However, Equation (5-60) shows that, for small steady-state phase errors, K has to be as large as possible, while now for good noise immunity K has to be as small as possible.

The above difficulty can be overcome by the use of a loop filter as shown in Figure 5-14. Here, $F(p) = (1 + \tau_1 p)/(1 + \tau_2 p)$ where $\tau_1 = R_1 C$ and $\tau_2 = (R_1 + R_2)C$. With this type of filter the noise bandwidth can be shown to be approximately (Gruen, 1953)

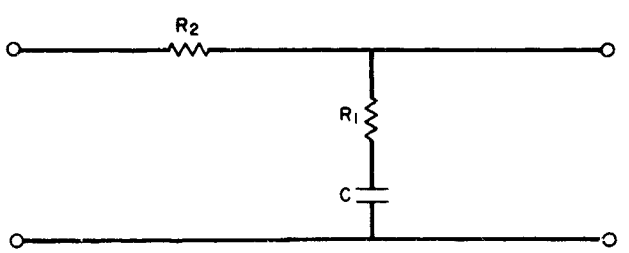

Figure 5-14. Proportional plus integral network.

$$2B \cong \frac{4\zeta^2 + 1}{4\zeta}\,\omega_n \tag{5-61}$$

for $\omega_n/K \ll 1$ where ω_r

$$= \sqrt{\frac{K}{(R_1 + R_2)C}}$$

is the natural frequency of the loop, and $\zeta = [\omega_n/2]\left[R_1C + \frac{1}{K}\right]$. If $4\zeta^2 \gg 1$, $R_1C \gg (1/K)$, the noise bandwidth becomes

$$2B \propto K \tag{5-62}$$

Since K is the open loop gain,

$$K = K_V k_\phi E_R E_M \tag{5-63}$$

where K_V is the VCO gain, k_ϕ the phase detector gain, E_R the reference signal amplitude, and E_M is the mixer output signal amplitude. It is seen from Equations (5-62) and (5-63) that $2B \propto E_s$ and, consequently, that the noise bandwidth is proportional to the input signal strength. It is this property of phase-locked loops which makes the system adaptive since the acquisition time is dependent on the noise power. It can be shown that the pull-in range of the loop with the filter shown in Figure 5-14 is $|\Delta\omega| = \sqrt{2\zeta\omega_n K}$. Therefore a high loop gain K, a high frequency ω_n, and a large damping constant ζ enable the system to have a wide pull-in frequency range. Too large a damping constant makes the phase-locked loop too sluggish and increases the time it takes for the loop to come to equilibrium. A large ω_n requires a large input signal to maintain a certain signal-to-noise ratio in the noise bandwidth 2B, while a very large K can cause the system to oscillate.

5.4.3 Sum Signal Reference Configuration

It can be shown that in the sum signal reference configuration the output voltage from the phase detector is proportional to the square of the signal voltage. Equation (5-62) becomes

$$2B \propto K \propto E_s^2 \tag{5-64}$$

for $\omega_n/K \ll 1$ where ω_r

$$= \sqrt{\frac{K}{(R_1 + R_2)C}}$$

is the natural frequency of the loop, and $\zeta = [\omega_n/2]\left[R_1C + \frac{1}{K}\right]$. If $4\zeta^2 \gg 1$, $R_1C \gg (1/K)$, the noise bandwidth becomes

$$2B \propto K \tag{5-62}$$

Since K is the open loop gain,

$$K = K_V k_\phi E_R E_M \tag{5-63}$$

where K_V is the VCO gain, k_ϕ the phase detector gain, E_R the reference signal amplitude, and E_M is the mixer output signal amplitude. It is seen from Equations (5-62) and (5-63) that $2B \propto E_s$ and, consequently, that the noise bandwidth is proportional to the input signal strength. It is this property of phase-locked loops which makes the system adaptive since the acquisition time is dependent on the noise power. It can be shown that the pull-in range of the loop with the filter shown in Figure 5-14 is $|\Delta\omega| = \sqrt{2\zeta\omega_n K}$. Therefore a high loop gain K, a high frequency ω_n, and a large damping constant ζ enable the system to have a wide pull-in frequency range. Too large a damping constant makes the phase-locked loop too sluggish and increases the time it takes for the loop to come to equilibrium. A large ω_n requires a large input signal to maintain a certain signal-to-noise ratio in the noise bandwidth 2B, while a very large K can cause the system to oscillate.

5.4.3 Sum Signal Reference Configuration

It can be shown that in the sum signal reference configuration the output voltage from the phase detector is proportional to the square of the signal voltage. Equation (5-62) becomes

$$2B \propto K \propto E_s^2 \tag{5-64}$$

If the noise spectral density remains constant, the signal-to-noise ratio in the phase-locked loop bandwidth will remain constant, independent of the input signal strength. However, this relationship is true only over the range of signal strengths over which the inequalities $4\zeta^2 > 1$ and $R_1 C > 1/K$ are valid. The sum signal reference configuration can also be made adaptive to changes in the noise spectral density by the use of band pass limiters immediately following the mixers. These limiters have the property of maintaining approximately the same signal-to-noise ratio in their output as in their input. They also tend to keep the output power constant. Therefore,

$$\frac{S_i}{N_i} \cong \frac{S_o}{N_o}$$

and

$$S_o + N_o \cong C \qquad (5\text{-}65)$$

It is seen that

$$S_o \cong \frac{S_i/N_i}{1 + S_i/N_i} C \qquad (5\text{-}66)$$

where S_i and N_i are the input signal and noise powers, respectively, and S_o and N_o are the equivalent output powers. For large S_i/N_i the output signal is essentially constant. For low S_i/N_i the output signal is proportional to S_i/N_i. At these small ratios an increase in the noise spectral density will give a smaller output power, thus lowering the gain of the phase-locked system and in turn reducing its bandwidth. Consequently, a relatively constant signal-to-noise ratio is maintained in the bandwidth when the noise spectral density increases.

5.4.4 Experimental Phase-Locked Loops

An eight-channel antenna array utilizing phase-locked loop principles has been simulated (Gangi, 1963). A block diagram of the simulator is shown in Figure 5-15. The signal picked up by the individual antennas was simulated by a 1-Kc sinusoid, and the zero-voltage VCO frequencies were approximately 1300 cps, giving an i-f frequency of 300 cps. The phase shifts in each antenna were simulated by resolver phase shifters.

To measure the system adaptiveness, the acquisition time as a function of signal level was measured (Figure 5-16). The noise bandwidth of the loop was 3.2 cps, the damping constant ζ was equal to 2, and $K = 2260\ \text{sec}^{-1}$. The sum signal was held constant as the input signal was changed.

It was found that the acquisition time decreased as the signal strength increased, thus indicating an increase in the noise bandwidth. Oscillograms of the VCO phase jitter (Figure 5-17) also indicated an increase in the noise bandwidth with signal strength by the presence of higher frequency components in the oscillograms for large signal strength.

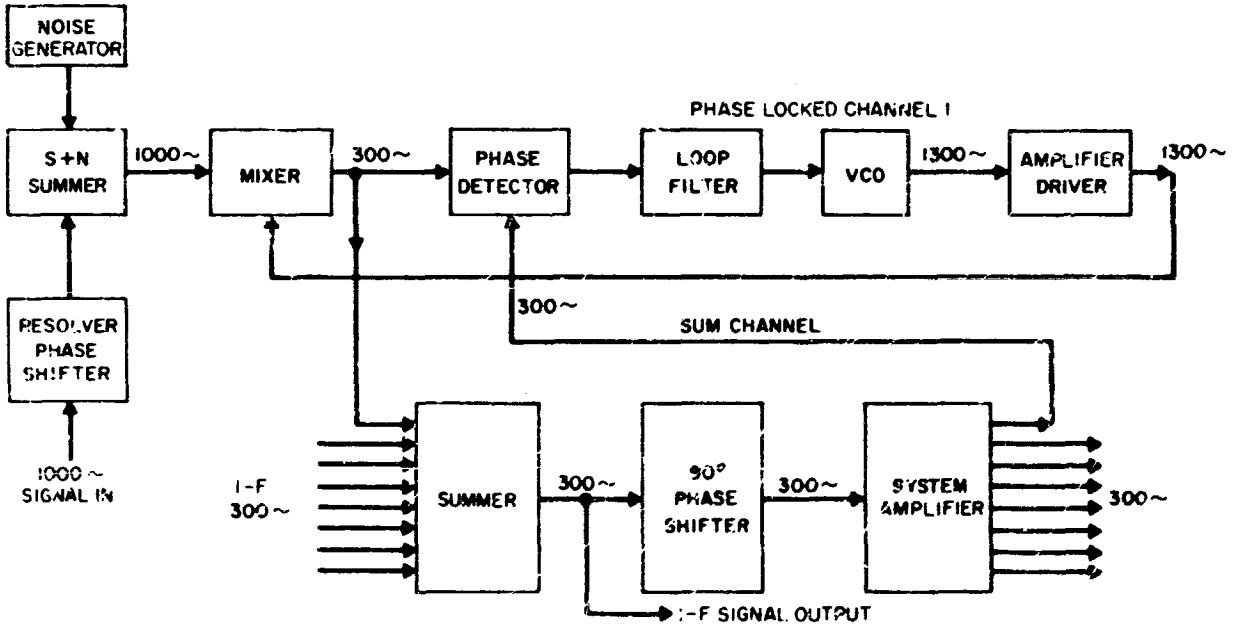

Figure 5-15. Block diagram of the active adaptive antenna array system simulator (Gangi, 1963).

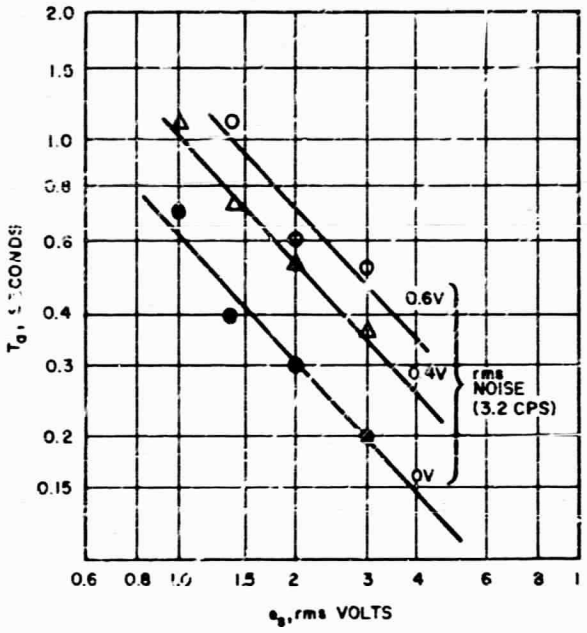

Figure 5-16. Acquisition time of the 8-channel antenna array simulator vs. mixer output voltage (Gangi, 1963).

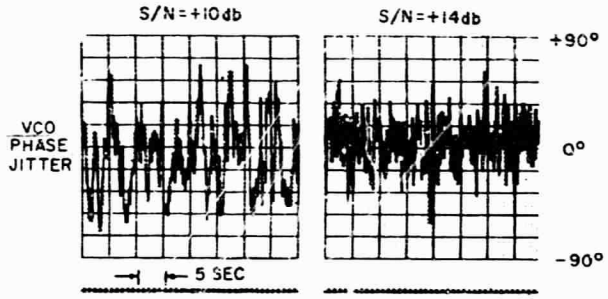

Figure 5-17. Oscillograms showing the adaptiveness of the phase-locked system (Gangi, 1963).

5.4.5 Adaptive Arrays used as Retrodirective Antennas

The preceding section treated adaptive arrays which are used for receiving only. It is possible to make the arrays retrodirective as well, by modifying their circuitry in an appropriate manner. Methods of accomplishing this modification are illustrated in Figure 5-18. In one configuration (Figure 5-18a), the operation is very similar to that of the retrodirective arrays discussed previously, except that now the characteristics of the phase-locked loop are also included.

A second configuration, (Margerum, 1965) shown in Figure 5-18b, uses an electronically controlled reciprocal phase shifter in conjunction with a phase-locked loop to achieve retrodirective action. The phase-locked loop automatically adjusts the phase shifter to keep the r-f signal in phase with the reference oscillator. The transmitted signal then automatically undergoes the correct phase shift to cause the beam to be directed back in the direction from which the pilot signal came. The wave shape of the voltage controlled oscillator must be tailored to the characteristic of the phase shifter. For example, if the phase shifter were of the synchronous type as discussed

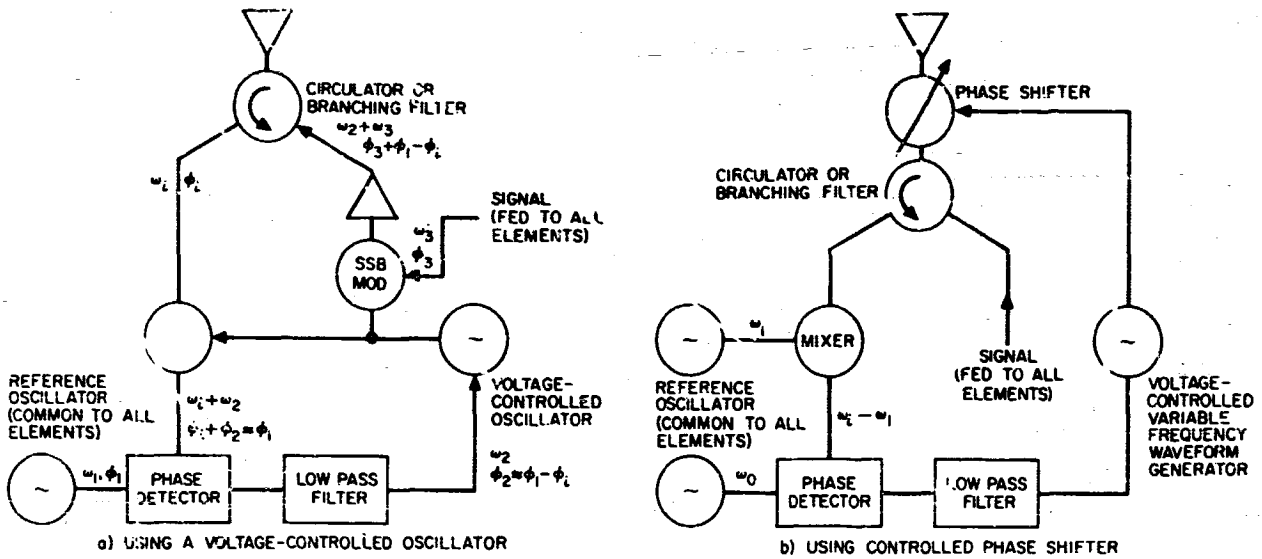

Figure 5-18. Adaptive retrodirective antenna modules.

in Section 3.1.4, then a two-phase sinusoidal voltage-controlled oscillator might be required; while if the phase shifter had a linear range of only 2π radians, a single-phase VCO with a sawtooth wave shape would be required to drive the phase shifter.

The arrangement of Figure 5-18b has the advantage of not requiring a separate power amplifier at each element since the phase shifters may carry relatively large powers. However, the weight of the phase shifters may be a problem and the required waveform generators would be more complex than a single VCO with a sinusoidal output.

6. NEW TECHNOLOGY SECTION: THE TRANS-DIRECTIVE ARRAY

A new type of electronically self-steering array has been formulated and named the Trans-Directive Array. Basically, this array is a new kind of retrodirective array.

6.1 GENERAL DESCRIPTION

The Trans-Directive Array utilizes a multibeam antenna, such as the Butler array, to receive and reradiate incident signals at several frequencies with high directivity and gain. The incident signals may be from one or more arbitrary or varying directions, and the reradiated signals may be transmitted toward one or more arbitrary or varying directions.

The most common antenna system presently used for this purpose incorporates one or two quasi-omnidirectional antennas together with signal processing instrumentation. Incident signals from arbitrary directions are received with the nearly omnidirectional, but low gain, receiving antenna and are processed by the signal processing instrumentation to have arbitrary amplification and frequency. They then are reradiated by the same or a different omnidirectional antenna.

The Trans-Directive Array allows the use of one high-gain, high directivity antenna to receive incident signals from arbitrary directions and to reradiate those signals, after they have been processed to have arbitrary amplification and frequency, toward arbitrary, desired directions. With this antenna economical low-power levels can be used both in this system and in all other participating systems. Signal information would be securely or privately radiated only to those receiving stations desired.

6.2 TWO-STATION OPERATION

Stations A and B, wishing to communicate with one another, each transmit a pilot tone and a band of information signals of slightly different frequencies to the Trans-Directive Array. In particular, station A might transmit a pilot tone of frequency $f_c + 20\ M_c$ and information signals at frequencies from $f_c + 5\ M_c$ to $f_c + 15\ M_c$. Similarly, station B might transmit a pilot tone of frequency $f_c - 20\ M_c$ and information signals at frequencies $f_c - 5\ M_c$ to $f_c - 15\ M_c$. The various output channels of the multiple-beam array antenna each receive incident signals from different portions of the field of view of the antenna.

Depending on the location of station A with respect to the Trans-Directive Array, its incident signals will be directed mainly into one particular channel (see Figure 6-1). The input circulator of that channel will direct these signals to the mixer where they are reduced to a lower frequency, the intermediate frequency (i-f). The strongest pilot tone A (which is in that channel) will be detected by the upper band pass filter which rejects all frequencies other than that of pilot tone A. The detection of the strongest pilot tone A generates a signal which directs the r-f switch to connect the right-hand transmitter being modulated by information from station B to radiate out the same channel of the antenna (towards station A) through the input circulator of that channel, and directs the i-f switch to allow the information from station A to modulate the left-hand transmitter.

Depending on the location of station B with respect to the Trans-Directive Array, its incident signals will be directed mainly into some other channel. The input circulator of that channel will direct these signals to the mixer where they are reduced to a lower frequency, the i-f. The strongest pilot tone B (which is in that channel) will be detected by the lower band pass filter which rejects all frequencies other than that of pilot tone B. The detection of the strongest pilot tone B generates a signal which directs the r-f switch to connect the left-hand transmitter being modulated by information from station A to radiate out the same channel of the antenna (towards station B) through the input circulator of that

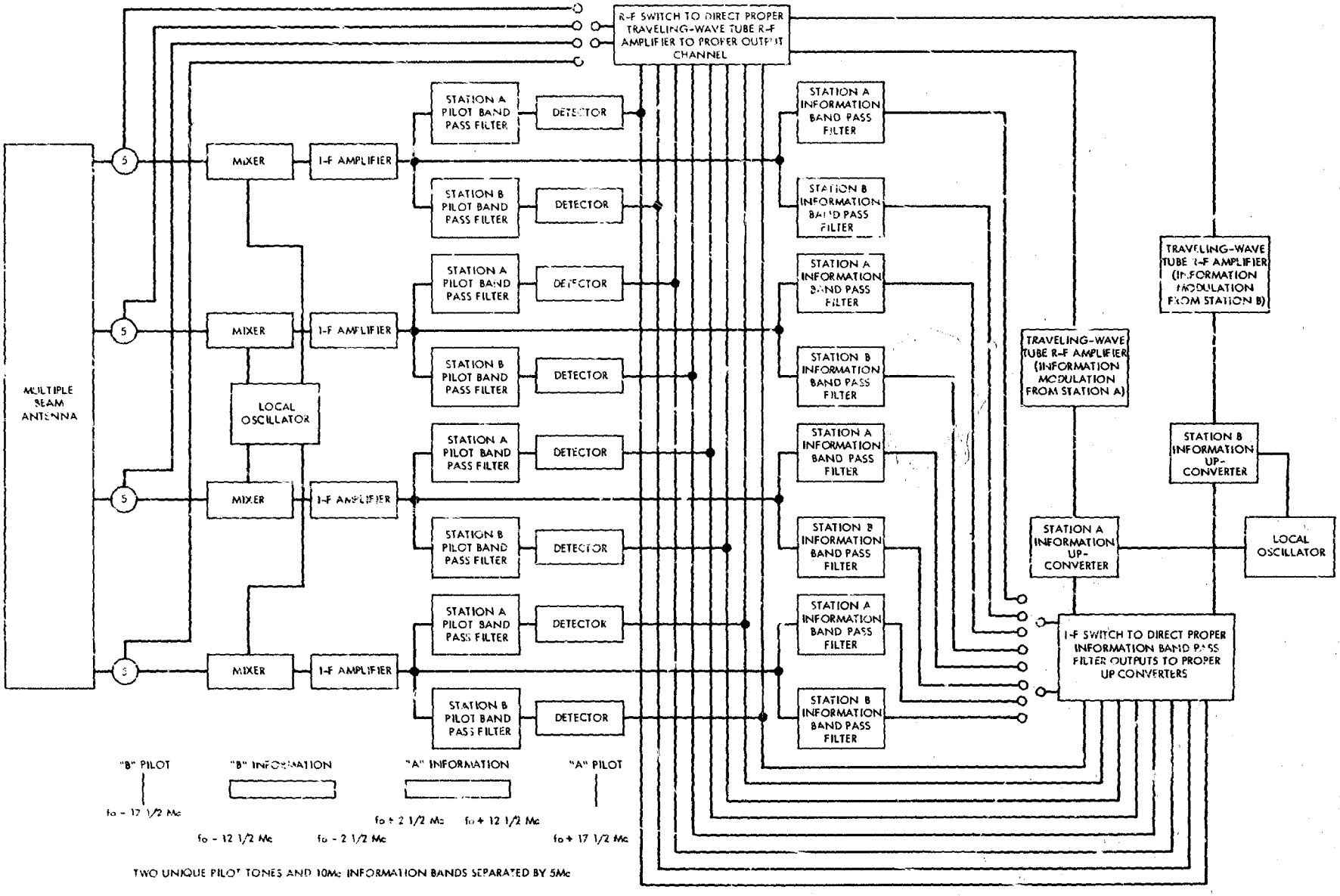

Figure 6-1. Trans-Directive Array.

channel, and directs the i-f switch to allow the information from station B to modulate the right-hand transmitter.

The net result is that the information from station A is reradiated toward station B and, simultaneously, the information from station B is reradiated toward station A at a different carrier frequency.

6.3 MULTI-STATION OPERATION

The description of operation with two stations communicating with one another through the Trans-Directive Array applies equally when additional stations are involved. When each station transmits a unique pilot tone and information band of frequencies to the Trans-Directive Array, the information from any or all stations can be reradiated to any or all stations. To perform this more complicated task, the Trans-Directive Array would either have to include one transmitter for each station whose information is to be reradiated, or time share a fewer number of transmitters, or use only a portion of the re-transmitted bandwidth of one transmitter for each station. It would also have to include a more complex r-f switch which could be programmed so as to connect the proper transmitters, appropriately modulated, to the proper output channels when directed by signals generated by the various pilot tones. Furthermore, the Trans-Directive Array would have to include a more complex i-f switch which could similarly be programmed to connect the station information signal of the various input channels to modulate the proper transmitters.

The several stations could be ground stations far apart, communicating with one another through the Trans-Directive Array in a satellite. The high gain and directivity of the Trans-Directive Array would allow the ground stations to use minimum transmitted power and to have physically smaller transmitting and receiving antennas. Or they could have a wider transmitting bandwidth to assure speedy information flow. Additionally, each station would not have to share its information with as many other stations as will be involved when a less directive satellite transmitting antenna is used.

A retrodirective system has been proposed by Belfi et al. (1964). Their article discusses a planar array backed by a beam-forming matrix. The proper transmitting beam is selected by using logic circuitry which automatically selects the coded input having the greatest signal strength. Typical logic circuitry is described. The system was not constructed, however.

A specific configuration of this system, designed in the Hughes Antenna Department, is shown in Figure 6-2. This particular system is designed for a 6,000 n. mi. orbit with a bandwidth of 10 M_c.

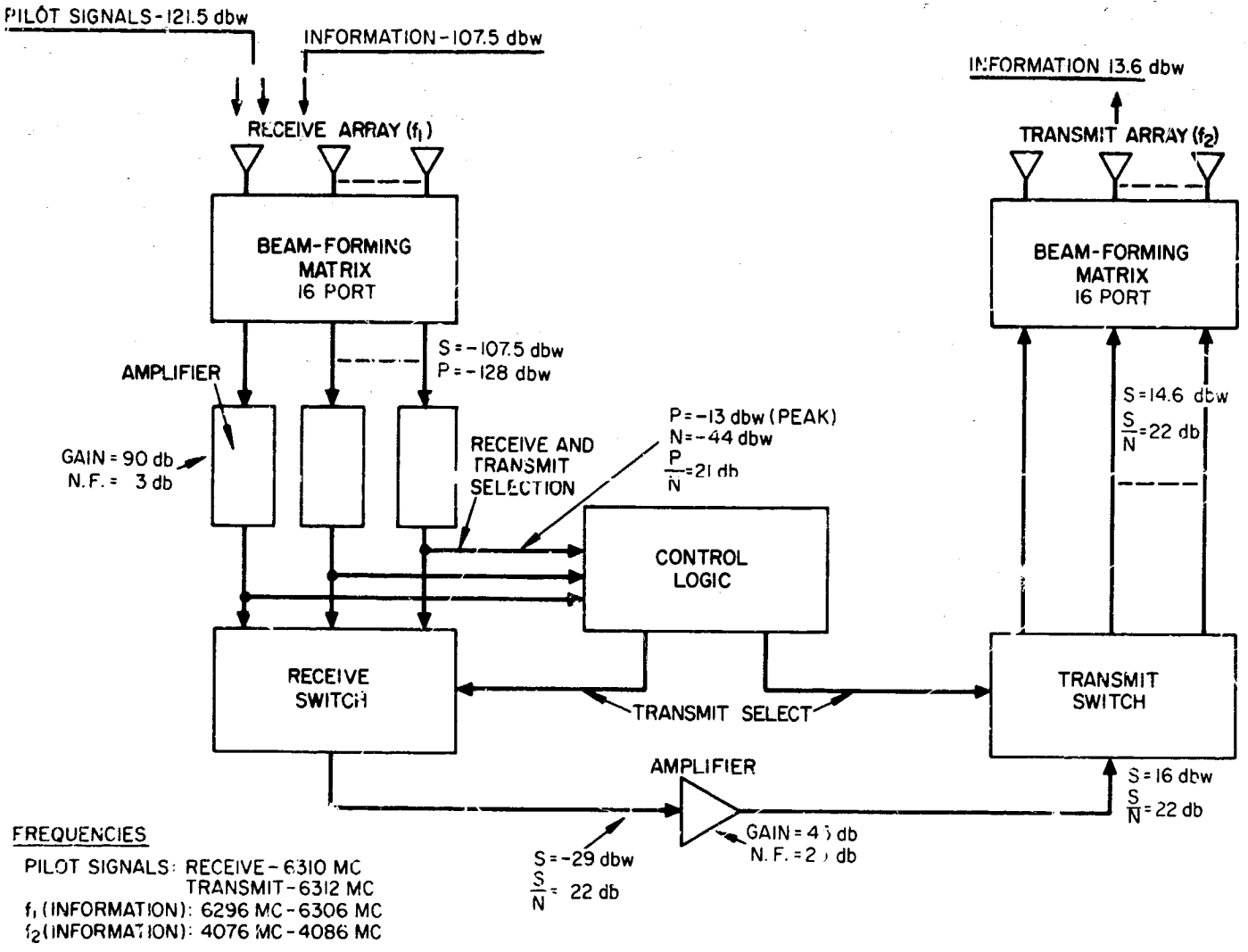

Figure 6-2. Specific configuration for a Trans-Directive Array.

BLANK PAGE

7. MILLIMETER-WAVE ANTENNAS

There is a growing interest in the use of millimeter waves in earth-spacecraft and spacecraft-spacecraft communication links. The vast distances alone require antennas with high gain to reduce the transmission loss. The narrow beams achievable with millimeter-wavelength systems make possible smaller, lighter weight components. The frequency bands involved at these higher ranges are not crowded as are those in the lower regions. Such potential advantages emphasize the need to extend the techniques of scanning and tracking into the millimeter-wave band and to develop new high-speed techniques and components. The frequency range from 30-100 Gc is of greatest current interest, especially the two window frequencies of 35 and 94 Gc.

Scaling lower frequency components and designs into the millimeter bands has become fairly standard, at least in the 10-30 Gc band. A second technique involves the possibility of phase shifters as the elements of millimeter planar arrays to provide beam forming and scanning. Another, relatively undeveloped, technique depends on the bulk behavior of a slab of ferrite material extending across a wavefront to change the direction of the beam. And, finally, beams have been formed by circular or spherical lenses and scanned by the mechanical or electronic movement of point sources. These methods and a brief summary of millimeter component development are considered in the following sections.

7.1 SCALING CONSIDERATIONS

One way of extending known technology into the higher frequencies involves scaling. In the 10-30 Gc band, the scaling of waveguide designs is straightforward and raises no serious problems in the mechanical and electrical design. In this band a wide range of strip transmission line components (corporate feeds, isolators, hybrids, mixers, phase shifters,

etc.) have been developed which exhibit low loss and excellent performance. In the band that extends from 30 to 300 Gc, however, the variety of presently developed components is more limited. Scaling can be accomplished, if with difficulty, through the K_a-band of frequencies (26.5 to 40 Gc); precision milling techniques have been developed that can achieve the tight tolerances required. For example, the usual requirement for good aperture efficiencies is $\lambda/20$ or better on the shape of a reflector or the surface flatness of a slot array. To achieve this efficiency requires a tolerance of ±0.010 inch at K_a-band. At the higher millimeter frequencies, such as the window frequency of 94 Gc, tolerance limitations decrease to ±0.003 inch. New techniques and methods that may not be scalar are needed.

Round-hole radiating elements are being investigated by the Hughes Antenna Department as one new technique for achieving the stringent tolerances. A round-hole element has only two parameters that affect tolerance in fabrication, diameter and location; in contrast, the milling of slot elements involves not only displacement from center line, but also the slot length, width, and angle of inclination. A 1000-element round-hole array, shown in Figure 7-1, has been designed for

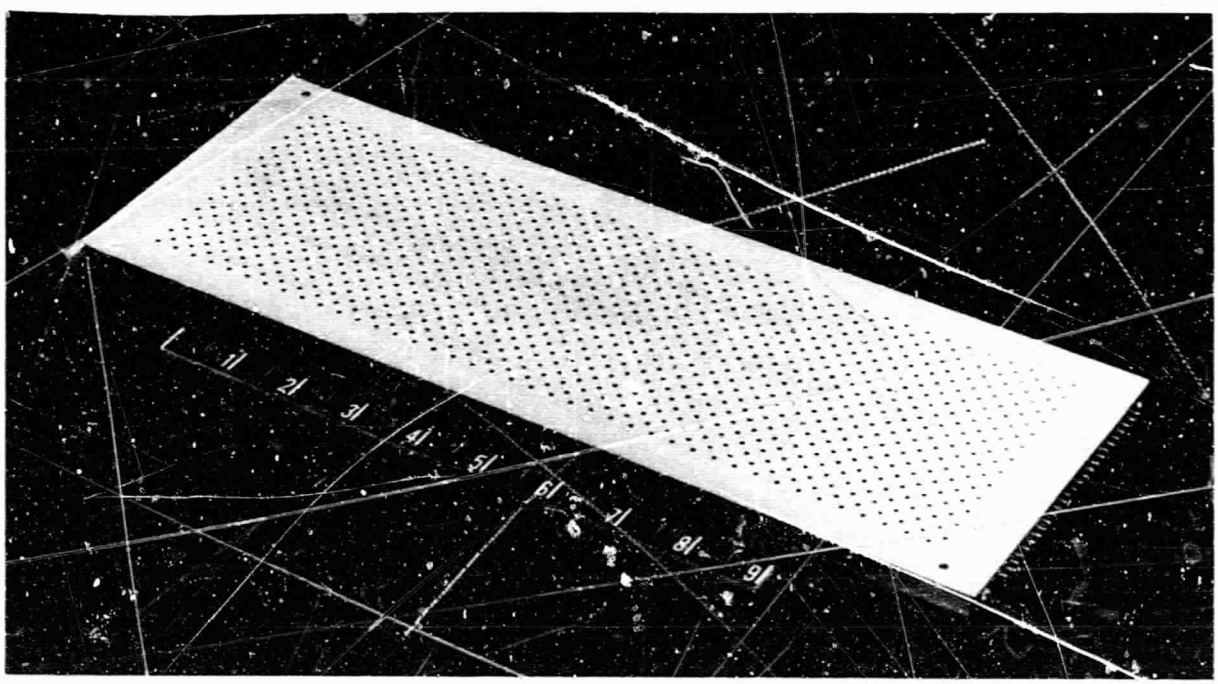

Figure 7-1. 1000-element round-hole 56-Gc array.

operation at 56 Gc with 40-db gain and a 1-by-3-degree beam. It is thought that round-hole elements offer considerable promise for the higher millimeter range.

Another approach has been the use of optical lens antenna systems which do not require the milling of radiating elements to stringent tolerances. Lens systems, constructed for operation at 56 Gc (section 7.5.1) with 6-inch lenses, have exhibited 3-degree beamwidths. The success of scaling such a system to 94 Gc, or higher, depends on the homogeneity of the lens. A small discontinuity in the lens is not too evident at the lower millimeter frequency, but at higher frequencies it would appear as a larger portion of a wavelength. In addition to the effects of lens discontinuities, the relationship of lens diameter to beamwidth is unknown for apertures greater than 30 wavelengths. Plans are underway at Hughes to test a fused quartz lens, 18 inches in diameter, at 56 Gc with the expectation of achieving a 1-degree beamwidth. Scaling this antenna system to 94 Gc, then, would entail the use of a lens of correspondingly smaller diameter to retain an equally narrow beam.

Beyond the 30-100 Gc range, very little is known empirically of the effects of scaling. The variety of presently developed components is extremely limited and the mechanical tolerances on waveguide transmission lines and components become difficult with available materials and techniques. The increased circuit losses imposed by the waveguide runs and components would appreciably impair the efficiency of the antenna. Minimizing these losses will probably entail the use of radically new antenna techniques.

7.2 PHASE SHIFTERS FOR THE RADIATING ELEMENTS OF A HIGH-GAIN PLANAR ARRAY

The technical difficulties of the multi-element scanning structure are so great that as yet no high-gain electronically scanned millimeter-wave antenna has been built. The reason for the problem can be illustrated by a discussion of a nonscanned planar array.

High-gain antennas at millimeter-wave frequencies that use an array of phased elements to form and scan the beam can become very

complex because of the number of elements required. Typical design parameters at the 35 and 94 Gc window frequencies are illustrated in Table 7-1 for nonscanned antennas. As is indicated, antenna gains in the 40 ± 5 db range require the use of thousands of radiating elements. The additional phase-shifting elements for beam scanning in a high-gain antenna would result in a structure that would be impossibly bulky, heavy, and costly.

Parameter	Frequency							
	35 Gc				94 Gc			
Antenna Gain, db(1)	45	40	35	30	45	40	35	30
Antenna diameter, inches(2)	24	15.6	7.8	4.6	9.2	5.3	3.9	1.7
Beamwidth, degrees(3)	0.75	1.4	2.2	4.3	0.75	1.4	2.2	4.3
No. of elements (square array)(4)	12000	5000	1500	500	12000	5000	1500	500
No. of elements (circular array)	9400	3900	1200	390	9400	3900	1200	390

Notes: (1) Absolute gain

(2) Diameter based on the effective area, A_e, and the actual area, A, as $A_e = 0.6A$

(3) Beamwidth total angle between points 3 db down

(4) Number of elements based on 0.6 λ_o spacing of elements

Table 7-1. Typical Design Parameters for Nonscanned Millimeter-wave Antennas (after Southworth, 1950).

An additional basic disadvantage with beam scanning relative to a fixed aperture plane is a lower gain because of a decreased effective aperture as the angle of the beam decreases relative to the aperture plane.

In view of these problem areas, mechanically scanned planar arrays may be more feasible than electronically scanned systems. The solution of such mechanical problems as bearings in space environments

may be easier for some applications than the fabrication of an electronic steering structure with thousands of elements. At millimeter wavelengths, the planar array is small (see Table 7-1), can be made very light, and can be designed with a high efficiency and good sidelobe control. For applications that require a limited number of elements or a limited scan angle, electronic phase shifting might be feasible.

7.3 FERRITE PHASE SHIFTERS

Three types of electronically controlled phase shifters have been considered – the ferrite, the ferroelectric, and the diode. Of these three, the use of ferrite is the most attractive since the magnetic field control is quite easily implemented and, at millimeter-wave frequencies, the losses are acceptable. The use of ferroelectric material has been studied to some extent (Cohn and Eikenberg, 1962), but with the material available so far, the losses are undesirably high and require voltages in the kilovolt range for phase control. The use of diodes mounted in a waveguide to give a controlled phase shift is dependent upon the development of suitable diodes for millimeter use. The problem areas in this development are expected to be the power handling capability and the insertion loss.

7.3.1 Applications to Arrays

Some thought has been given to the use of ferrite phase shifters in antenna arrays. For example, one preliminary study has been performed of an electronic scanning antenna operating at millimeter wavelengths (Republic, 1963). This antenna is described as a linear array of 16 conical horns that radiate a circularly polarized wave. The antenna is divided into two sections of 8 horns each to provide 2-port monopulse operation. Electronic scanning is presumably by the type of ferrite phase shifters described by F. Reggia (1961a) and McCarter and Landry (1961). These employ cylindrical ferrite rods in rectangular waveguide. The conical tapering of the ends of the ferrite rod provide a match (VSWR) of better than 1.2:1 over a 10-percent band and for a wide variation in applied magnetic field. No details of the phase shifter or of the circuit

arrangement are given in the preliminary report, nor are the desirable characteristics of such phase shifters mentioned. However, an article in Aviation Week and Space Technology (Miller, 1964) gives a summary of the program:

> Flight tests of a feasibility breadboard, broadband millimeter digital communications system are being conducted by USAF's Aeronautical Systems Division. The 100-mc bandwidth system was built for the Air Force by the Electronic Products Division of Republic Aviation. It operates at 50 to 55 Gc., a region where there is relatively high atmospheric attenuation, suggesting that it may be intended ultimately for secure communications among aircraft or space vehicles. The transmitter puts out about 10 w. and the receiver, including its preamplifier, has a noise figure of 10 db.
>
> An unusual feature of the system is its electronically steerable phased array antenna which can search, acquire and maintain target lock-on. One of the highest frequency radio frequency scanning antennas ever built, it consists of a linear array of 16 circularly polarized circular waveguide apertures protected by a radome. It was built by TRG, Inc.
>
> Each half of the array is excited by a waveguide input through an 8-to-1 matched balanced power divider and eight ferrite phase shifters. The two inputs are combined in a hybrid, the two outputs of which are the 16 element sum signal and a monopulse difference signal for boresighting. The phase shifters, according to TRG, have identical current characteristics with less than ±40 degree error for a zero to 360 degree phase shift. The antenna has 17 db gain, an azimuth beamwidth of 3.5 degrees, an elevation beamwidth of 70 degrees, a scanning range of ±30 degrees, and a beam switching time of three microsec.

The added complexity of the waveguide runs in arrays using ferrite phase shifters may be a problem. With an interelement spacing of less than the free space wavelength and with phase shifters whose length is a number of wavelengths, the length and complexity of the waveguide runs must be increased to make room for the phase shifter. One possible arrangement to produce a more compact unit is to fold the structure to shorten its length. A development of this form has been described by Jones and Reggia (1964) and is shown in Figure 7-2.

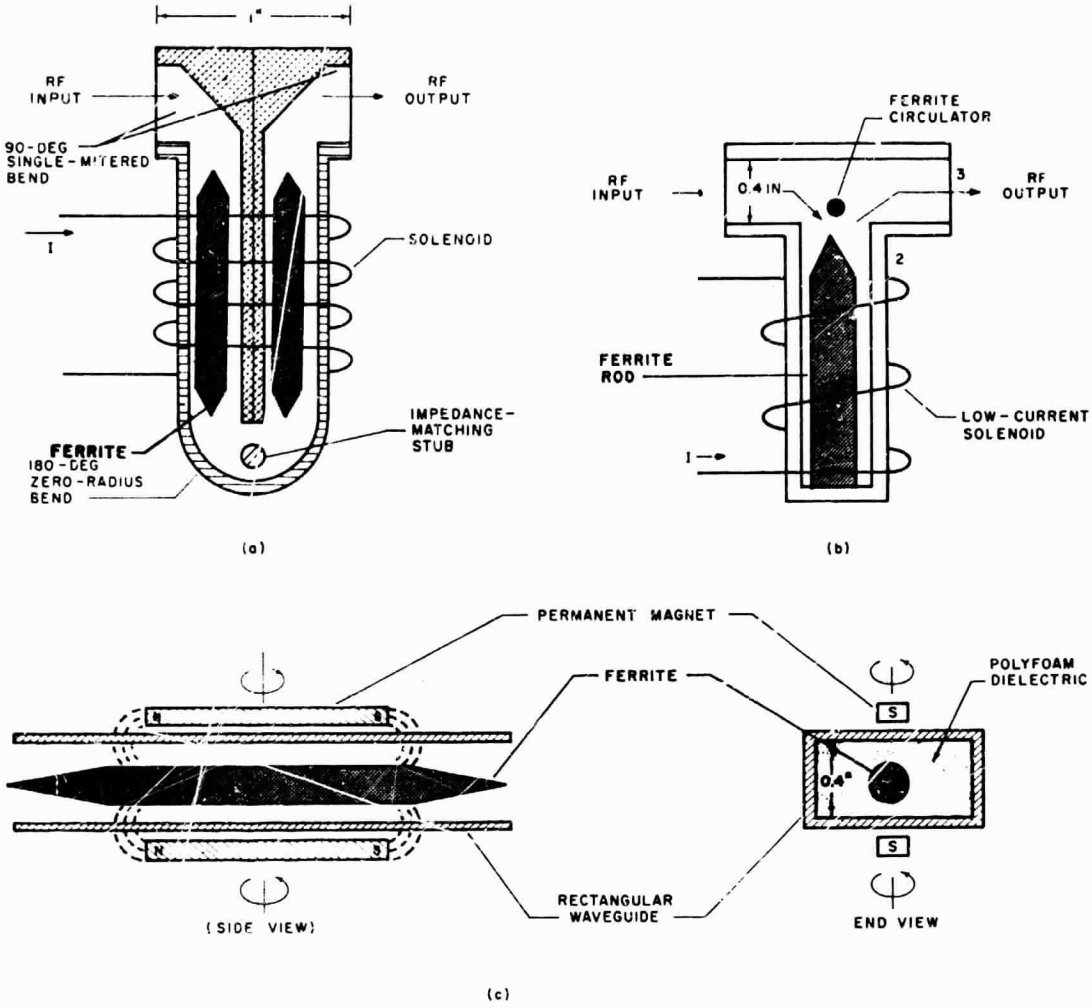

Figure 7-2. Detail of small ferrite phase shifters (Jones and Reggia, 1964).

7.3.2 Linearity

A characteristic which assumes an increasing importance is the linearity of phase shift in degrees with the magnetizing field in degrees. Linearity is feasible but does require an increase in length if non-linearity, due to saturation effects, is to be avoided. There is also some non-linearity in phase shift present at very low magnetizing fields. Biasing with a low magnetic field and making the ferrite unit long enough to operate only over the linear region for the required phase shift, of say 360 degrees, will tend to minimize undesirable non-linear behavior. Extending the dynamic range beyond the amount of phase shift required will permit some magnetic biasing with a fixed current to facilitate tracking of the different ferrite units.

7.3.3 Insertion Loss

Another factor involved with ferrite phase shifters is the insertion loss which tends to increase with frequency. The losses at K-band and K_a-band are less than 0.5 db for a phase shifter (Reggia, 1961b) which will give a substantially linear phase shift of 360 degrees. It is expected that the use of a low-loss ferrite (Reggia, 1961c) will decrease the loss somewhat at the higher frequencies, for example at 90 Gc.

7.4 SCANNING BY CONTROL OF FERRITE SLAB IN WAVEFRONT

A novel electronic scanning antenna has been reported by Sylvania (Schiller, 1964). The general purpose of this program is a millimeter-wave antenna in the 30-100 Gc band for use aboard spacecraft. The desired objectives include a 1-degree pencil beam capable of scanning ±45 degrees in both planes, a 40-db gain, and a peak-power handling capability of 5 Kw.

The scanning is achieved by control of the electrical properties of a bulk material in the wavefront of the beam. Specifically, a thin slab of ferrite is placed in the wavefront as shown in Figure 7-3. The function of the ferrite is to change the beam direction as the magnetic field is varied in a very special manner. A nonuniform magnetic field ($n_i \cdots n_k \cdots n_j$) parallel to the axis of this incident field is used. A variation of the magnetic field across the aperture changes the wave front in a linear manner to point the beam in a new direction. Scanning is obtained by appropriate variation of the applied axial field.

The basic principle is indicated in Figure 7-4. The magnetization of the ferrite is varied over a range of values n_i, n_k, and n_j, as indicated, so that

$$\theta_s = \sin^{-1} \frac{T}{D} \Delta n \qquad (7\text{-}1)$$

where

T = the thickness of the slab

D = the width of the slab

$n = \sqrt{\mu\epsilon}$

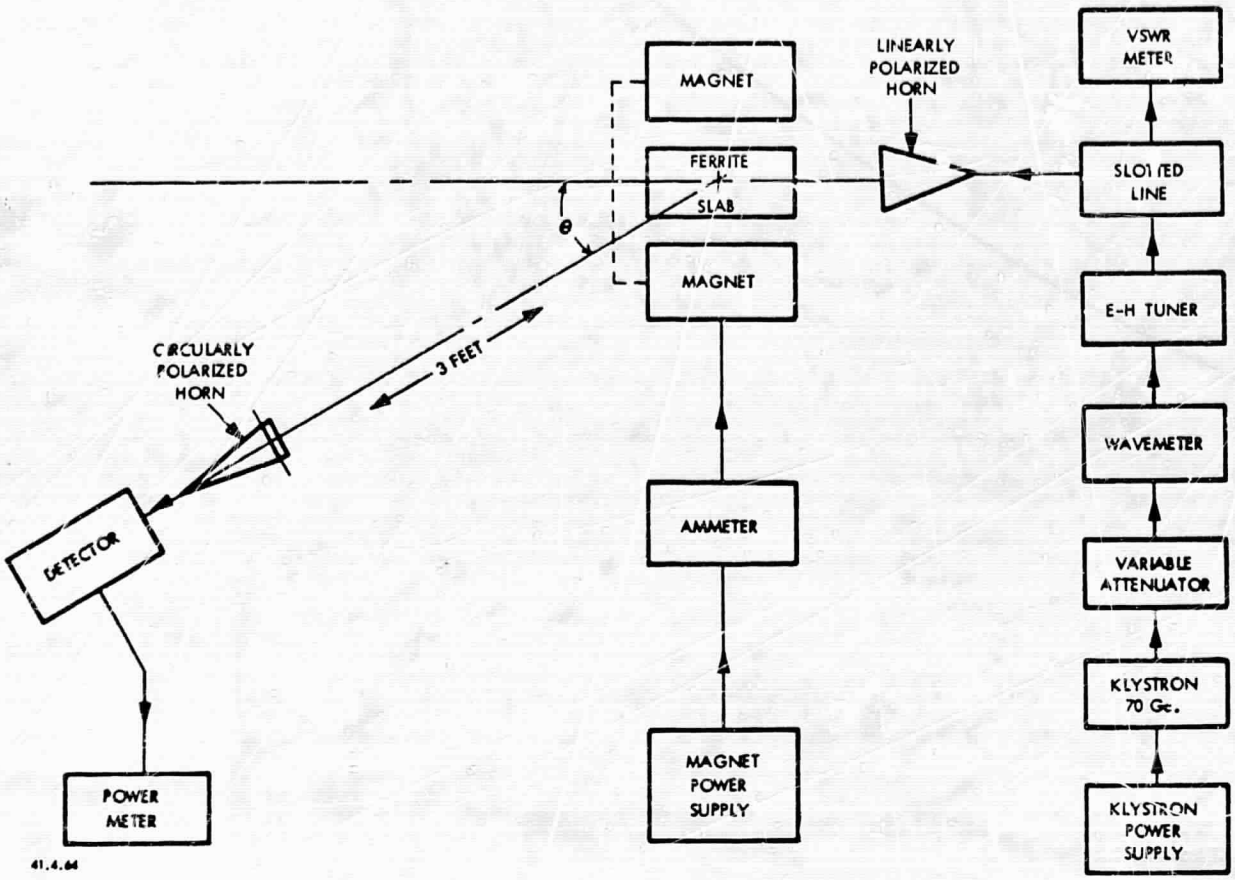

Figure 7-3. Ferrite slab in wavefront (Schiller, 1964).

$$\mu = \text{permeability} = 1 - \frac{4\pi M_s}{f/\gamma - H_i}$$

$4\pi M_s$ is the saturation moment and $f = \gamma H_i$

ϵ = permittivity (dielectric constant)

Using this principle of variation of the ferrite magnetization, a number of radiation patterns were made that indicate a shift in the direction of the beams with different magnetizations. Shifts in the direction of the beam axis of over 20 degrees can be seen in the patterns of Figure 7-5. Figure 7-5a indicates the radiation pattern through the ferrite slab with no external magnetic field applied (0 ampere turns). This pattern is essentially that of the antenna without the ferrite inserted in the beam. Patterns at several angles up to 20 degrees (Figures 7-4b and c) indicate

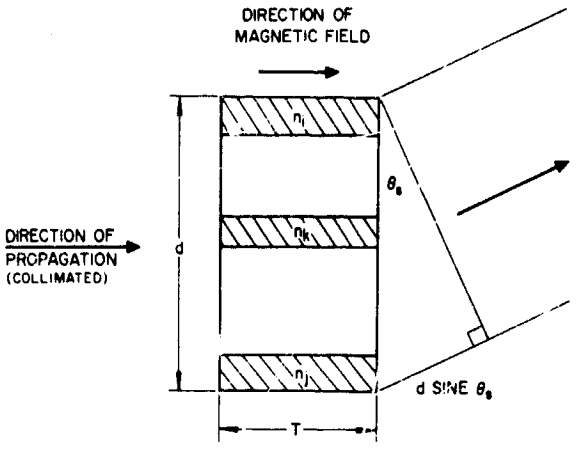

Figure 7-4. Basic arrangement of ferrite slab scanner (Schiller, 1964).

only slight degradation in performance: a slight increase in beamwidth (≈8° to 10°), an increase in sidelobe level from -13 to -10 db, and a slightly lower gain (by ≈1 db). For a shift of the beam by more than 20 degrees, the loss increased by 3-4 db and the minor sidelobe level increased to a value comparable to the major lobe, as shown in Figure 7-4d.

Other patterns are shown (Schiller, 1964) to illustrate other conditions, such as hysteresis of the ferrite: a reversal of the magnetic field does not return the beam to the same position it occupied before the reversal. Problems in the control of the magnetic field distribution indicate that further effort is required to realize a practicable system. The beam can be shifted by this ferrite slab technique but a feasible scanning system has not yet been demonstrated.

7.5 OPTICAL ANTENNAS

Application of the well-known principles of optics offers some attractive possibilities in the design of millimeter-wave antennas, particularly for the higher frequencies. Optical antennas are attractive for use at microwave frequencies and even more attractive at the higher millimeter-wave frequencies because they are simple, lightweight structures. Optical millimeter-wave systems employ reflective or refractive optics or combinations of the two.

Antennas employing reflective optics include the well known paraboloidal antenna or the horn reflector antenna (Hines et al., 1963). The paraboloid is widely used at millimeter-wave frequencies, and even at 94 Gc, a wide range of paraboloid diameters are available commercially (TRG, 1962).

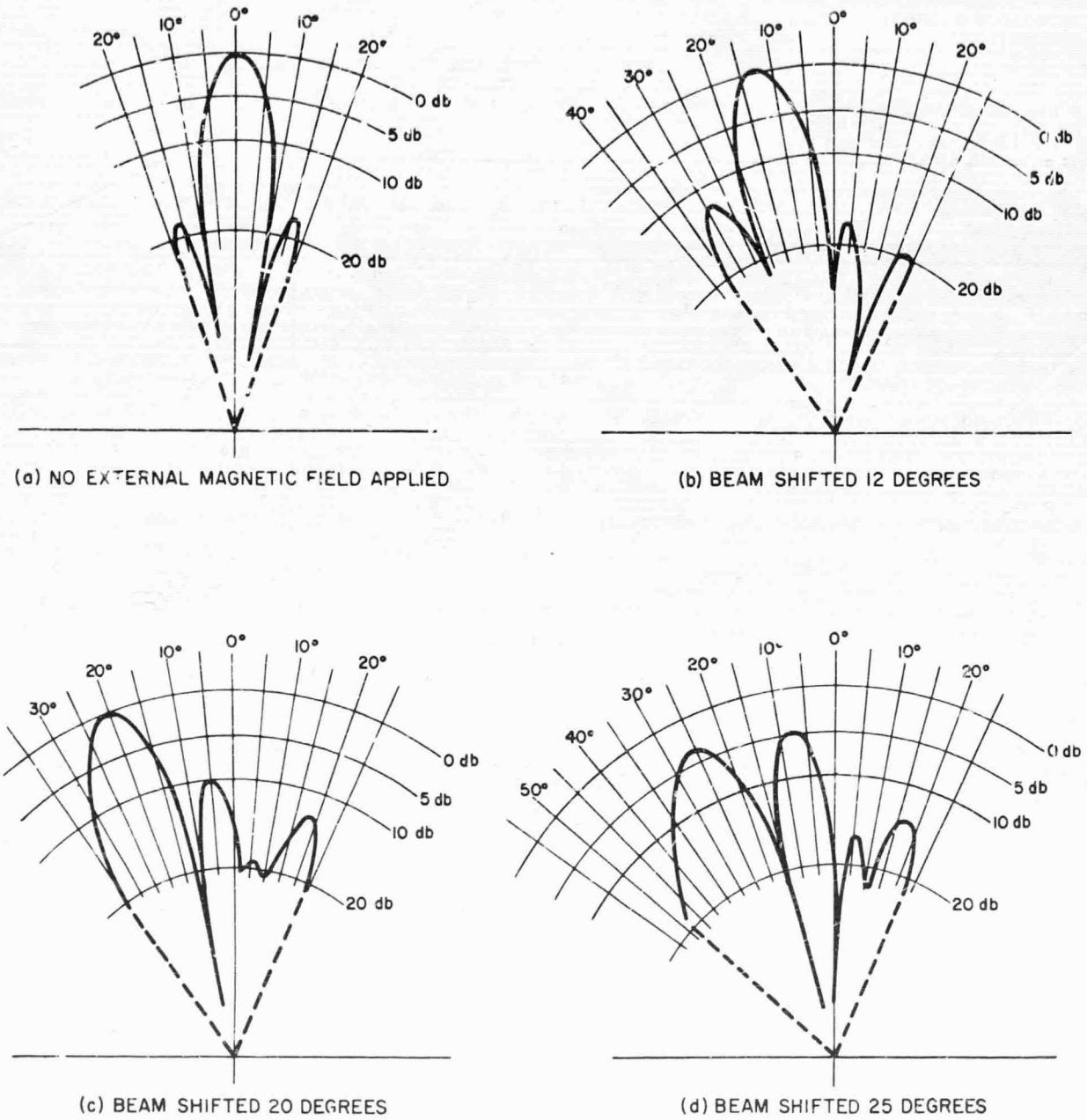

Figure 7-5. Radiation patterns of ferrite slab scanner (Schiller, 1964).

The diffractive properties of a dielectric are utilized in such antennas as the Luneberg lens (Luneberg, 1944); a point source with a convex lens; a spherical lens that is a special application of the Luneberg lens (Cheston and Luoma, 1963); and a multiple lens system such as the zoom lens (Kott, 1964) which varies the antenna beamwidth. The well-established optical methods for making dielectric lenses of plastic and ceramic materials are applicable to millimeter-wave antennas. The weight of the plastic lens can be markedly reduced by the use of a Fresnel lens of comparable design.

Combinations of both reflective and diffractive optics include the Schmidt lens (Jasik, 1961d) in which a spherical reflecting surface is utilized with a dielectric correcting or compensating lens. Another form of this type of optical antenna employs a short conical horn with a corrective lens mounted in the aperture to convert the spherical wavefront to a plane wavefront.

Scanning of optical antennas in the millimeter-wave ranges by displacement of the primary feed relative to the reflector axis is limited to a few beamwidths if serious beam deterioration is to be avoided. For larger scan angles, the entire antenna structure can be moved. With lenses having a circular symmetry, scanning can be accomplished over large angles by moving the feed only or, alternatively, by switching between feeds. Some methods of achieving this type of scan are considered in the next sections.

7.5.1 Lens Scanning Antennas

In one class of antennas the beam may be formed by a lens with a circular or spherical symmetry. The beam is developed from a small area feed or point source and expanded to a plane wavefront with the lens. At millimeter wavelengths the lens may be a dielectric lens of the Luneberg type with a dielectric constant that varies with the radius of the sphere. Scanning can be achieved by the movement of the feed point over the surface of the sphere. A variation of the Luneberg configuration is a spherical lens with a uniform dielectric constant throughout its volume (Cheston and Luoma, 1963). A geodesic lens (Horner et al., 1953)

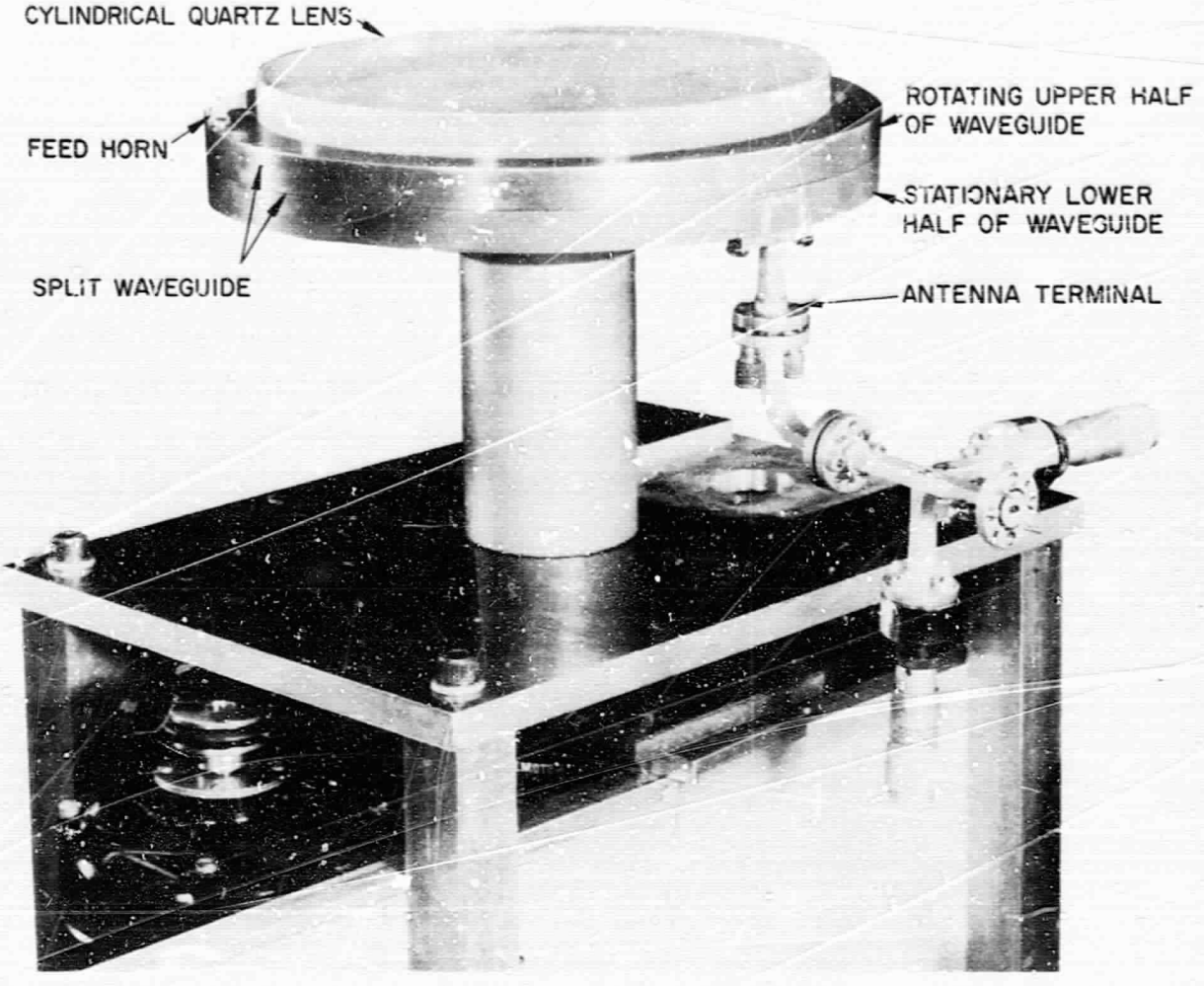

Figure 7-6. Cylindrical lens scanner.

which consists of two specially curved and uniformly spaced metallic surfaces can also form the beam in a manner analogous to a dielectric lens.

A short dielectric cylinder can be used in place of a spherical lens for scanning in one plane. The correct choice of dielectric constant will focus a plane wave along the periphery of the cylinder. One arrangement of this type of antenna is shown in Figure 7-6 (Behnke, 1964). A section of a quartz cylinder acts as a lens to collimate the beam and radiate a plane wave. The feed horn is placed at the periphery of the cylinder and is connected by an H-plane junction to the upper half of a split ring waveguide that is rectangular in cross section. The upper half of this waveguide ring and the feed horn rotate together to produce

a circular scan. The lower half of the waveguide is stationary and is connected, also by an H-plane junction, to the antenna terminal. A broadband match produces a small coupling restriction when the feed horn junction crosses the waveguide terminal to restrict the scanning to about 355 degrees at 56 Gc, but a full 360 degrees of scan could easily be obtained with a rotary joint.

The cylindrical lens scanner of Figure 7-6 was measured with a 6-inch diameter lens at 56 Gc, and the radiation pattern in the plane of scan is presented in Figure 7-7. The beamwidth is 3 degrees, and the minor sidelobes are 15.5 db down. The measured axial gain was 25 db. Both senses of linear polarization resulted in practically the same behavior, which suggests that the antenna would work with a circularly polarized feed source. Two or four-port monopulse operation could be used; several beams at the same or different frequencies could be operated simultaneously. The weight of the quartz lens in such a scanning system might be excessive for application to spacecraft, but possibilities do exist for lessening the weight since a lighter weight dielectric lens can be used in place of the quartz.

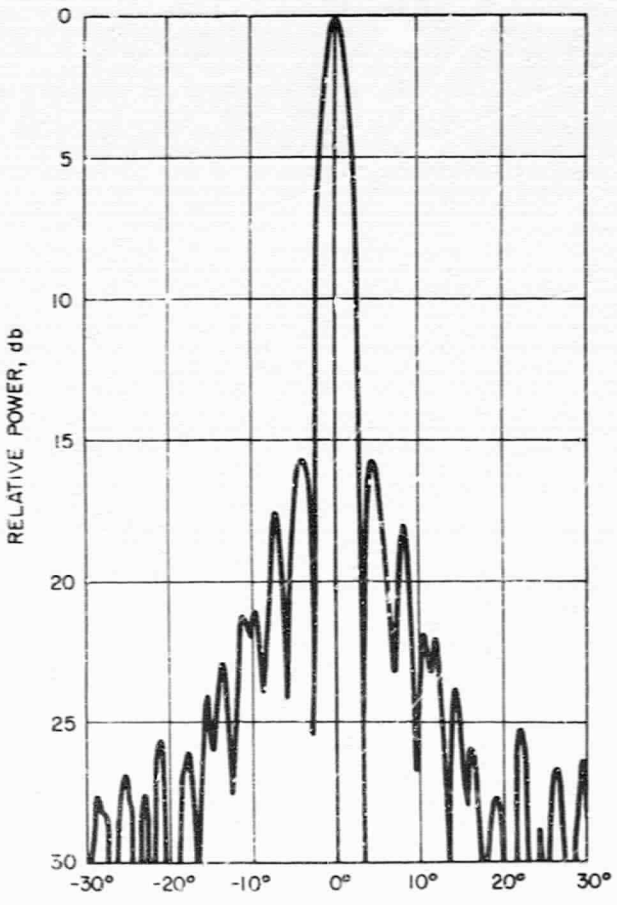

Figure 7-7. Radiation pattern at 56 Gc in the plane of scan of the cylindrical lens scanner.

The cylindrical lens scanner is a device with several possible applications. One, for example, is beam steering on a spin-stabilized spacecraft, such as the Applications Technology Satellite. Another application would employ several of the lens scanners in an array to provide a system with milliradian beamwidths and scannable over a limited angle. An interesting by-product of the lens

scanner is the application of the split ring waveguide as a phase shifter. One embodiment, as used in the antenna of Figure 7-6, is a phase shifter with rotation relative to a moving feed point. In another form both terminals of the phase shifter might be stationary. In either configuration, large phase shifts that are linear with rotation could be realized. Other possible applications of the device are as a multiple-pole switch or as a device to produce sector scanning. Other forms of the split ring waveguide to provide either scanning or switching have also been reported (Johnson et al., 1960).

7.5.2 Hemispherical Mechanical Scanning

Another novel form of optical antenna which is capable of scanning a full hemisphere has also been described (Cochrane, 1956). The essential details of this system are shown in Figure 7-8. This antenna is composed of a fixed feed source that illuminates a fixed paraboloid. The collimated beam is reflected from a plane surface which can be rotated in either plane to provide a scan (Figure 7-8a). To avoid blockage of the plane wavefront by the paraboloid, the following technique is employed: the paraboloid is constructed of a series of parallel plates spaced less than $\lambda_o/2$ apart so that complete reflection occurs when the electric field polarization from the feed aperture is parallel to the slats of the paraboloid. After collimation, the beam strikes the flat surface of the reflector. This surface is designed as a half-wave plate and consists of a flat, solid, reflecting plate with a grid of plates, $\lambda_o/4$ in height and also spaced at intervals of less than $\lambda_o/2$. The grid is mounted on the surface of the flat plate and oriented at 45 degrees relative to the electric field. For this orientation, the reflected wave will be rotated 90 degrees in polarization. Under these conditions, the parallel plates of the paraboloid are now perpendicular to the electric field and quite transparent to the emerging beam.

Figure 7-9b indicates the variation in gain with beam scan angle. It is interesting to note that a relatively small gain penalty is imposed in the scanning over such a wide angle. The increased losses at scan angles greater than 50-60 degrees are believed to be caused by the plane

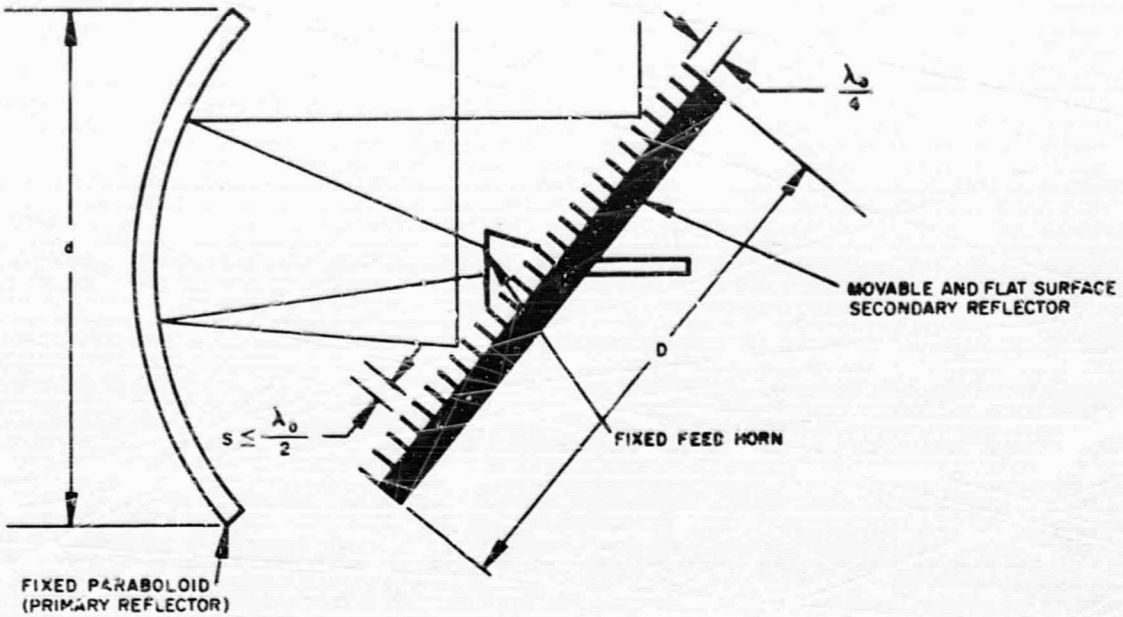

(a) BASIC CONFIGURATION

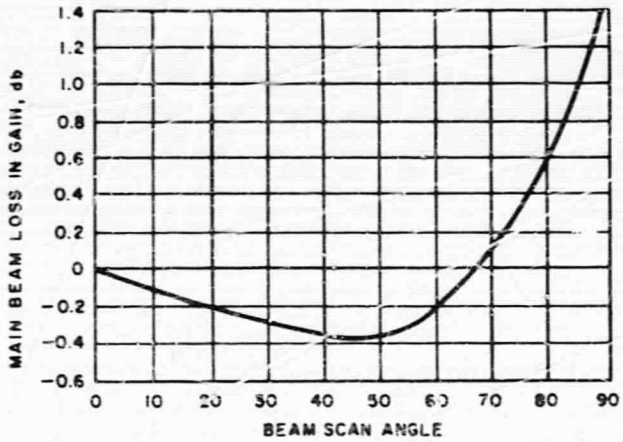

(b) VARIATION IN GAIN WITH SCAN ANGLE

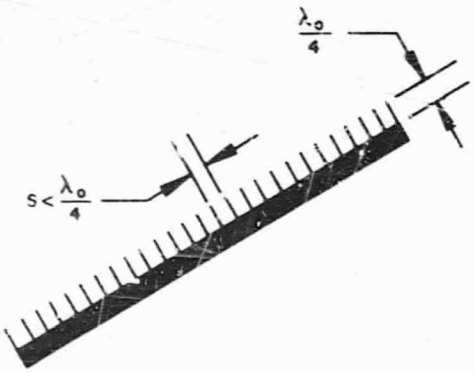

(c) SECONDARY REFLECTOR WITH CLOSER SPACING

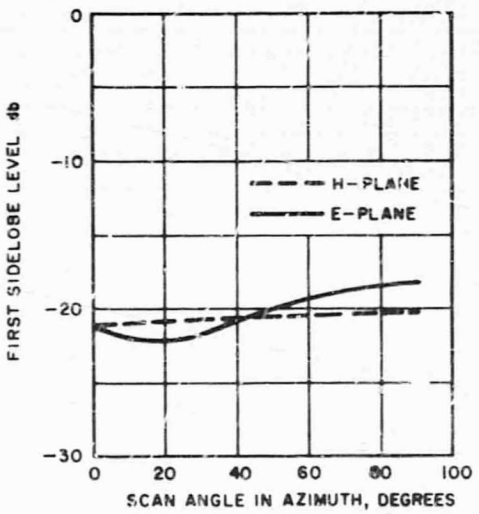

(d) FIRST SIDELOBE LEVEL VS. SCAN ANGLE

Figure 7-8. Hemispherical mechanical scanner.

reflector departing from a $\lambda_o/2$ plate and introducing slight loss and increased wave ellipticity. The performance of the half-wave plate secondary reflector can be improved by the use of closer spacing, for example, by $\lambda_o/8$ (Figure 7-8c). In addition, the larger scan angles, for example 90 degrees, require the secondary reflector to be larger by the ratio D/d = 1.4 if a lower gain due to a decrease in the aperture is to be avoided. The level of the first sidelobes as a function of the scan angle is indicated in Figure 7-8d.

7.5.3 Electronic Switches

To convert the mechanical movement of a lens scanning system such as the cylindrical lens scanner to electronic control will require switches. These would be used to provide a connection between the antenna terminal and one of the feed lines while the other feed lines were disconnected. The direction of the beam is shifted by discrete amounts preferably less than the 3-db beamwidth to limit the scanning loss to less than 3 db. In one sense this switching action can be considered a digital scanning technique.

A number of different switches have been explored, including diode, ferrite, reed, plasma, and secondary emission types. Some very satisfactory low-power diode waveguide switches have been developed at 10 Gc, but there appears to be no developed product at millimeter-wave frequencies. Low-power ferrite switches (Turner, 1958) have been built at frequencies up to 70 Gc. These switches utilize the Faraday rotation principle and switch the signal between two output ports. The speed of a switch is governed by the desired rate of scan. For example, to give the cylindrical lens scanner electronic scan capability would require, say, 120 switches for 360-degrees of scan (1 switch for each 3 degrees of scan). With these switches, three complete 360-degree scans per second would be possible, requiring a switching time of 1 millisecond. Different systems and different scan times would present different switching time requirements. The switching speed for the ferrite switches is dependent on the magnetic circuit design. For the ferrite switch, speeds in the megacycle region are possible.

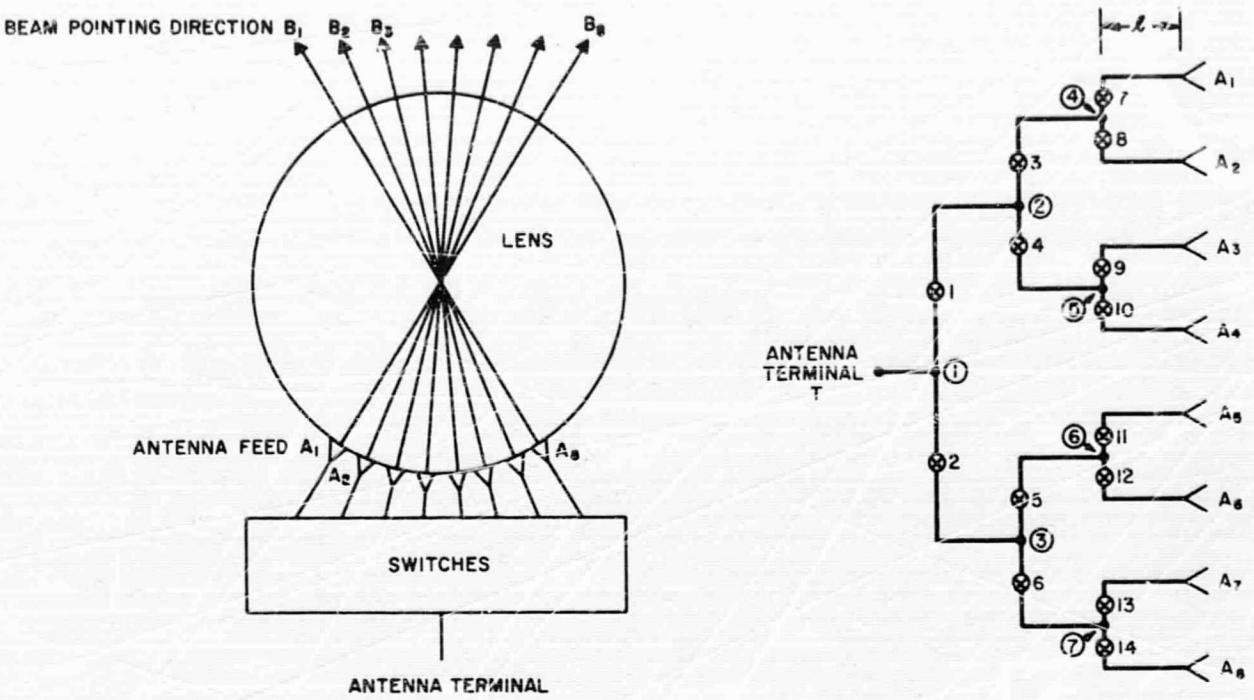

$A_1 \ldots A_8$	FEEDS DISTRIBUTED OVER SURFACE OF SPHERE OR ALONG PERIPHERY OF CYLINDRICAL LENS
$B_1 \ldots B_8$	BEAM POINTING DIRECTIONS FOR FEED $A_1 - A_8$, RESPECTIVELY
⊗1. ... ⊗14	SWITCHES
①, ②, ... ⑧	JUNCTIONS

ANTENNA FEED CONNECTED	SWITCHES ACTUATED
A_1	2,4,8
A_2	2,4,7
A_3	2,3,10
A_4	2,3,9
A_5	1,6,12
A_6	1,6,11
A_7	1,5,14
A_8	1,5,13

Figure 7-9. Multiple feed scanning antenna utilizing switches.

There are a number of ways in which a waveguide switch can be used with an optical antenna. As an example, the multiple feed lens antenna of Figure 7-9 can be considered. In this arrangement, the switches are associated with junctions (Figure 7-9b). At junction ① there are two switches, one in each branch line. The tee is designed so that when switch 2 is actuated, it shorts the line and acts as a piston. By suitable design (distance of short to the piston and junction design), line T is terminated and the power flows in line 1 past switch ⊗1. Similarly for the other switch-junctions. To actuate any of feeds A_1 to A_8 requires the operation of the switches, as indicated in Figure 7-9b. The number of junctions required is n - 1 where n is the number of feed elements, and the number of switches is twice as many. For the

particular arrangement illustrated the number of switches (X) which must be actuated to excite each element is 2(n - 1). It becomes evident that, as n becomes large and the number of switches also increases, the loss of each switch must be low in order to keep the total loss within reasonable limits. For the arrangement of Figure 7-9, the excitation of feed A_1 requires that 3 switches (2, 4, 8) be actuated to short the line. In addition, power will flow past three additional switches (1, 3, 4).

The combined loss of the switches involved in this kind of circuit must be kept to a reasonably low value. In addition, loss in a switch (shorted case) due to leakage to an adjacent feed will tend to degrade the antenna pattern. Another objectionable feature is the coupling between an active feed and the adjacent ones. The circuit must be arranged to minimize this effect, possibly by adjustment of the length ℓ between the feed and the switch of the adjacent feeds.

7.6 MILLIMETER-WAVE COMPONENTS

The stimulated interest in millimeter-wave antenna systems has been reflected in the development of new and improved components. Several backward-wave oscillators show promise and a number of traveling-wave amplifiers are available. Lightweight waveguide ferrite isolators have also been developed.

7.6.1 Power Sources

The development of higher powered tubes at lower frequencies has benefited the development of millimeter-wave sources. Improved techniques and fabrication have greatly extended the available power and upper frequencies of millimeter wave tubes. Table 7-2 indicates the frequency range and CW powers available with oscillator tubes that have been successfully built and tested. Some are now commercially available.

Very likely the highest CW powers obtained have been with tubes developed by the Hughes Malibu Research Laboratories (Forster, 1964). One backward-wave oscillator traveling-wave tube has an output in the 1500-watt range. A recently developed tube (814H) delivers 150 watts of CW power at 94 Gc. Some development has also been done with a tube designed to produce 5 watts at 120 Gc.

CW Output Power	Frequency Range	Notes
1 - 1500 watts	50 - 80 Gc	Klystrons and backward-wave oscillators
10 mw - 5 watts	100 - 150 Gc	Klystrons and backward-wave oscillators
1 - 10 mw	to > 400 Gc	(No sources available 150-250 Gc)

Table 7-2. Power Characteristics of Available Oscillators (Forster, 1964).

CSF is currently working on a backward-wave oscillator (Carcinotron) that is estimated to produce 1 watt of CW power at 300 Gc and higher powers at lower frequencies.

Pulsed magnetrons with peak power outputs of 100 Kw at 34-35 Gc (SFD) and peak powers of 5-10 Kw in the 50-100 Gc band have been developed and are commercially available. A few tubes with peak powers of 25-35 Kw in the 50-75 Gc range are also available.

7.6.2 Amplifiers

A number of traveling-wave tube amplifiers are available at 50-60 Gc with gains in the 30-db range and CW power outputs of fractions of a watt. Both BTL and CSF have amplifiers of the crossed-field type in the 1-10 watt range, and the Hughes Research Laboratories have a tube with a CW power output of 1500 watts and a gain of about 18 db in the 51-56 Gc frequency range. Presumably, these tubes will deliver appreciably higher power when operated on a pulsed basis. There still appear to be no amplifier tubes available that will compete with pulsed magnetrons in peak power output.

7.6.3 Hexagonal Ferrite Isolators

A series of lightweight rectangular waveguide ferrite isolators have been developed in which the weight is minimized by the use of hexagonal ferrites to reduce the size of the external magnet (Taft et al., 1963). There has been a general improvement in ferrite mixtures which produce

isolators with a lower forward transmission loss. The results of the development program are summarized in Table 7-3. The lower three bands (18-50 Gc) cover the full bandwidth with forward losses ranging from 0.6-1.5 db and a reverse loss in the 24-40 db range. At higher frequencies (50-110 Gc) the forward loss is over 1 db and the minimum reverse loss drops to the 15-20 db range. The wide band is achieved through the use of several ferrites (4-6) in each unit.

Characteristic	Frequency Range, Gc				
	18-26.5	26.5-40.0	33-50	50-75	75-110
Reverse loss, db	28 - 32	24 - 40	24 - 37	20 minimum	15 minimum
Forward loss, db	0.6-0.8	0.6-1.1	0.7-1.5	1.0+	1.0+
Input VSWR	1.1	1.04-1.1	1.0-1.5	1.2:1 maximum	1.2:1 maximum
Waveguide	RG-53/U	RG-96/U	RG-97/U	RG-98/U	RG-138/U
Minimum CW power	10 watts	10 watts	10 watts	10 watts	10 watts

Table 7-3. Characteristics of Hexagonal Ferrite Isolators (after Taft et al., 1963).

8. ACKNOWLEDGMENTS

The authors wish to acknowledge the assistance of several colleagues in the Hughes Antenna Department: A. P. King for Section 3.4 on solid-state components and for the section on millimeter-wave antennas (7); S. S. Shapiro for much of the ferrite material in Section 3.1 and for the New Technology section (6); B. F. Forman and F. J. Goebels, Jr., for the diode and diode-iris material in Sections 3.2 and 3.3, and F. A. Lauriente for Sections 5.4.1 through 5.4.4. The authors also wish to acknowledge the diligent editorial assistance of M. Delzell.

Several sections of this report were abstracted from W. H. Kummer's chapter on Feeding and Phase Scanning in Microwave Scanning Antennas, Vol. II, R. Hansen, editor, (Academic Press, 1965).

Acknowledgment is also made to the NASA Goddard Technical Officer, Mr. A. Kampinsky, for his many helpful suggestions and criticisms.

PRECEDING PAGE BLANK NOT FILMED.

9. REFERENCES

Andre, S. N., and D. J. Leonard (1964). An active retrodirective array for satellite communications. IEEE Trans. AP-12, 181-186.

Ashmead, J., and A. B. Pippard (1964). The use of spherical reflectors as microwave scanning aerials. Journal IEE (London) 93, Pt. III-A, 627-632.

Assaly, R. N. (1953). Experimental investigation of a homogeneous dielectric sphere as a microwave lens. Can. J. Physics 36, 1430-1435.

Atalla, M. (1964). Private communication. Hewlett-Packard Associates, Palo Alto, California.

Bangert, J. T., R. S. Engelbrecht, E. T. Harkless, R. V. Sperry, and E. J. Walsh (1963). The spacecraft antennas. Bell System Tech. J. 43, 869-892.

Behnke, M. C. (1964). High-speed, millimeter-wave lens scanner. Unpublished technical memo. Hughes Aircraft Company, Culver City, California.

Bekefi, G., and G. W. Farnell (1956). A homogeneous dielectric sphere as a microwave lens. Can. J. Physics 34, 790-803.

Belfi, C. A., C. Rothenberg, L. Schwartzman, R. E. Tilley, and A. Wills (1964). A satellite data transmission system. IEEE Trans. AP-12, 200-206.

Bowness, C. (1957). Contribution to Discussion on microwave apparatus. Proc. IEE (London) 104B, suppl. 6, 366.

Brooks, R. O. (1963). Unpublished work. Raytheon Company, Bedford, Massachusetts.

Bugnolo, D. S. (1962). A quasi-"isotropic" antenna in the microwave spectrum. IRE Trans. AP-10, 377-383.

Bush, D. (1957). Contribution to Discussion on microwave apparatus. Proc. IEE (London) 104B, suppl. 6, 366.

PRECEDING PAGE BLANK NOT FILMED

Button, K. J., and B. Lax (1962). Microwave Ferrites and Ferrimagnetics. McCraw-Hill Book Co., Inc., New York.

Chadwick, G. G., and J. C. Glass (1962). Investigation of a Multiple Beam Scanning Circular Array. Scientific Rept. No. 1 on Contract AF19(628)-367; Rept. No. AFCRL-63-136 TR31. Radiation Systems, Inc., Alexandria, Virginia.

Cheston, T. C., and E. J. Luoma (1963). Constant-K lenses. APL Technical Digest, March-April, 8-11.

Clavin, A. (1958). Reciprocal ferrite phase shifters in rectangular waveguide. IRE Trans. MTT-6, 334.

Clavin, A. (1960). (a) Reciprocal ferrite phase shifters. IRE Trans. MTT-8, 254; (b) IRE National Symposium on Microwave Theory and Techniques, Coronado, California.

Cochrane, C. A. (1956). Scanning Antennas. U. S. Patent No. 2736895.

Cohn, M., and A. F. Eikenberg (1962). UHF Ferroelectric Phase Shifter Research. Final Rpt. No. AFCRL-62-319 on Contract AF19(604)-8349. Electronic Communications, Inc., Timonium, Maryland.

Cutler, C. C., R. Kompfner, and L. C. Tillotson (1963). A self-steering array repeater. Bell System Tech. J. 42, 2013-2032.

Dawirs, H. N., and W. G. Swarner (1962). A very fast, voltage-con rolled, microwave phase shifter. Microwave Journal 5, no. 6, 99-107.

DeSize, L. K. (1957). An investigation of the feasibility of obtaining a constant beamwidth Luneberg lens. Abstracts of the Seventh Annual Symposium on the USAF Antenna Research and Development Program. Doc. No. AD-13850. University of Illinois.

Duhamel, R. H., and M. E. Armstrong (1964). 1964 PTGMTT Internat'l Symposium Digest. (a) Characteristics of log-periodic transmission-line circuits, pp. 9-12; (b) Log-periodic phase difference circuits, pp. 13-16; (c) Log-periodic octaline hybrid junctions, pp. 18-20.

Drude, P. (1925). Theory of Optics, pp. 58-63. Longmans, Green, New York.

Eaton, J. E. (1953). An Extension of the Luneberg-type Lens. Rpt. No. 4110, p. 13. Naval Research Laboratory, Washington, D. C.

Erhardt, H. R., G. Gerson, and D. C. Mead (1963). The advanced Syncom communication antenna system: a directive array for spin-stabilized satellites. IRE Nat'l Symposium on Space Electronics and Telemetry Record.

ESSA (1959). Electrical Scanning and Stabilizing of Antennas, pp. 51-53. Final Report No. WADD-TR-60-284 on Contracts AF33(616)-2971, 5499. Bell Telephone Laboratories, Inc., New York, New York.

Feiner, A. (1964). The ferreed. Bell System Tech. J. 43, no. 1, pt. 1, 1-15.

Fletcher, A., T. Murphy, and A. Young (1954). Solutions of two optical problems. Proc. Royal Soc. (London) 223, 216-225.

Forman, B. J., and F. J. Goebels, Jr. (1962). Electronic amplitude control of a slot radiator in an X-band waveguide by means of a varactor diode-iris. Unpublished technical memo. Hughes Aircraft Company, Culver City, California.

Forster, D. C. (1964). Review of available millimeter wave sources. IEEE Wescon Convention Record.

Fox, A. G. (1947). An adjustable waveguide phase changer. Proc. IRE 35, 1489.

Friedlander, F. C. (1946). A dielectric-lens aerial for wide angle beam scanning. Journal IEE (London) 93, pt. III-A, 658.

Gangi, A. F. (1963). The active adaptive antenna array system. IEEE Trans. AP-11, 405-414.

Ghose, R. N. (1964). Electronically adaptive antenna systems. IEEE Trans. AP-12, 161-169.

Goodwin, F. and T. Nussmeier (1959). A Ferrite Volumetric Scanning Array. Rpt. No. 102. Research Laboratories, Hughes Aircraft Company, Culver City, California.

Gruen, W. J. (1953). Theory of AFC synchronization. Proc. IRE 41, 1043-1048.

Gruenberg, E. L., and C. M. Johnson (1964). Satellite communication relay system using a retrodirective space antenna. IEEE Trans. AP-12, 215-223.

Hamasaki, J. (1963). A wideband high-gain transistor amplifier at L band. IRE Internat'l Solid-State Circuits Conference Digest, 48-49.

Hansen, R. C. (1961). Communications satellites using arrays. Proc. IRE 49. (a) pp. 1066-1074; (b) "Correction," pp. 1340-1341.

Hardin, R. H., E. J. Downey, and J. Munushian (1960). Electronically-variable phase shifters utilizing variable capacitance diodes. Proc. IRE 48, 944-945.

Harrington, R. F. (1961). Time Harmonic Electromagnetic Fields, pp. 17-20. McGraw-Hill, New York.

Higgins, V. J. (1963). X-band semiconductor switching and limiting using waveguide series tees. Microwave Journal 6, no. 11, 67-77.

Hines, J. N., T. Li, and R. H. Turrin (1963). The electrical characteristics of the conical horn reflector antenna. Bell System Tech. J. 42, part 2, 1187-1213.

Horner, R. T., J. S. Hollis, M. W. Long, et al. (1953). A Two-beam 16,000-Mc Modified Luneberg Lens Scanning System, p. 13. Final Rpt. on Contract DA-36-039, SC-15566. Georgia Institute of Technology.

Houlding, N. (1960). Measurement of varactor quality. Microwave Journal 3, no. 1, 40-45.

Jasik, H., ed. (1961). Antenna Engineering Handbook. McGraw-Hill, New York. (a) pp. 15-19 to 15-21; (b) pp. 10-4 to 10-5; (c) pp. 14-1 to 15-19; (d) p. 15-12; (e) pp. 14-12 to 14-15.

Johnson, R. C., A. L. Holliman, and J. S. Hollis (1960). A waveguide switch employing the offset ring-switch junction. IRE Trans. MTT-8, 532-537.

Jones, H. S., and F. Reggia (1964). Design of three miniature ferrite phase shifters. Microwaves 3, no. 7, 28-32.

Kay, A. F. (1959). Spherical symmetric lenses. IRE Trans. AP-7, 32-38.

Kelleher, K. S., and H. P. Coleman (1952). Off-axis Characteristics of the Paraboloidal Reflector. Rpt. No. 4088, Naval Research Laboratory, Washington, D. C.

Kott, M. A. (1964). A variable beamwidth millimetric wave antenna. IEEE Trans. AP-12, 662-668.

Kummer, W. H., A. T. Villeneuve, and F. G. Terrio (1963). Scanning without phase shifters. Electronics 36, 27.

Kummer, W. H., A. T. Villeneuve, T. S. Fong, and F. G. Terrio (1963). Ultra-low sidelobes from time-modulated arrays. IEEE Trans. AP-11, 633-639.

Lauriente, F. A., and F. G. Terrio (1963). Electronic amplitude scan of a 27-element slot array. Unpublished technical memorandum. Hughes Aircraft Company. Culver City, California.

Lax, B., and K. J. Button (1962). Microwave Ferrites and Ferrimagnetics. McGraw-Hill, New York. This book contains many references to various ferrite microwave devices.

Li, T. (1959). A study of spherical reflectors as wide angle scanning antennas. IRE Trans. AP-7, 223-226.

Luneberg, R. K. (1944). Mathematical Theory of Optics, pp. 189-212. Brown University Press.

Margerum, D. L. (1965). Self-phased arrays. Chap. 7, vol. 2. Microwave Scanning Antennas, R. C. Hansen, ed. Academic Press.

Margerum, D. L., and A. B. Lees (1964). Private communication. Electronic Speciality Company, Los Angeles, California

Matthei, W. C. (1964). Advances in solid-state microwave devices. Microwave Journal 7, no. 7. (a) pp. 41-47; (b) p. 45; (c) p. 46; (d) p. 56.

Maxum, B. J. (1957). Resonant Slot with Independent Control of Amplitude and Phase. Tech. Memo No. 573. Hughes Aircraft Company, Culver City, California.

McCarter, R. S., and E. F. Landry (1961). K_a-band ferrite phase shifter. IRE Trans. MTT-9, 271.

Microwave Associates (1964). Microwave Semi-Conductors, Catalog SF-4001/February 1964, p. 4. Microwave Associates, Inc.

Miller, B. (1964). Millimeter waves hold aerospace promise. Aviation Week and Space Technology, 24 August 1964, p. 71.

Morgan, S. P. (1959). Generalizations of spherically symmetric lenses. IRE Trans. AP-7, 342-345.

Mortenson, K. E. (1964). Microwave semiconductor control devices. Microwave Journal 7, no. 5, 49-57.

Neff, H. P., D. R. Stephens, and J. D. Tillman (1961). Electronic Scanning of Circular Antenna Arrays. Scientific Report No. 5 on Contract AF19(604)-4967; AFCRL 989. University of Tennessee, Knoxville, Tennessee.

Pon, C. Y. (1964). Retrodirective array using heterodyne technique. IEEE Trans. AP-12, 176-180.

Reggia, F. (1961). K-band reciprocal ferrite phase modulator. IRE Trans. MTT-9. (a) pp. 269-270; (b) p. 270; (c) See footnote 5, p. 269.

Reggia, F., and E. G. Spencer (1957). A new technique in ferrite phase shifting for beam scanning of microwave antennas. Proc. IRE 45, 1510

Republic (1963). Feasibility Study and Investigation of EHF Communication Techniques. Interim Engineering Rpt. No. 1, prepared for Aeronautical Systems Div., Wright-Patterson AFB, on Project No. 4335. Electronic Products Division, Republic Aviation Corp., Farmingdale, L. I., New York.

Ricardi, L. J., J. B. Rankin, and R. N. Assaly (1964). Private communication. Lincoln Laboratory, Mass. Inst. Technology.

Rizzi, P. A., and B. Gatlin (1959). Rectangular guide ferrite phase shifters employing longitudinal magnetic fields. Proc. IRE 47, 446.

Rofuse, R. P., and D. Steinbracher (1964). A 22 Gc balanced varactor quadrupler with 50 mwatt power. IEEE Internat'l Solid-State Circuits Conference Digest, 22-23.

Rutz-Philipp, E. M. (1964). Spherical retrodirective array. IEEE Trans. AP-12, 187-194.

Ruze, J. (1950). Wide angle metal plate optics. Proc. I. R. E. 38, 53-59.

Ryerson, J. L. (1960). Passive satellite communication. Proc. IRE 48, 613-619.

Schiller, T. R. (1964). Electronically Steerable Array for Space Vehicle Application. Report No. RADC-TDR-64-222 on Contract AF30(602)-3041. Sylvania Electronic Systems-Central, Williamsville, New York.

Schwartz, S., and J. Bagby (1964). Rigidized inflatable solar energy concentrators. Final Rpt. No. P64-123 on Contract NAS 1-3244. Hughes Aircraft Company, Culver City, California.

Sepoff, J. H., and G. J. Wheeler (1964). Octave bandwidth tunnel-diode amplifier. IEEE Trans. MTT-12, 21-26.

Shanks, H. E., and R. W. Bickmore (1959). Four-dimensional electromagnetic radiators. Can. J. Physics 37, 263.

Shapiro, S. S., ed. (1962). Mosaic Radar Study Program. Contract NOrd-19179. Hughes Aircraft Company, Culver City, California. (a) Semiannual progress report, p. 57, Table III; (b) Semiannual progress report, p. 53, Fig. 12; (c) Final Technical Report, pp. 7-8, Fig. 2.

Shapiro, S. S., ed. (1963). Quarterly Progress Report for Mosaic Radar Study Program, p. 20, Fig. 20. Contract NOw 63-0156-d. Hughes Aircraft Company, Culver City, California.

Shnitkin, H. (1961). Survey of electronically scanned antennas -- Pt. II. Microwave Journal 4, no. 1, 57-64.

Sichelstiel, B. A., W. M. Waters, and T. A. Wild (1964). Self-focusing array research model. IEEE Trans. AP-12, 150-154.

Silver, S. (1949). Microwave Antenna Theory and Design. MIT Rad. Lab. Series Vol. 12. McGraw-Hill, New York. (a) p. 195; (b) pp. 415-420; (c) pp. 497-502; (d) pp. 89-90.

Skolnik, M. I., and D. D. King (1964). Self-phasing array antennas. IEEE Trans. AP-12, 142-149.

Sletten, C. J., P. Blacksmith, Jr., and L. F. Shodin (1958). Amplitude Scanning of Antenna Arrays. Rept. No. TR-58-124. Antenna Laboratory, Air Force Cambridge Research Center.

Southworth, G. C. (1950). Principles and Applications of Waveguide Transmission. D. Van Nostrand, New York.

Steinhoff, R., and F. Sterzer (1964). Microwave tunnel diode amplifiers with large dynamic range. RCA Review 25, 54-66.

Sylvania (1965). Advertisement. Microwave Journal 8, no. 1, 53.

Taft, D. R., L. R. Hodges, and G. R. Harrison (1963). Millimeter Wave Components (Hexagonal Ferrite Isolators). Tech. Repts 1, 2, 3, 4, and 6 on Contract DA-36-039-89193. Microwave Electronics Company, Division of Sperry Rand Corporation, Clearwater, Florida.

Tang, R. (1956). A Slot with Variable Coupling and Its Application to a Linear Array. Rept. No. RLM(M)S6-15. Hughes Aircraft Company, Culver City, California.

TRG (1962). Millimeter Microwave Components. Catalog 162. TRG, Inc., East Boston, Massachusetts.

Turner, E. H. (1958). A fast ferrite switch for use at 70 KMC. IRE Trans. MTT-6, 300-303.

Van Atta, L. C. (1959). Electromagnetic Reflector. U. S. Patent No. 2,908,002.

Weiss, J. A. (1959). (a) The Reggia-Spencer phase shifter. JAP 30, 1538; (b) A phenomenological theory of the Reggia-Spencer phase shifter. Proc. IRE 47, 1130.

White, W. D., and L. K. DeSize (1963). Electronically steerable antenna-feed techniques (ESAFT). 1963 PTGAP International Symposium Digest, 73-77.

10. APPENDIX: ESTABLISHMENTS AND PERSONNEL VISITED

As part of the survey phase of the study program, a number of establishments were visited to obtain data from which the state-of-the art in electronic scanning and steering techniques could be evaluated. The names of the establishments visited, the key personnel interviewed, and the applicable subjects discussed are given..

1. Air Force Cambridge Research Laboratories, Bedford, Massachusetts: W. Rotman, P. Blacksmith.

   Bibliographical data on multiple-beam scanning circular array by G. C. Chadwick and J. C. Glass of RSI, Inc.; on the circular array work at the University of Tennessee; on the multibeam volumetric scan work by Chu Associates; and on the Georgia Institute of Technology work on scanning antennas.

2. Wright-Patterson Air Force Base, Directorate of Communications and Systems Engineering Group: R. B. Stimmel, Acting Director; G. Sheer, Acting Assistant Director; M. A. Hill; D. Guidice; J. Pashek; Harold Weber and Captain Juan Butto.

   Millimeter-wave array at 50 Gc under contract to Republic Aviation; retrodirective array work at Sylvania, Buffalo.

   E. Turner, D. Horton, L. Brown

   Teledyne's inflatable antenna for vehicle orientation that uses log-periodic spirals; Butler arrays with beam shift over an octave bandwidth; and reed switches for electro-mechanical switching of Butler-type arrays.

3. Rome Air Development Center, Rome, New York

H. Hoffman, D. Baerwald, A. Snyder

Pseudo-passive satellites that increase radar cross section of a passive reflector satellite by distribution of active devices over reflecting surface; tests of S-band arrays of 3 elements; use of tunnel-diode reflection amplifiers over portion of a spherical surface.

C. Pankiewicz, C. Malagisi

a) Sylvania (Buffalo) Electronic Scanning for Space Platform; millimeter-wave techniques for electronic steering using ferrite slab in wavefront and optical focusing.

b) HICAT program at Philco; very narrow scanning beams at low microwave frequencies using X-band Luneberg lens as phase processor; frequency conversion scheme to reduce physical size.

c) L-band Van Atta array at Electronic Specialty Company (R. Johnson).

d) Phase backscatter array (J. Blass); Dorne and Margolin's reflect-array antenna system.

e) Pseudo-passive satellites; replacement of a 1000-foot diameter echo balloon with smaller one of equally effective cross section; 25-element array at X-band.

f) Retrodirective arrays; 3-by-3 S-band array.

A. Blymiller

Electronically switched L-band Wullenweber array (Motorola's Electric Goniometer).

4. Bell Telephone Laboratories, Crawford Hill Laboratory, Holmdel, New Jersey:

L. C. Tillotson, A. B. Crawford, C. Ruthroff

a) STAR array

b) Development of lightweight, reliable, efficient, small components of the type needed to implement novel array techniques.

5. Space-General, El Monte, California:

A. F. Gangi

Adaptive antennas using phase-locked loops.

6. Sylvania Electronic Systems, Buffalo, New York:

D. Leonard, G. Vlay

Electronically steerable array for space vehicle applications; objective is a millimeter-wave (30-100 Gc) antenna for a space platform.

7. Dalmo-Victor, Belmont, California

J. B. Damonte, W. F. Rock, D. Stoddard

a) S-band varactor phase shifting array using short-slot hybrids between elements.

b) LEM steerable communication antenna with mechanical scanning; a mechanically erectable paraboloid and crossed-dipole antenna; wire mesh reflectors for erectable lunar antenna.

c) Mariner and Ranger omnidirectional antenna; a slotted circular waveguide with fill-in spirals to complete the coverage.

d) Retrodirective array.

8. Electronic Communications, Inc., Timonium, Maryland:

a) M. I. Skolnik: STAFT program, self-focusing array.

b) D. D. King: Millimeter-wave program.

9. Electronic Specialty Company, Glendale, California:

D. Margerum, A. B. Lees

a) Self-phasing arrays such as the Van Atta array.

b) Pseudo-passive devices similar to the STAR array.

10. Lincoln Laboratory, Massachusetts Institute of Technology, Cambridge, Mass.:

L. J. Ricardi, J. B. Rankin, R. N. Assaly

a) Satellite that uses multiple-beam horn antennas; near synchronous unstabilized system.

b) Switches for beam switching.

11. Lockheed Aircraft Company, Sunnyvale, California

E. Blasi, A. Dunbar, A. Gaetano

a) High-gain and steerable data link; lightweight and steerable mechanical erectable reflector and feed.

b) Sequential lobing techniques.

c) Inertialess mechanical techniques that involve compensating motion for mechanical scanning.

d) Bearings of high reliability.

R. Davis, D. Hochman, C. Kortmann, D. Payne

e) Lockheed's laser acquisition and track system (LOCAT); transvideo system; a gravity-gradient stabilized vehicle using extended boom techniques.